NASA Contractor Report 3727

Helicopter Rotor Wake Geometry and Its Influence in Forward Flight

Volume II - Wake Geometry Charts

T. Alan Egolf and Anton J. Landgrebe

CONTRACT NAS1-14568
OCTOBER 1983

25th Anniversary
1958-1983

NASA

NASA Contractor Report 3727

Helicopter Rotor Wake Geometry and Its Influence in Forward Flight

Volume II - Wake Geometry Charts

T. Alan Egolf and Anton J. Landgrebe
United Technologies Research Center
East Hartford, Connecticut

Prepared for
Langley Research Center
under Contract NAS1-14568

NASA
National Aeronautics
and Space Administration
Scientific and Technical
Information Branch
1983

PREFACE

This investigation was sponsored by the Structures Directorate, U. S. Army Research and Technology Laboratories, Langley Research Center, Virginia, and administered by the National Aeronautics and Space Administration at Langley Research Center under Contract NAS1-14568. The Army technical representative for this contract was Wayne R. Mantay. Henry E. Jones was the technical representative during the initial period of the contract. The Principal Investigator was T. Alan Egolf, Research Engineer, United Technologies Research Center (UTRC). The Program Manager and Co-investigator was Anton J. Landgrebe, Manager, Aeromechanics Research, UTRC. Donna Edwards, Engineering Assistant, UTRC, contributed significantly to the development of the computer graphics used to provide the wake charts presented herein.

This report consists of two volumes:

Volume I - Generalized Wake Geometry and Wake Effect on Rotor Airloads and Performance

Volume II - Wake Geometry Charts

SUMMARY

Wake geometry charts and figures are presented which provide the necessary information to estimate the location of tip vortices trailed from helicopter rotor blades for a range of parameters representative of steady level forward flight. The charts are based on theoretical wake geometries from the classical undistorted wake equations and the generalized distorted wake equations described in Volume I. The charts can be used for a variety of applications which require the geometric relationship between the tip vortices and spatial locations relative to the helicopter. In addition to tip vortex geometry, the geometry related to blade/tip vortex interactions and wake boundaries beneath the rotor can be rapidly defined using these charts. An example application is included as an instructional tool for the use of the charts.

TABLE OF CONTENTS

LIST OF SYMBOLS

b	Number of rotor blades, dimensionless
C_T	Rotor thrust coefficient, dimensionless: $\frac{T}{\rho\pi R^2(\Omega R)^2}$
E_f	Generalized wake envelope function, nondimensional
G_f	Generalized wake shape function, nondimensional
PR	Functional notation defining the operation of taking the positive residual of the specified quantity.
R	Rotor radius, dimensional
T	Rotor thrust, dimensional
V	Rotor flight speed, dimensional
X	Longitudinal coordinate in the tip path plane, dimensional - Eq. 3
Y	Lateral coordinate in the tip path plane, dimensional - Eq. 4
Z	Axial coordinate in the tip path plane, dimensional - Eq. 2 or Eq. 6
α_{TPP}	Rotor disk attitude in tip path plane, degrees
β	Angle of intersection between blade and tip vortex based on tip path plane plan view projection, degrees
ΔZ	Axial coordinate distortion, dimensional, Eq. 7
λ_{TPP}	Rotor inflow ratio in tip path plane, Eq. 1
μ	Rotor advance ratio, $\frac{V}{\Omega R}$
μ_{TPP}	Tip path plane advance ratio, $\mu\cos\alpha_{TPP}$
π	Pi, 3.1415926...

LIST OF SYMBOLS (Cont'd)

ρ	Air density, dimensional, slugs/ft^3
ψ_{age}	Wake azimuth position or wake age, azimuth angle of vortex element (point on tip vortex) relative to the blade from which it originated; represents the blade azimuth travel between the time the vortex element was shed by the blade and the current blade azimuth, deg or rad
ψ_b	Azimuth position of the blade from which the tip filament is trailed, degrees or radians
ψ_o	Reference blade azimuth position, degrees
$\bar{\psi}$	Positive residual of the relative wake azimuth position as defined by Eq. 5, degrees or radians
ΩR	Rotor tip speed, dimensional

INTRODUCTION

The intent of this volume is to provide wake geometry data in the form of easily usable charts and figures which allow for the rapid estimation of the geometric position of the tip vortex of a specific rotor blade at any instant in time (blade azimuth). This information can then be used to determine the potential for rotor blade/tip vortex interactions and other spatial point/tip vortex interactions through comparison of the relative geometric position of the point of interest and the tip vortex position. These charts and figures provide this information based on both undistorted wake methodology and the generalized distorted tip vortex model developed and discussed in Volume I of this report. The charts and figures are presented progressing from the elementary to the more complex model. The charts consist of isometric and projection views of wake geometry, inflow ratio nomographs, undistorted axial displacement nomographs, undistorted, generalized longitudinal and lateral coordinate charts, generalized axial distortion nomographs, blade/vortex passage charts, blade/vortex intersection angle nomographs and fore and aft wake boundary charts. These charts and figures have been prepared as functions of the parameters found to be of primary interest in the first level wake generalization as described in Volume I of this report. The range of these parameters for most of the charts and figures is listed below.

Thrust Coefficient:	0.0025	$\leq$	C_T	$\leq .01$
Rotor Disk Attitude:	$-16°$	$\leq$	α_{TPP}	$\leq 4°$
Advance Ratio:	0	$\leq$	μ	≤ 0.5
Number of Blades:	2	$\leq$	b	≤ 6

The charts are presented in a format which allows for the rapid estimation of the geometric positions of the tip vortex. They were developed such that they require only a minimum amount of hand calculations to obtain the desired information. All coordinate values on the charts are normalized by the rotor radius and are in a right handed tip path plane coordinate system. This coordinate system is illustrated in Fig. 1. Figures 2 to 10 are presented as an introduction to the wake charts and their application. These figures illustrate the variety and use of the wake charts that have been developed by way of an example application.

WAKE CHART DESCRIPTION

Isometric and Projection View Plots

To provide for the fundamental understanding of the wake and its parametric variations and to provide a realistic pictorial wake representation which complements the wake information to follow, isometric and projection view plots of both the undistorted and distorted wake geometries for selected conditions are presented. These plots will give the wake chart user a physical feeling of the output from the two dimensional wake charts that follow in relation to the actual three dimensional wake geometry. All of the figures presented in this section will contain the standard projection views (top, side, and rear) and an isometric view. They are presented as functions of blade number, thrust level, tip path plane attitude, advance ratio, and blade azimuth position.

Figure 11 presents the effect of advance ratio on the wake geometry of a four bladed configuration for the undistorted wake model. The variation in advance ratio changes the inflow ratio for the condition selected (C_T = .005, α_{TPP} = -2.0 deg). This effect results in both an axial and longitudinal variation in the wake geometry with increasing advance ratio, as seen in Fig. 11.

Figure 12 presents the effect of thrust level on the wake geometry of a two bladed configuration for the undistorted wake model. The influence of thrust level is limited to changes in the axial coordinate as seen in this figure. Higher thrust creates a larger inflow, and thus, a larger axial displacement from the rotor tip path plane. Figure 13 presents the effect of tip path plane attitude on the wake geometry of a two bladed configuration for an undistorted wake model. Changes in rotor tip path plane attitude with the other parameters held constant result in changes in both axial and longitudinal coordinates since the definition used for the rotor advance ratio does not include the cos α_{TPP} term. The strongest influence of increasing (negatively) the tip path plane attitude is to displace the wake in an axially increasing (negative) direction. The effect of wake distortions as modeled by the generalized distorted tip vortex model is presented in Fig. 14 for the same conditions as presented in Fig. 12. As seen from the comparison of the undistorted and distorted wake geometries presented in these two figures, the effect of the distortions is a tendency for the tip vortex to rollup on the lateral edges of the wake. The increase in thrust level (Fig. 14c) is seen also to result in larger wake distortions from the comparatively undistorted position at the lower thrust level (Fig. 14a). The effect of wake distortion with changes in tip path plane attitude can be seen in a comparison of Fig. 15, the distorted wake model, with Fig. 13, the undistorted model.

Figure 16 presents the effect of advance ratio on the distorted wake geometries for the same conditions presented in Fig. 11. A comparison of these two figures shows the influence of the distorted wake model on the tip vortex geometry for changes in advance ratio. The effect of increasing advance ratio is seen to change the character of the wake distortions. This effect is better demonstrated in a following section on the generalized wake shape function. Figure 17 presents the specific condition presented in Fig. 11c for incremental values of the blade azimuth position using the distorted tip vortex model. From this figure, the variation of the wake geometry with blade azimuth position can be seen. A careful study of the plots of wake geometries presented in Figs. 11 to 17 should yield significant insight into the three dimensional representation of the tip vortex as modeled by either the undistorted or distorted wake models. This insight will be helpful in understanding the use of the following wake charts.

Inflow Ratio Nomographs

The first set of nomographic charts (Fig. 18) are used to determine the rotor tip path plane inflow ratio (λ_{TPP}) to define the axial displacement of the rotor wake. The inflow ratio is defined by momentum considerations in the tip path plane as a function of the rotor thrust coefficient (defined in the conventional sense, (C_T)), the rotor advance ratio (μ) defined as the ratio of the rotor flight speed to rotor tip speed, and the rotor tip path plane angle (negative nose down, α_{TPP}). Given these parameters, the rotor inflow ratio can be determined quickly by graphical means from these charts, or by finding the first positive root (λ_{TPP}) of the following relationship

$$\lambda_{TPP} = \mu \sin \alpha_{TPP} - \frac{C_T}{2} \left[(\mu \cos \alpha_{TPP})^2 + \lambda_{TPP}^2 \right]^{-1/2} \qquad (1)$$

These charts are presented in terms of the tip path plane inflow ratio as a function of the tip path plane rotor advance ratio ($\mu \cos \alpha_{TPP}$) from 0 to .5 and the thrust coefficient (C_T) from 0.0 to .010 for two degree incremental values of the tip path plane angle from -16 to 4 degrees. This range of values should be adequate for most conventional rotorcraft.

Undistorted Axial Displacement Nomographs

Once the tip path plane inflow ratio is known, the classical undistorted axial (normal) displacement of any tip vortex can be found. Figure 19 provides nomographic charts which are used to determine this normalized axial displacement of the tip vortex as functions of wake age and inflow ratio. The wake age is defined as the azimuthal variation in time from the instant in time that the filament is trailed off the blade to its current position in time. Zero wake age is thus physically referenced to the blade tip (quarter chordline).

$$Z/R = \lambda_{TPP}\ \psi_{age} \tag{2}$$

The axial displacement referenced to the tip path plane is normalized by the blade radius and is plotted for four revolutions of wake age (1400 degrees) in Parts I and II of Fig. 19. The third part of this figure is a table of the normalized axial displacement versus inflow ratio for integer multiples of 360 degrees of wake age. With this table, and the graphs of Parts I and II, the axial displacement can be found for any wake age by the appropriate addition of the axial displacement for integer multiples of 360 degrees of wake age and the displacement for the positive fractional remainder of the wake age for the condition of interest. Note that the variation of this displacement is linear in terms of either the inflow ratio or the wake age.

Undistorted Longitudinal and Lateral Coordinate

The axial displacement by itself does not allow for the determination of the relative distance between a point of interest and the tip vortex in three dimensional space. The longitudinal and lateral positions of the tip vortex are also necessary to determine the relative geometry. As noted in Volume I of this report, the longitudinal and lateral positions are not highly distorted from the undistorted helicoidal shape. Thus, the first order approximation to these coordinate positions can be simply determined by the use of the undistorted equations in the tip path plane.

$$X/R = \cos\ (\psi_B - \psi_{age}) + \mu\cos\ \alpha_{TPP}\ \psi_{age} \tag{3}$$

$$Y/R = \sin\ (\psi_B - \psi_{age}) \tag{4}$$

To avoid the necessity of calculating these functions to obtain the coordinate values, the charts in Figs. 20 and 21 are provided. These charts present the data as functions of the wake age, the blade azimuth position of the blade from which the wake is trailing (ψ_B), and the rotor advance ratio in the tip path plane ($\mu_{TPP} = \mu\cos\alpha_{TPP}$). Figure 20 provides sufficient information to determine the longitudinal position of the tip vortex. This figure has two parts, corresponding to the cyclic and steady terms in the above equation for the longitudinal term (X/R). The steady part is determined in a manner similar to the method for axial displacement and is linear with wake age. The table in Fig. 20a provides for the determination of the steady longitudinal displacement for integer multiples of 360 degrees of wake age for various tip path plane advance ratios. The steady longitudinal displacement for the positive fractional remainder of the wake age for a given condition is obtained graphically from the nomograph of displacement versus wake age, presented in the graphic part of Fig. 20a as a function of the appropriate tip path plane advance ratio. The addition of these two displacements results in the total steady longitudinal coordinate for a given tip path plane advance ratio and wake age. The cyclic portion is obtained by the use of the second portion of this figure (Fig. 20b). This figure presents the cyclic portion of the longitudinal coordinate as a function of the positive residual of the relative wake azimuth position ($\bar{\psi}$). The relative wake azimuth position is defined as the difference between the instantaneous blade azimuth position from which the filament is trailing (ψ_B) and the local wake age (ψ_{age}) of interest of the actual filament. The positive residual ($\bar{\psi}$) is defined as the remaining positive value after subtracting the largest integer multiple of 360 degrees which does not yield a negative fraction.

$$\bar{\psi} = PR\ [\psi_B - \psi_{age}] \tag{5}$$

It can be seen that this figure is simply a plot of the cosine function versus a reference angular position ($\bar{\psi}$). For a given blade azimuth position (ψ_B) from which a tip filament trails, and a particular wake age (ψ_{age}) of interest, the cyclic longitudinal position can then be obtained from this plot. The addition of the steady and cyclic portions results in the total longitudinal displacement of the tip vortex filament as a function of blade azimuth position, wake age and tip path plane advance ratio.

The lateral coordinate of the tip vortex is found by the use of the information presented in Fig. 21. Again, the positive residual of the relative blade wake azimuth position is used and the cyclic lateral position of the tip vortex is obtained from the plot for the particular combination of parameters of interest. These charts provide sufficient information to quickly determine the location of an undistorted tip vortex with respect to the rotor tip path plane based on rotor momentum transport concepts.

Generalized Axial Distortion Nomographs

As noted in Volume I of this report, the actual tip vortex does not follow the trajectory of the undistorted momentum wake. Thus, the use of the axial distortions based on momentum definitions will not accurately define the potential for strong close blade/vortex interactions. As an improvement to the estimate of this potential based on the undistorted wake, the generalized distorted wake model can be used. However, the complex nature of the relationships used in this model requires the use of somewhat more complex wake charts. It should also be noted that the wake charts provided for this model provide only an approximation to the actual wake geometry and that the use of the charts must be made with this understanding. Because it is only an approximation, the results obtained should be used only as an indicator of potential blade/vortex interactions, and not as an accurate measure of the relative distance between the blade (or field point) of interest. The generalized wake coordinates for a tip vortex are comprised of two parts, one of which is the undistorted wake position (Fig. 19) already described. Thus, it is only necessary to present the additional axial distortions from this momentum wake position

$$Z/R = \lambda_{TPP}\ \psi_{age} + \Delta Z/R. \tag{6}$$

The distortions from the momentum wake position ($\Delta Z/R$) are modeled by the combination of an envelope function (E_f) and a geometric shape function (G_f).

$$\Delta Z/R = E_f \cdot G_f \tag{7}$$

The exact expressions are presented in Volume I of this report and are functions of advance ratio, thrust level, blade number, blade azimuth position and wake age. Figures 22 through 25 present these functions as nomographic plots for the range in parameters for which they were developed. Figures 22 and 23 present the envelope function for 2 and 4 blades respectively at advance ratios of .05, .1, .15, .2, and .3, and for thrust coefficients of .0025 to .0075. Figures 24 and 25 present the generalized shape functions for 2 and 4 blades respectively for the same variation in parameters. Again, graphical means are used to obtain the appropriate values for these functions from the charts for the particular set of parameters of interest. The multiplication of these two values (Eq. 7) results in the axial displacement from the momentum wake position for the tip vortex. This value is then combined with the momentum wake position to define the axial position of the tip vortex (Eq. 6). With this information, an improved estimate can be made for the determination of the potential for close blade/vortex interaction.

Blade/Vortex Passage Charts

As noted earlier, the charts presented herein can be used to determine the relative position between a point in space and the tip vortex for any given time increment. The determination of the potential for a blade/tip vortex interaction to exist using these charts by themselves would be a tedious, time consuming task. To alleviate this tedious effort, the next set of charts was developed to simplify this task. These charts present the occurrence of an intersection of a rotor blade with the tip vortex of any of the blades of the rotor for a given tip path plane advance ratio. They are based only on the inplane projection of the longitudinal and lateral coordinates of the tip vortices and the intersection of the rotor blade of interest. The charts are presented in polar coordinate form where the axes represent the radial and azimuthal position of the blade of interest. These plots do not represent wake geometries, only the potential occurrence of an intersection. The occurrence of an intersection is represented by the solid lines and symbols. Superimposed at selected locations on these curves which correspond to the intersection occurrences are the wake ages for up to four revolutions of wake age (1440 degrees). Since these intersections are based on the projections of the tip vortices into the tip path plane, they do not recognize the axial displacement between the blade and vortex intersection of interest. However, the axial displacement for a potential intersection can be quickly obtained from the charts presented earlier if the thrust level, wake age, and rotor attitude are known (Figs. 18 and 19 and 22 through 25). Thus, the rapid determination for the potential for close blade/vortex interactions can be determined from these charts based on axially distorted wake considerations. These intersection plots are presented in polar coordinate format in Figs. 26 through 30 for two (2) through six (6) blades respectively as functions of the tip path plane advance ratios of .05, .1, .15, .2, .3 and .4. In addition, these results are also presented in rectilinear format, without the wake age indicated, on the plots in Figs. 31 and 32 for two (2) and four (4) blades respectively.

Blade/Vortex Intersection Angle Nomographs

The next set of charts, presented in Fig. 33, provides additional information about the intersections presented in Figs. 26 through 32. These charts provide the angle of intersection (β) of a potential blade/tip vortex intersection for the tip path plane advance ratios of .05, .1, .15, .2, .3 and .4. If the reference blade azimuth position (ψ_o), wake age at the point of intersection (ψ_{age}), azimuthal position of the blade trailing the tip vortex (ψ_b), and the tip path plane advance ratio ($\mu\cos\alpha_{TPP}$) are known, the angle of intersection can be obtained graphically from this figure. If the blade angle (ψ_o) is greater than 180 degrees, the value for use with the chart must be reduced by 180 degrees. This is because of the periodicity of the solution

for multiples of 180 degrees of blade azimuth angle position. This angle of intersection information can be useful in determining the nature of the intersection; for example, a normal or parallel encounter.

Fore and Aft Wake Boundary Charts

The information provided in the axial distortion charts (Figs. 19 and 22 through 25) can also be used to define fore and aft wake boundary information. However, to expedite this task, a set of wake boundary charts has been provided in Figs. 34 through 50. The use of these charts can be helpful in the determination of rotor/empennage/stores/body interactions beneath the rotor disk. In Fig. 34, the fore and aft wake boundary charts are presented based on the undistorted axial wake model. These boundaries are functions of the rotor attitude, inflow rotor and advance ratio. The lines representing the fore and aft boundaries for the zero lateral position (Y/R=0) along the centerline of the outer disk are presented in these charts. The use of the lateral position indicators provided in these charts also allows for the determination of the fore and aft boundaries for non-zero lateral positions by the appropriate parallel translation of the fore and aft reference lines to the appropriate lateral reference position. This procedure will be discussed in the example application section which follows.

In Figs. 35 through 50 the fore and aft boundaries based on the generalized distorted wake model are provided for various selected lateral positions, thrust levels, advance ratios, tip path plane attitudes, and two and four blades. A selection is necessary because the axial displacement based on the generalized distorted wake model must be determined numerically for each lateral position and would result in a very large number of plots. Careful examination of these selected charts indicates that the wake boundaries compress as the vertical and longitudinal sectional plane is moved in the lateral direction (advancing or retreating) toward the rotor tips. This is due to the wake rollup. It should also be noted that at the rotor centerline the distortions displace the wake toward the rotor.

The range of parameters is limited in scope due to the previously noted reason. Hopefully the selected range is sufficient for general applications and will give the user a "feel" for the distortion influence.

SAMPLE APPLICATION OF THE WAKE CHARTS

Example Condition

An example of the use of the provided charts is demonstrated for a fictitious aircraft operating at a prescribed flight condition. In this example, the objective is to determine whether or not a tip vortex passes close to a blade at 160 degrees azimuth. The parameters and the values for this example which are necessary for the use of these charts are:

Blade radius	20 ft
Blade number (b)	4
Thrust Coefficient (C_T)	.0075
Tip path plane attitude	-3°
ΩR	700 fps
V	161 fps
Advance ratio, μ	.23
Blade azimuth position, ψ_B	160°

The tip path plane advance ratio is calculated as

$$\mu_{TPP} = \mu \cos \alpha_{TPP} = 0.23$$

Inflow Ratio

The tip path plane inflow ratio (λ_{TPP}) for this particular condition is found by graphical means from Figs. 18g and 18h. This technique is demonstrated in Fig. 2, and the value obtained is approximately -.0283. An exact calculation for the inflow rotor to five places would yield -.02822 for this condition. This corresponds to a momentum induced velocity for the condition of 11.3 fps, using the relationship noted below.

$$V_{imom} = \frac{1}{2} C_T (\lambda_{TPP}^2)^{-1/2}$$

Undistorted Axial Location

With the above value for the tip path plane inflow ratio, the undistorted axial displacement of a tip vortex can be found using Fig. 19. To illustrate this procedure, consider a rotor blade's relationship to the tip vortex trailed from the preceding blade (one of four). For this condition, the blade azimuthal spacing is 90 degrees (360°/b). Thus, the wake age is approximately 90 degrees. From Fig. 19, Part I, the axial displacement for 90 degrees wake age is found by graphical means. This procedure is demonstrated in Fig. 3 for two methods, one of which allows for an increased graphical accuracy. For this condition, the displacement is found to be about -.0425 R using the more accurate method. The exact value is -.044328 R. This represents a relatively close blade/vortex interaction. For example, if the magnitude of the induced velocity of such an encounter can be modeled for first order accuracy by a straight infinite vortex with circulation strength of 250 ft^2/sec, not an unreasonable value for this aircraft, the induced velocity using the Biot-Savart law for an infinite vortex filament would be about 45 fps.

$$V_i \cong \frac{\Gamma}{2\pi R}\frac{1}{h} = \frac{250}{2\pi \cdot 20 \cdot (.044)} = 45.2$$

This corresponds to four (4) times the momentum value for this condition. At the azimuthal position of 160 degrees at the .75 R radial location, this could represent a significant change in the induced angle of attack compared with that predicted based on the momentum value. As a result of this study, it is seen that a blade vortex interaction of potential significance could occur.

Longitudinal and Lateral Coordinates

Consider now that the preceding blade is at an azimuthal position (ψ_B) of 250 degrees for the above example, the longitudinal and lateral positions of the tip vortex shed from this blade near the reference blade of interest (ψ_o = 160°) can approximately be found by the use of Figs. 20 and 21. Since the approximate wake age (ψ_{age}) in this example is known to be about 90 degrees for the close interaction noted above, the relative wake azimuth position ($\bar{\psi}$) is simply 160°.

$$\bar{\psi} = PR\ [\psi_B - \psi_{age}] = 250 - 90 = 160$$

From Fig. 20, Part I, the steady longitudinal component based on the wake age (90°) is found to be .37 R. From Fig. 20, Part II, the cyclic portion based on the relative wake age position ($\bar{\psi}$ = 160°) is found to be -.93 R. The total of these two values results in a longitudinal coordinate of -.56 R. This technique is demonstrated in Fig. 4. The lateral coordinate is found from Fig. 21 in a manner similar to the cyclic portion of the longitudinal coordinate as shown in Fig. 5. The value obtained for the lateral coordinate is .34 R. The resulting undistorted coordinates for the tip vortex near the following blade at 160° for this condition are then:

	Graphical	Exact
X/R =	-.56	-.57841
Y/R =	.34	.34202
Z/R =	-.043	-.04432

Axial Coordinate Distortions

Since it is known that the actual tip vortices trailed by the rotor blades can undergo significant axial distortions, the occurrence of such distortions should be considered when studying close blade/vortex interaction. In order to provide additional insight into this problem, the use of the UTRC Generalized Wake Model can be used to further refine the axial displacement. Figures 22 and 24, and 23 and 25, for two and four blades respectively, present the generalized wake modeling functions for a range of advance ratios and thrust loads. For the example condition, the envelope function, E_f, is found by graphical means from Figs. 23d and 23e to be .035. This procedure is illustrated in Fig. 6. The generalized shape function, G_f, for this condition is also found by graphical means from Fig. 25 to be .90. This procedure is illustrated in Fig. 7. The multiplication of these values results in the distortion, $\Delta Z/R$, from the undistorted wake model.

$$\Delta Z/R = E_f \cdot G_f = .0350 \times .90 = .0315$$

The addition of the undistorted and distorted displacement values results in the generalized wake distortion model value for the condition of interest,

$\psi_o = 160°,$

$\psi_b = 250°,$

$\psi_{age} = 90°,$

$\mu_{TPP} = .23,$

$\lambda_{TPP} = -.0283.$

$$Z/R = \lambda_{TPP}\ \psi_{age} + \Delta Z/R = -.043 + .0315 = -.0115$$

This value for the axial displacement places the tip vortex very near the rotor tip path plane for this condition. The implication of this result is that there is a very strong potential for a close blade/tip vortex interaction to occur. It should be noted that the exact wake age was not used, only an approximate value ($\psi_{age} = 90°$). The exact value will be obtained in the next section.

Blade/Tip Vortex Intersections

For the example condition, it has been shown that there is the potential for a blade vortex interaction to be occurring based on the tip vortex trailed from the preceding blade. The potential for blade/tip vortex intersections can quickly be determined for any azimuthal position due to any tip vortex by the use of Figs. 26 to 32. For the example condition, Figs. 28d and 28e are used to determine the desired information using graphical interpolation techniques. This procedure is illustrated in Fig. 8. The radial position of the blade at 160 degrees, which intersects the tip filament trailed by the preceding blade, is found to be about .68 R and the actual wake age noted at discrete intervals on the intersection curves is determined graphically to be about 84 degrees. For this wake age the exact value for the radial coordinate is .6781 R. This information could have been obtained from Figs. 32d and 32e which present the same information in a rectilinear format. With this more exact value for the wake age, a slightly more exact value for the axial displacement of the tip vortex can be found by repeating the above procedures.

These blade/vortex intersection plots (Figs. 26 to 32) are of significant value if the user is basically interested in only tip vortex intersections. By first using these figures to determine if any intersection is possible from a plan view projection basis, the axial position can be rapidly determined by the use of Fig. 18 for the inflow ratio, Fig. 19 for the undistorted axial displacement, and if desired, Figs. 22 to 25 for the generalized wake distortions. The longitudinal and lateral coordinates for the intersection point are determined graphically from Figs. 20 and 21, or by the use of the trigonometric relationships between polar and cartesian coordinates, since the radial and azimuthal coordinates (polar) are now known from Figs. 26 to 32.

Angle of Intersection

Figure 33 can be used to obtain the relative angle of intersection between the blade and tip vortex for a plan view intersection obtained from the blade/tip vortex intersection plots. For the example condition, Fig. 9 illustrates this procedure, and the angle of intersection is found to be about 90 degrees. Note that 180 or 0 degrees represents a parallel blade/vortex encounter. As a further note, if the blade angle (ψ_o) is greater than 180 degrees, the value should be reduced by 180 degrees for use on the chart as noted in the earlier section describing this type of chart.

Fore and Aft Wake Boundaries

Now assume that the wake boundary defined by the passage of the tip vortices beneath the rotor is of interest. For instance, the geometric relationship between the launch point location of rocket stores and the rotor wake boundary of an attack helicopter might be of importance because the strong downwash of the wake could influence the rocket trajectory. For this example, the wake boundary location is significant for low speed rocket firings, since the downwash can strongly affect the accuracy of the rocket. Assume for illustrative purposes that a rocket launcher is located in the tip path plane coordinate system .4 R beneath the rotor, .05 R ahead of the hub center, and displaced laterally on the advancing side by .5 R. For this example flight condition, the undistorted fore and aft wake boundaries can be determined using Fig. 34c. Figure 10 illustrates this procedure for the determination of the position of the wake boundary relative to the rocket launch location. In this particular example, the results obtained in Fig. 10 indicate that there is no intersection of the rocket launch point, or trajectory with the wake boundary.

The wake boundaries are, in reality, changed due to the actual wake distortions. The approximate boundaries can be found for selected conditions by the use of Figs. 35 to 50. For the above example of a rocket launch point, the distorted wake boundaries can be found using a similar procedure (Fig. 50c).

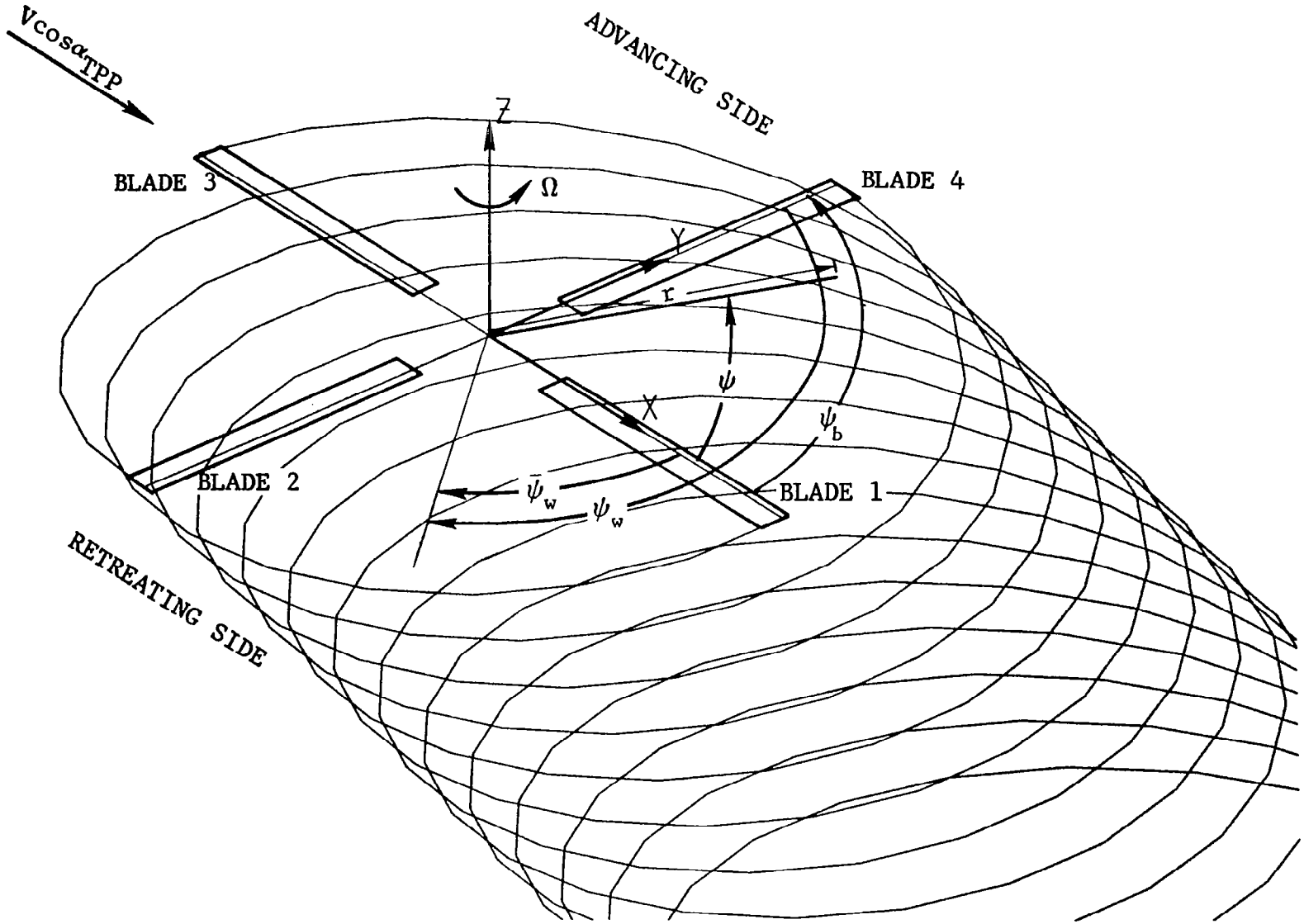

FIGURE 1. COORDINATE DEFINITION AND BLADE NUMBERING SYSTEM

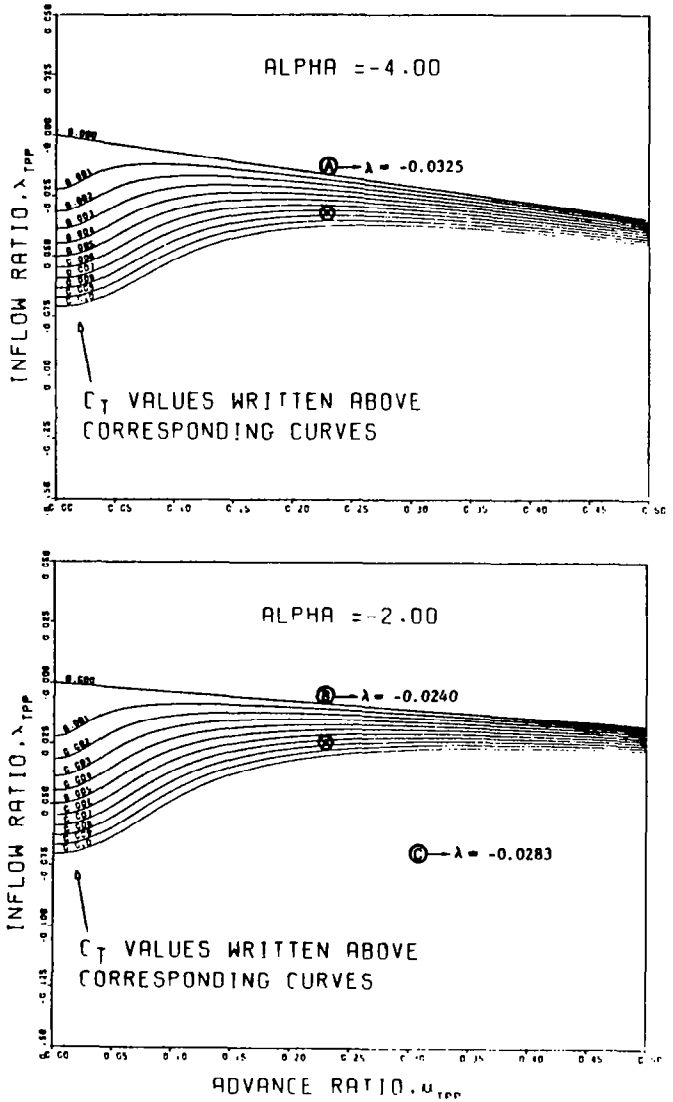

Information Desired

Inflow ratio (λ_{TPP})

Information Required

Thrust coefficient (C_T = .0075), tip path plane advance ratio (μ = .23), tip path plane attitude (α_{TPP} = -3°).

Instructions

Ⓐ For μ_{TPP} = .23 and C_T = .0075 the inflow ratio for a -4° tip path plane is found by graphical means to be -.0325.

Ⓑ For μ_{TPP} = .23 and C_T = .0075 the inflow ratio for a -2° tip path plane is found by graphical means to be -.0240.

Ⓒ Since the desired value is for a tip path plane of -3°, the average of the two values can be used.

λ_{TPP} = (-.0325 + -.0240) / 2
= -.0283

FIGURE 2. EXAMPLE USE OF THE INFLOW RATIO NOMOGRAPHS

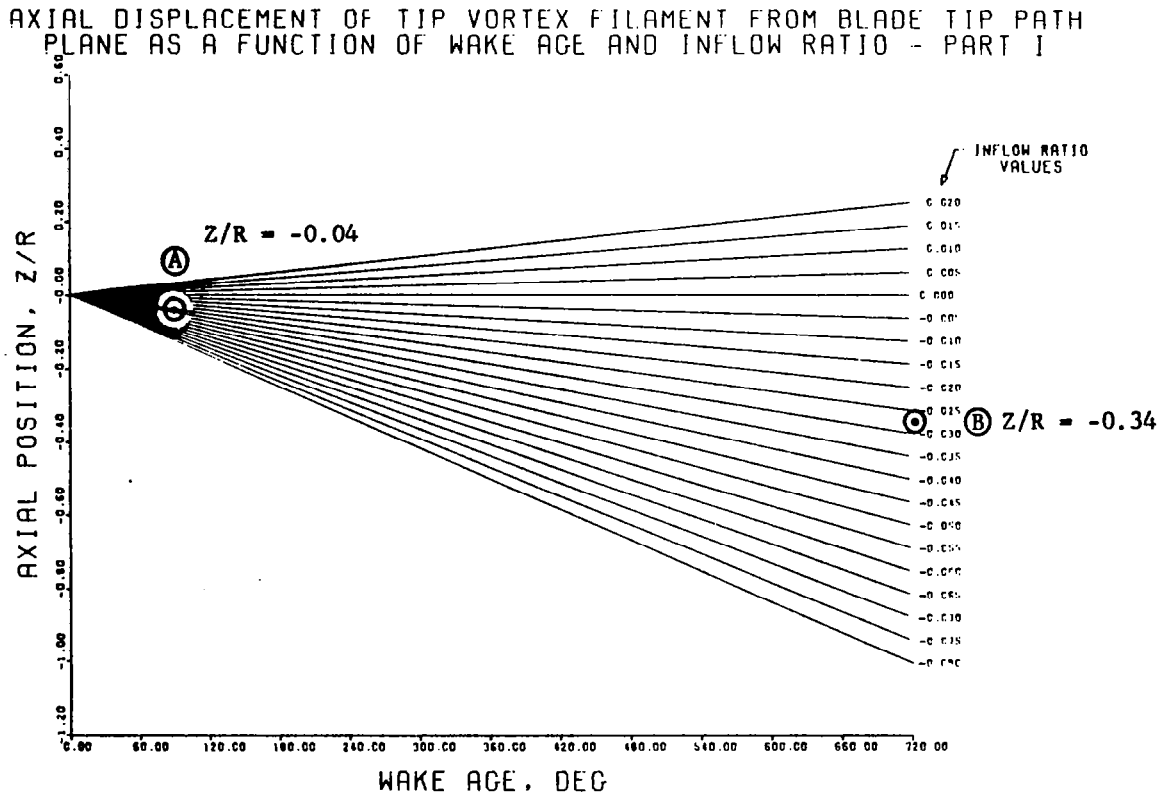

Information Desired

Undistorted axial displacement

Information Required

Inflow ratio (λ = -.0283), wake age (ψ_{age} = 90°).

Instructions

Ⓐ Determine Z/R by graphical interpolation for λ = -.0283 at ψ_{age} of 90°.

Z/R = -0.04

Ⓑ Determine Z/R by graphical interpolation for λ = -.0283 at a larger ψ_{age} (720°) and divide answer by appropriate value to obtain more accurate estimate.

Z/R (720) = -0.34
Divide by 8
Z/R (90) = -0.0425

FIGURE 3. EXAMPLE USE OF THE AXIAL DISPLACEMENT CHART

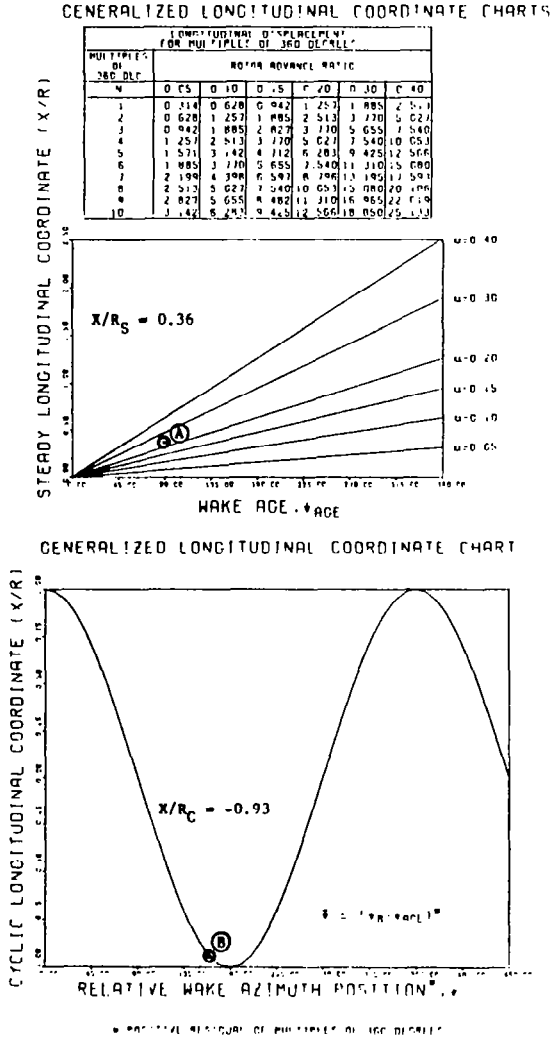

Information Desired
Longitudinal coordinate, X/R

Information Required
Tip path plane advance ratio (μ_{TPP}), wake age (ψ_{age}), and blade azimuth position from which the tip vortex trails (ψ_B)

Instructions

Ⓐ By graphical means the steady longitudinal component is found for a given μ_{TPP} (.23) and ψ_{age} (90^{o}).

$X/R_S = .36$

Ⓑ By graphical means the cyclic longitudinal component is found for the relative wake azimuth position $\bar{\psi}$.

$\bar{\psi} = PR\ |\psi_B - \psi_{age}|$

$\bar{\psi} = PR\ |250 - 90| = 160$

$X/R_C = -.93$

Ⓒ $X/R = X/R_S + X/R_C = -.56$

FIGURE 4. EXAMPLE USE OF THE GENERALIZED LONGITUDINAL COORDINATE CHART

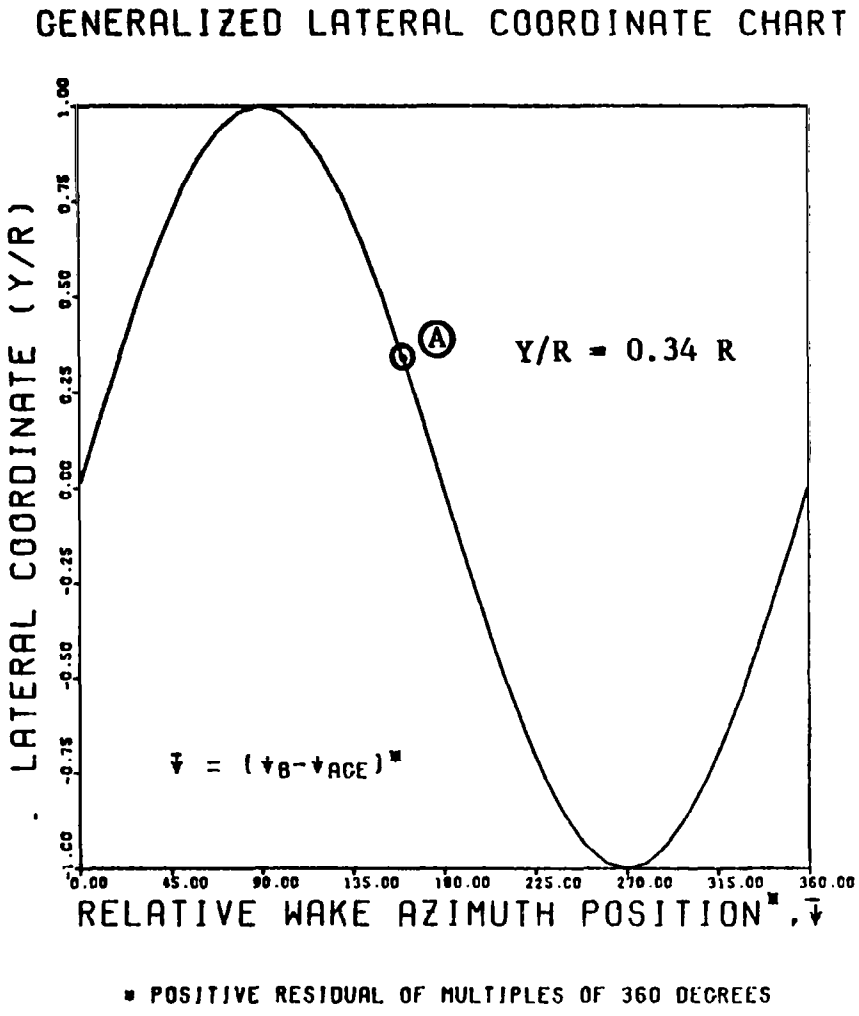

Information Desired

Lateral coordinate

Information Required

Relative wake azimuth position, $\bar{\psi}$

Instructions

Ⓐ By graphical means, the lateral coordinate for the relative wake azimuth position ($\bar{\psi}$ = 160) is found.*

Y/R = 0.34

*See Figure 4.

FIGURE 5. EXAMPLE USE OF THE GENERALIZED LATERAL COORDINATE CHART

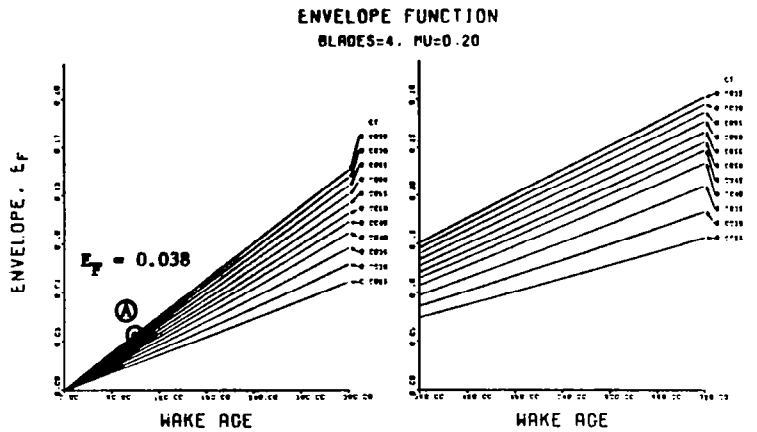

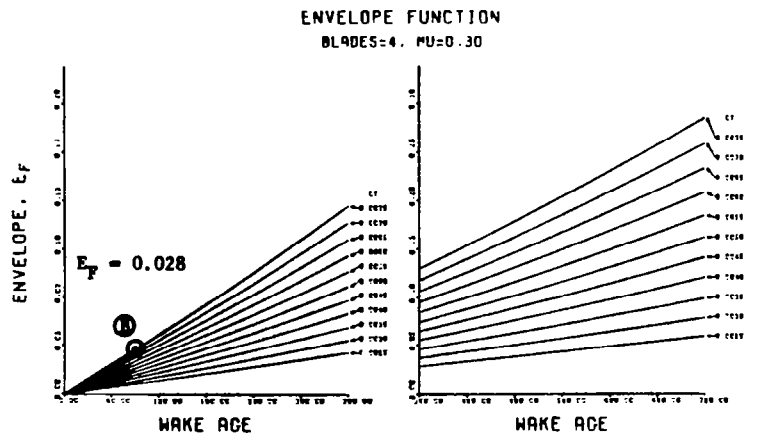

Information Desired

Envelope function for a particular thrust and wake age.

Information Required

Thrust coefficient (C_T), wake age (ψ_{age}), number of blades (b), and advance ratio ($\mu = \frac{V}{\Omega R}$)

Instructions

(A) Interpolate by graphical means on the thrust level (C_T = .0075), wake age (ψ_{age} = 90°), blade number (b = 4), and advance ratio (μ = .2).

ε_F = .038

(B) Interpolate by graphical means on the thrust level (C_T = .0075), wake age (ψ_{age} = 90°), blade number (b = 4), and advance ratio (μ = .3).

ε_F = .028

(C) Using linear interpolation in the advance ratio (μ = .23) and envelope functions found in A and B, the actual envelope function is found.

ε_F = .035

(C) $$\varepsilon_F = 0.038 + \frac{0.028 - 0.038}{0.3 - 0.2}(0.23 - 0.2)$$

$$= 0.035$$

FIGURE 6. EXAMPLE USE OF THE GENERALIZED WAKE ENVELOPE FUNCTION CHART

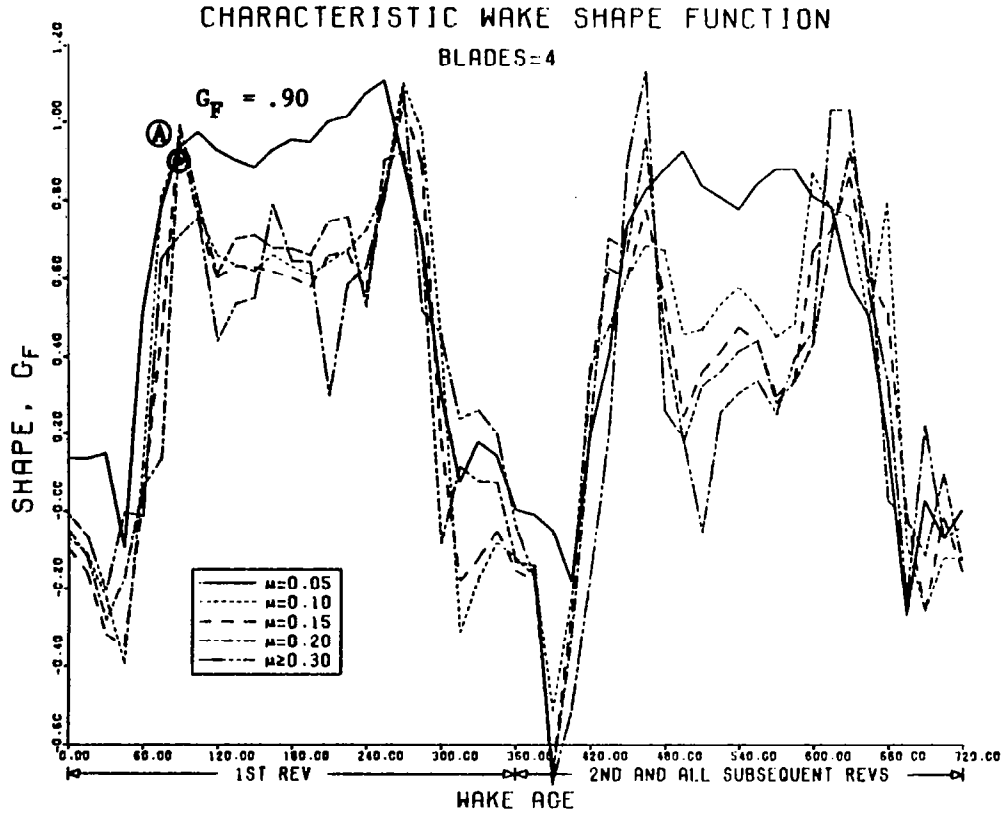

Information Desired

Wake shape function (G_F)

Information Required

Rotor advance ratio ($\mu = \frac{V}{\Omega R}$), wake age (ψ_{age}), and number of blades.

Instructions

Ⓐ For the selected wake age ($\psi_{age} = 90^{o}$), the shape function (G_F) is found by graphical interpolation between the advance ratios which bound the actual value ($\mu = .23$).

$G_F = .90$

FIGURE 7. EXAMPLE USE OF THE GENERALIZED WAKE SHAPE FUNCTION CHART

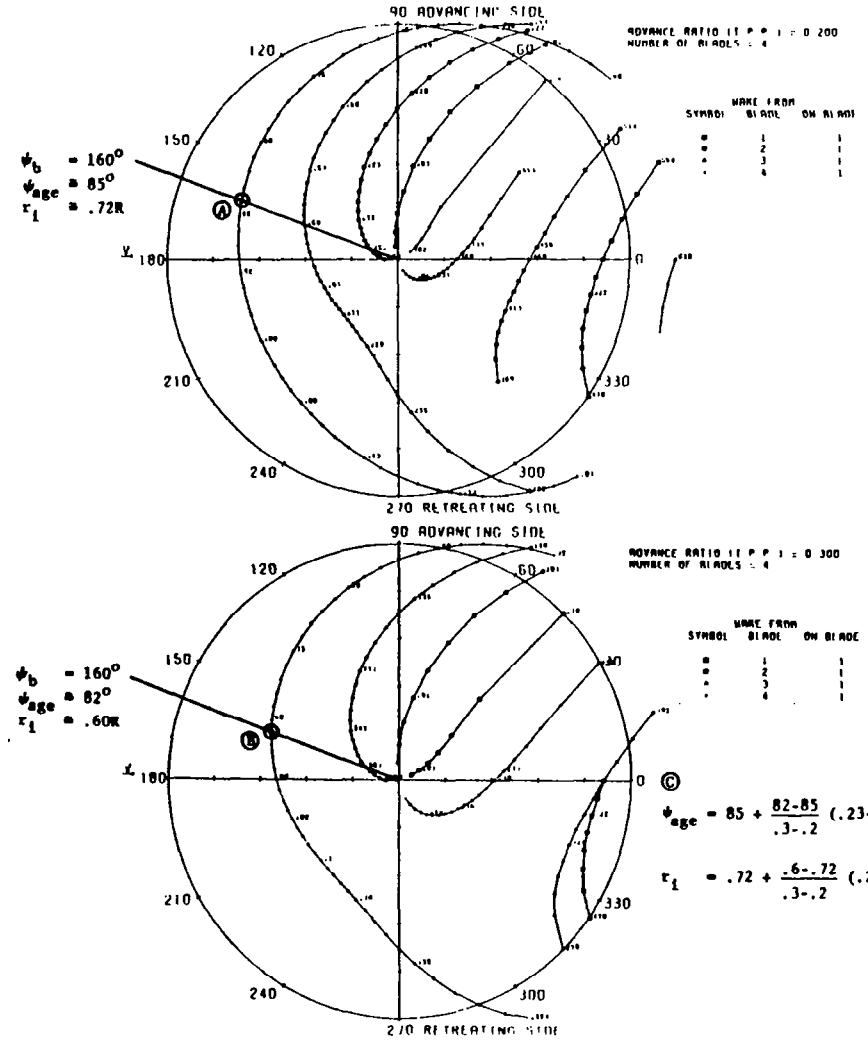

Information Desired

Radial and azimuthal location of a blade/tip vortex intersection and the associated wake age.

Information Required

Tip path plane advance ratio (μ_{TPP}) and number of blades.

Instructions

Ⓐ At a selected blade azimuthal position ($\psi_b = 160^\circ$) for a selected advance ratio ($\mu = .2$) determine by graphical means the radius of intersection and wake age for the tip filament of interest ($\psi_o = 250^\circ$, blade 4).

$\psi_{age} = 85^\circ$, $r_i = .72R$

Ⓑ At a selected blade azimuthal position ($\psi_b = 160^\circ$) for a selected advance ratio ($\mu = .3$) determine by graphical means the radius of intersection and wake age for the tip filament of interest ($\psi_o = 250^\circ$, blade 4).

$\psi_{age} = 82^\circ$, $r_i = .60R$

Ⓒ By linear interpolation on the solutions for the advance ratios bounding the desired value ($\mu = .23$) obtain the estimate for the wake age and radius of intersection.

$$\psi_{age} = 85 + \frac{82-85}{.3-.2}(.23-.2) = 84$$

$$r_i = .72 + \frac{.6-.72}{.3-.2}(.23-.2) = .68$$

$\psi_{age} = 84^\circ$, $r_i = .68R$

FIGURE 8. EXAMPLE USE OF THE BLADE/TIP VORTEX INTERSECTION PLOTS

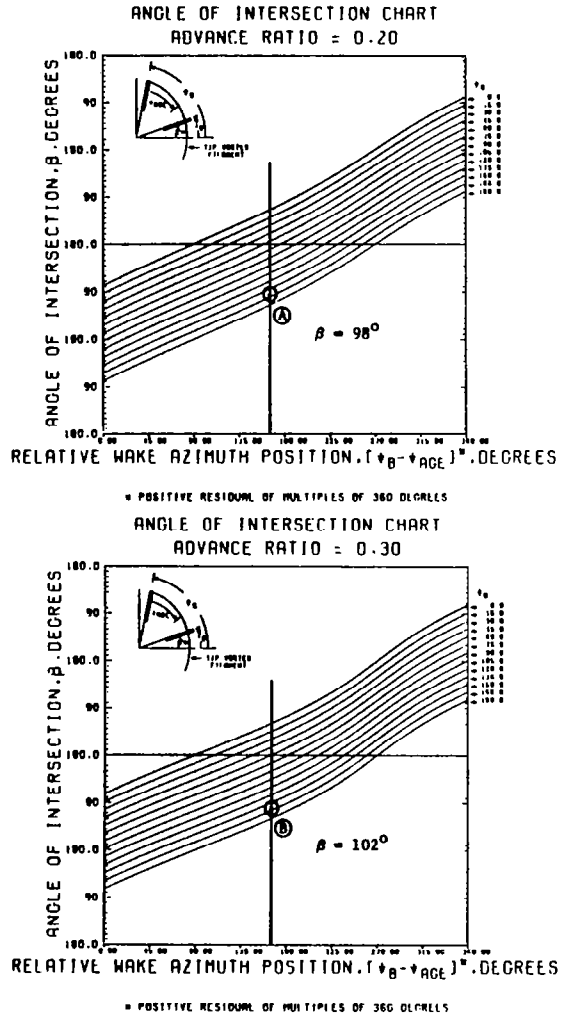

Information Desired

Angle of intersection

Information Required

Tip path plane advance ratio, ($\mu\cos\alpha_{TPP}$), reference blade azimuth position (ψ_o), and blade azimuth position from which tip filament trails (ψ_B).

Instructions

(A) The positive residual of the relative wake azimuth position ($\psi_B - \psi_{age} = 250 - 84 = 166$) on the bounding advance ratio ($\mu = .2$) is determined, and the angle of intersection (β) is found by graphical means for the selected reference blade azimuth position ($\psi_o = 160$).

$$\beta \cong 98^\circ$$

(B) This procedure is repeated for the other bounding advance ratio ($\mu = .3$) to determine the corresponding angle of intersection.

$$\beta \cong 102^\circ$$

(C) The angle of intersection for the actual advance ratio ($\mu = .23$) is then determined by interpolation.

$$\beta \cong 99.2^\circ$$

(C) $$\beta = 98 + \frac{102 - 98}{.3 - .2}(.23 - .2) = 99.2$$

FIGURE 9. EXAMPLE USE OF THE ANGLE OF INTERSECTION CHART

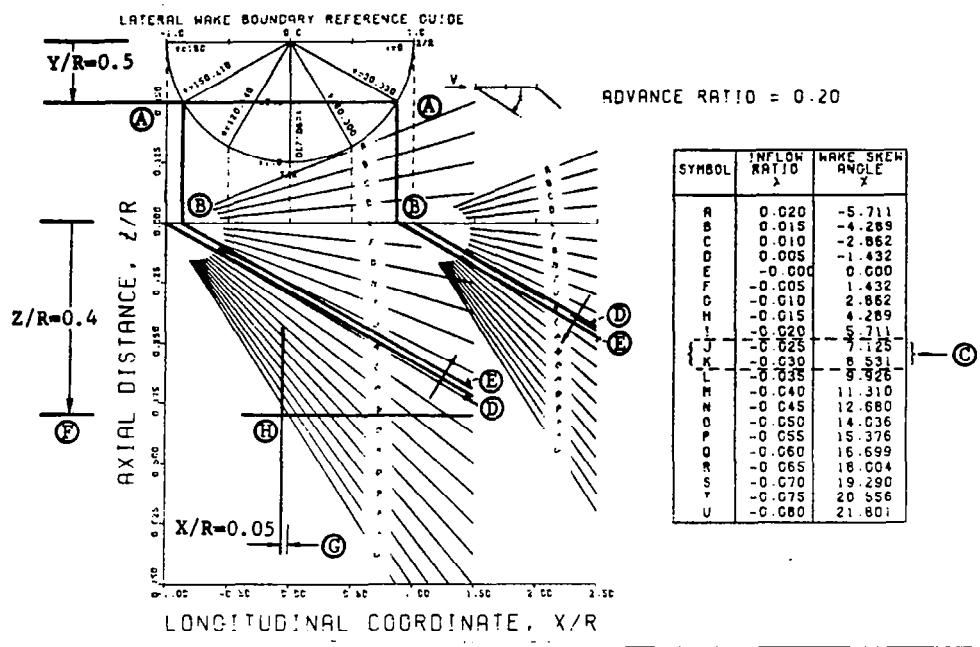

SYMBOL	INFLOW RATIO λ	WAKE SKEW ANGLE χ
A	0.020	-5.711
B	0.015	-4.289
C	0.010	-2.862
D	0.005	-1.432
E	-0.000	0.000
F	-0.005	1.432
G	-0.010	2.862
H	-0.015	4.289
I	-0.020	5.711
J	-0.025	7.125
K	-0.030	8.531
L	-0.035	9.926
M	-0.040	11.310
N	-0.045	12.680
O	-0.050	14.036
P	-0.055	15.376
Q	-0.060	16.699
R	-0.065	18.004
S	-0.070	19.290
T	-0.075	20.556
U	-0.080	21.801

C

Information Desired	Information Required
Location of fore and aft wake boundary and wake skew angle relative to a reference point.	Tip path plane advance ratio, inflow ratio, and desired reference locations if needed.

Instructions

Ⓐ With a known lateral reference value (Y/R = .5) the lateral reference guide can be used to determine, by construction, the appropriate lateral reference location Ⓑ on the Z/R axis.

Ⓒ For the desired inflow ratio (λ = -.0283) the indices can be determined which define the fore and aft wake boundary reference lines. (Symbol from col. 1.)

Ⓓ The wake boundary lines can be determined by graphical interpolation for the zero lateral location.

Ⓔ The parallel translation of the graphically obtained wake boundary lines for the fore and aft coordinates is made to the appropriate lateral position Ⓑ .

Ⓕ, Ⓖ The determination of the rocket launch point in the tip path plane is made on the selected graph (X/R = -.05, Z/R = .4), resulting in Ⓗ.

Ⓗ From this determination it is found that the wake has been displaced rearward from the launch point. Since the μ = .23 condition will have the wake displaced further rearward there is no need to use any additional figures for interpolation on advance ratio.

FIGURE 10. EXAMPLE USE OF THE FORE AND AFT WAKE BOUNDARY CHARTS

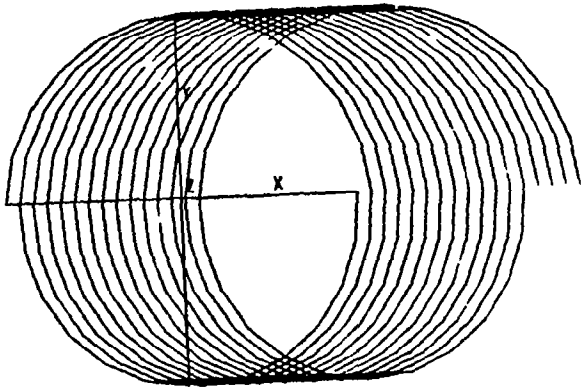

TOP VIEW

NUMBER OF BLADES = 4
CT = 0.005
ALPHA = -2.0
MU = 0.05
Ψ_B = 0.0

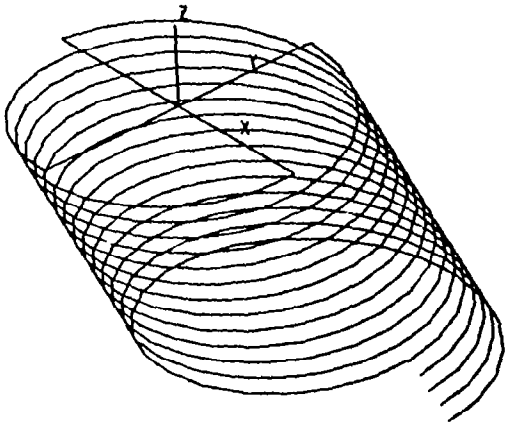

ISOMETRIC VIEW

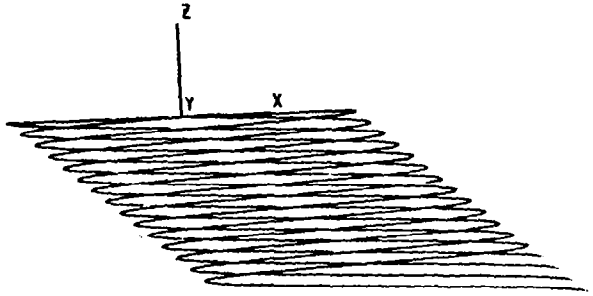

SIDE VIEW

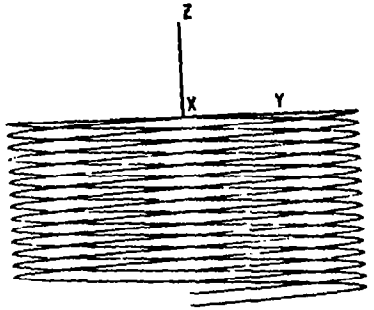

REAR VIEW

FIGURE 11A. PROJECTION AND ISOMETRIC VIEWS OF UNDISTORTED TIP VORTEX, VARYING ADVANCE RATIO ($V/\Omega R$ = .05)

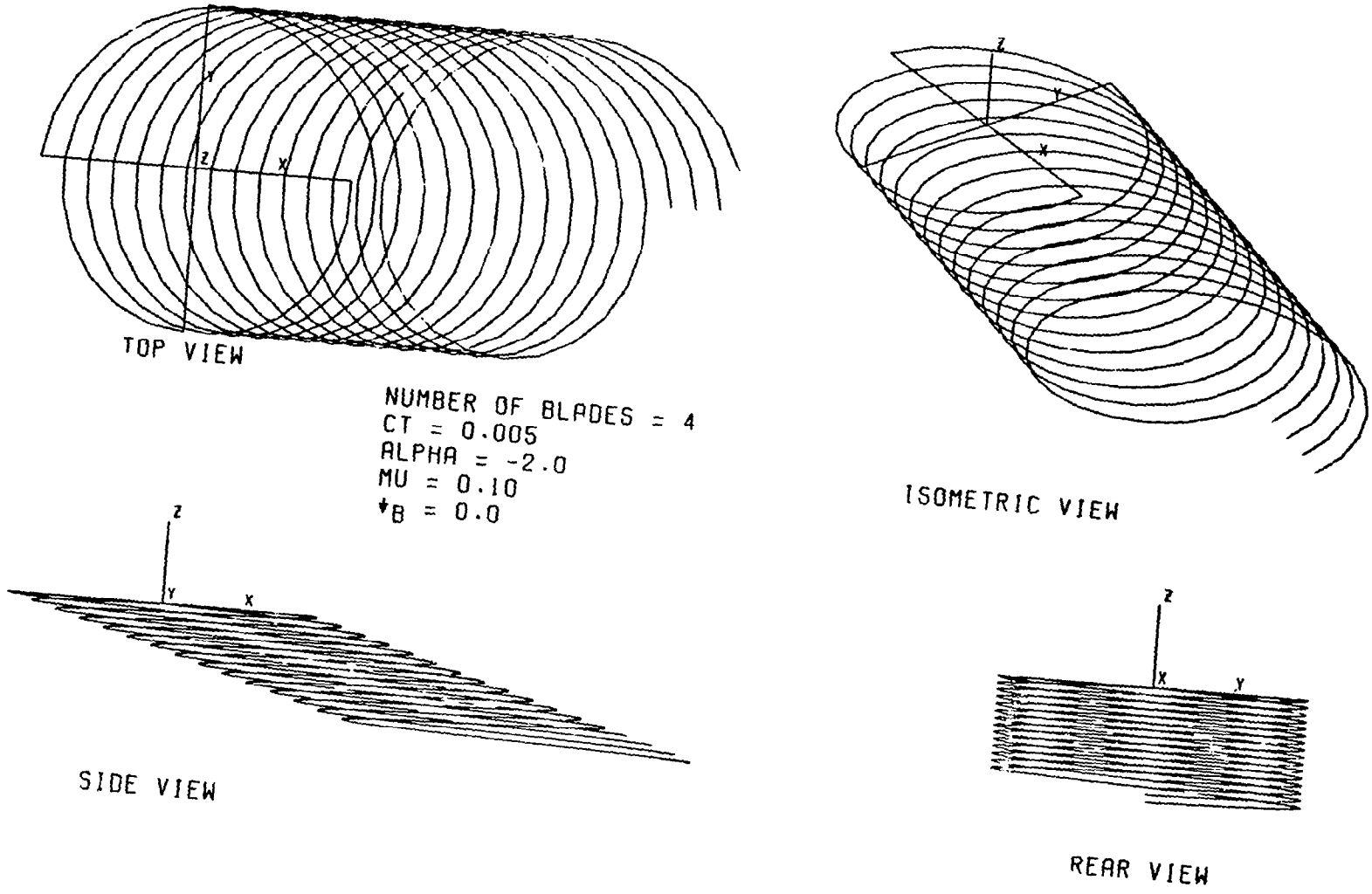

FIGURE 11B. PROJECTION AND ISOMETRIC VIEWS OF UNDISTORTED TIP VORTEX, VARYING ADVANCE RATIO ($V/\Omega R$ = .10)

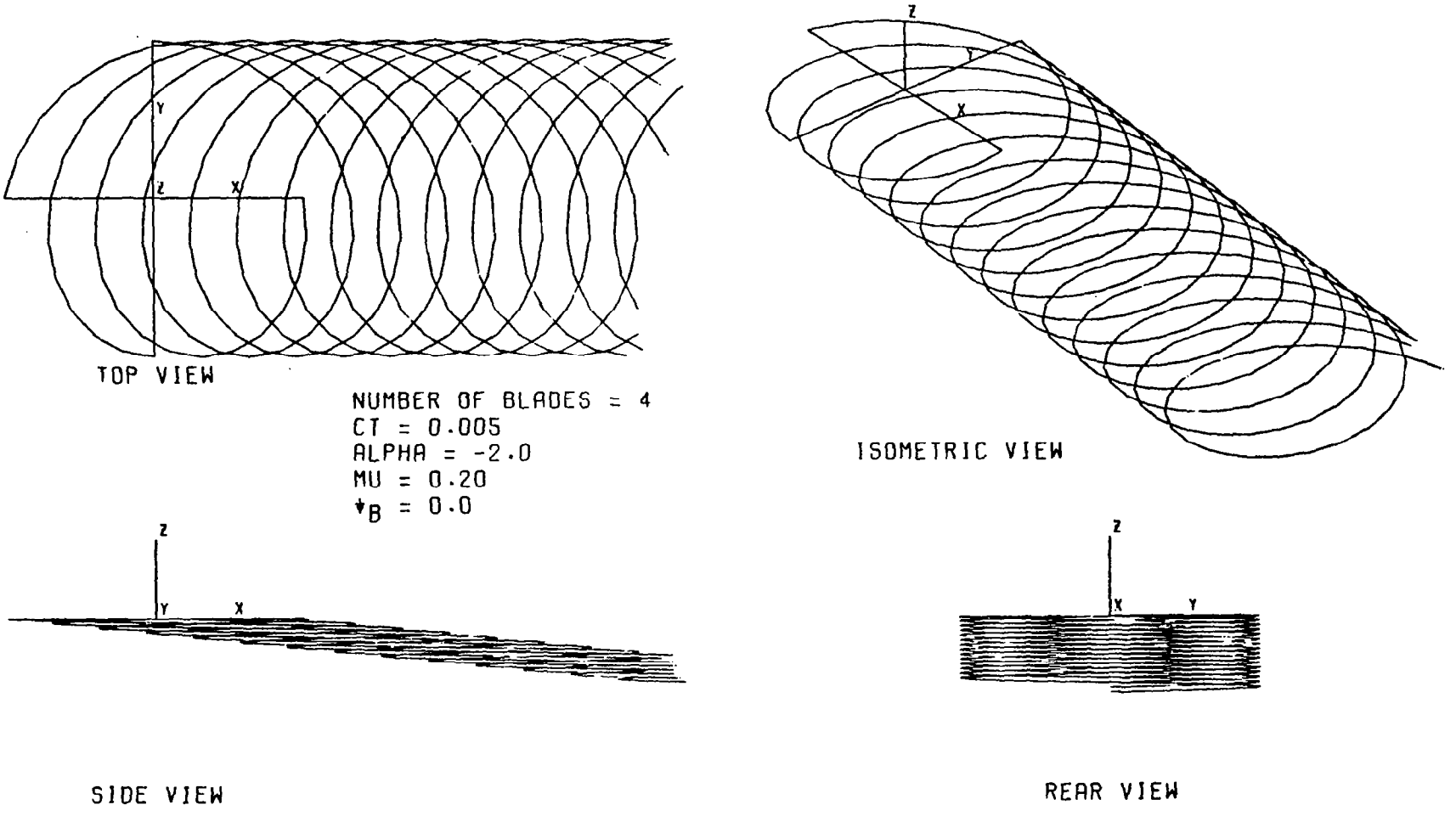

FIGURE 11C. PROJECTION AND ISOMETRIC VIEWS OF UNDISTORTED TIP VORTEX, VARYING ADVANCE RATIO ($V/\Omega R$ = .20)

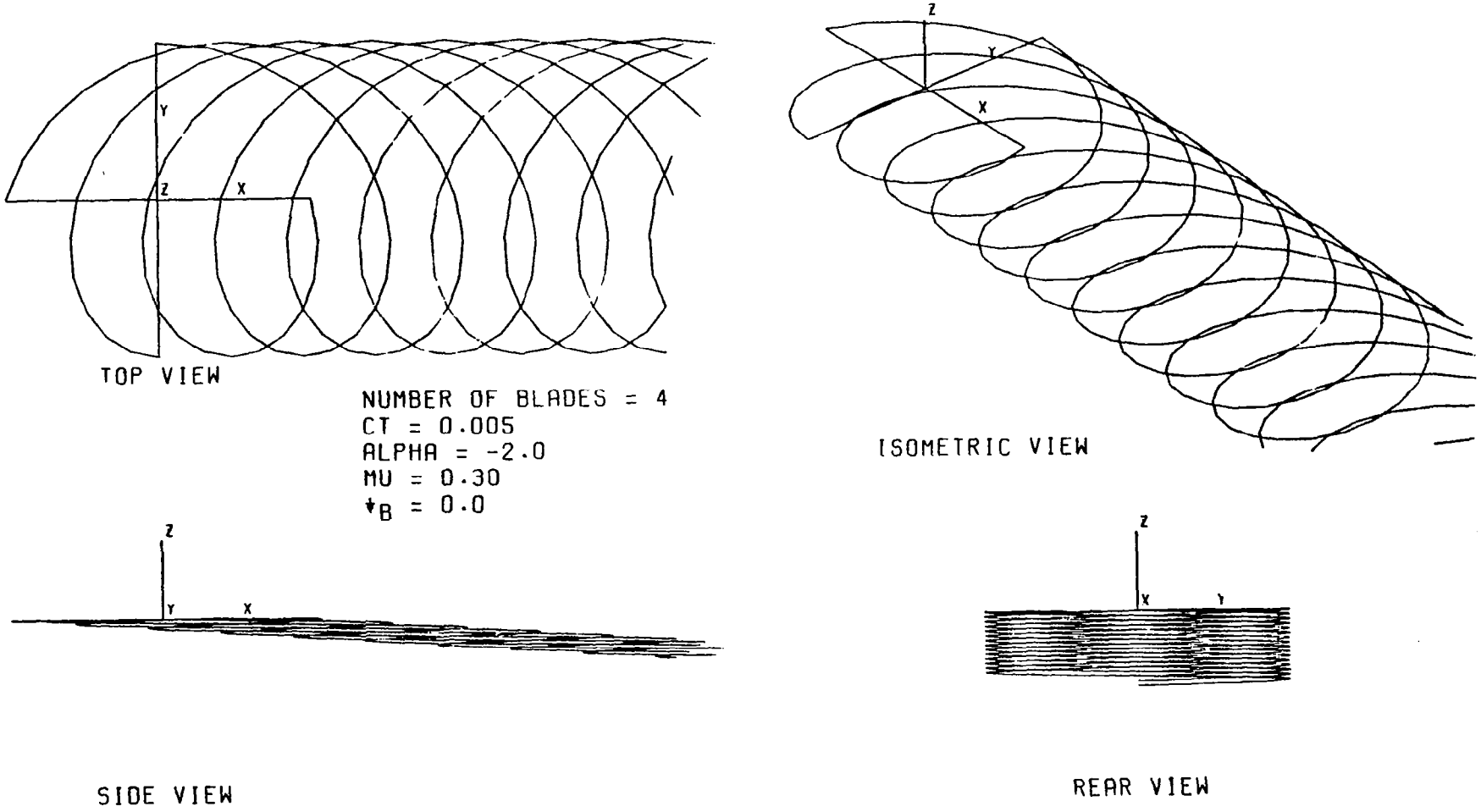

FIGURE 11D. PROJECTION AND ISOMETRIC VIEWS OF UNDISTORTED TIP VORTEX, VARYING ADVANCE RATIO ($V/\Omega R$ = .30)

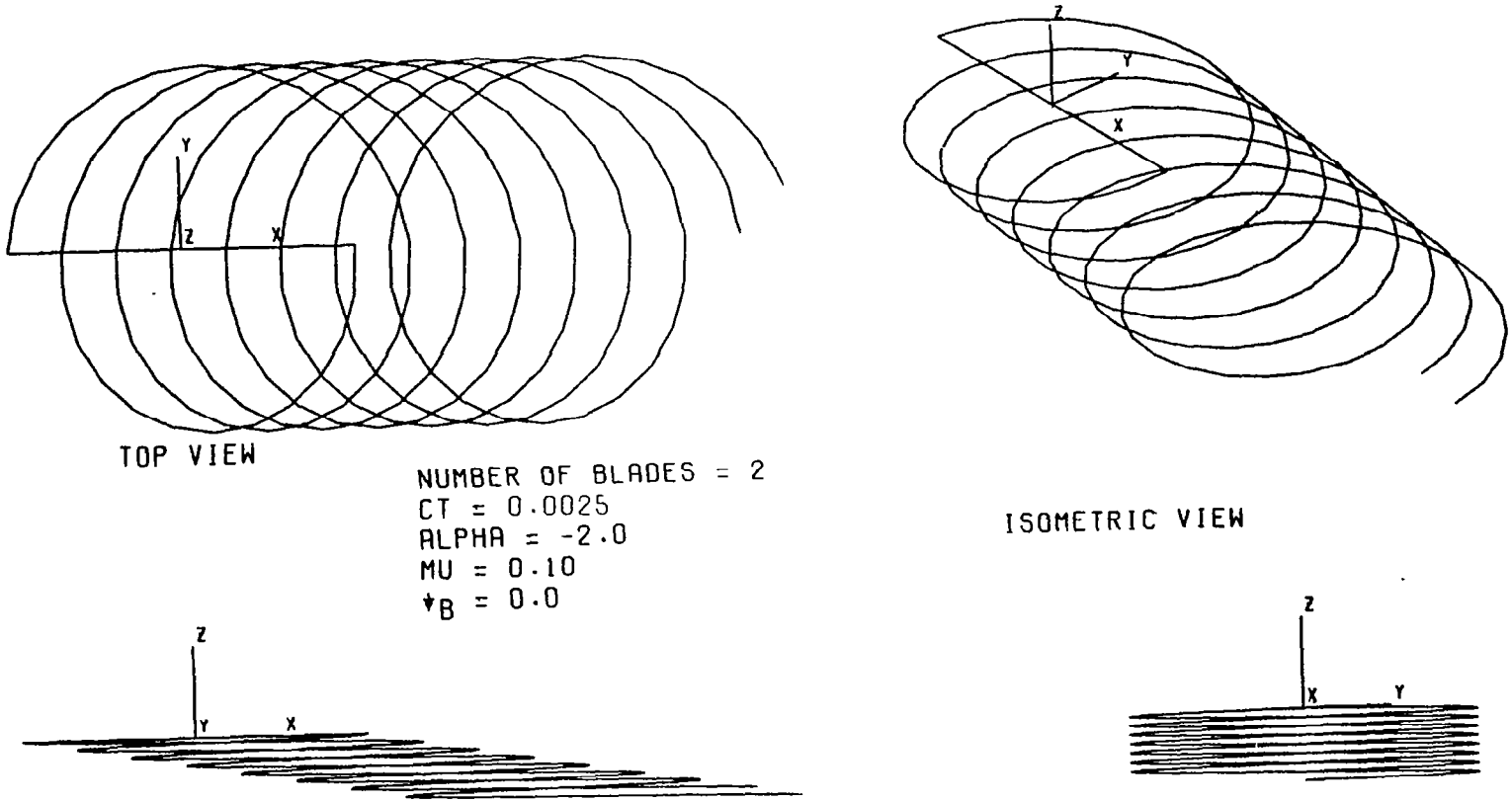

FIGURE 12A. PROJECTION AND ISOMETRIC VIEWS OF UNDISTORTED TIP VORTEX, VARYING THRUST LEVEL (C_T = .0025)

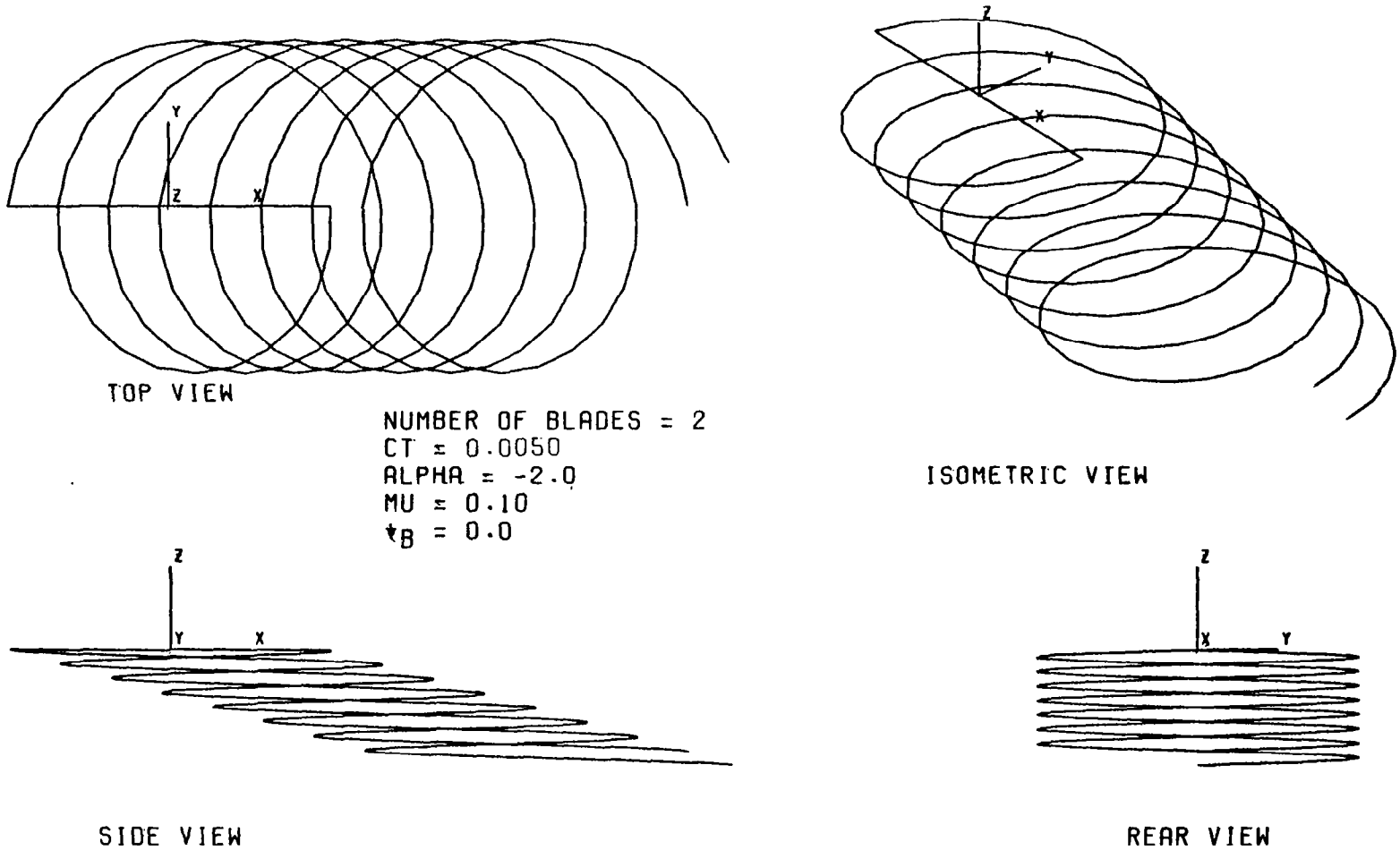

FIGURE 12B. PROJECTION AND ISOMETRIC VIEWS OF UNDISTORTED TIP VORTEX, VARYING THRUST LEVEL (C_T = .0050)

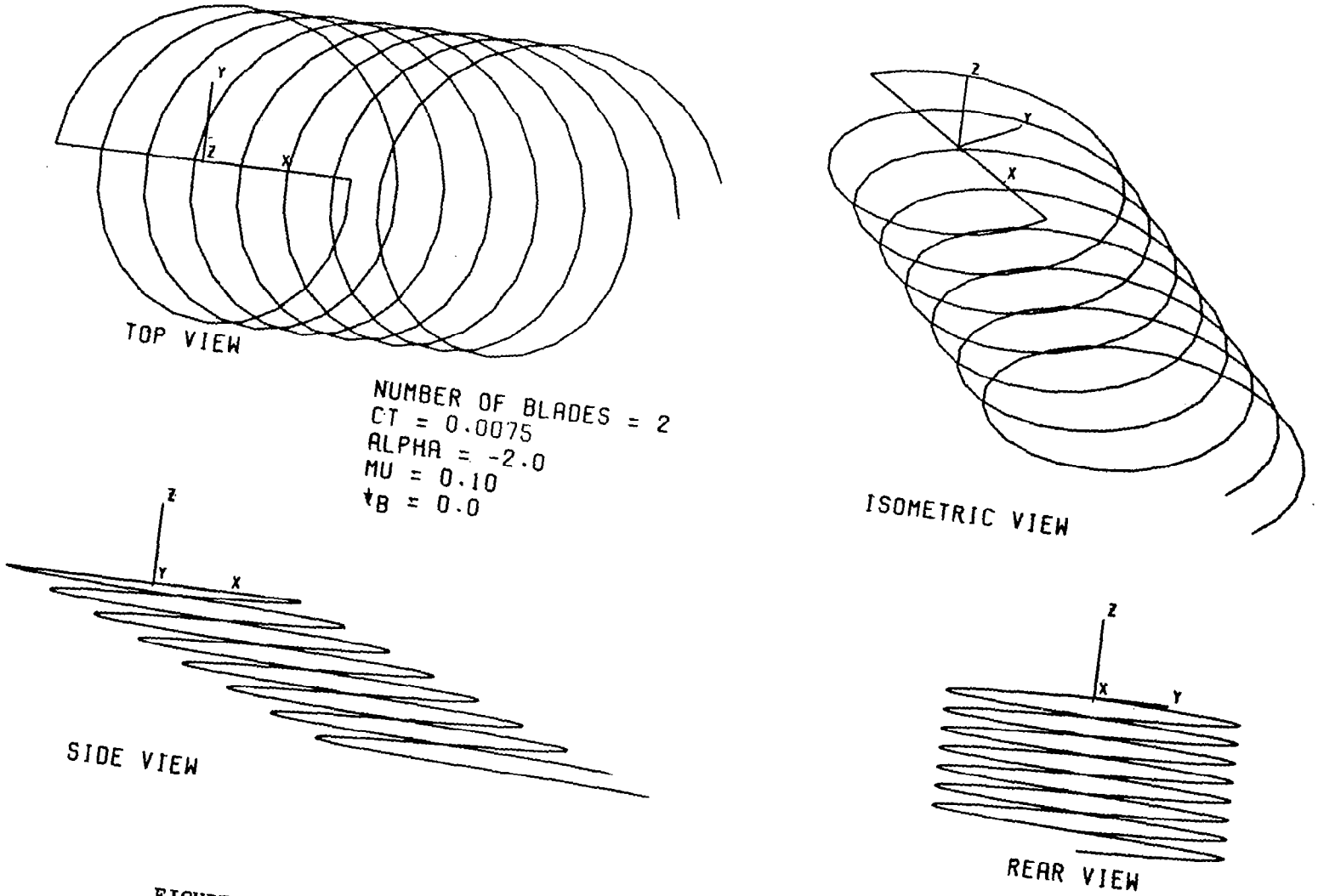

FIGURE 12c. PROJECTION AND ISOMETRIC VIEWS OF UNDISTORTED TIP VORTEX, VARYING THRUST LEVEL (C_T = .0075)

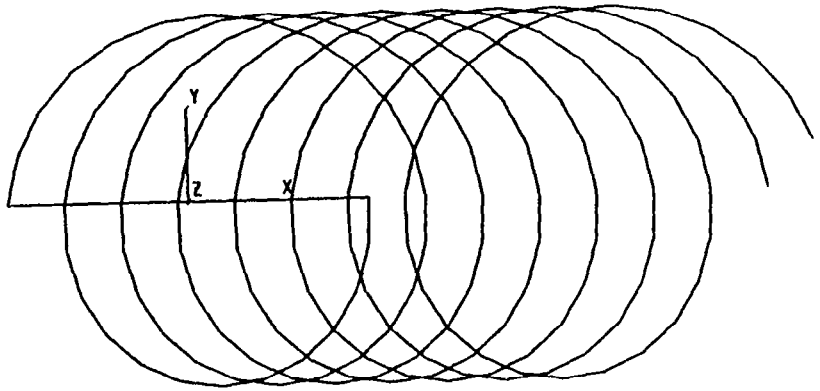

TOP VIEW

NUMBER OF BLADES = 2
CT = 0.005
ALPHA = 0.0
MU = 0.10
Ψ_B = 0.0

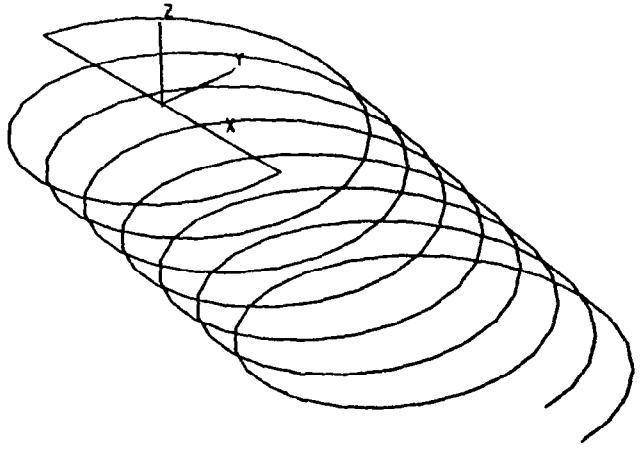

ISOMETRIC VIEW

SIDE VIEW

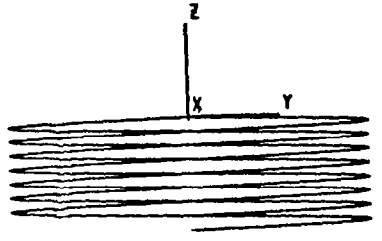

REAR VIEW

FIGURE 13A. PROJECTION AND ISOMETRIC VIEWS OF UNDISTORTED TIP VORTEX, VARYING TIP PATH PLANE ALTITUDE (α = 0.0)

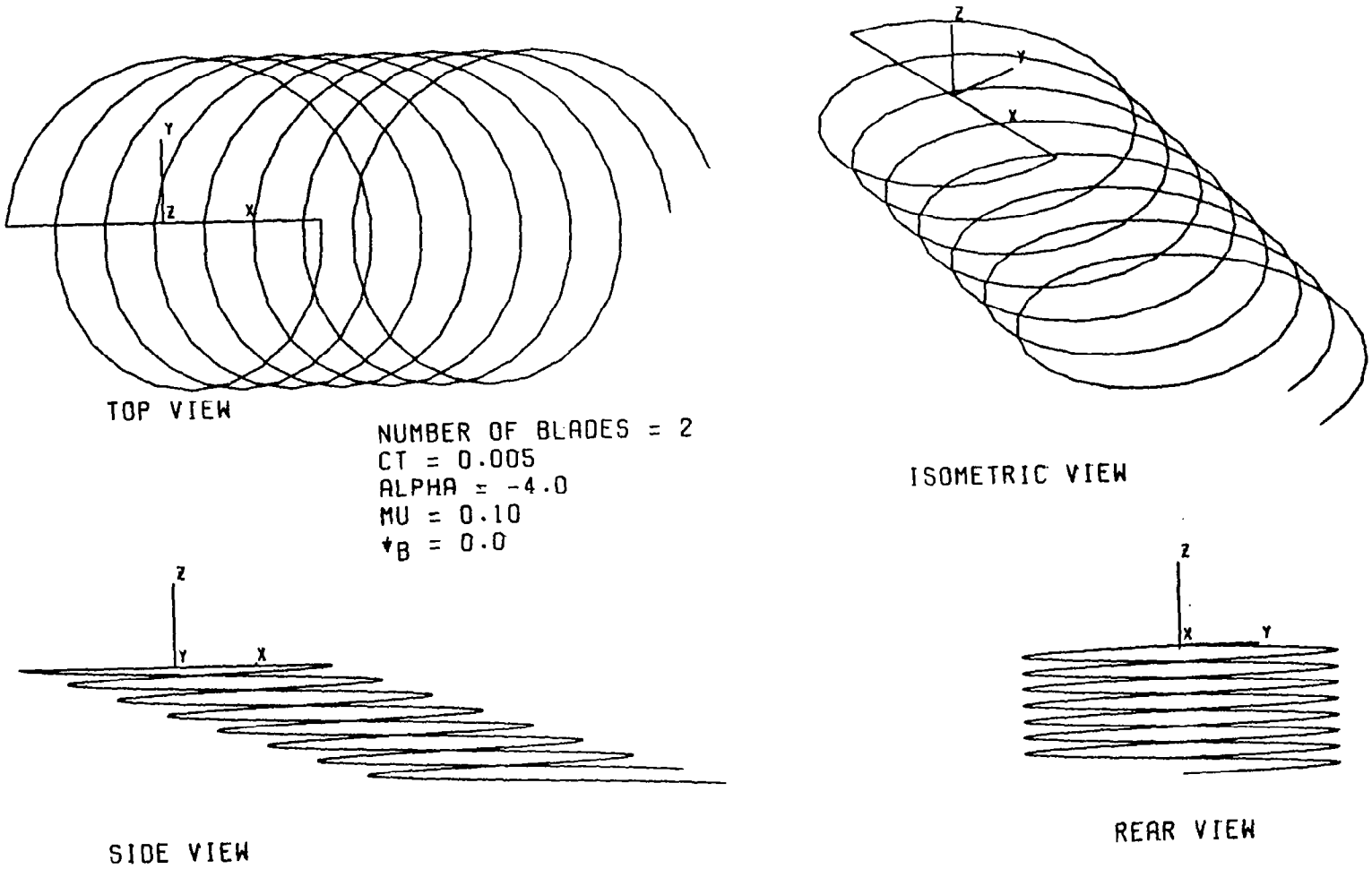

FIGURE 13B. PROJECTION AND ISOMETRIC VIEWS OF UNDISTORTED TIP VORTEX, VARYING TIP PATH PLANE ALTITUDE (α = -4.0)

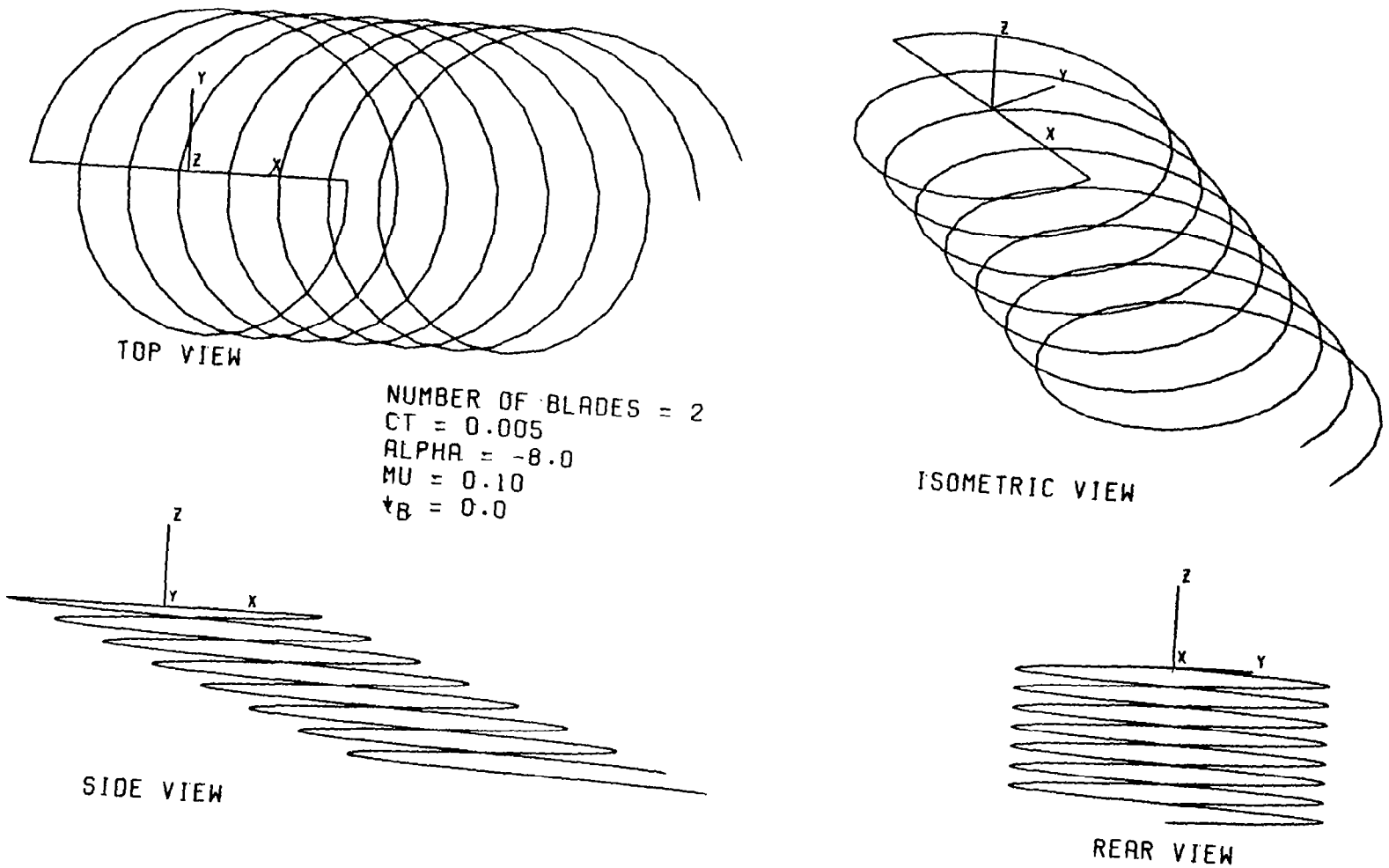

FIGURE 13C. PROJECTION AND ISOMETRIC VIEWS OF UNDISTORTED TIP VORTEX, VARYING TIP PATH PLANE ALTITUDE (α = -8.0)

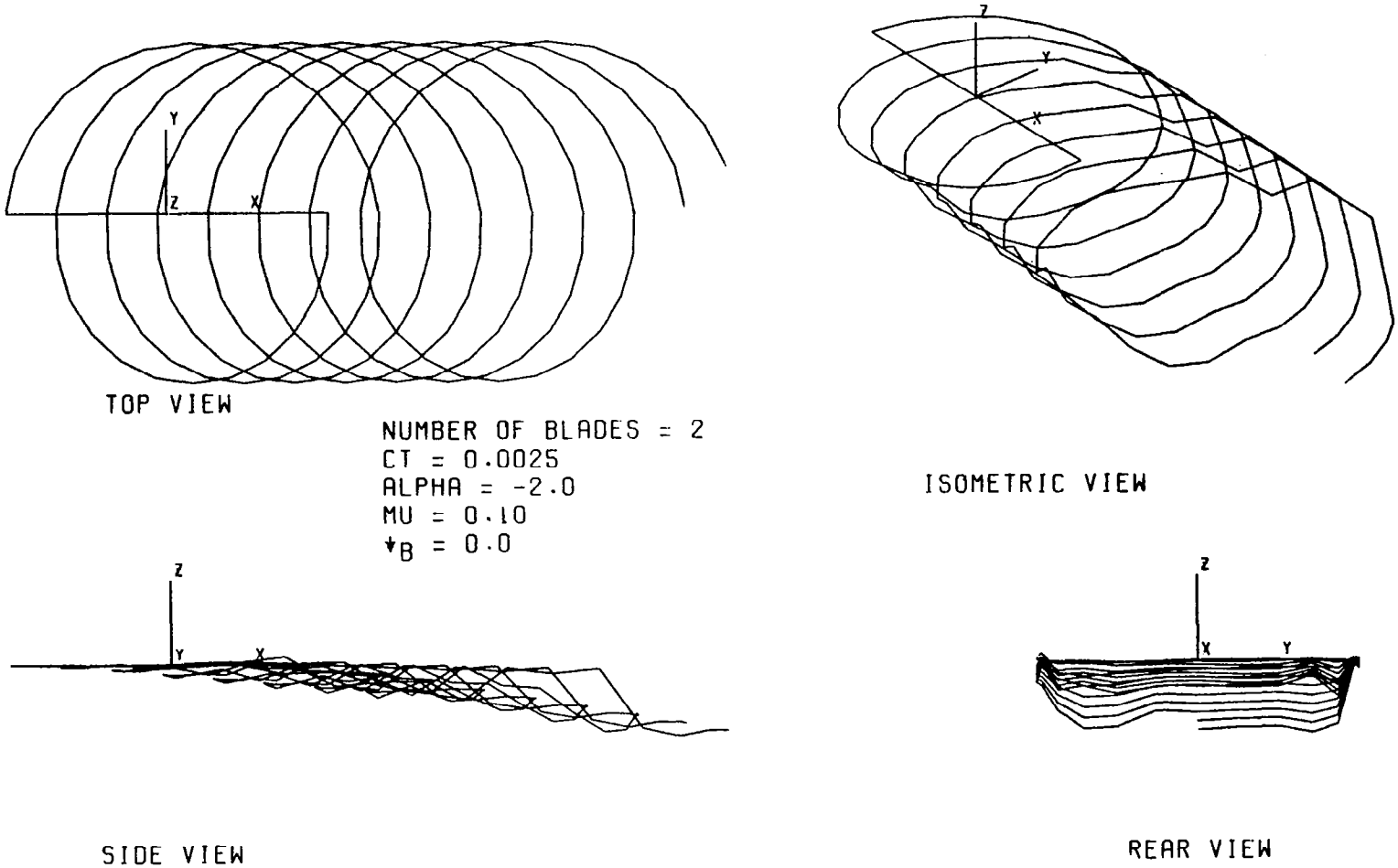

FIGURE 14A. PROJECTION AND ISOMETRIC VIEWS FOR GENERALIZED DISTORTED TIP VORTEX, VARYING THRUST LEVEL (C_T = .0025)

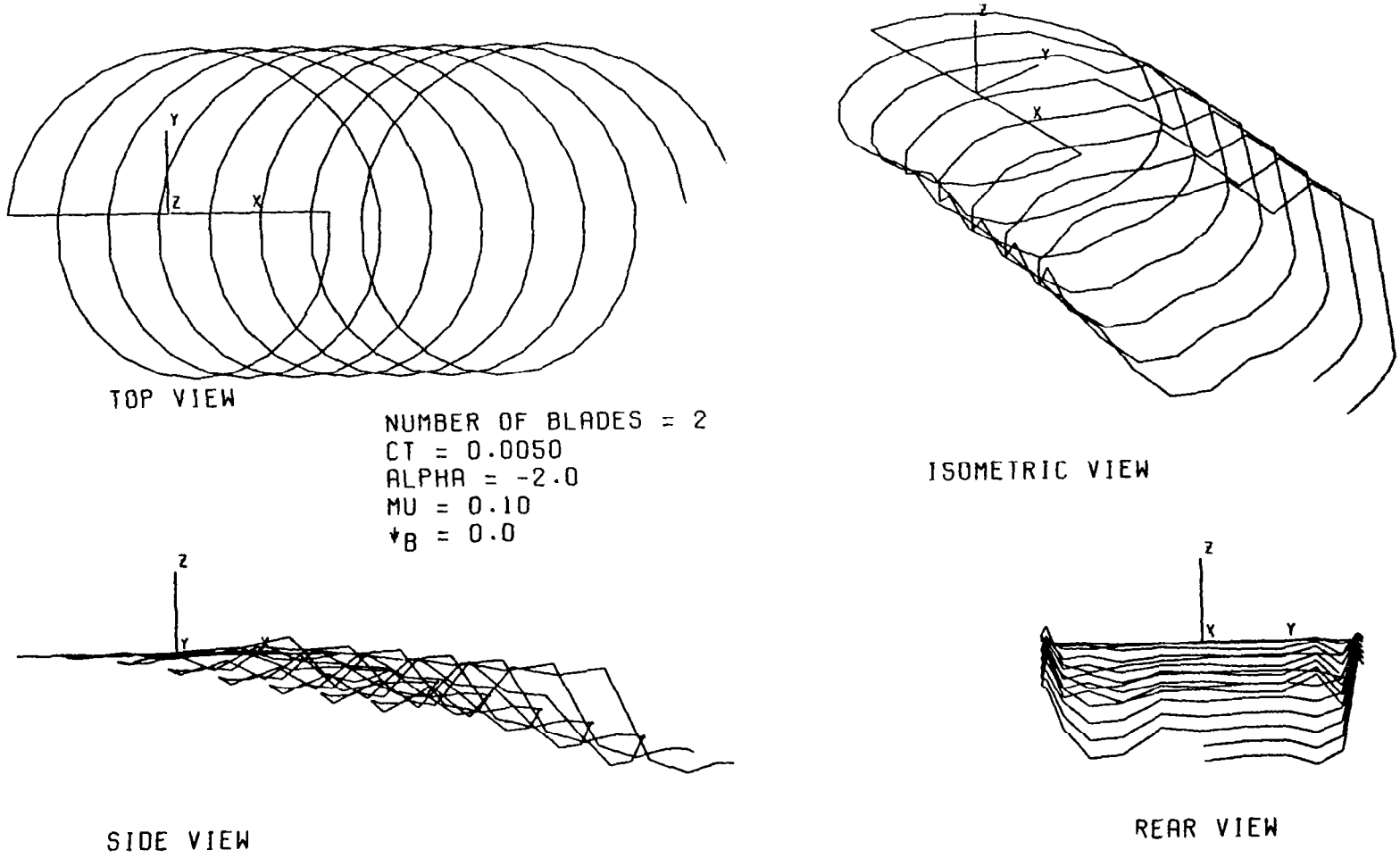

FIGURE 14B. PROJECTION AND ISOMETRIC VIEWS FOR GENERALIZED DISTORTED TIP VORTEX, VARYING THRUST LEVEL (C_T = .0050)

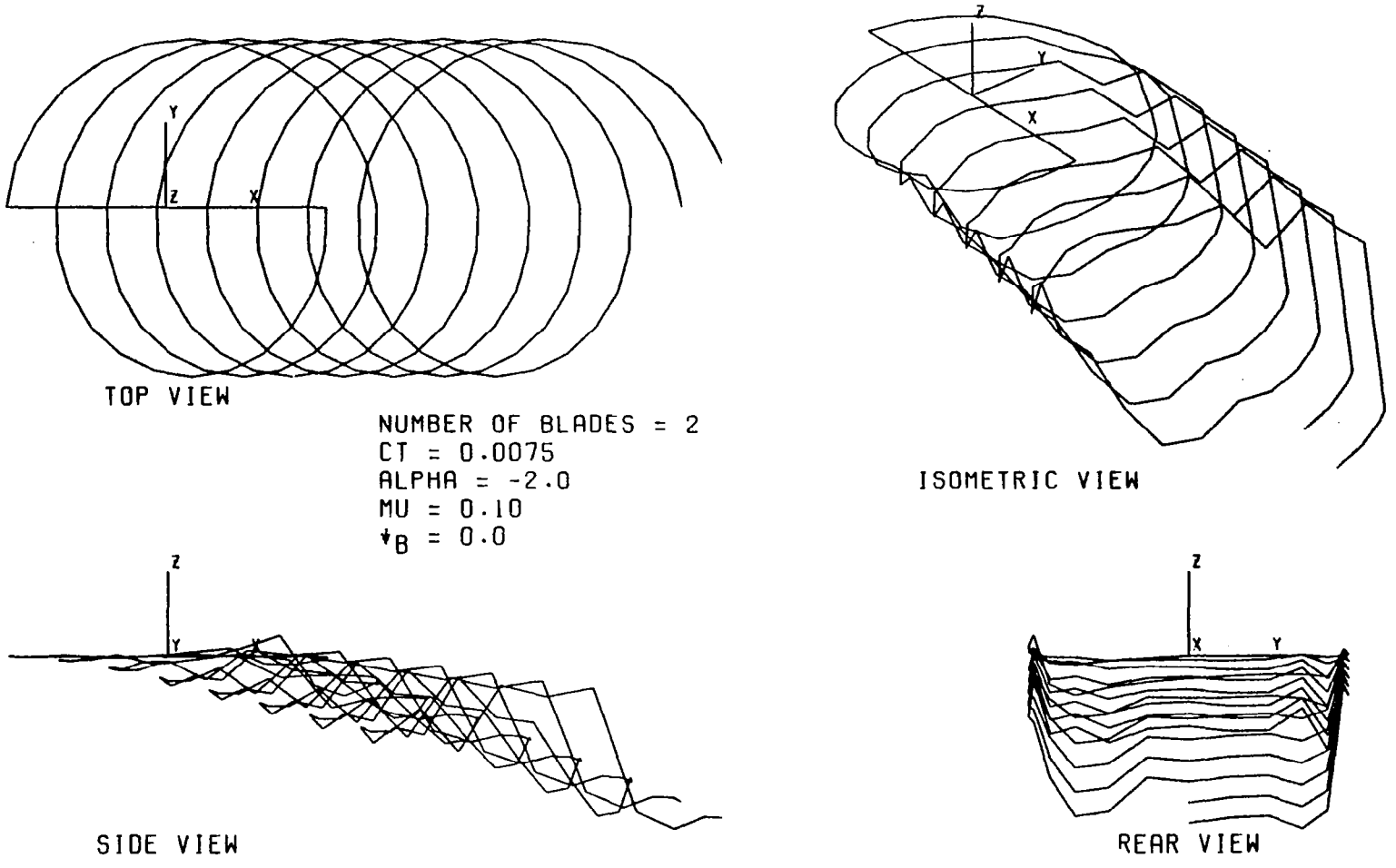

FIGURE 14C. PROJECTION AND ISOMETRIC VIEWS FOR GENERALIZED DISTORTED TIP VORTEX, VARYING THRUST LEVEL (C_T = .0075)

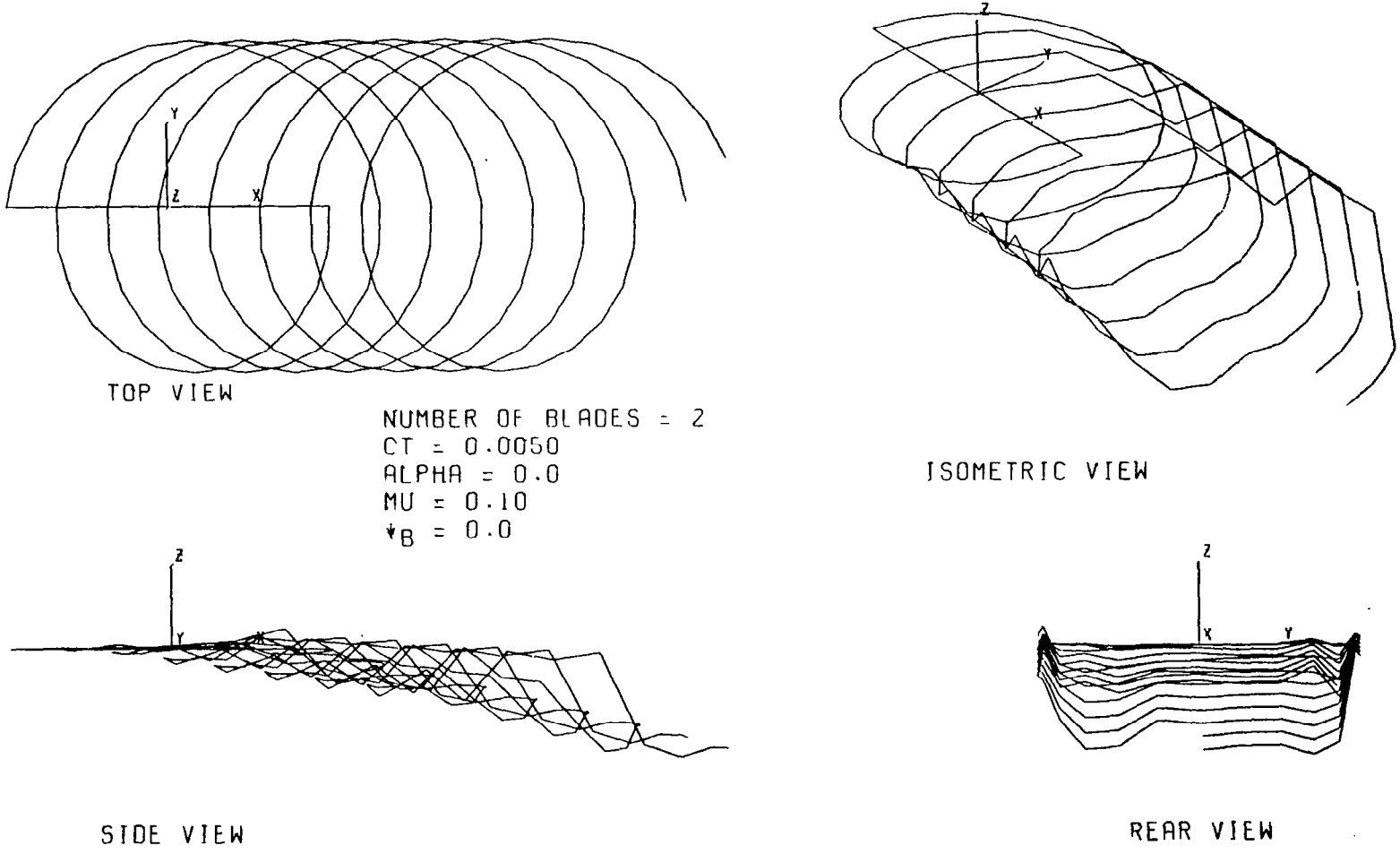

FIGURE 15A. PROJECTION AND ISOMETRIC VIEWS FOR GENERALIZED DISTORTED TIP VORTEX, VARYING TIP PATH PLANE ALTITUDE (α = 0.0)

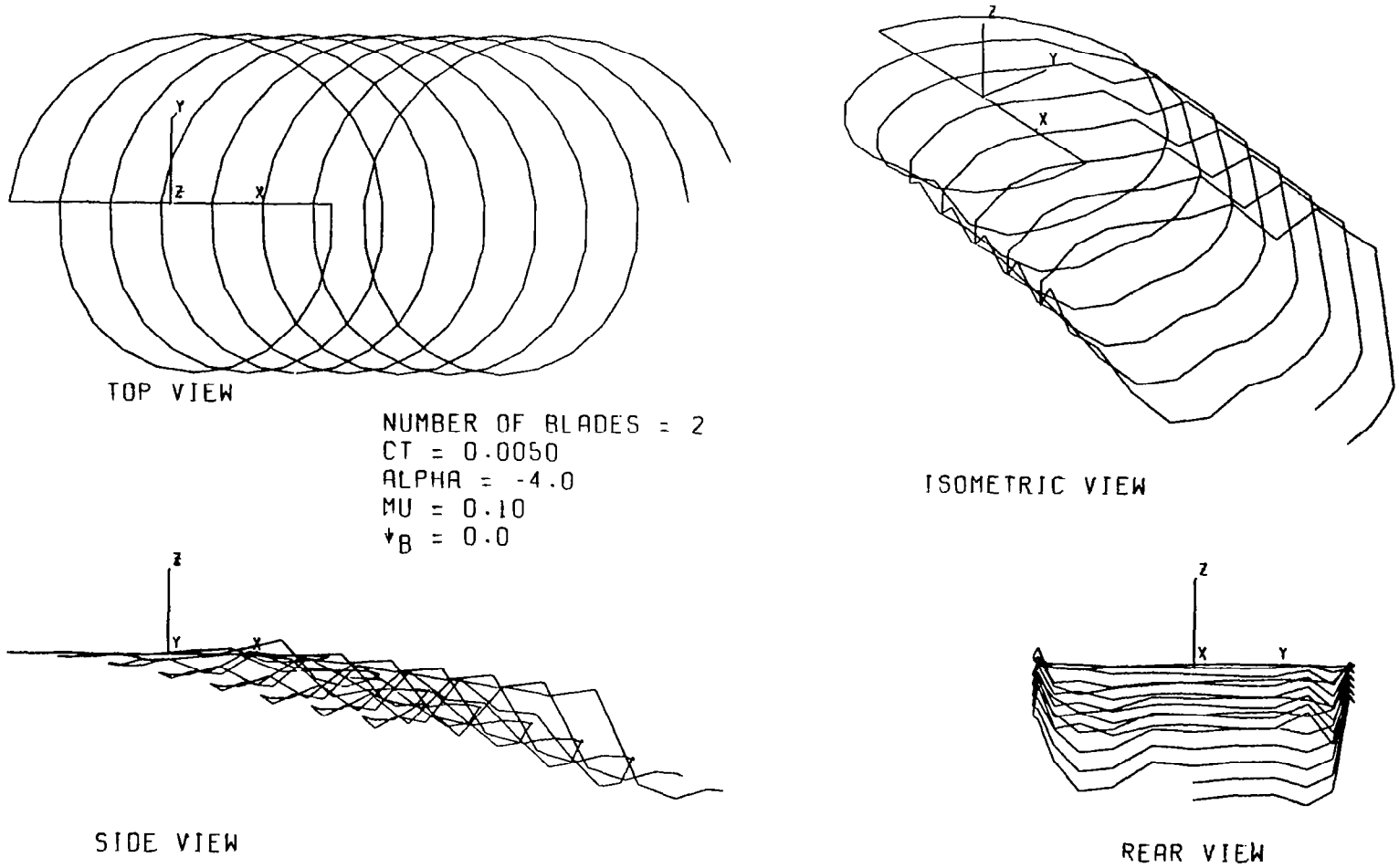

FIGURE 15B. PROJECTION AND ISOMETRIC VIEWS FOR GENERALIZED DISTORTED TIP VORTEX, VARYING TIP PATH PLANE ALTITUDE (α = -4.0)

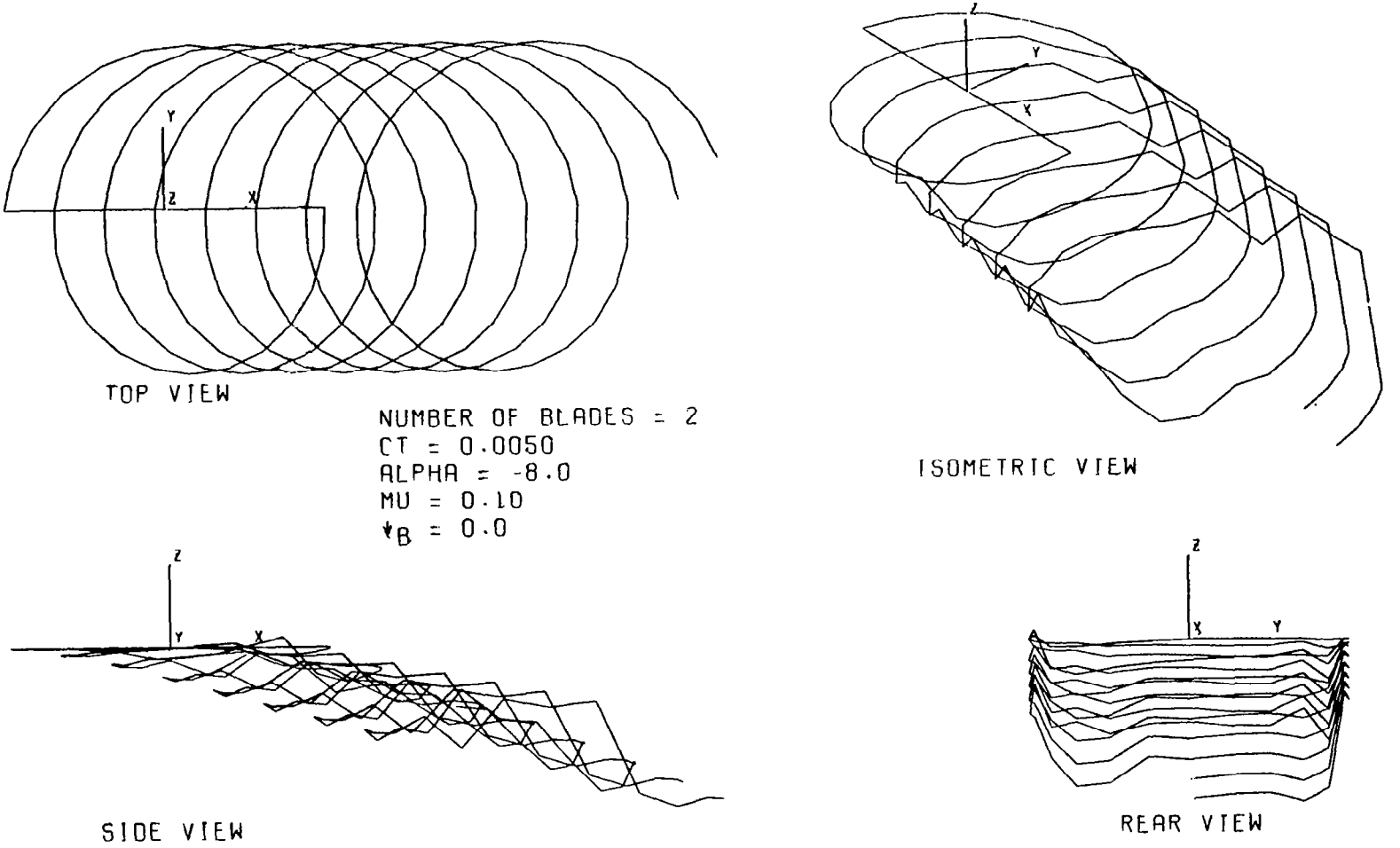

FIGURE 15C. PROJECTION AND ISOMETRIC VIEWS FOR GENERALIZED DISTORTED TIP VORTEX, VARYING TIP PATH PLANE ALTITUDE (α = -8.0)

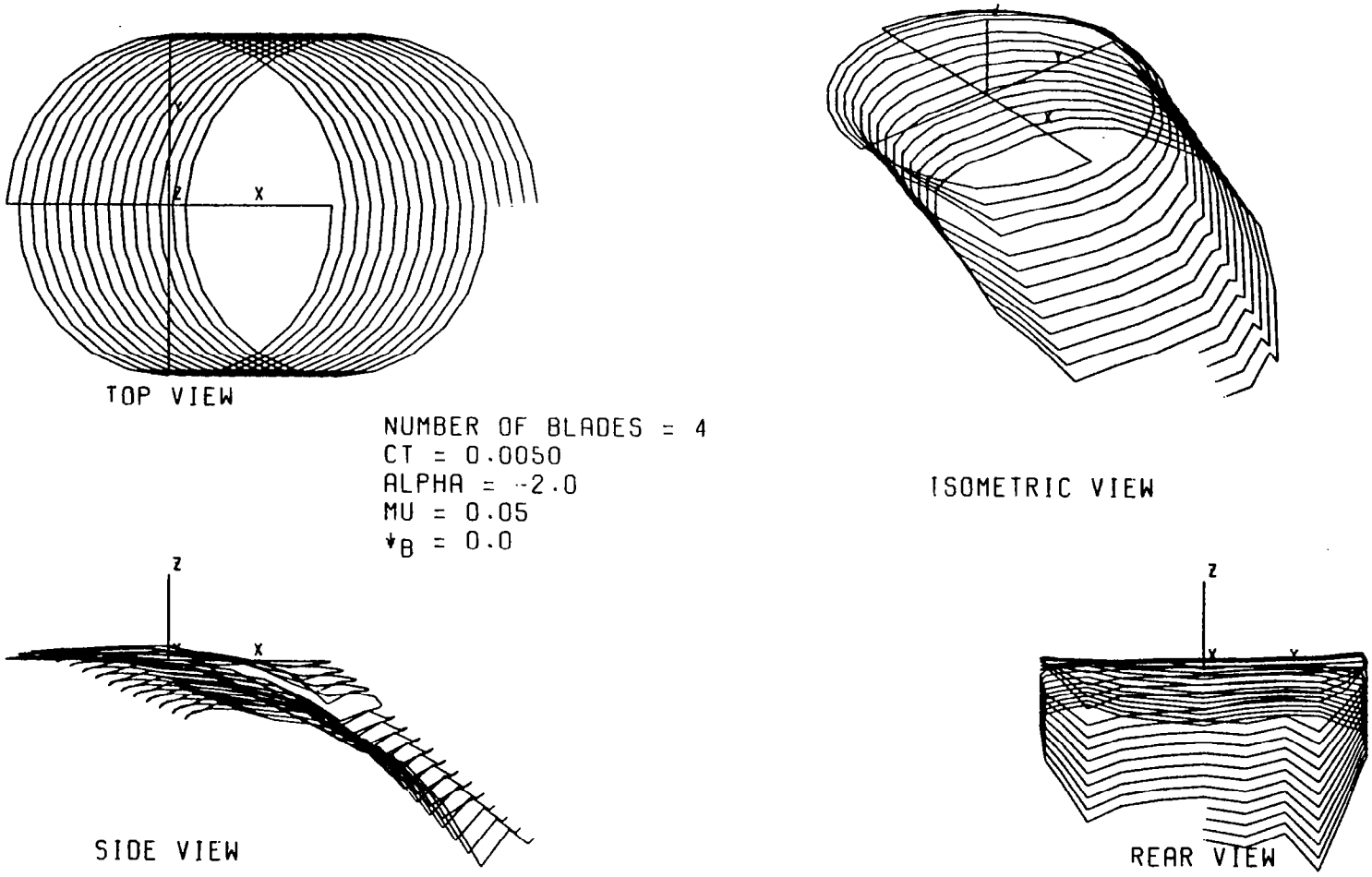

FIGURE 16A. PROJECTION AND ISOMETRIC VIEWS FOR GENERALIZED DISTORTED TIP VORTEX, VARYING ADVANCE RATIO ($V/\Omega R$ = .05)

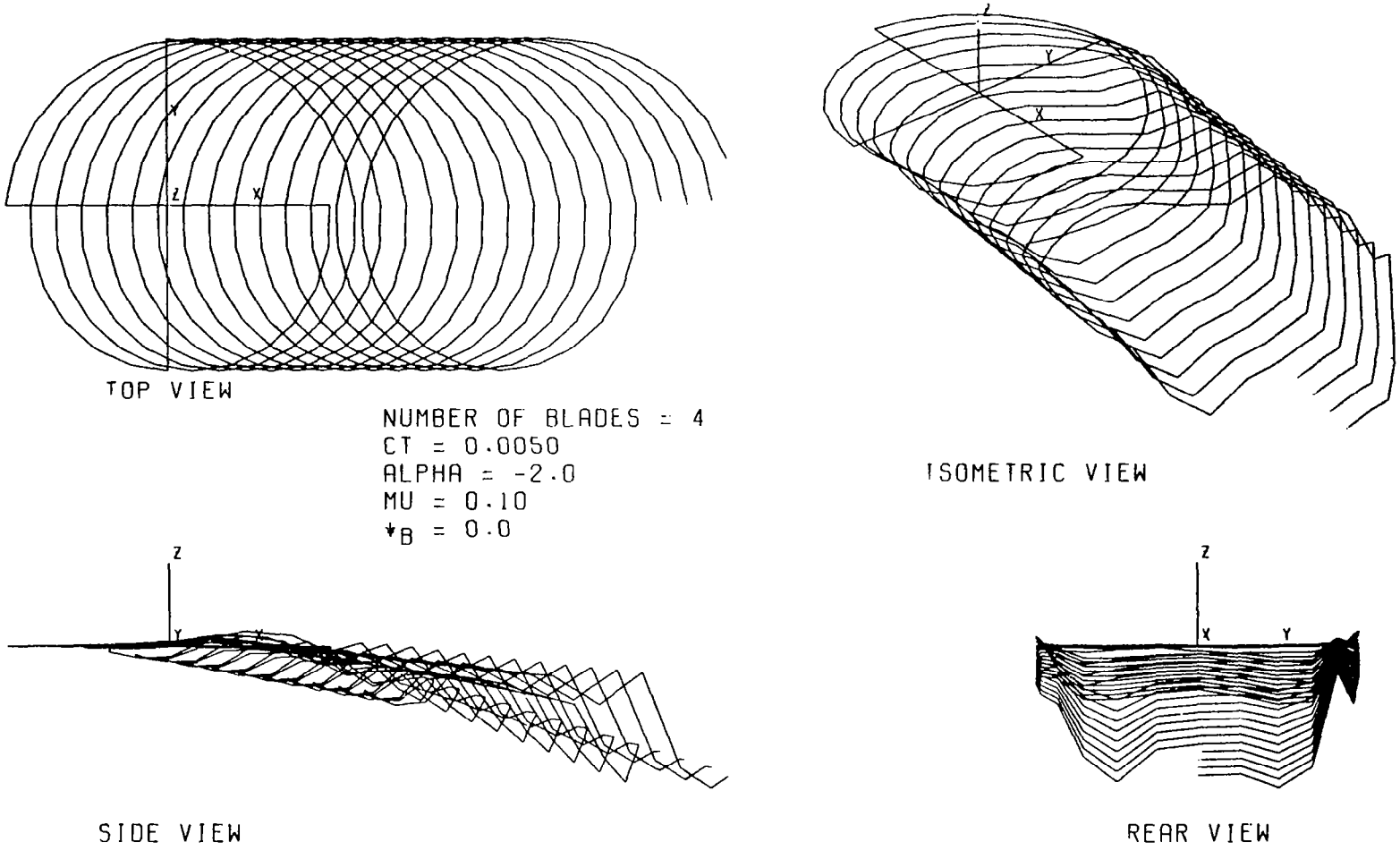

FIGURE 16B. PROJECTION AND ISOMETRIC VIEWS FOR GENERALIZED DISTORTED TIP VORTEX, VARYING ADVANCE RATIO ($V/\Omega R$ = .10)

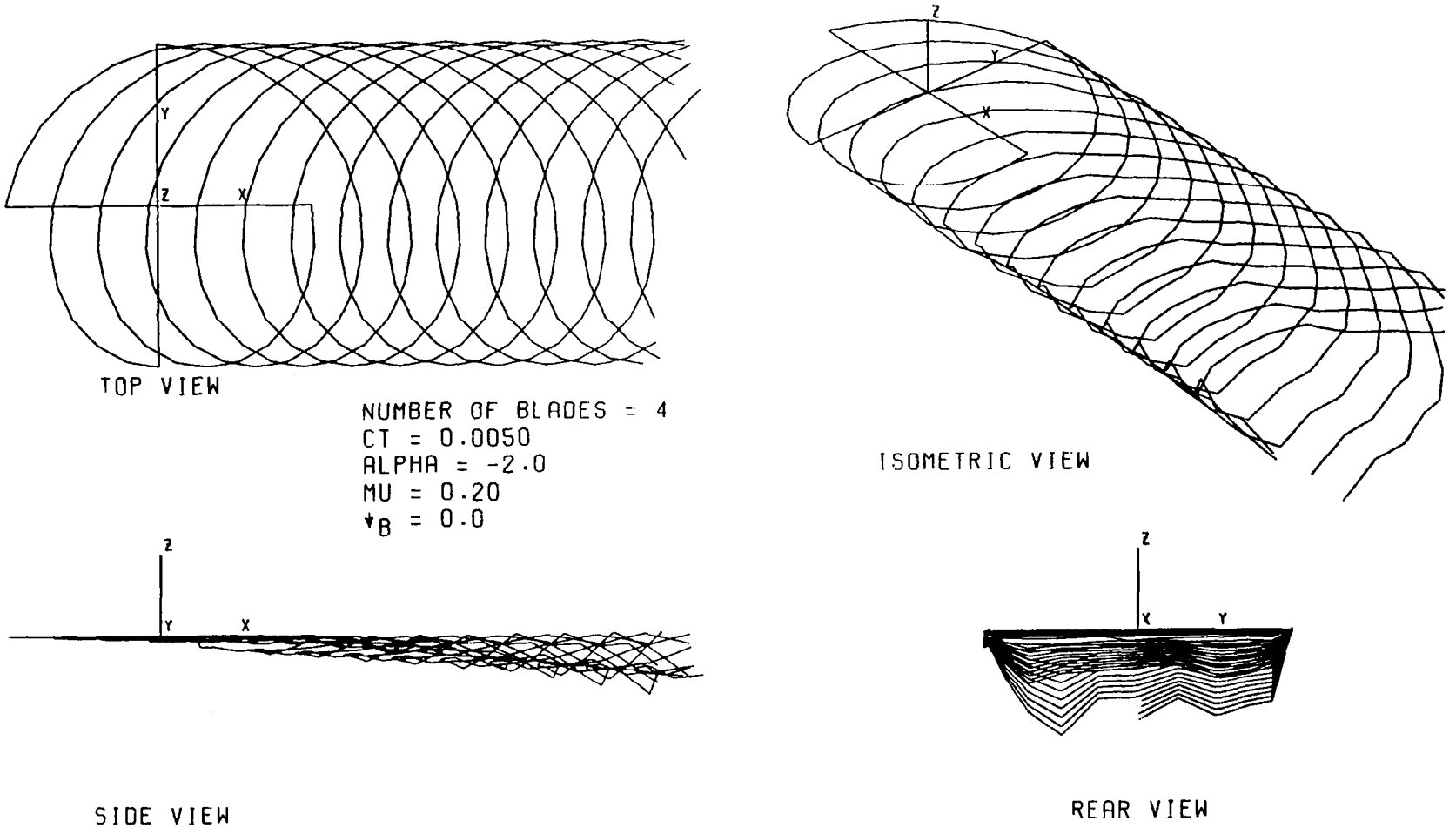

FIGURE 16C. PROJECTION AND ISOMETRIC VIEWS FOR GENERALIZED DISTORTED TIP VORTEX, VARYING ADVANCE RATIO ($V/\Omega R$ = .20)

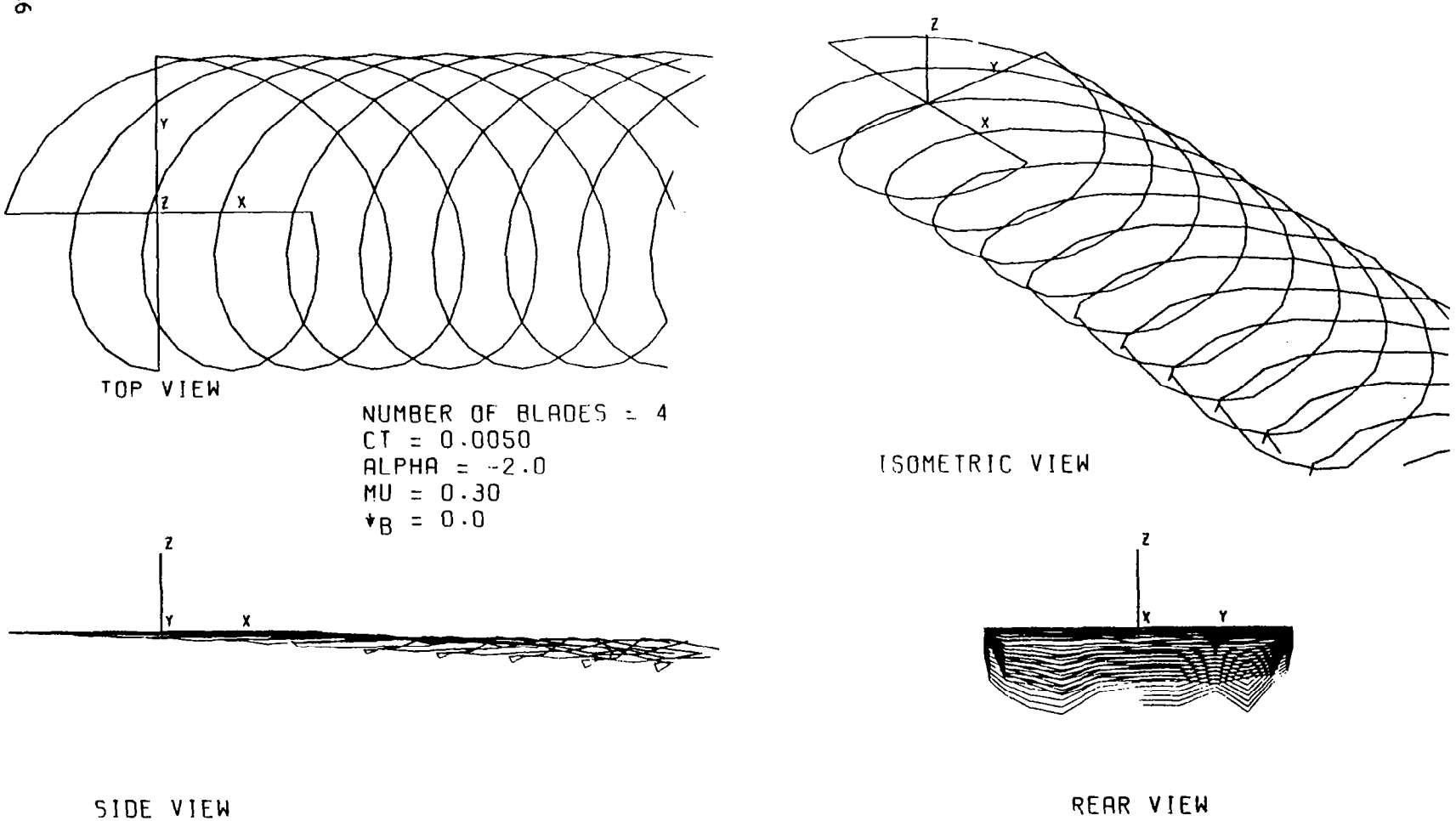

FIGURE 16D. PROJECTION AND ISOMETRIC VIEWS FOR GENERALIZED DISTORTED TIP VORTEX, VARYING ADVANCE RATIO (V/ΩR = .30)

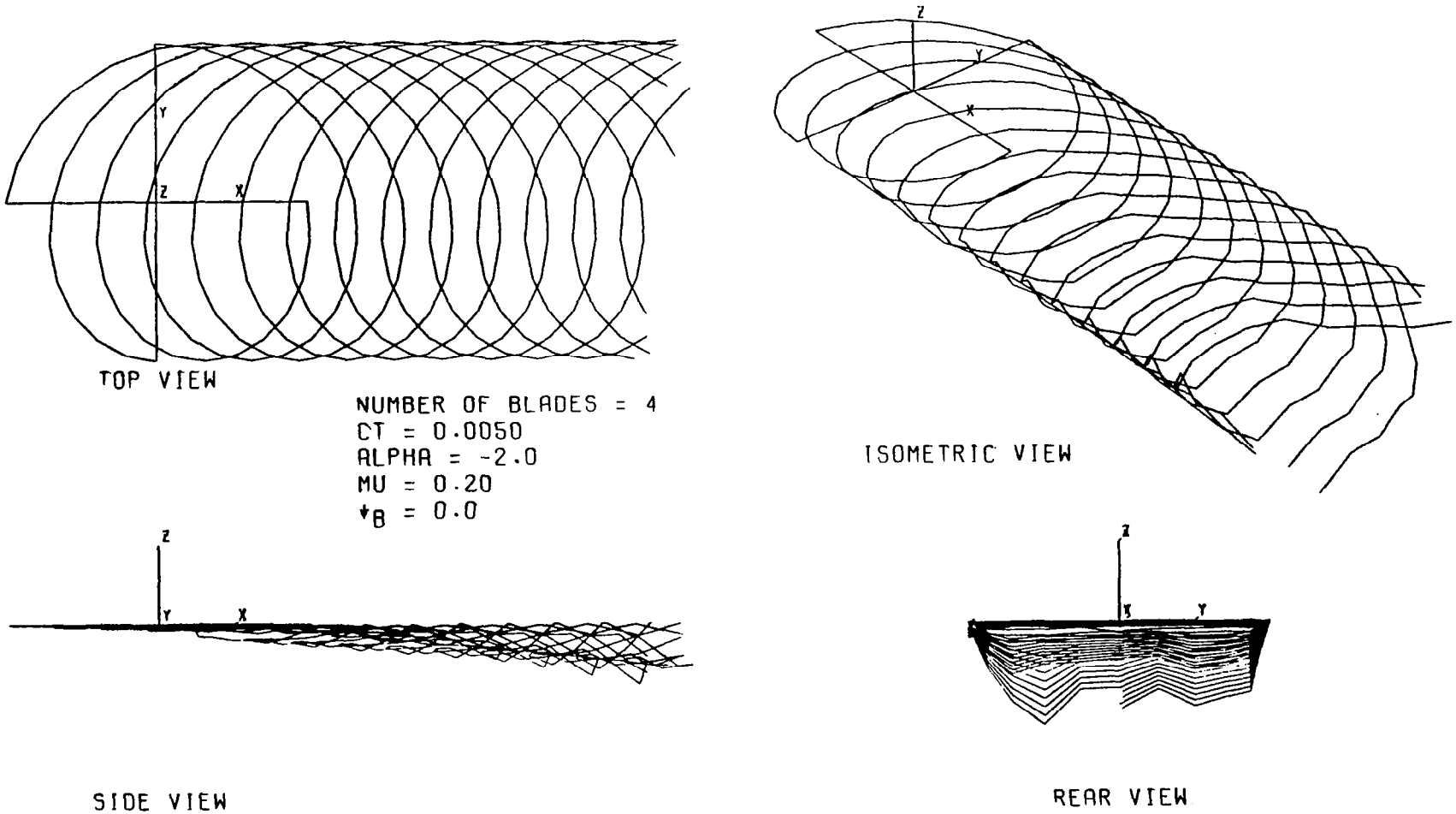

FIGURE 17A. PROJECTION AND ISOMETRIC VIEWS FOR GENERALIZED DISTORTED TIP VORTEX, VARYING BLADE AZIMUTH POSITION (ψ_B = 0.0)

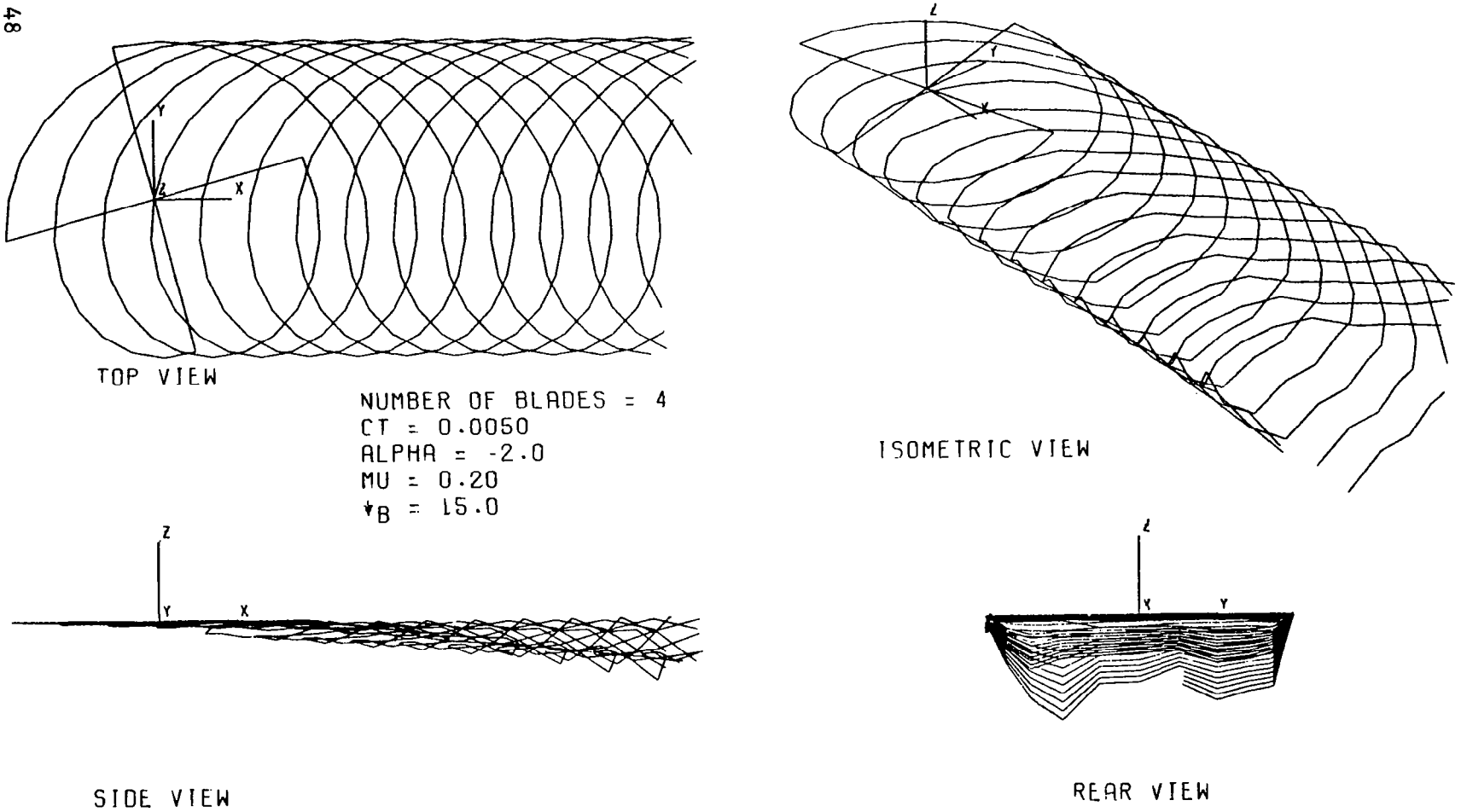

FIGURE 17B. PROJECTION AND ISOMETRIC VIEWS FOR GENERALIZED DISTORTED TIP VORTEX, VARYING BLADE AZIMUTH POSITION (ψ_B = 15.0)

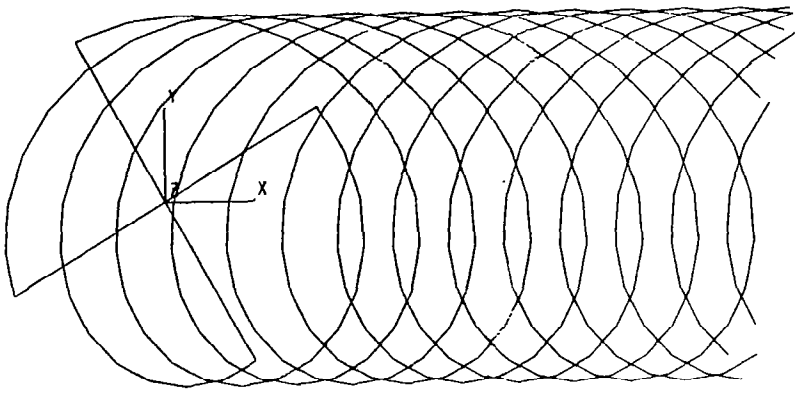

TOP VIEW

NUMBER OF BLADES = 4
CT = 0.0050
ALPHA = -2.0
MU = 0.20
Ψ_B = 30.0

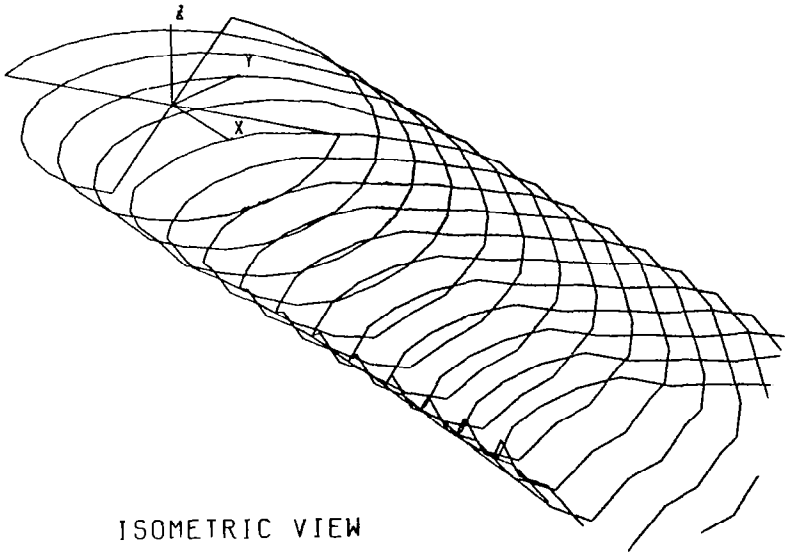

ISOMETRIC VIEW

SIDE VIEW

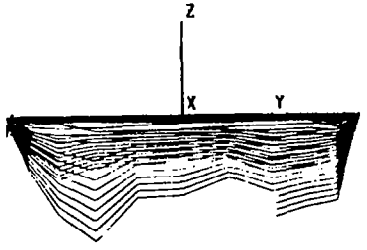

REAR VIEW

FIGURE 17C. PROJECTION AND ISOMETRIC VIEWS FOR GENERALIZED DISTORTED TIP VORTEX, VARYING BLADE AZIMUTH POSITION (ψ_B = 30.0)

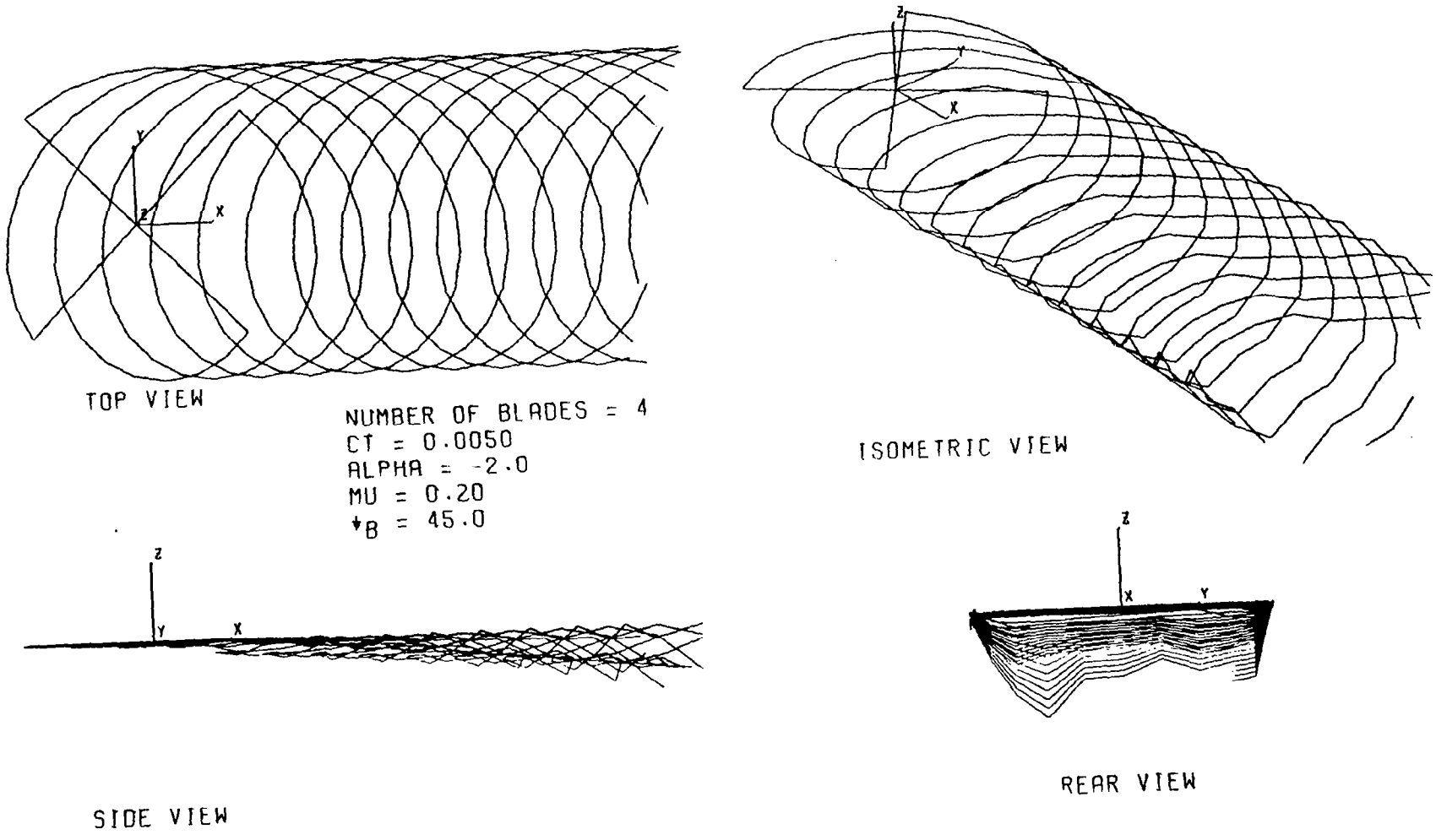

FIGURE 17D. PROJECTION AND ISOMETRIC VIEWS FOR GENERALIZED DISTORTED TIP VORTEX, VARYING BLADE AZIMUTH POSITION (ψ_B = 45.0)

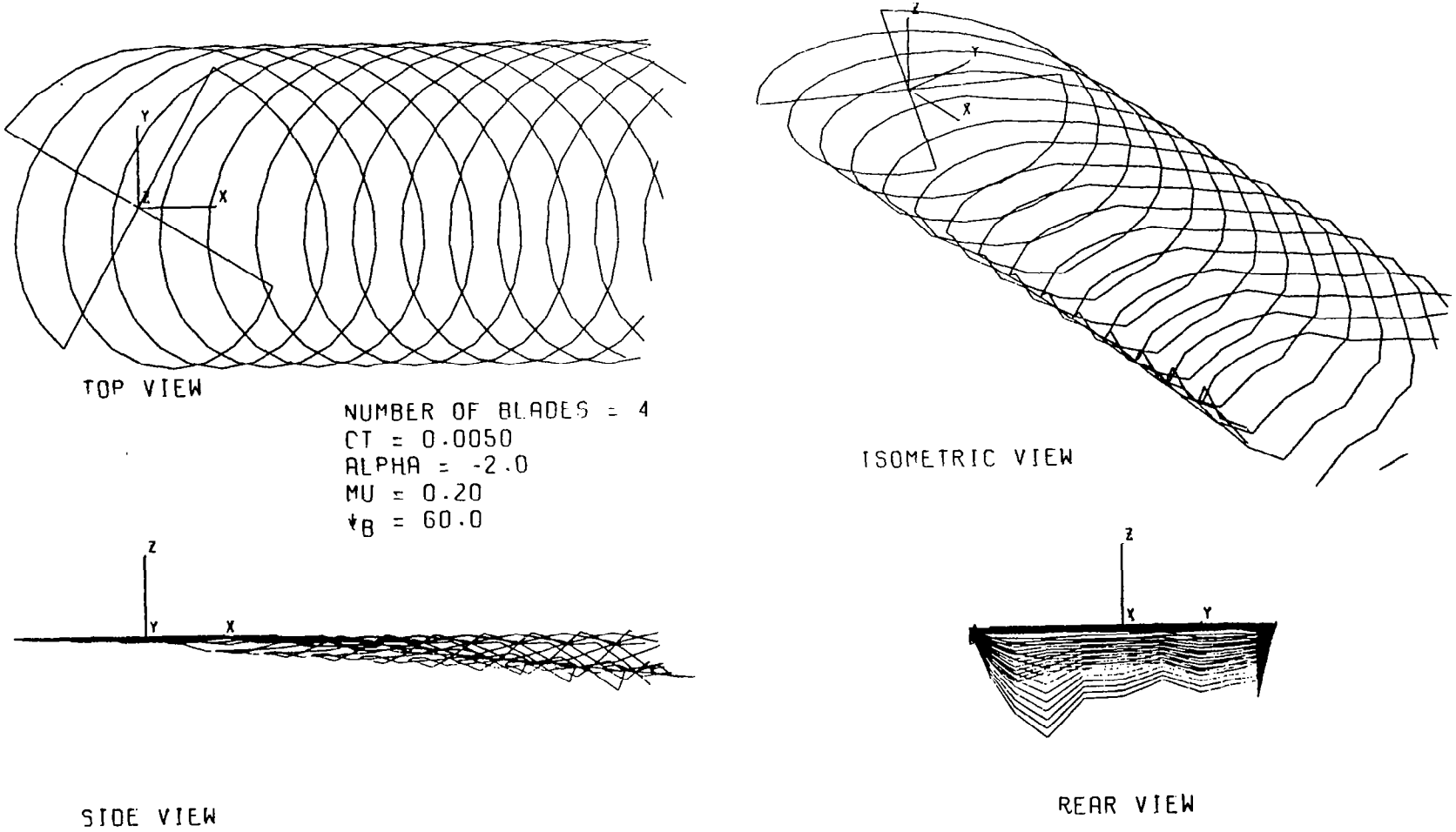

FIGURE 17E. PROJECTION AND ISOMETRIC VIEWS FOR GENERALIZED DISTORTED TIP VORTEX, VARYING BLADE AZIMUTH POSITION (ψ_B = 60.0)

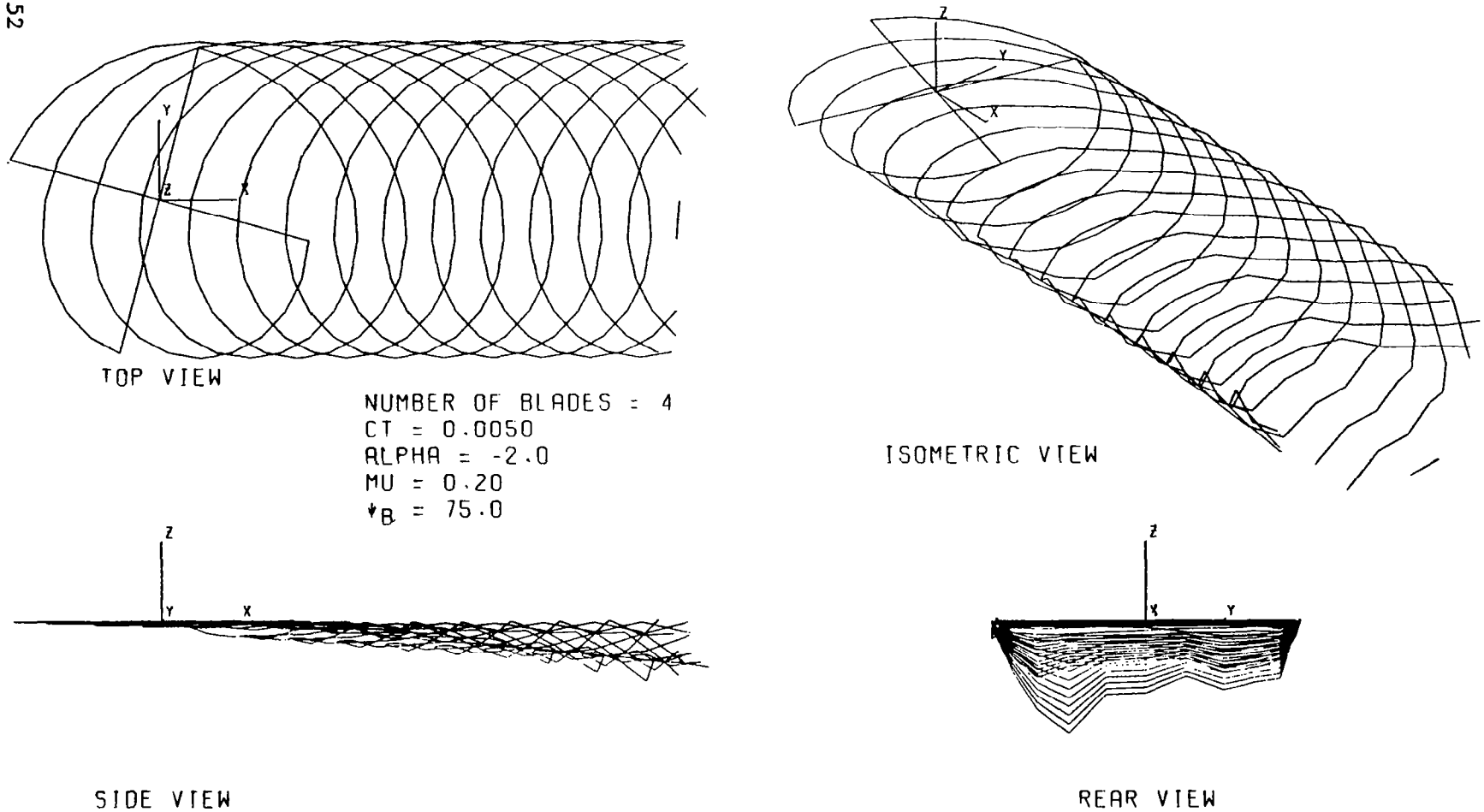

FIGURE 17F. PROJECTION AND ISOMETRIC VIEWS FOR GENERALIZED DISTORTED TIP VORTEX, VARYING BLADE AZIMUTH POSITION (ψ_B = 75.0)

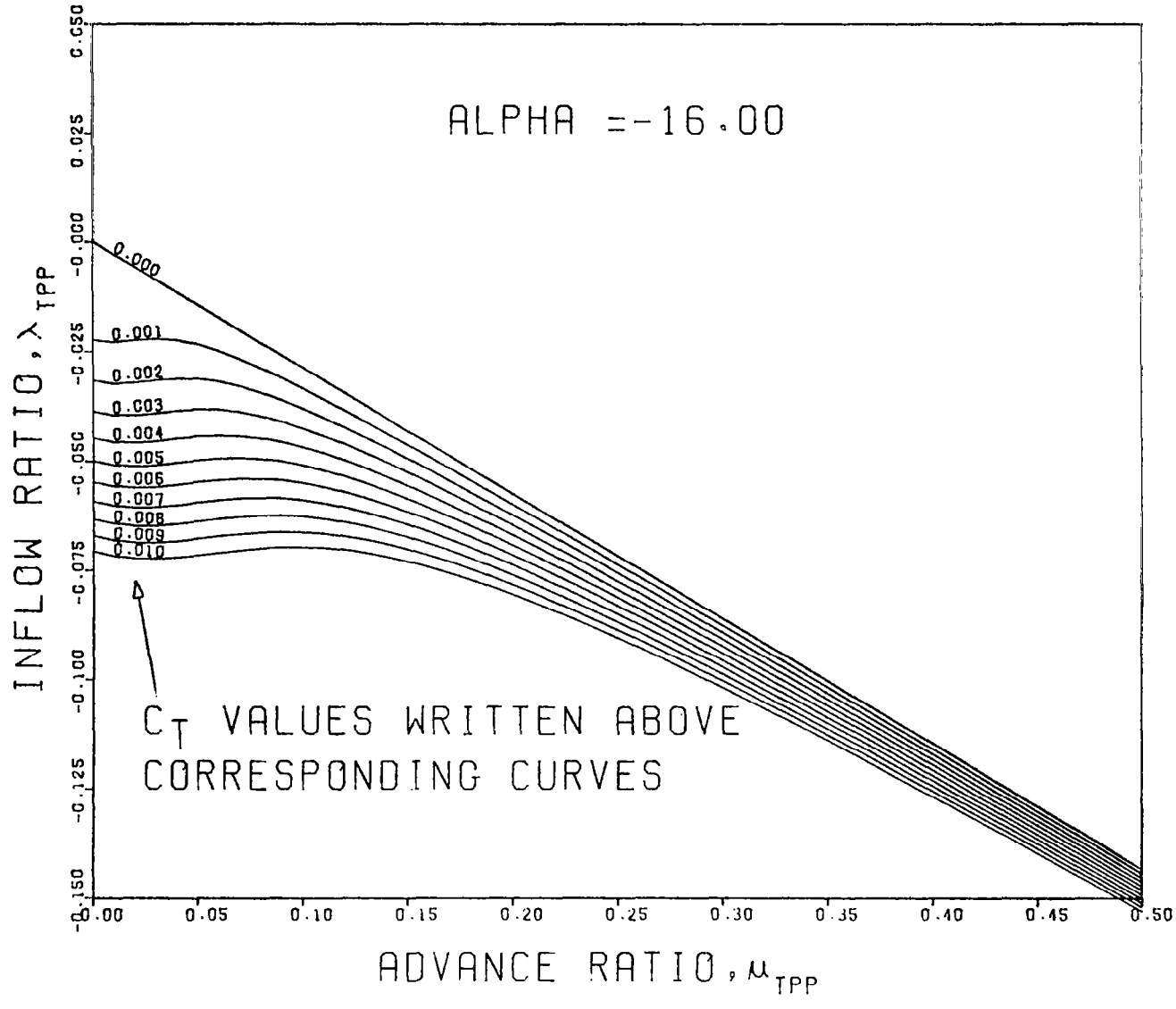

FIGURE 18A. INFLOW RATIO NOMOGRAPH (α_{TPP} = -16.0)

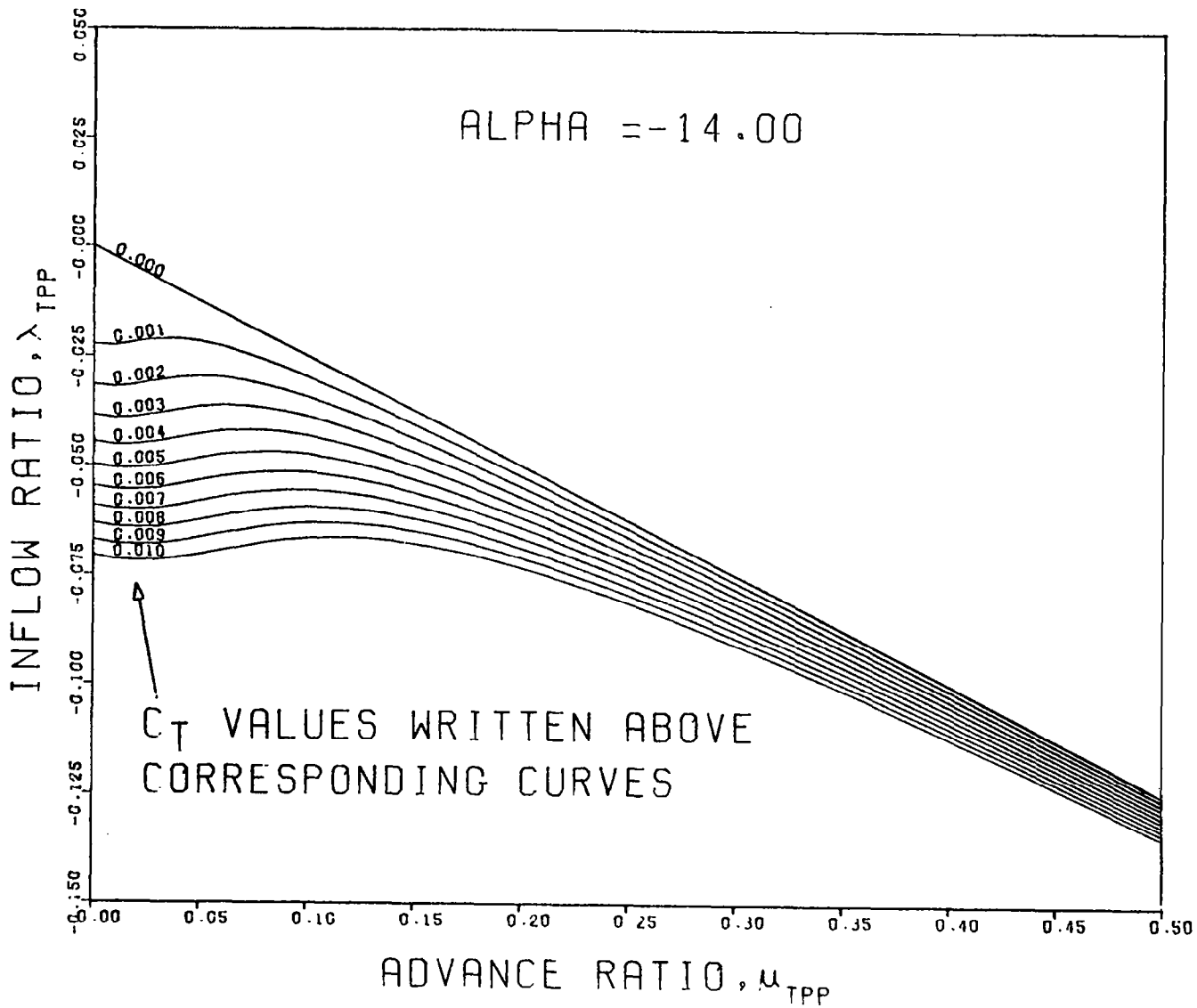

FIGURE 18B. INFLOW RATIO NOMOGRAPH (α_{TPP} = -14.0)

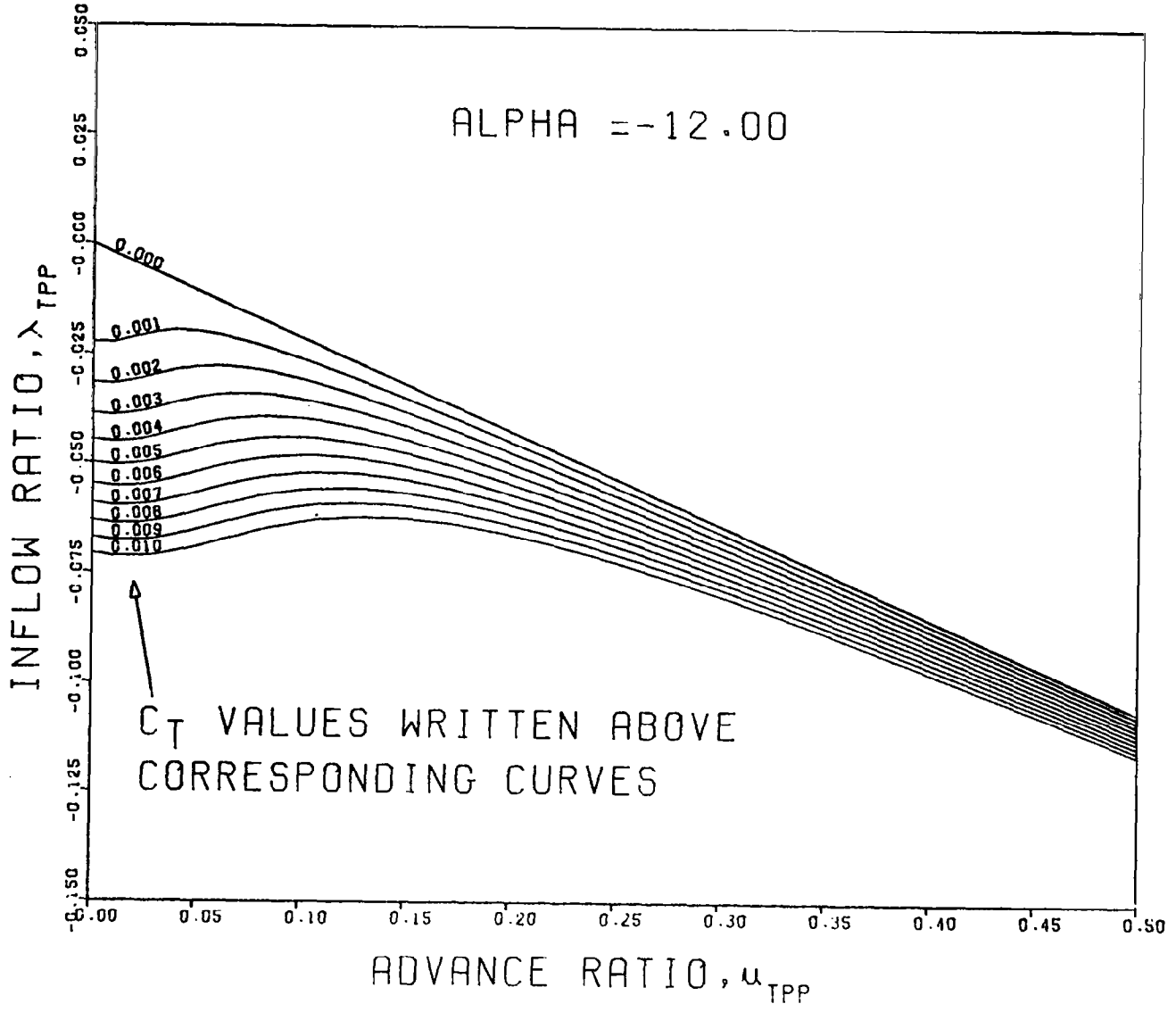

FIGURE 18C. INFLOW RATIO NOMOGRAPH (α_{TPP} = -12.0)

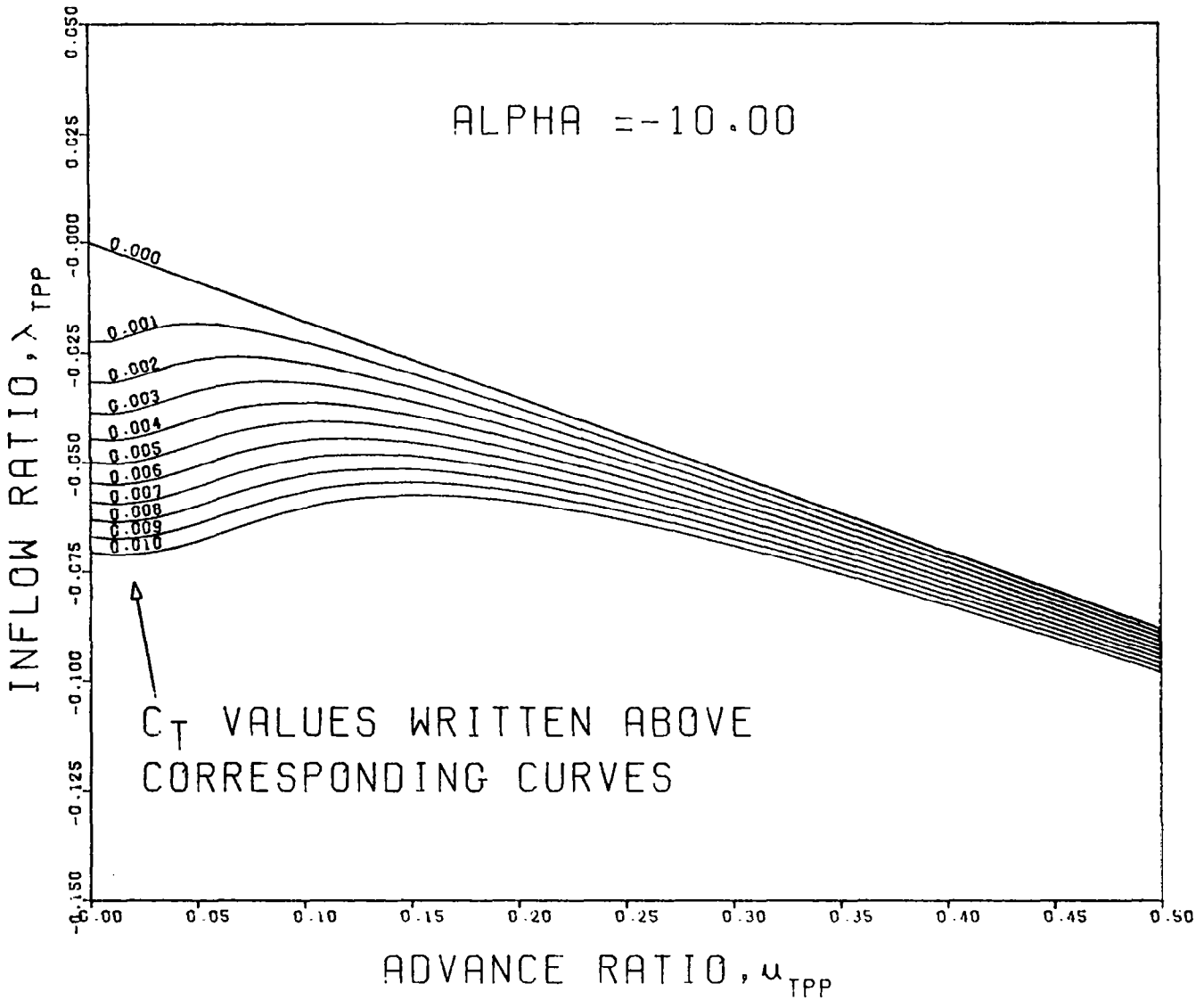

FIGURE 18D. INFLOW RATIO NOMOGRAPH (α_{TPP} = -10.0)

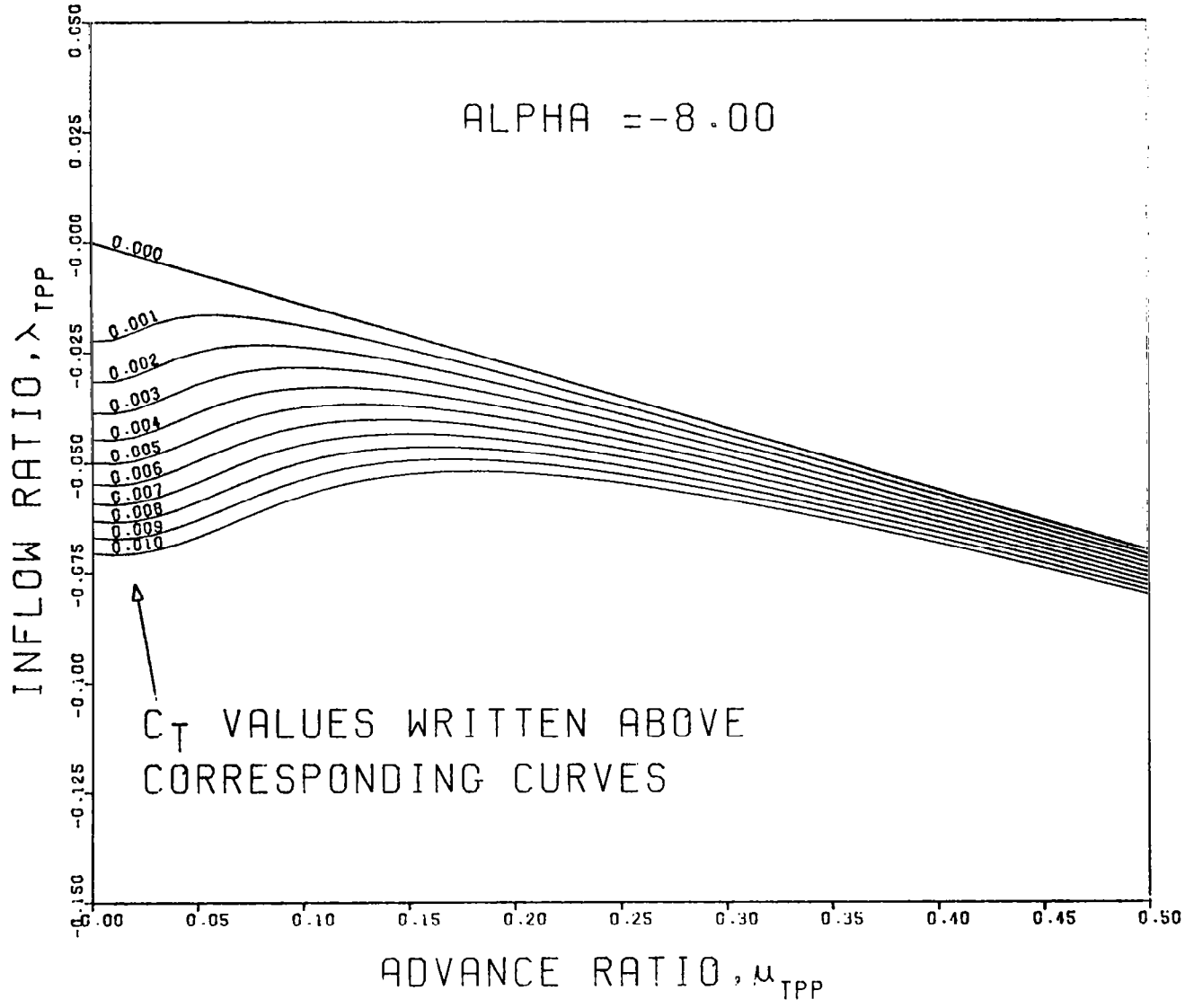

FIGURE 18E. INFLOW RATIO NOMOGRAPH (α_{TPP} = -8.0)

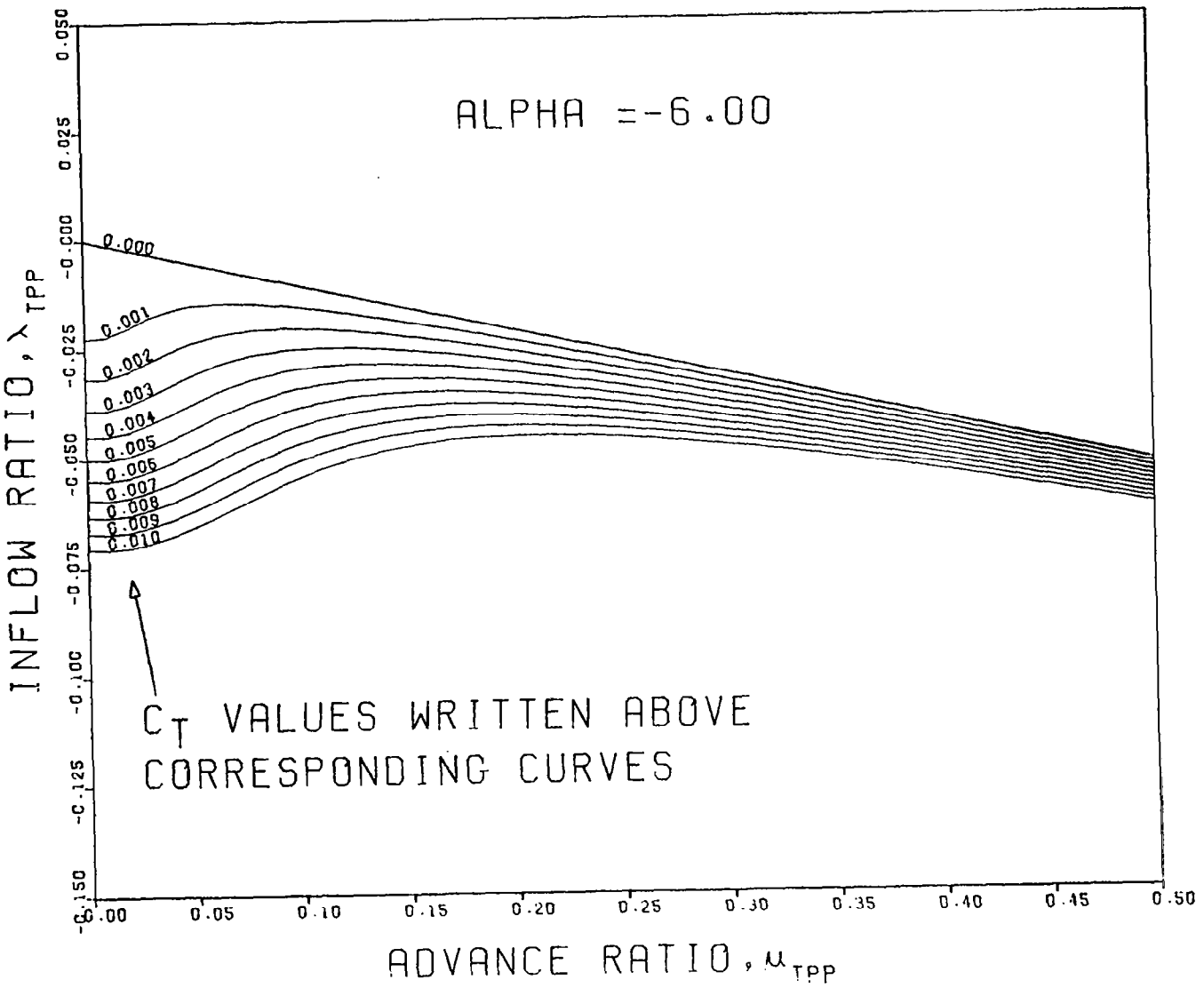

FIGURE 18F. INFLOW RATIO NOMOGRAPH (α_{TPP} = -6.0)

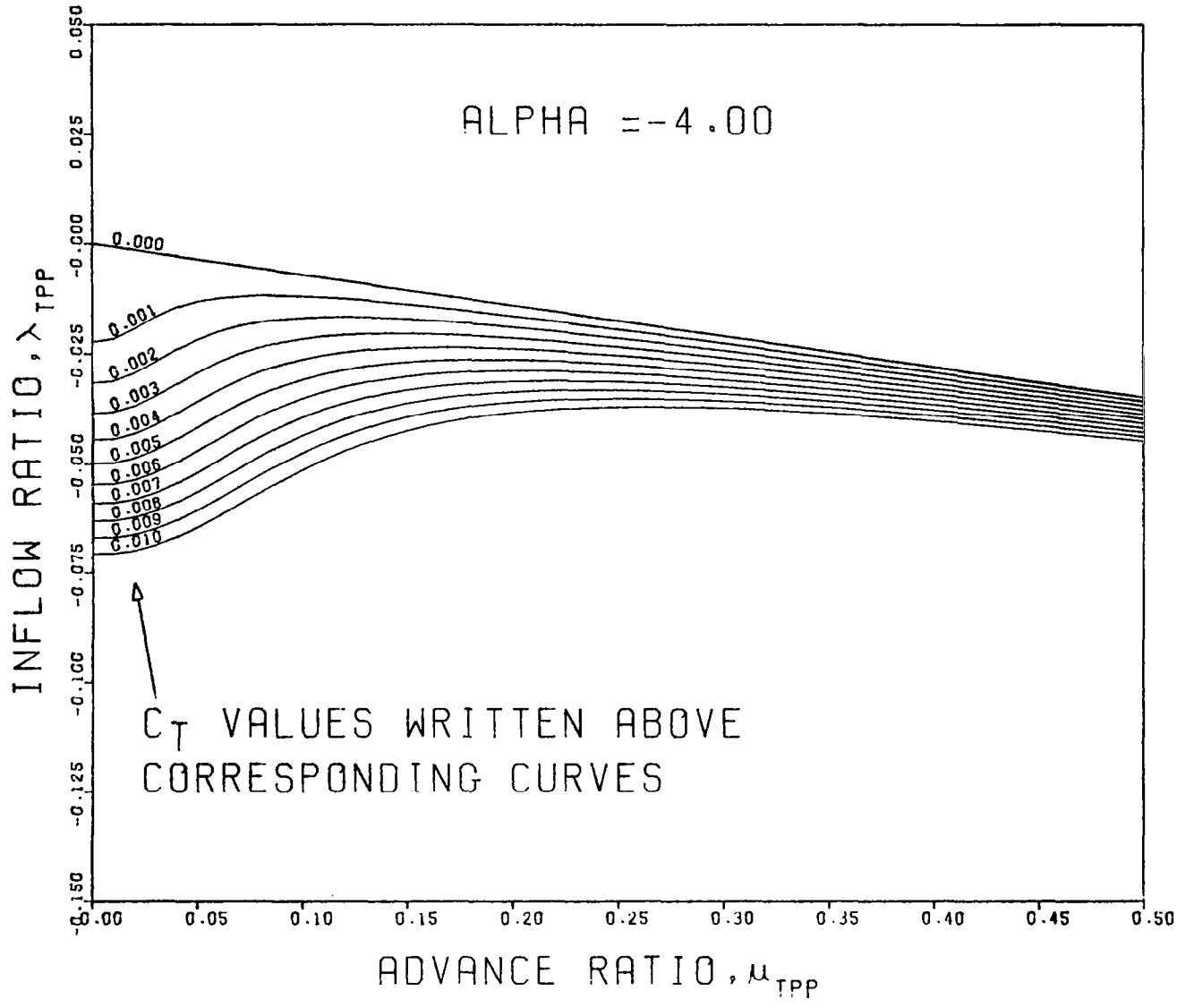

FIGURE 18G. INFLOW RATIO NOMOGRAPH (α_{TPP} = -4.0)

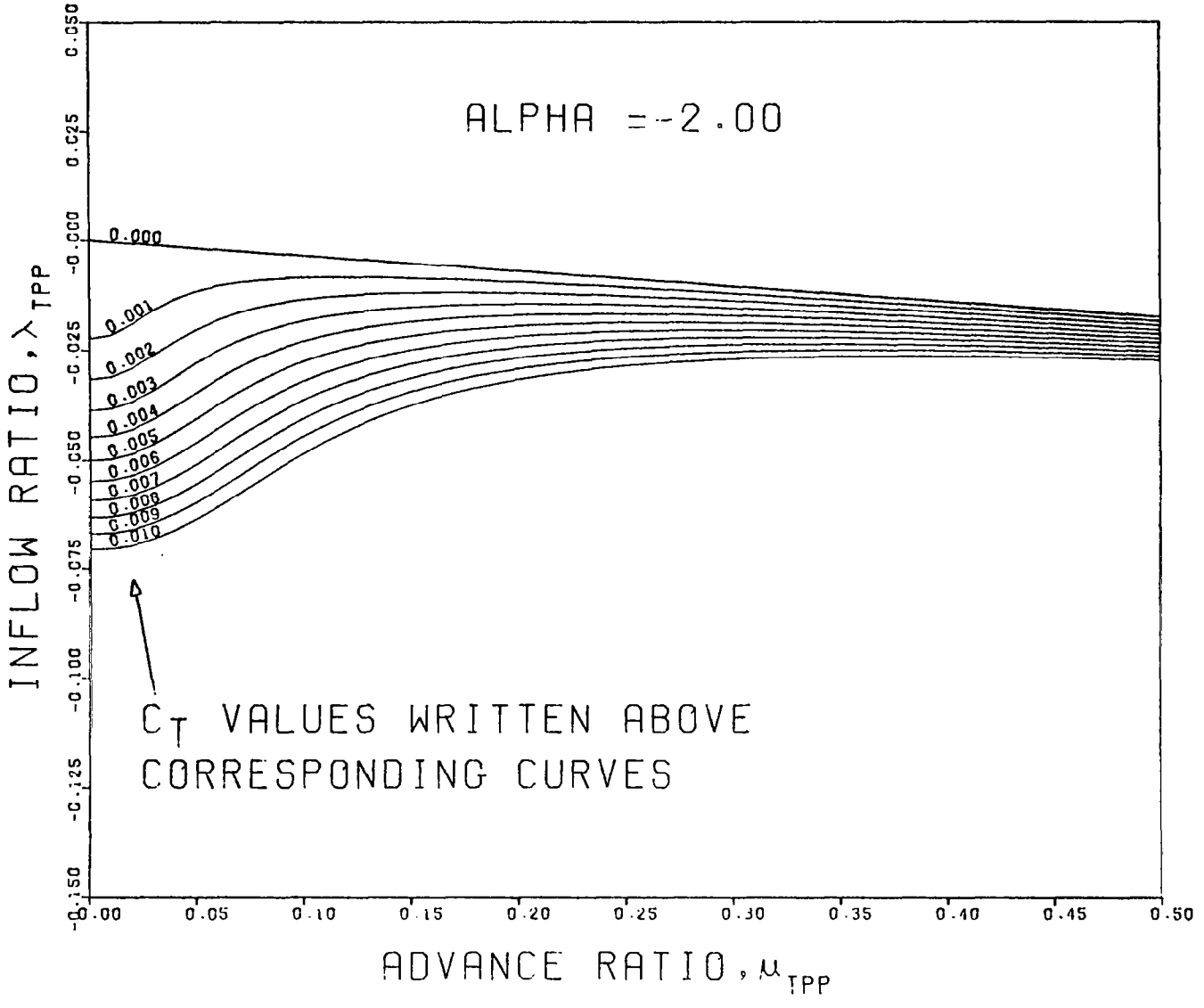

FIGURE 18H. INFLOW RATIO NOMOGRAPH (α_{TPP} = -2.0)

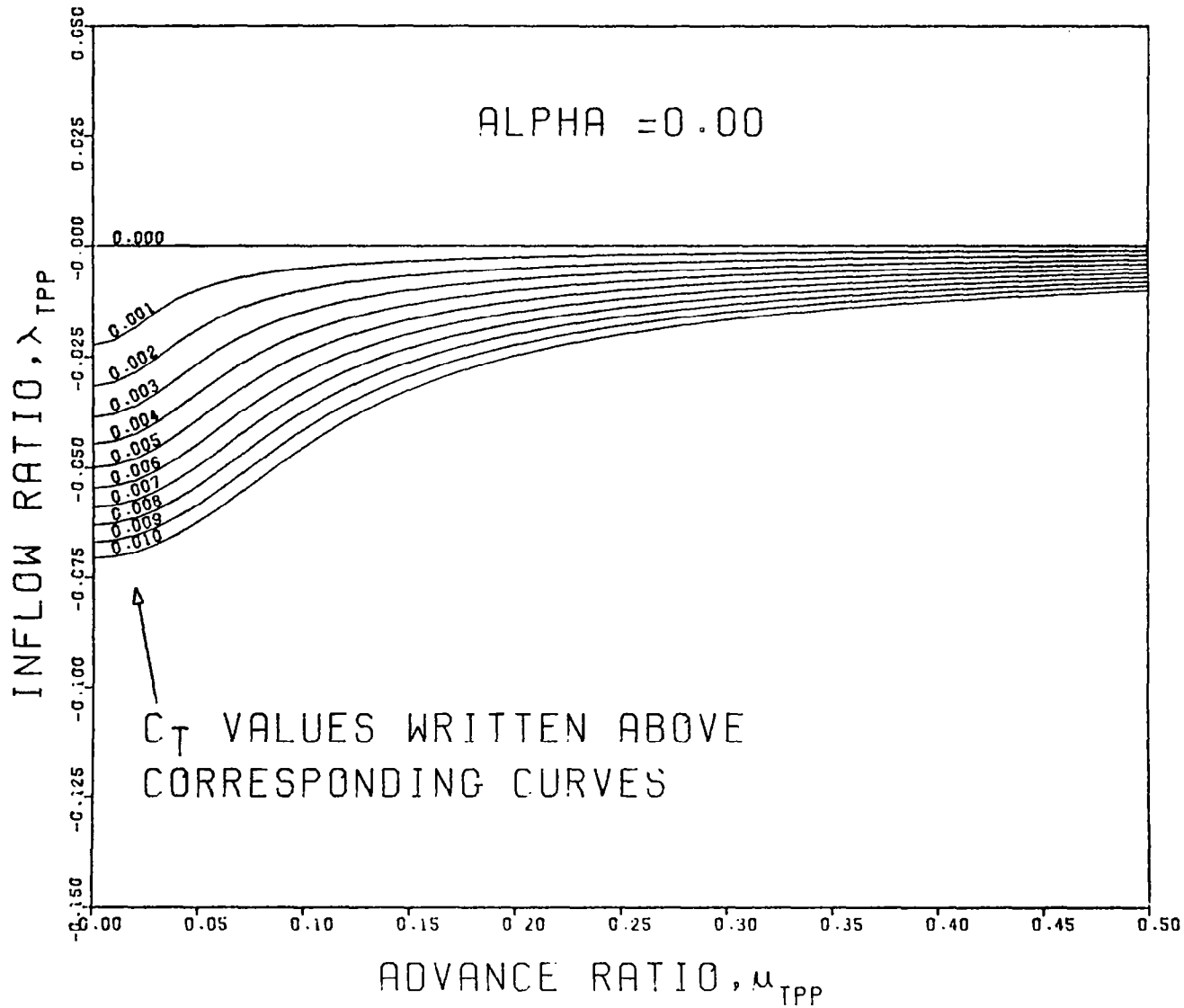

FIGURE 18I. INFLOW RATIO NOMOGRAPH (α_{TPP} = 0.0)

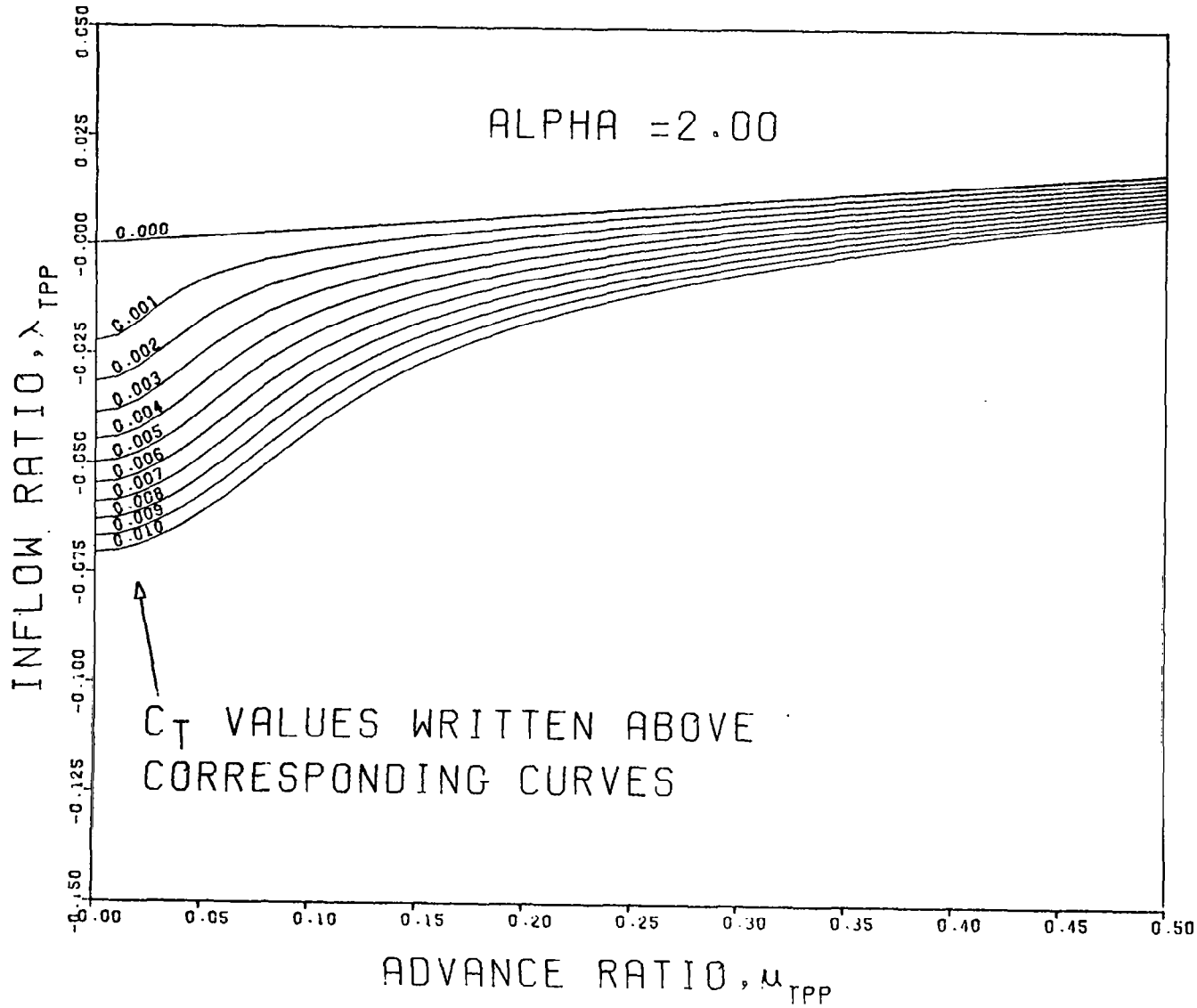

FIGURE 18J. INFLOW RATIO NOMOGRAPH (α_{TPP} = 2.0)

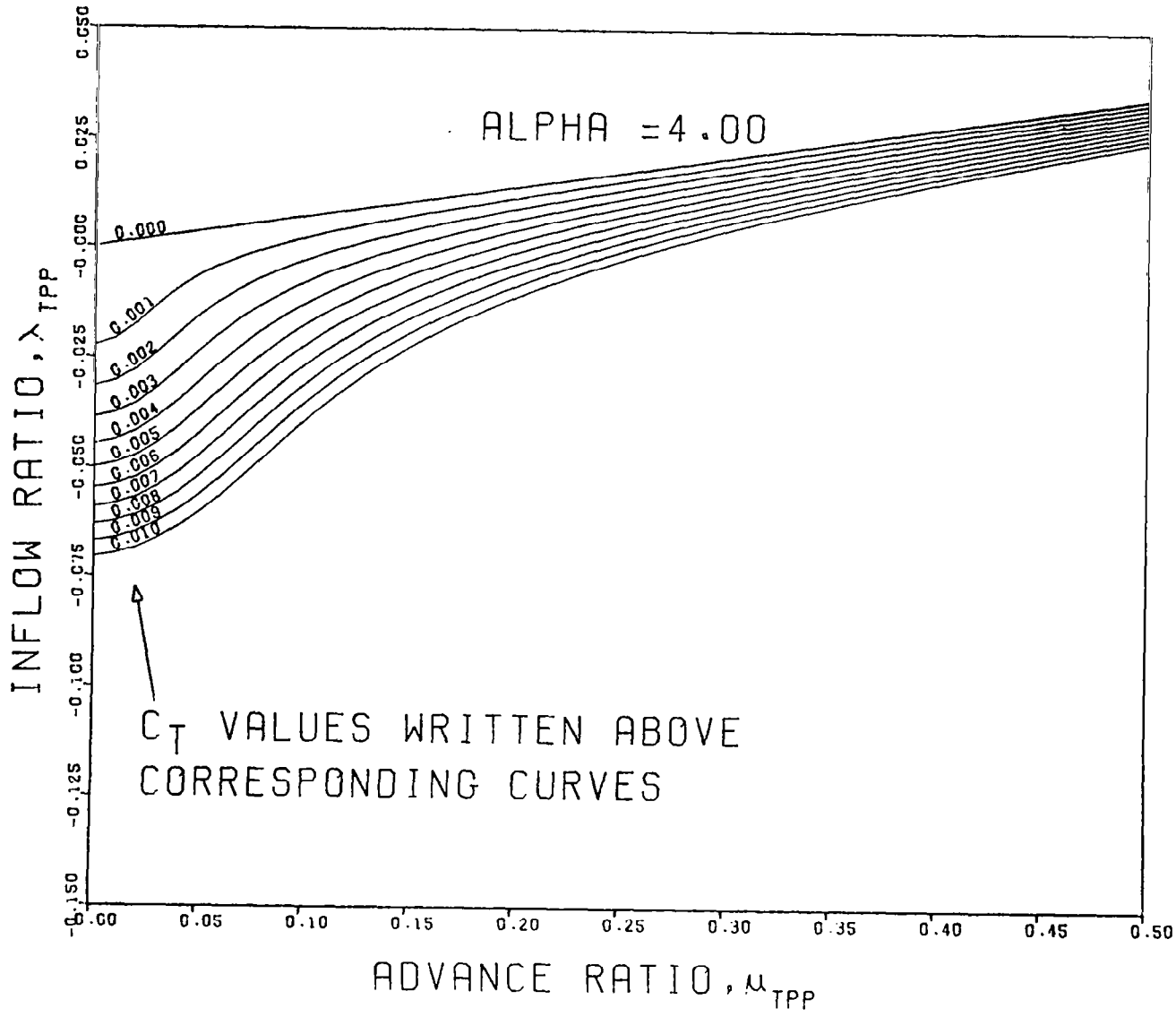

FIGURE 18K. INFLOW RATIO NOMOGRAPH (α_{TPP} = 4.0)

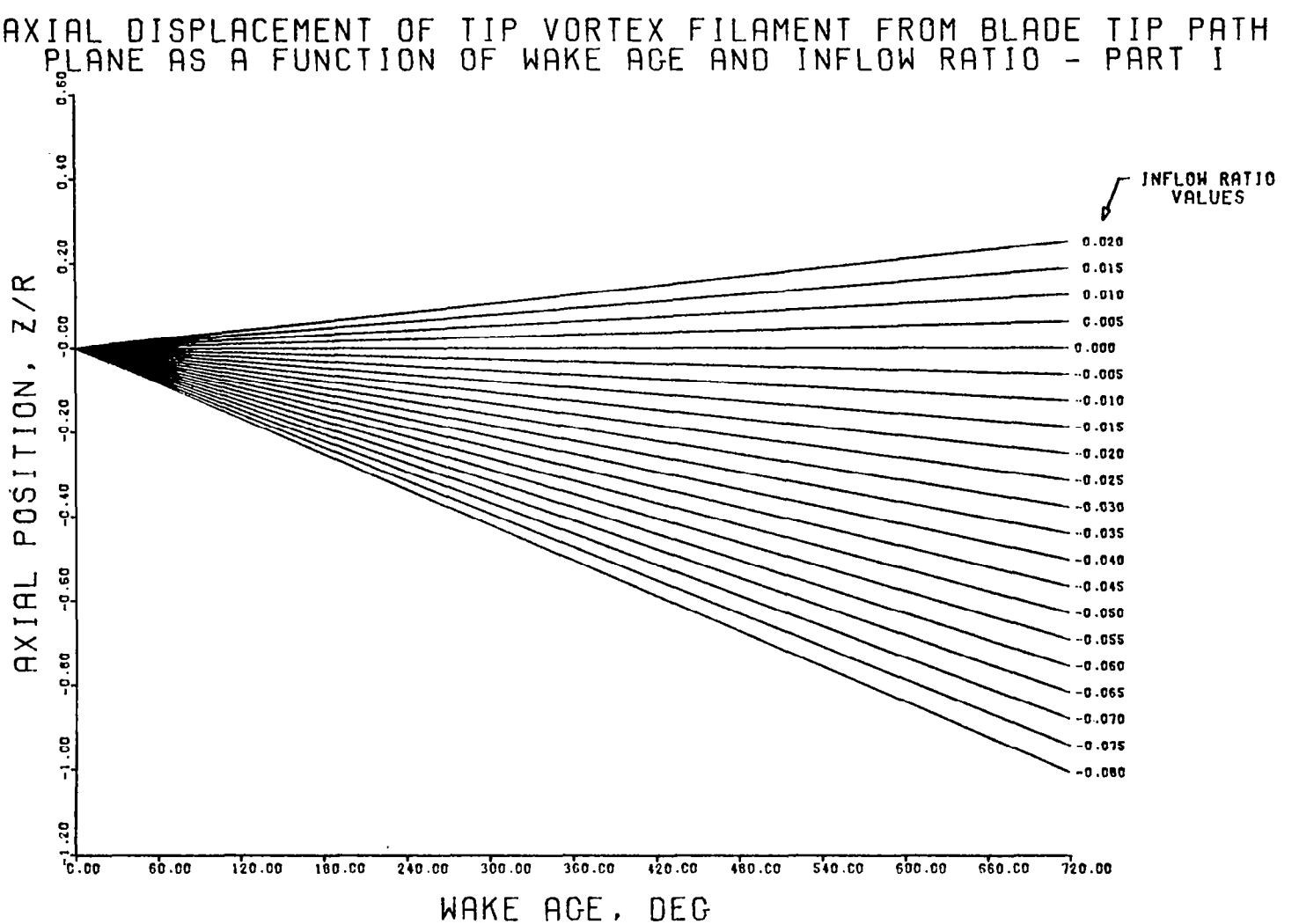

FIGURE 19A. UNDISTORTED AXIAL DISPLACEMENT NOMOGRAPHS - PART I

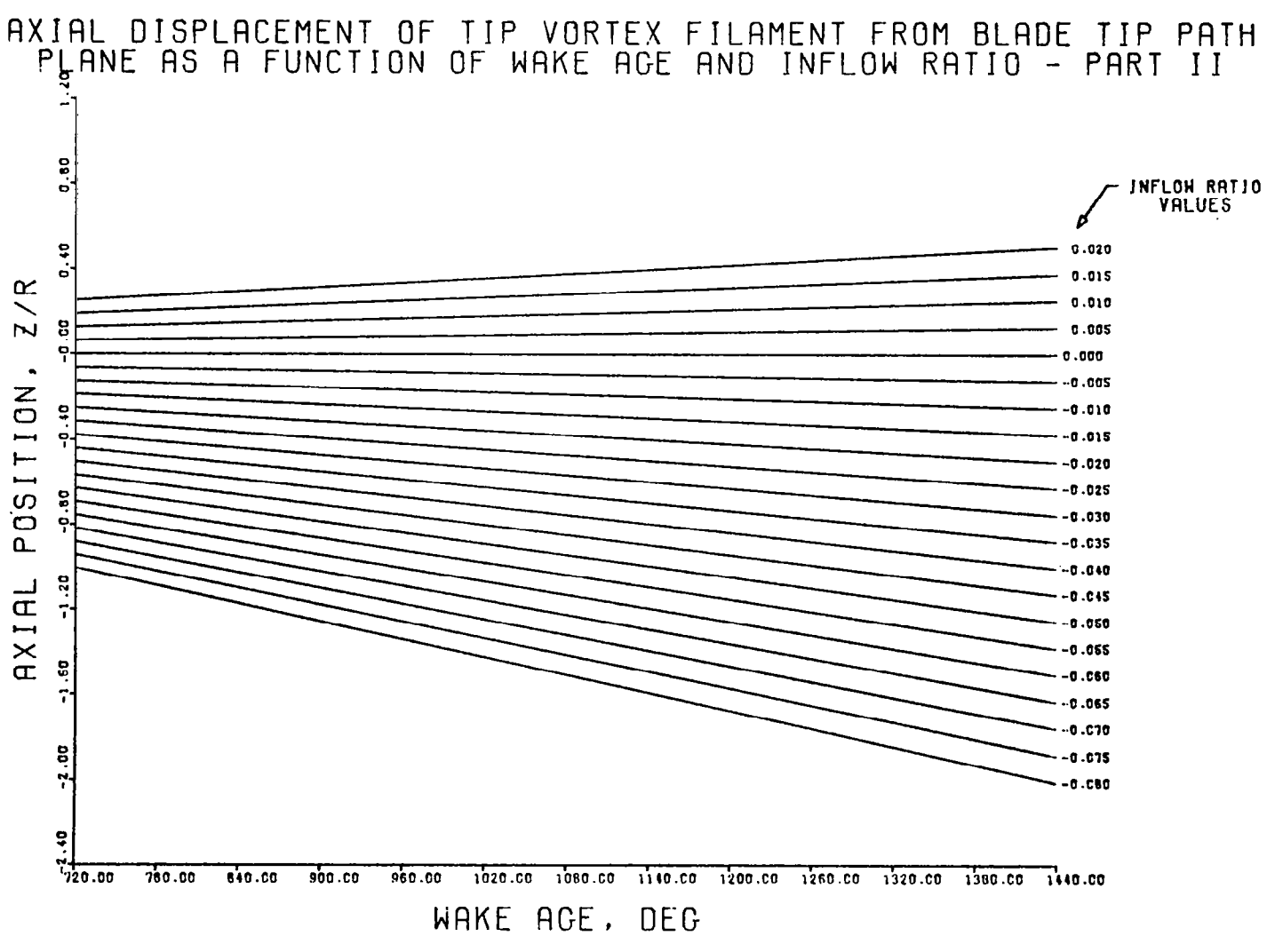

FIGURE 19B. UNDISTORTED AXIAL DISPLACEMENT NOMOGRAPHS - PART II

AXIAL DISPLACEMENT IN THE TIP PATH PLANE FOR INTEGER MULTIPLES OF 360 DEGREES OF WAKE AGE

INFLOW RATIO λ	Z/R FOR INTEGER MULTIPLES OF 360 DEGREES OF WAKE AGE									
	1	2	3	4	5	6	7	8	9	10
0.050	0.314	0.628	0.942	1.257	1.571	1.885	2.199	2.513	2.827	3.142
0.040	0.251	0.503	0.754	1.005	1.257	1.508	1.759	2.011	2.262	2.513
0.030	0.188	0.377	0.565	0.754	0.942	1.131	1.319	1.508	1.696	1.885
0.020	0.126	0.251	0.377	0.503	0.628	0.754	0.880	1.005	1.131	1.257
0.010	0.063	0.126	0.188	0.251	0.314	0.377	0.440	0.503	0.565	0.628
0.000	0.000	0.000	0.000	0.000	0.000	0.000	0.000	0.000	0.000	0.000
-0.010	-0.063	-0.126	-0.188	-0.251	-0.314	-0.377	-0.440	-0.503	-0.565	-0.628
-0.020	-0.126	-0.251	-0.377	-0.503	-0.628	-0.754	-0.880	-1.005	-1.131	-1.257
-0.030	-0.188	-0.377	-0.565	-0.754	-0.942	-1.131	-1.319	-1.508	-1.696	-1.885
-0.040	-0.251	-0.503	-0.754	-1.005	-1.257	-1.508	-1.759	-2.011	-2.262	-2.513
-0.050	-0.314	-0.628	-0.942	-1.257	-1.571	-1.885	-2.199	-2.513	-2.827	-3.142
-0.060	-0.377	-0.754	-1.131	-1.508	-1.885	-2.262	-2.639	-3.016	-3.393	-3.770
-0.070	-0.440	-0.880	-1.319	-1.759	-2.199	-2.639	-3.079	-3.519	-3.958	-4.398
-0.080	-0.503	-1.005	-1.508	-2.011	-2.513	-3.016	-3.519	-4.021	-4.524	-5.027
-0.090	-0.565	-1.131	-1.696	-2.262	-2.827	-3.393	-3.958	-4.524	-5.089	-5.655
-0.100	-0.628	-1.257	-1.885	-2.513	-3.142	-3.770	-4.398	-5.027	-5.655	-6.283
-0.110	-0.691	-1.382	-2.073	-2.765	-3.456	-4.147	-4.838	-5.529	-6.220	-6.912
-0.120	-0.754	-1.508	-2.262	-3.016	-3.770	-4.524	-5.278	-6.032	-6.786	-7.540
-0.130	-0.817	-1.634	-2.450	-3.267	-4.084	-4.901	-5.718	-6.535	-7.351	-8.168
-0.140	-0.880	-1.759	-2.639	-3.519	-4.398	-5.278	-6.158	-7.037	-7.917	-8.796
-0.150	-0.942	-1.885	-2.827	-3.770	-4.712	-5.655	-6.597	-7.540	-8.482	-9.425

FIGURE 19C. UNDISTORTED AXIAL DISPLACEMENT NOMOGRAPHS - PART III

GENERALIZED LONGITUDINAL COORDINATE CHART

LONGITUDINAL DISPLACEMENT FOR MULTIPLES OF 360 DEGREES						
MULTIPLES OF 360 DEG	TIP PATH PLANE ROTOR ADVANCE RATIO					
N	0.05	0.10	0.15	0.20	0.30	0.40
1	0.314	0.628	0.942	1.257	1.885	2.513
2	0.628	1.257	1.885	2.513	3.770	5.027
3	0.942	1.885	2.827	3.770	5.655	7.540
4	1.257	2.513	3.770	5.027	7.540	10.053
5	1.571	3.142	4.712	6.283	9.425	12.566
6	1.885	3.770	5.655	7.540	11.310	15.080
7	2.199	4.398	6.597	8.796	13.195	17.593
8	2.513	5.027	7.540	10.053	15.080	20.106
9	2.827	5.655	8.482	11.310	16.965	22.619
10	3.142	6.283	9.425	12.566	18.850	25.133

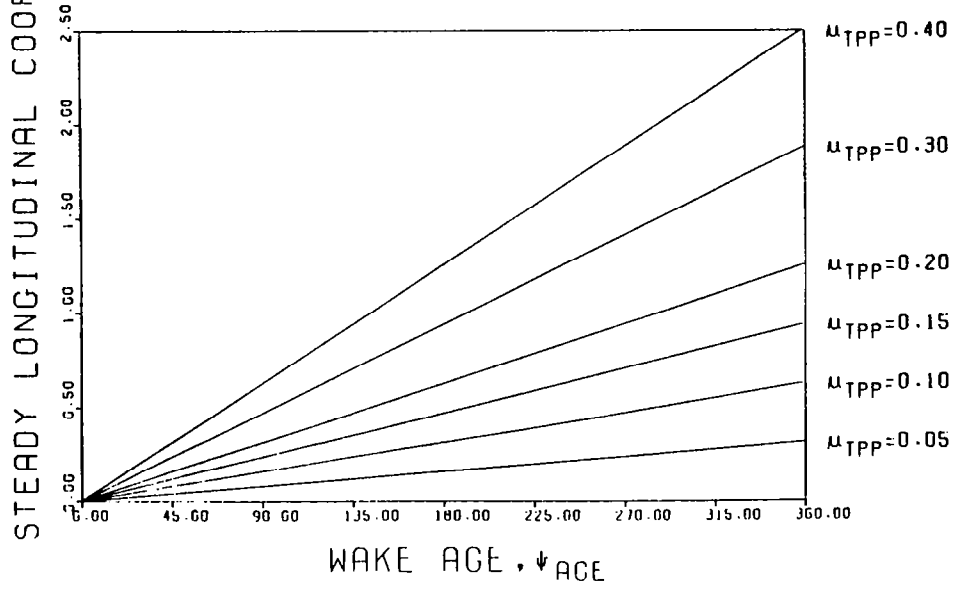

FIGURE 20A. GENERALIZED LONGITUDINAL COORDINATE CHART - PART I, STEADY PORTION

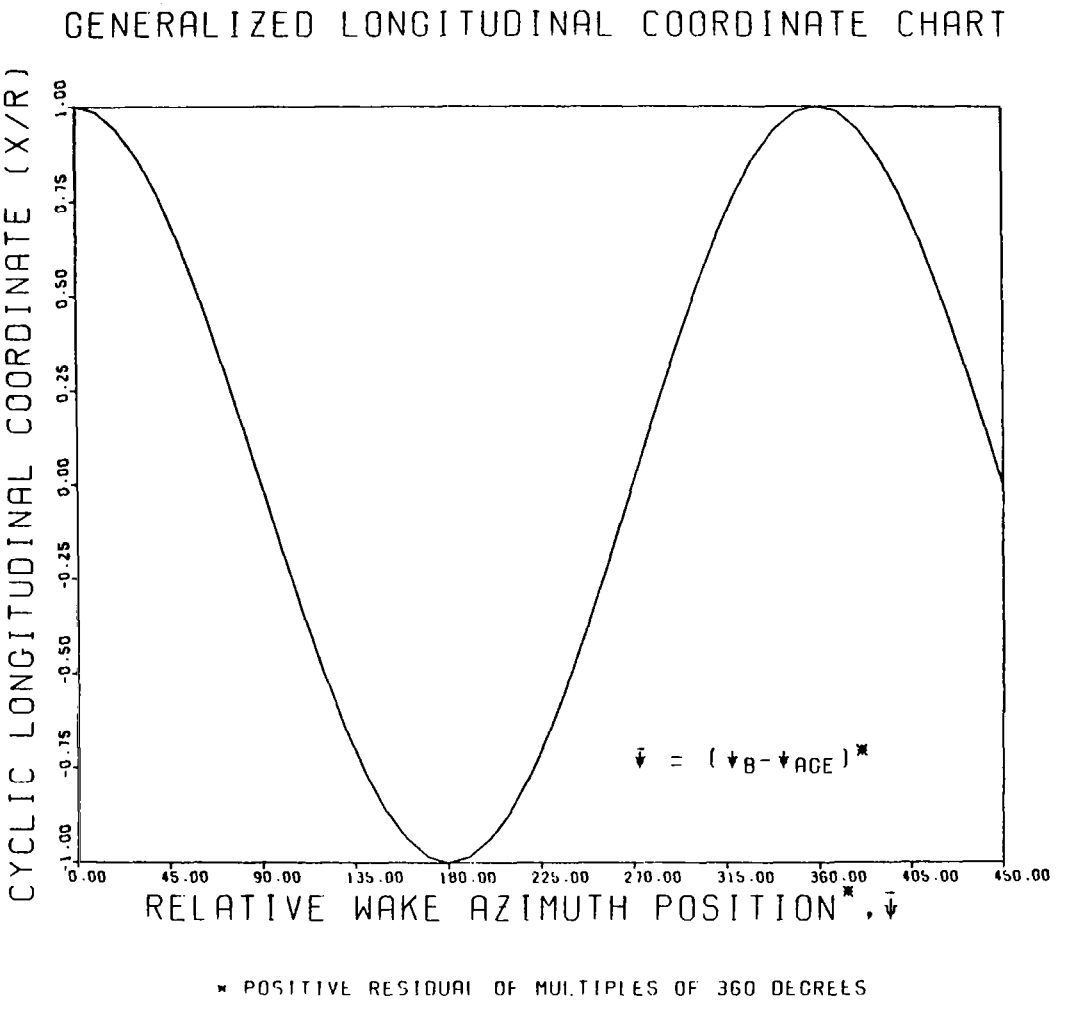

FIGURE 20B. GENERALIZED LONGITUDINAL COORDINATE CHART - PART II, CYCLIC PORTION

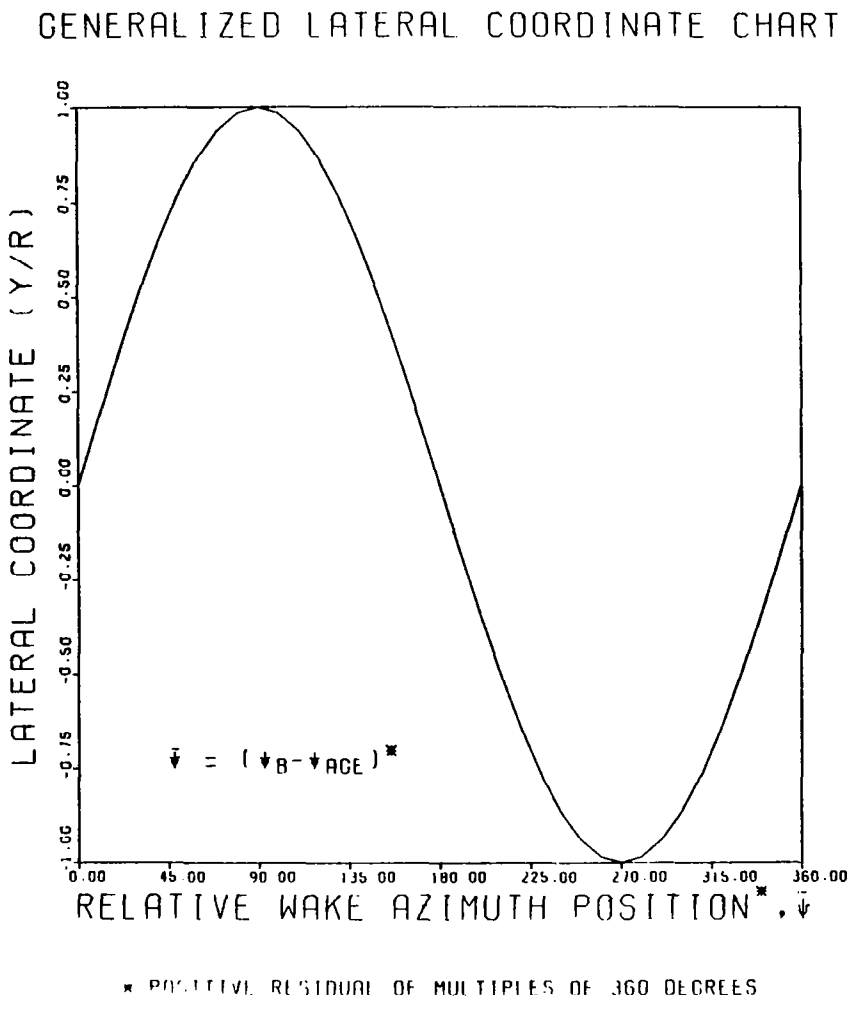

FIGURE 21. GENERALIZED LATERAL COORDINATE CHART

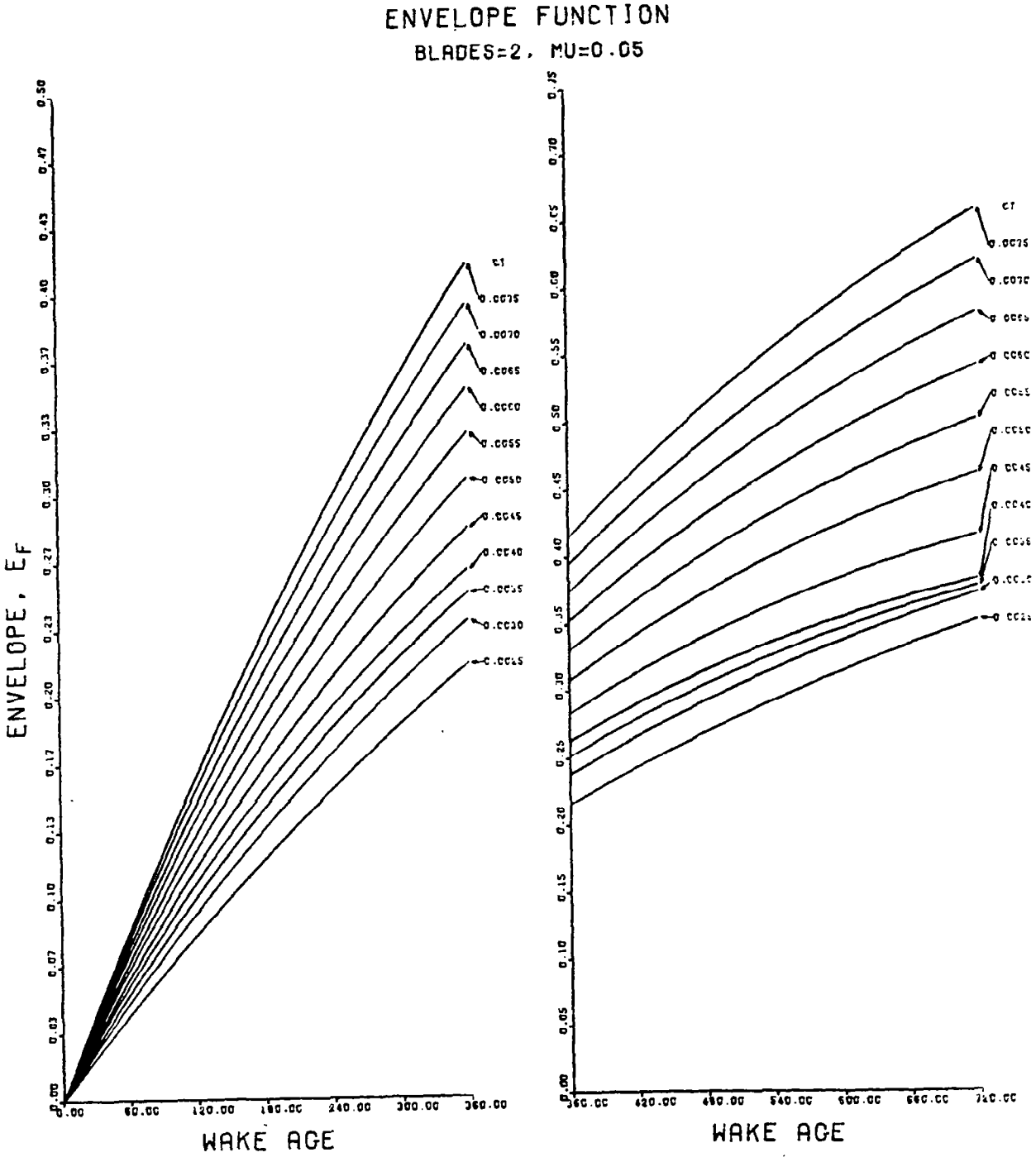

FIGURE 22A. GENERALIZED WAKE ENVELOPE FUNCTION CHARTS FOR TWO BLADES (μ = .05)

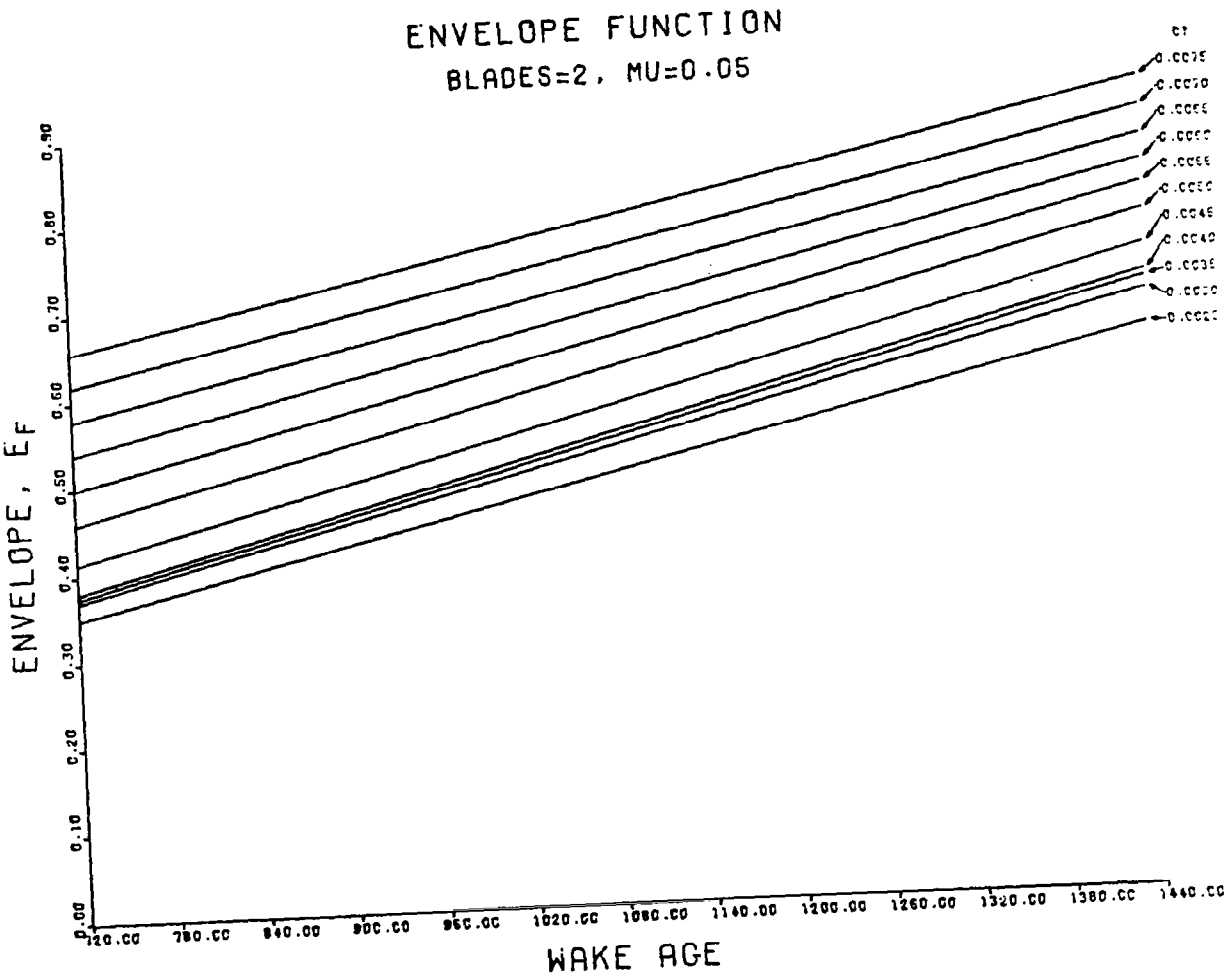

FIGURE 22A. CONTINUED

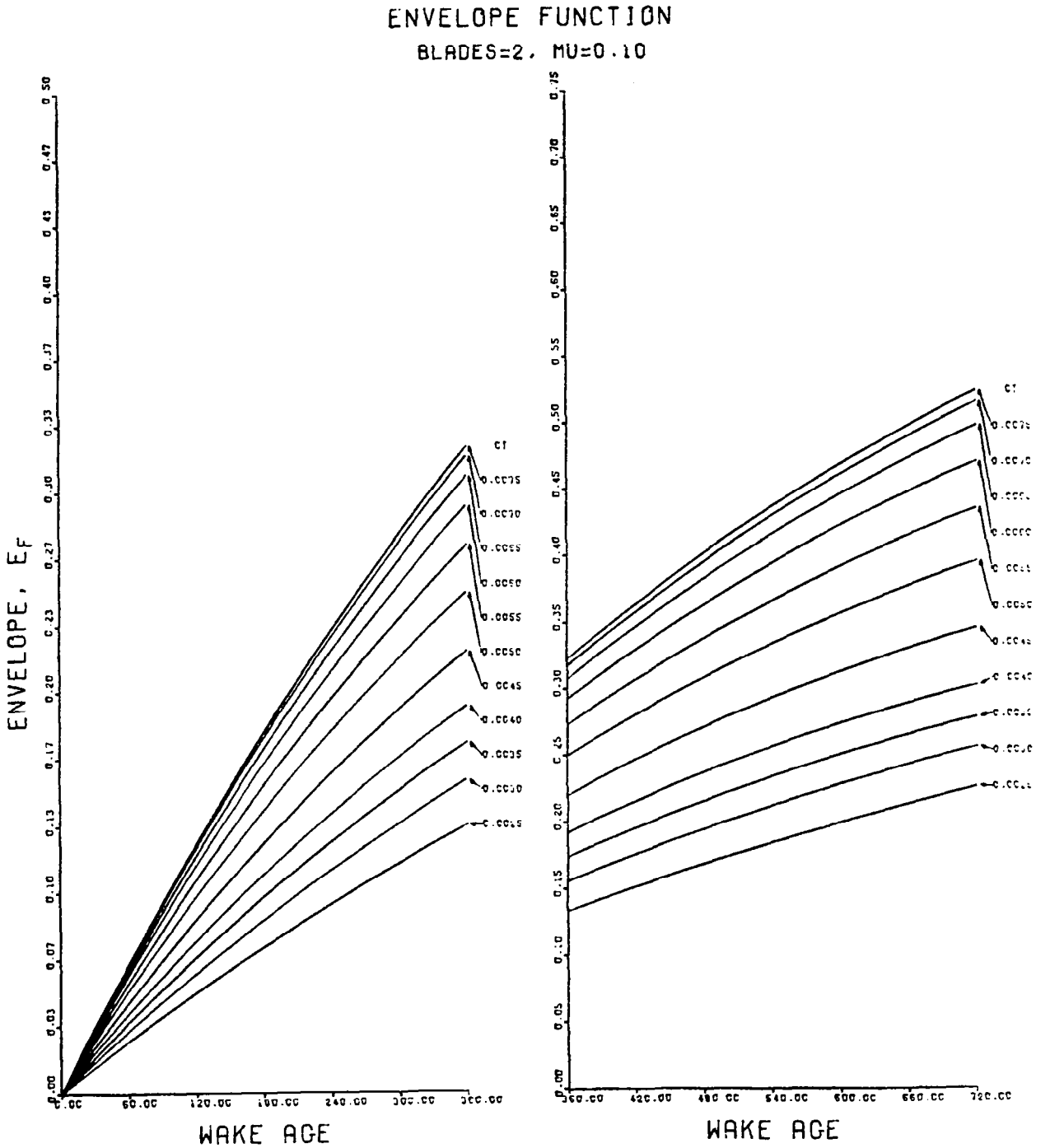

FIGURE 22B. GENERALIZED WAKE ENVELOPE FUNCTION CHARTS FOR TWO BLADES (μ = .10)

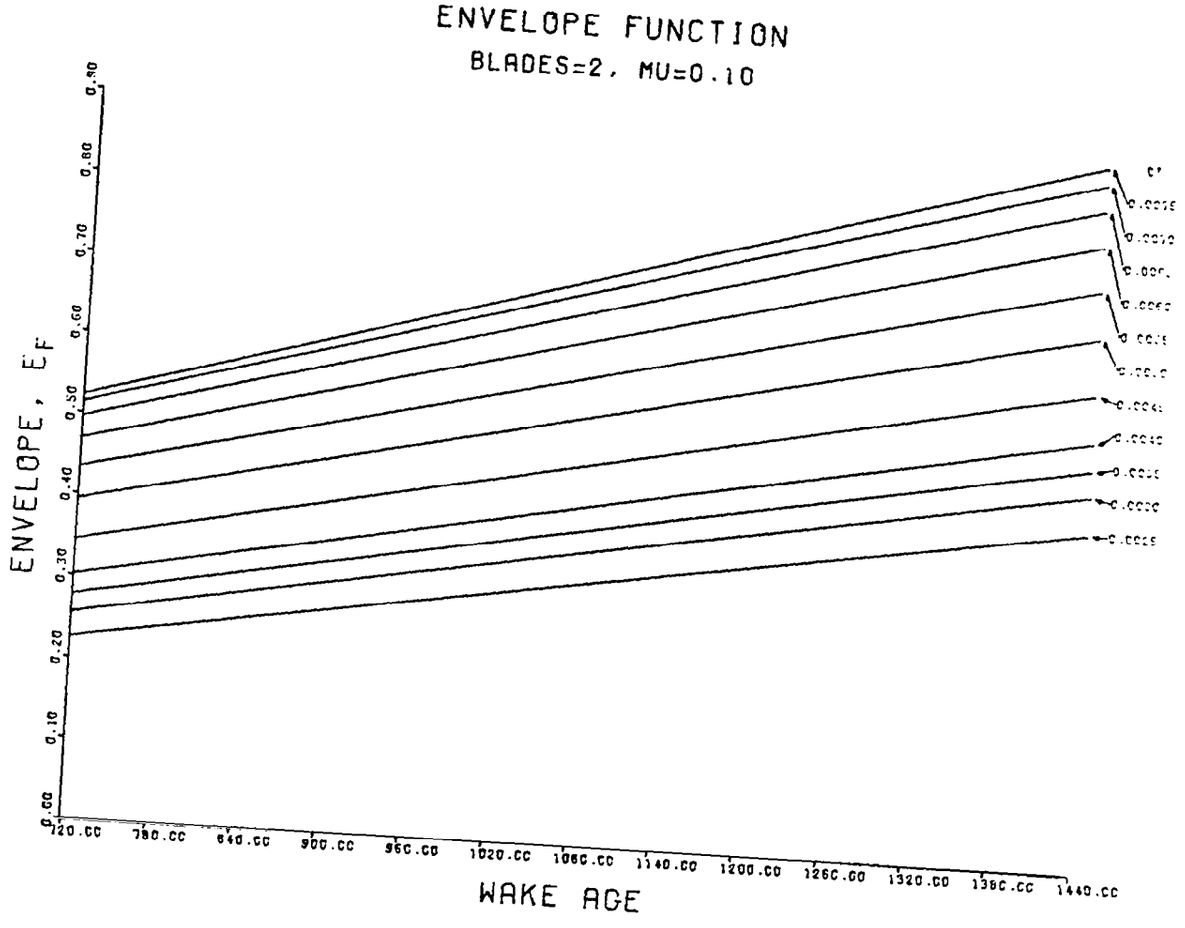

FIGURE 22B. CONTINUED

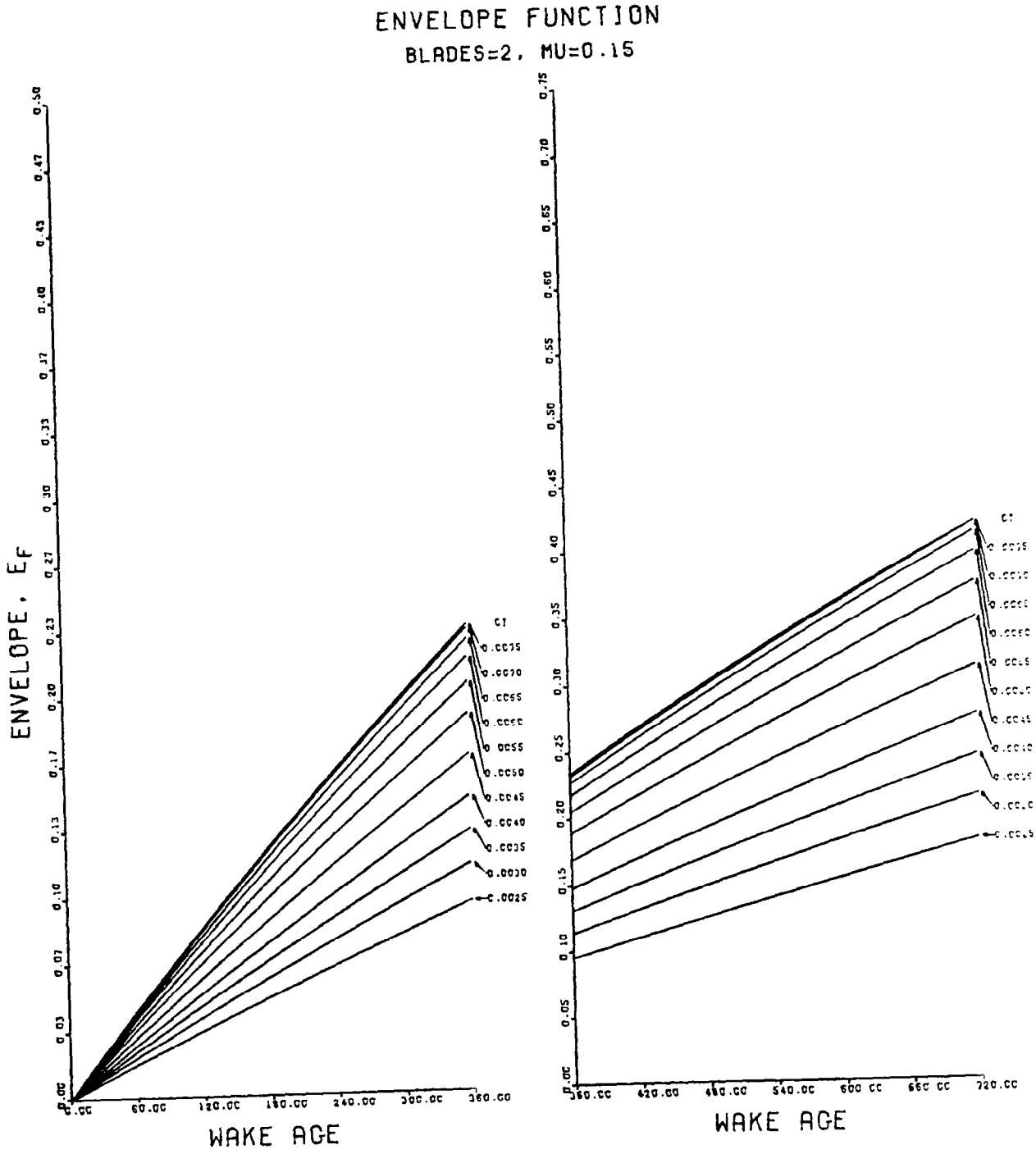

FIGURE 22C. GENERALIZED WAKE ENVELOPE FUNCTION CHARTS FOR TWO BLADES (μ = .15)

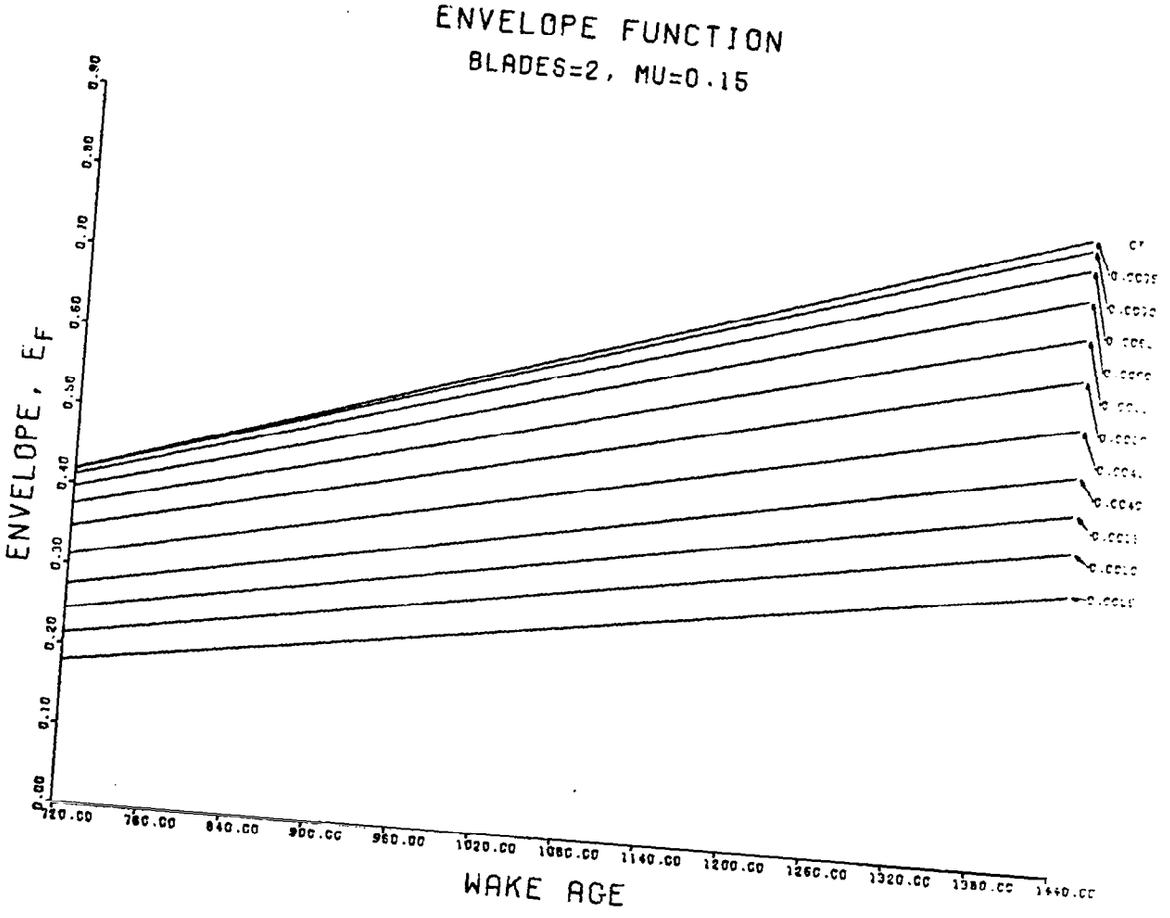

FIGURE 22C. CONTINUED

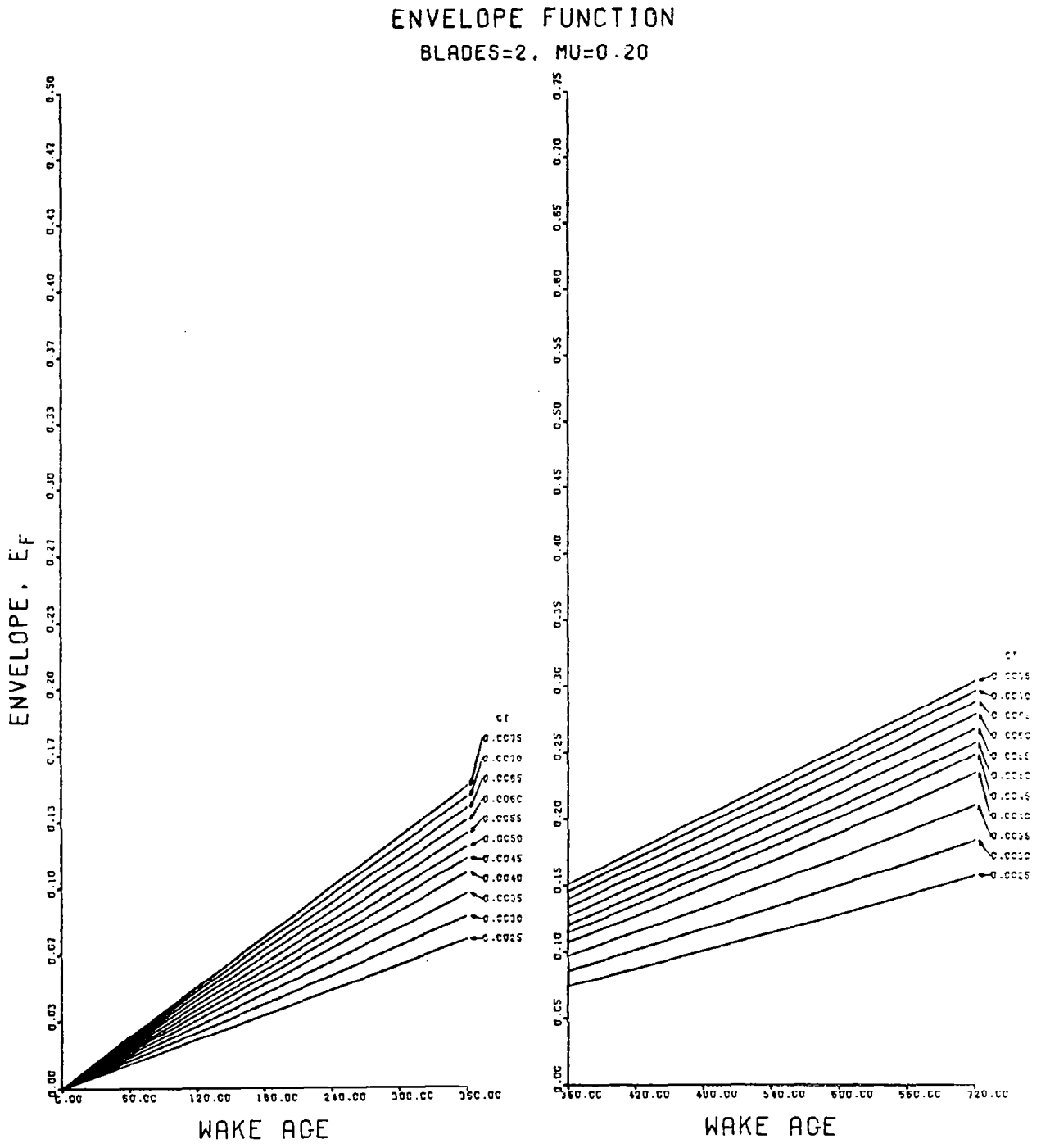

FIGURE 22D. GENERALIZED WAKE ENVELOPE FUNCTION CHARTS FOR TWO BLADES (μ = .20)

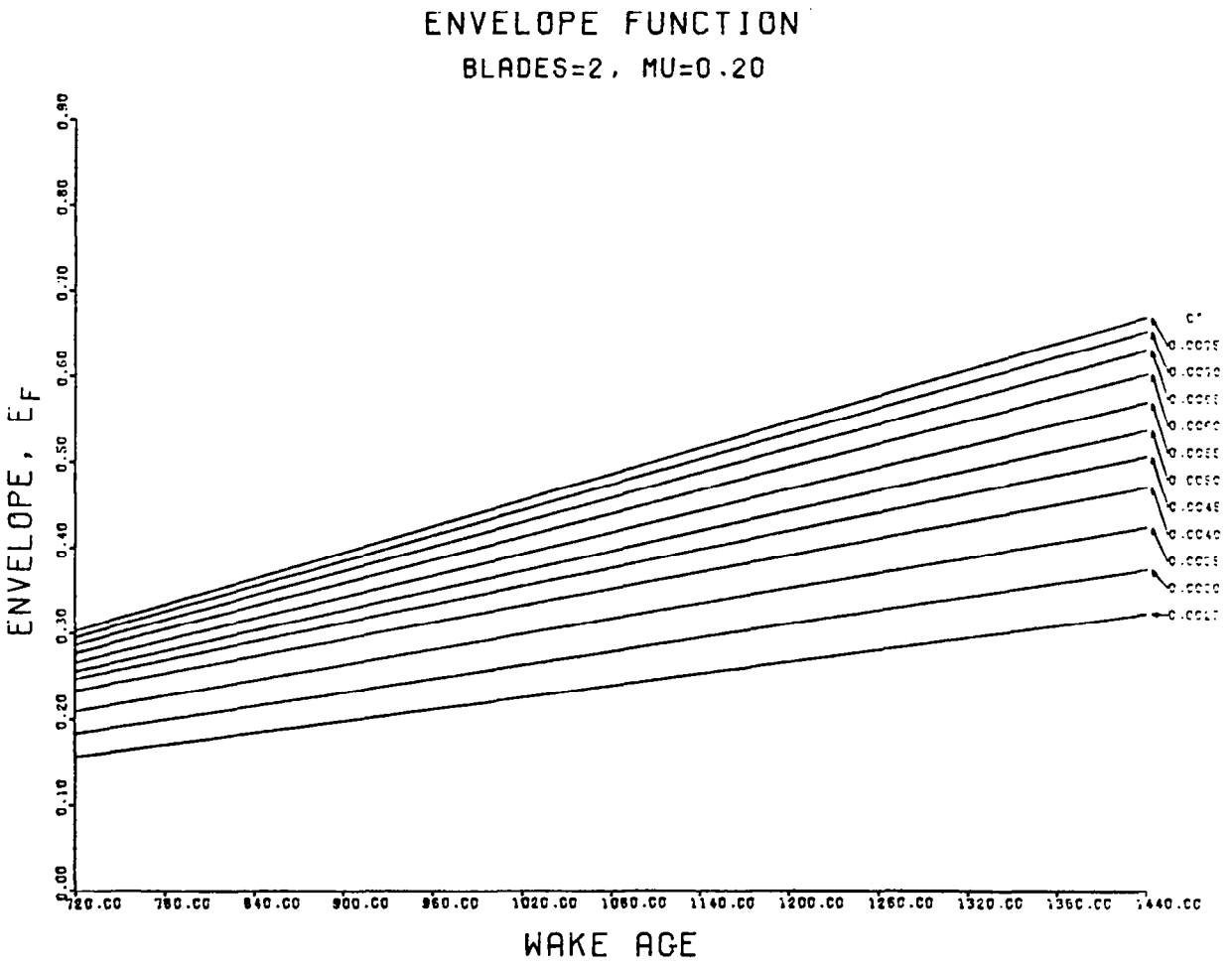

FIGURE 22D. CONTINUED

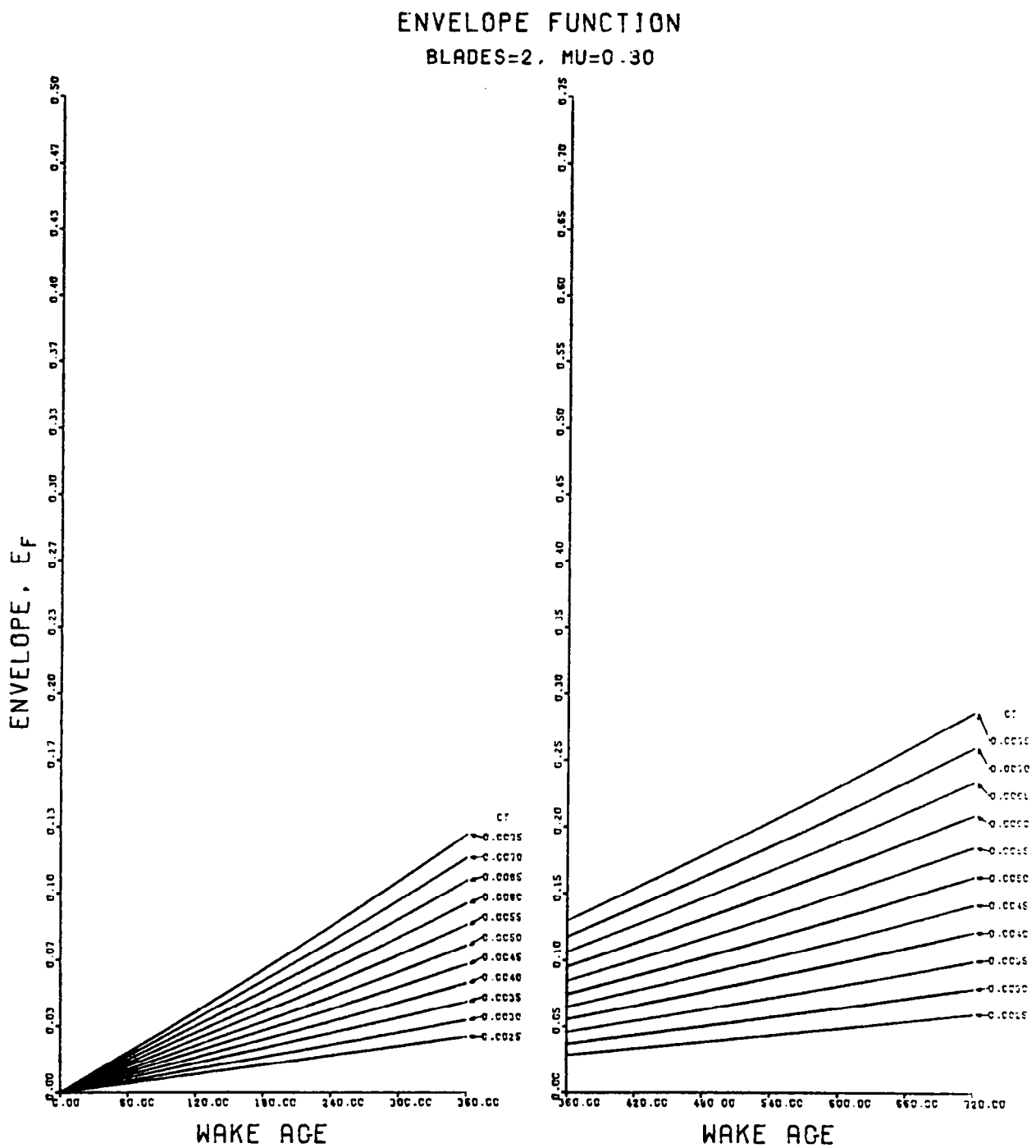

FIGURE 22E. GENERALIZED WAKE ENVELOPE FUNCTION CHARTS FOR TWO BLADES (μ = .30)

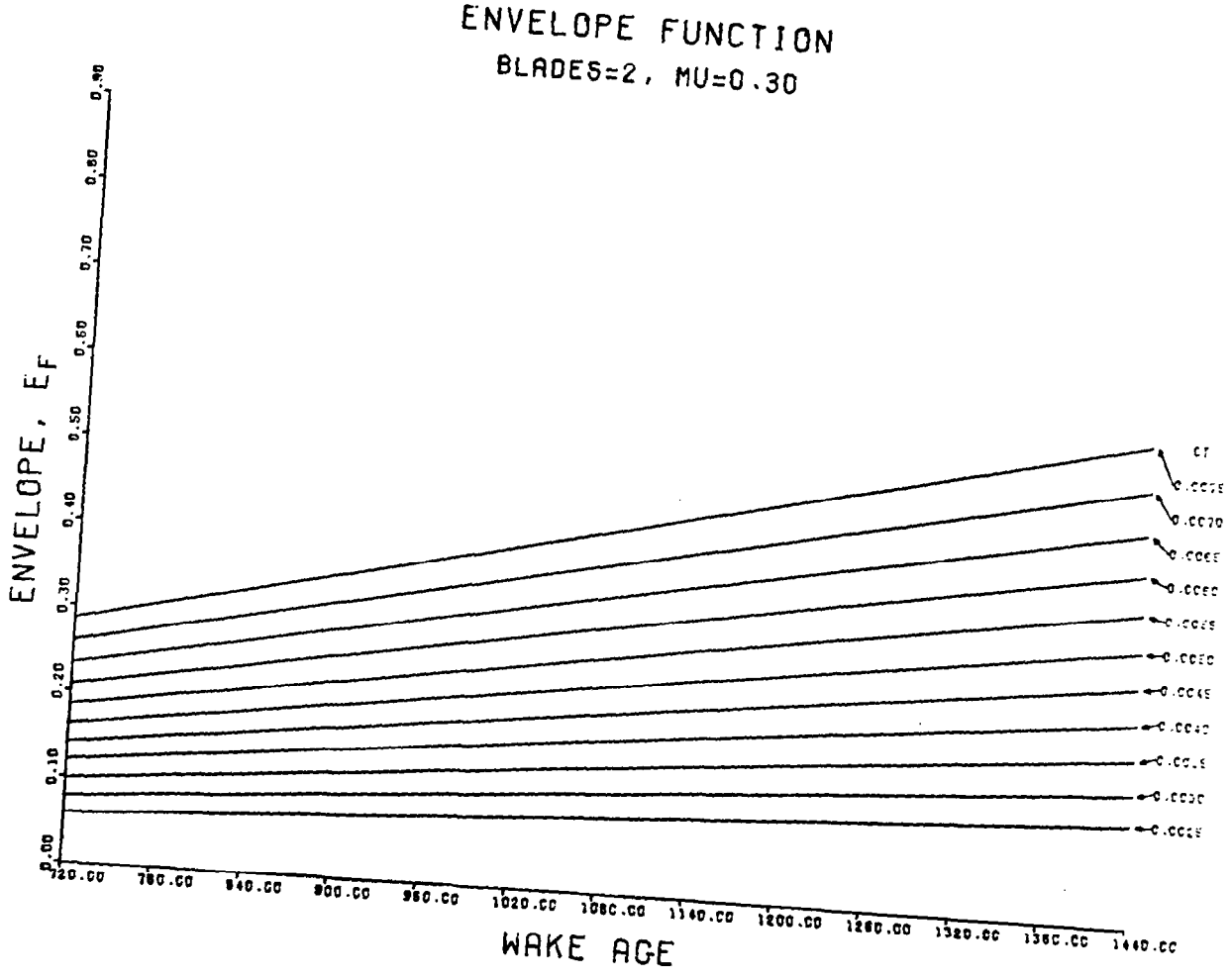

FIGURE 22E. CONTINUED

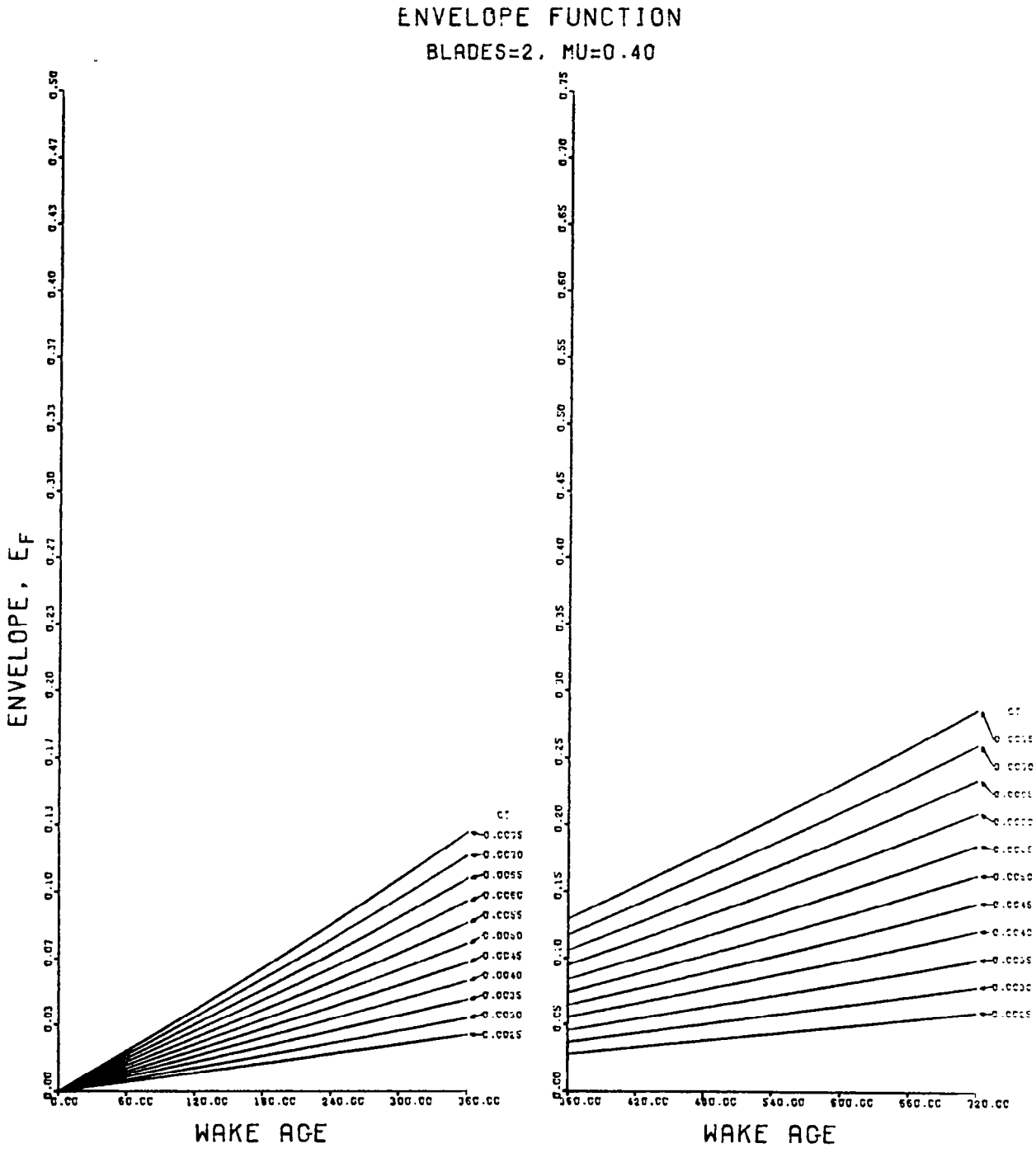

FIGURE 22F. GENERALIZED WAKE ENVELOPE FUNCTION CHARTS FOR TWO BLADES (μ = .40)

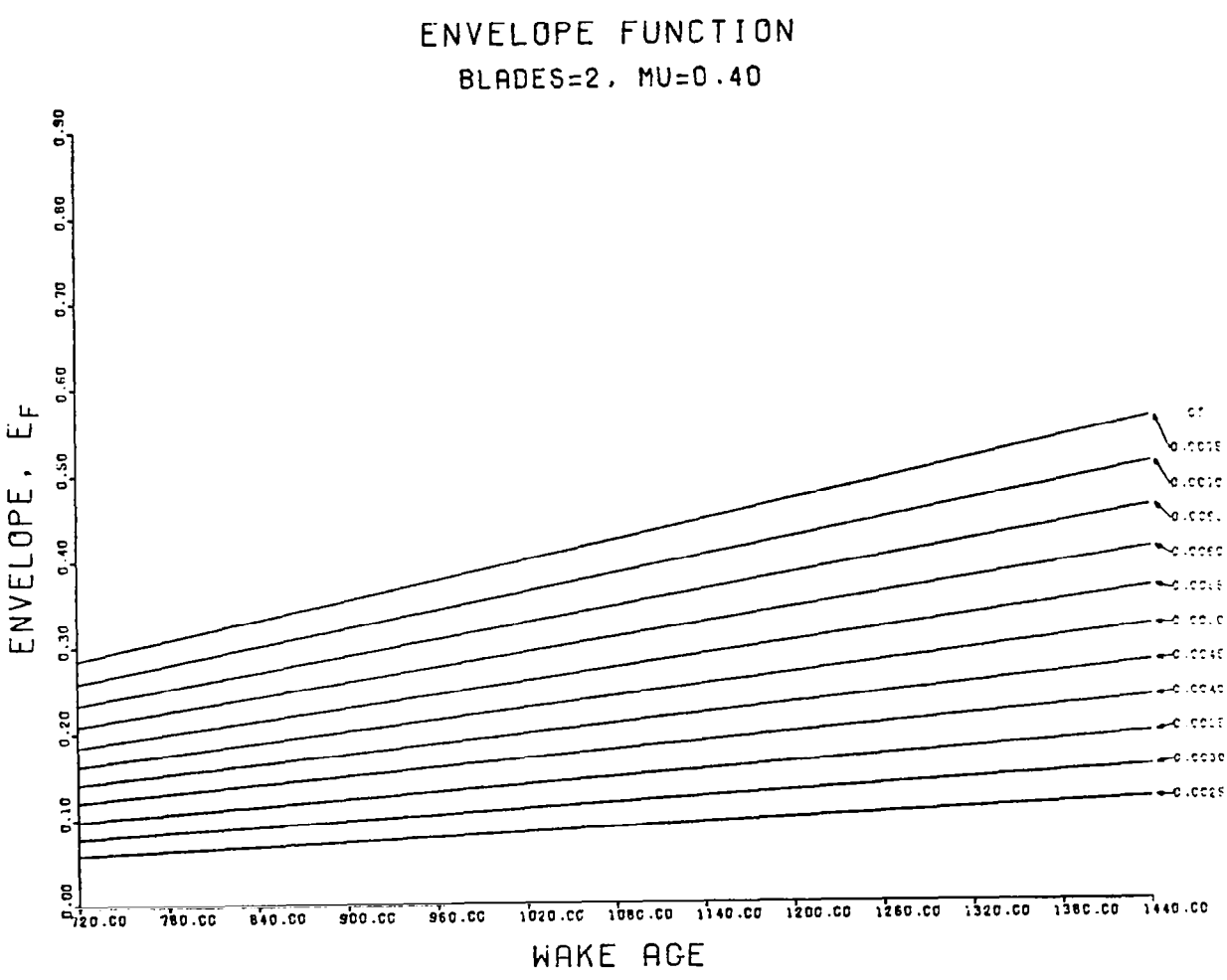

FIGURE 22F. CONTINUED

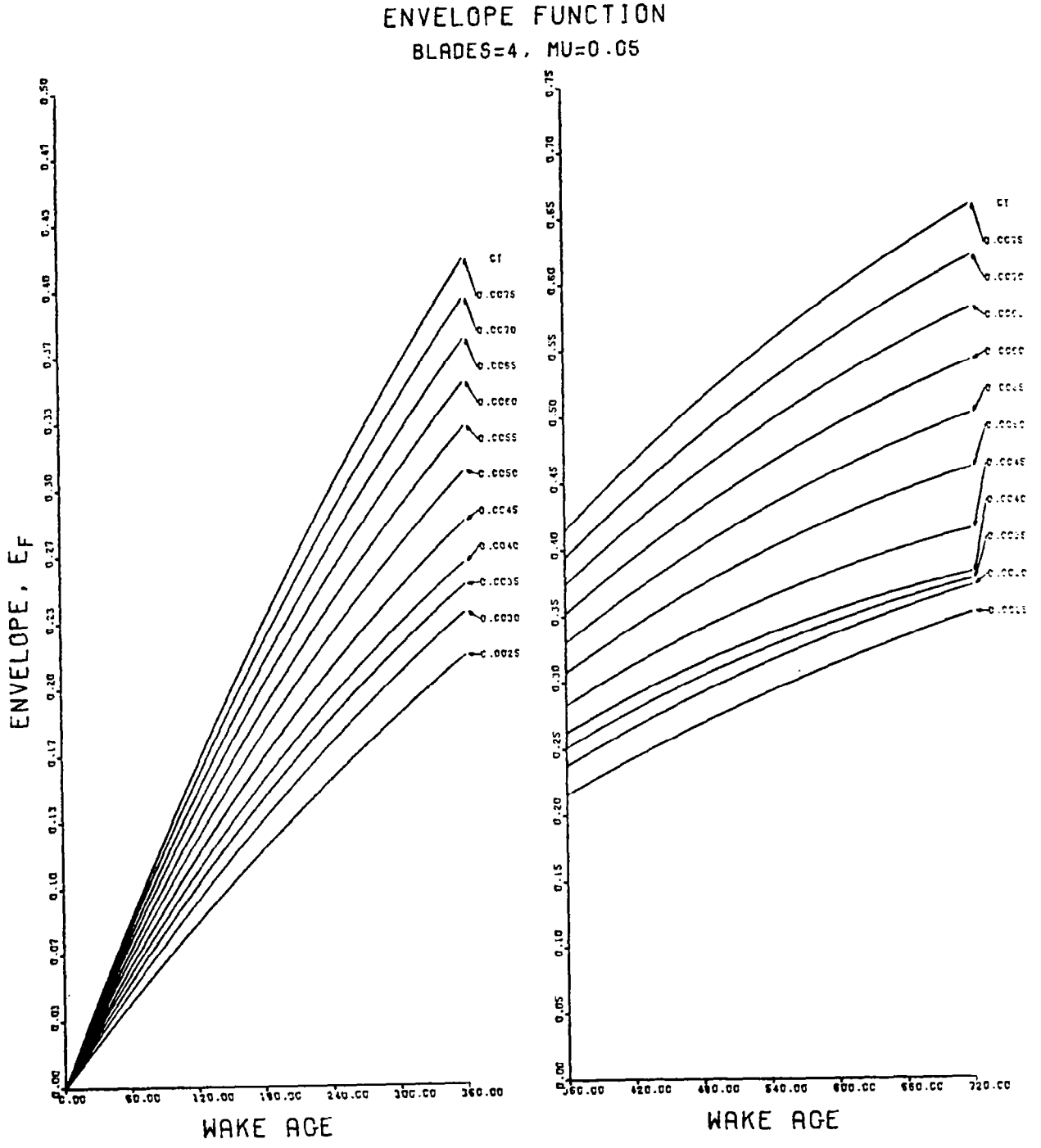

FIGURE 23A. GENERALIZED WAKE ENVELOPE FUNCTION CHARTS FOR FOUR BLADES (μ = .05)

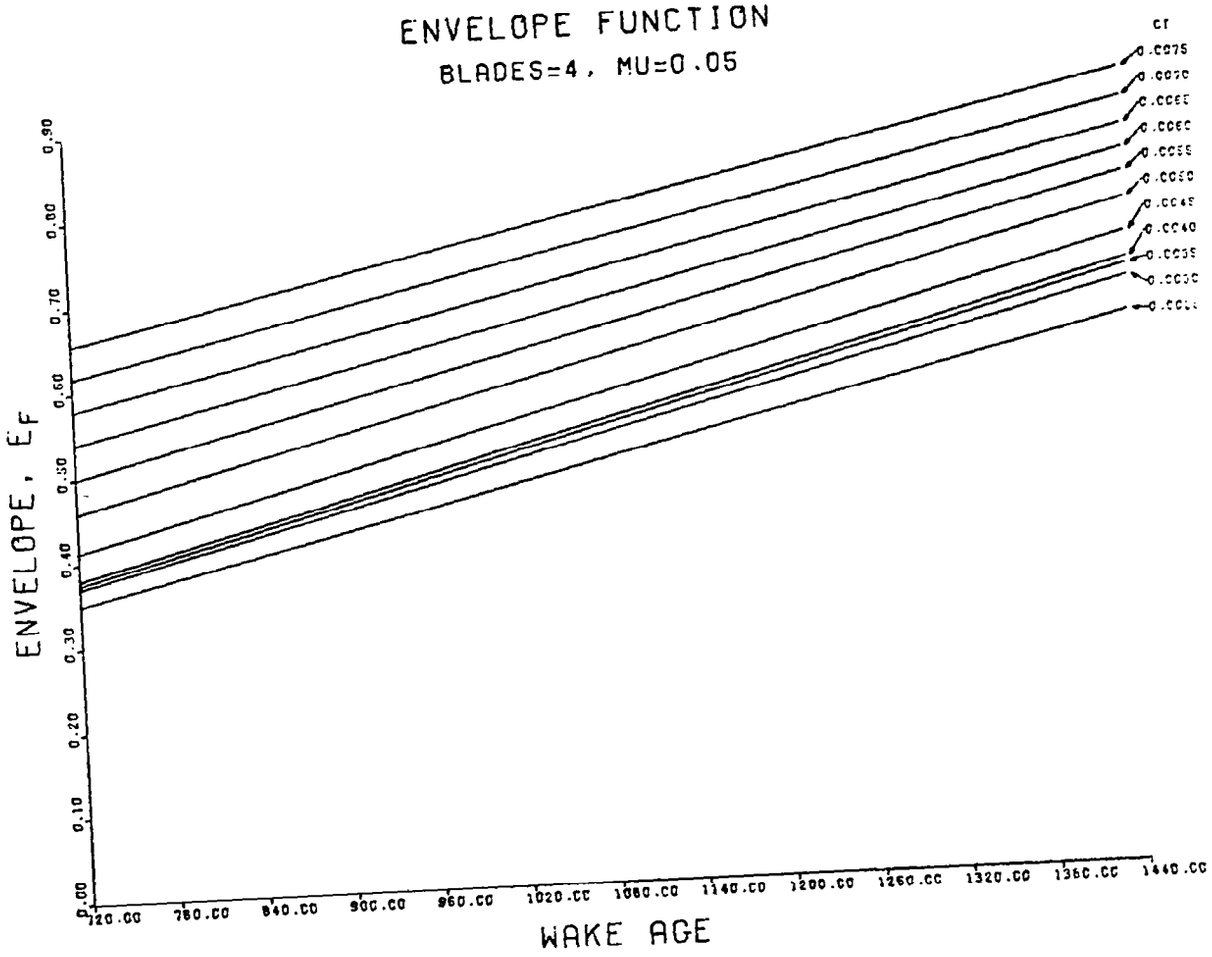

FIGURE 23A. CONTINUED

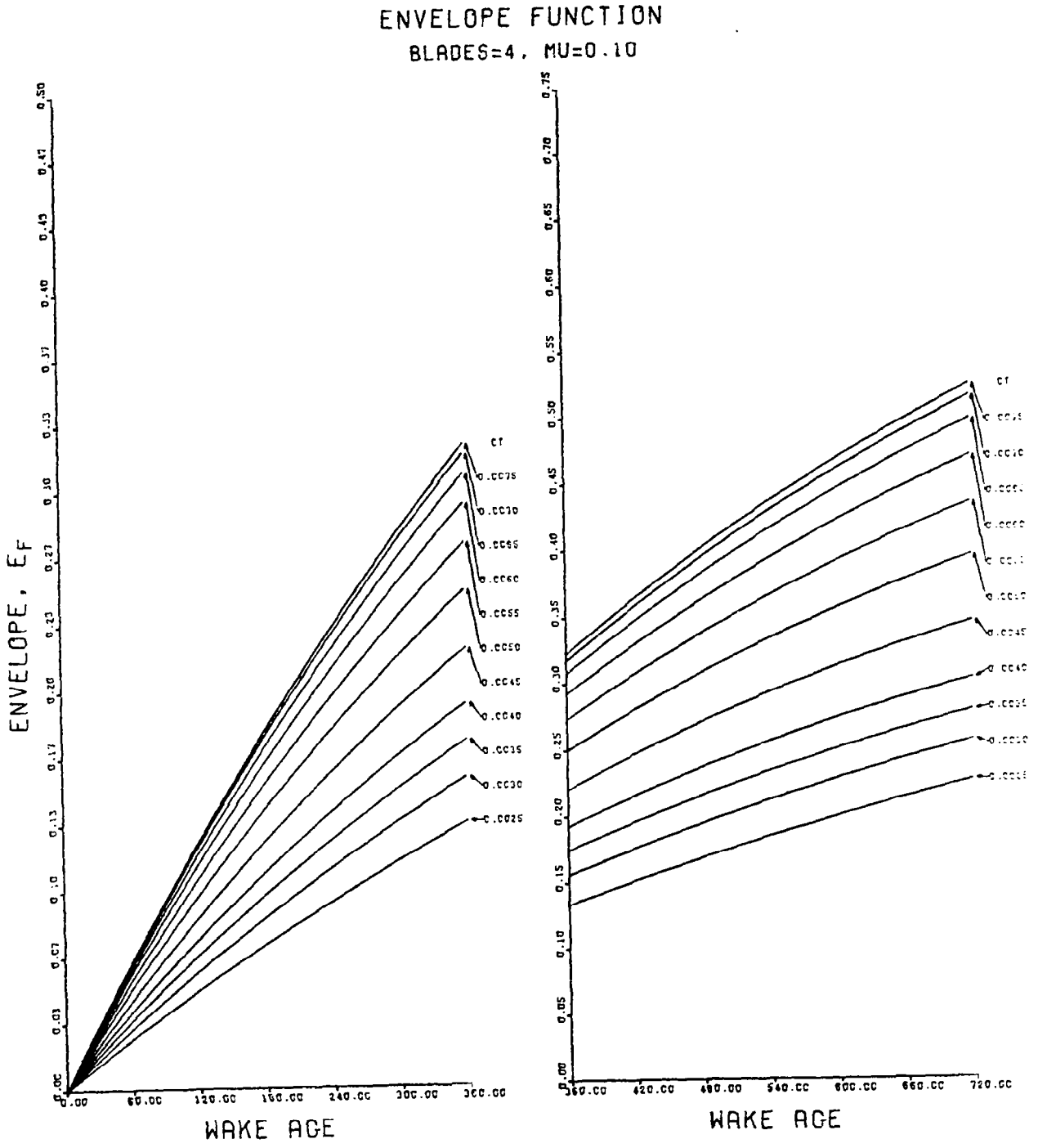

FIGURE 23B. GENERALIZED WAKE ENVELOPE FUNCTION CHARTS FOR FOUR BLADES (μ = .10)

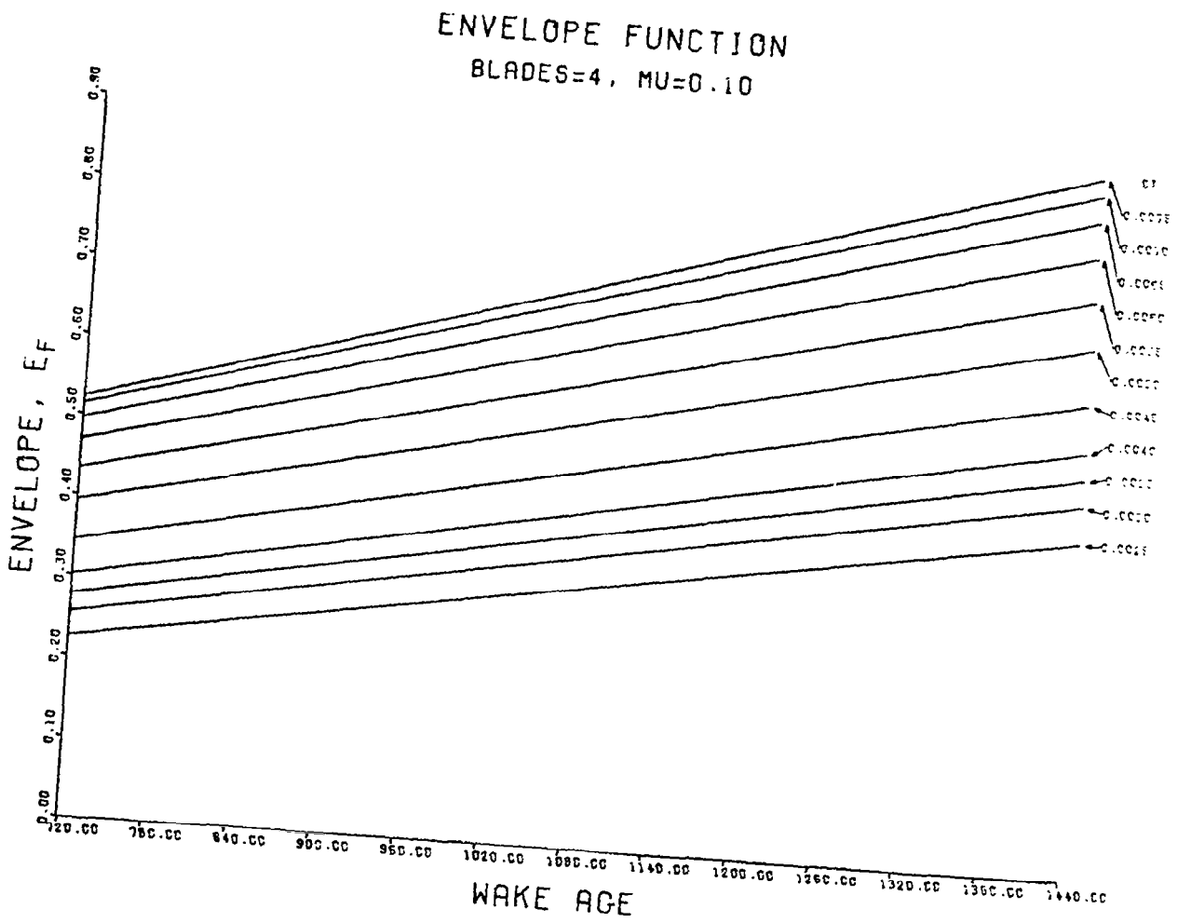

FIGURE 23B. CONTINUED

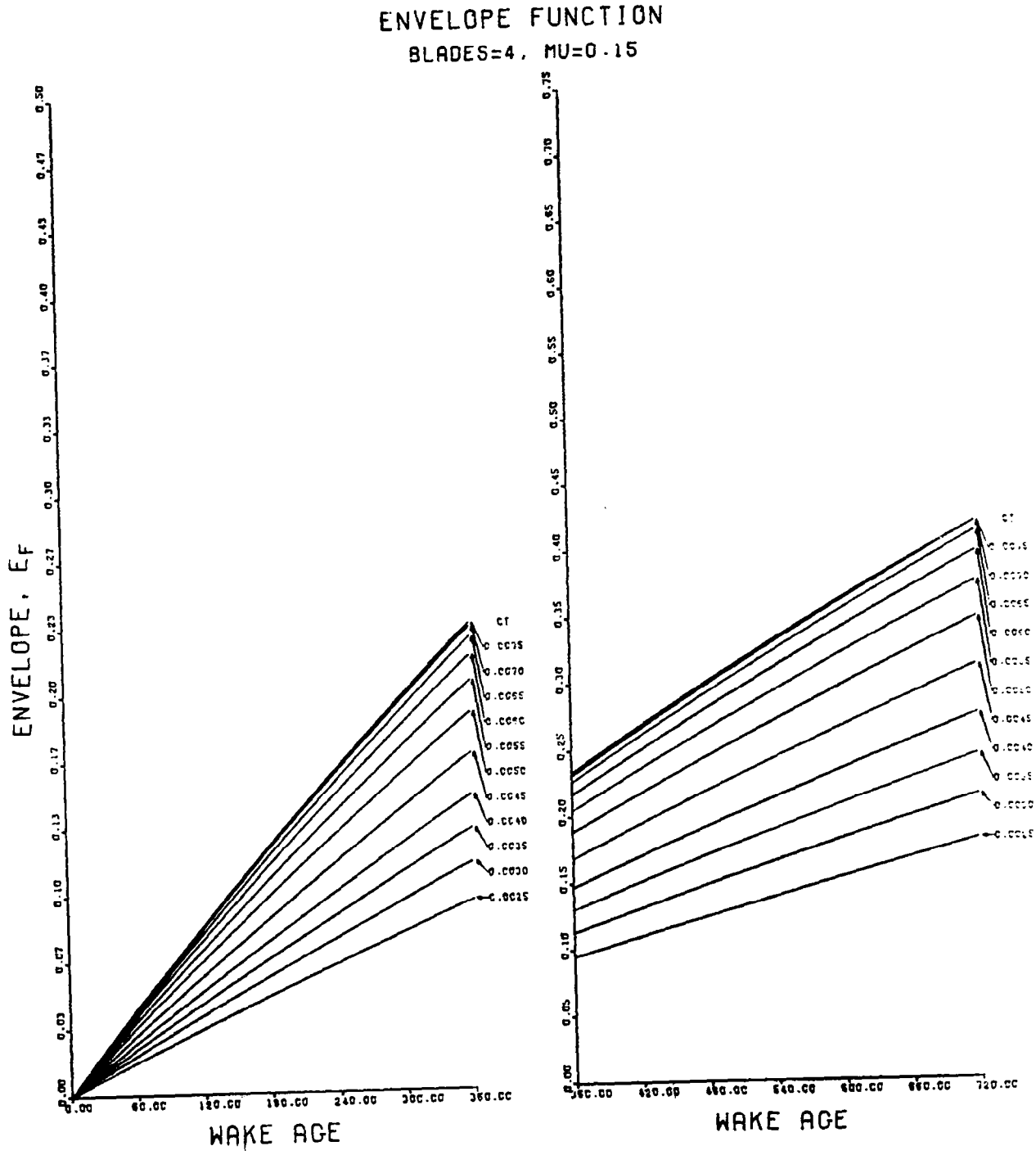

FIGURE 23C. GENERALIZED WAKE ENVELOPE FUNCTION CHARTS FOR FOUR BLADES (μ = .15)

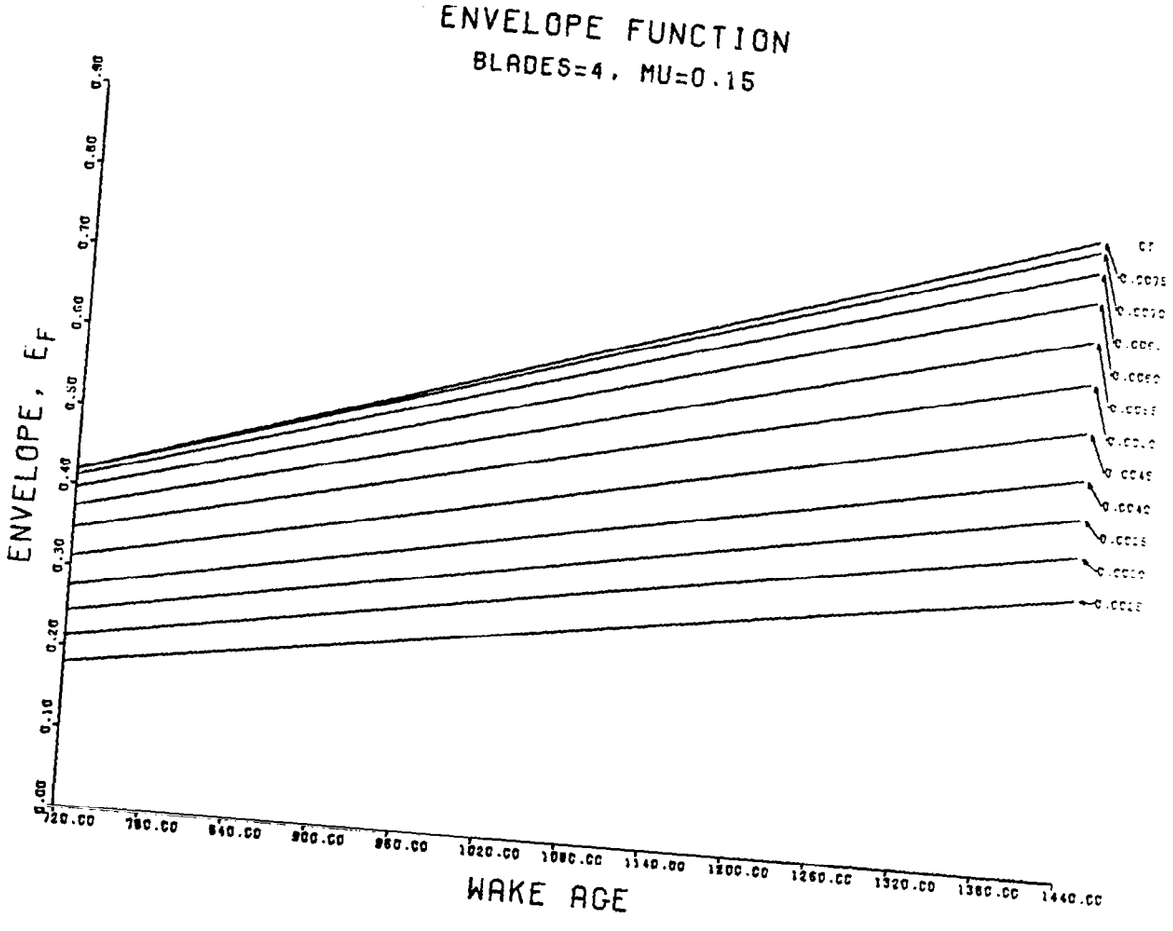

FIGURE 23C. CONTINUED

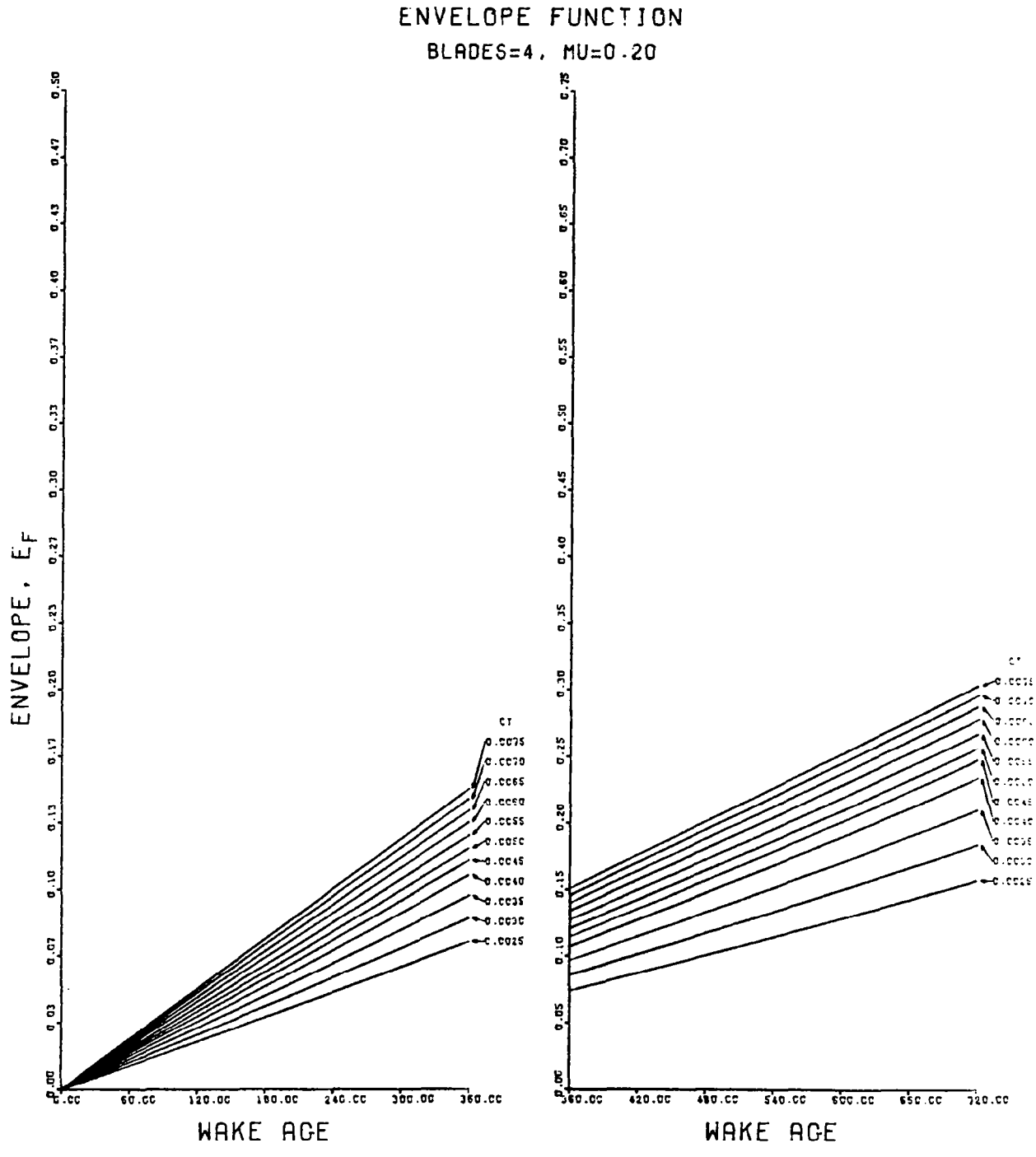

FIGURE 23D. GENERALIZED WAKE ENVELOPE FUNCTION CHARTS FOR FOUR BLADES (μ = .20)

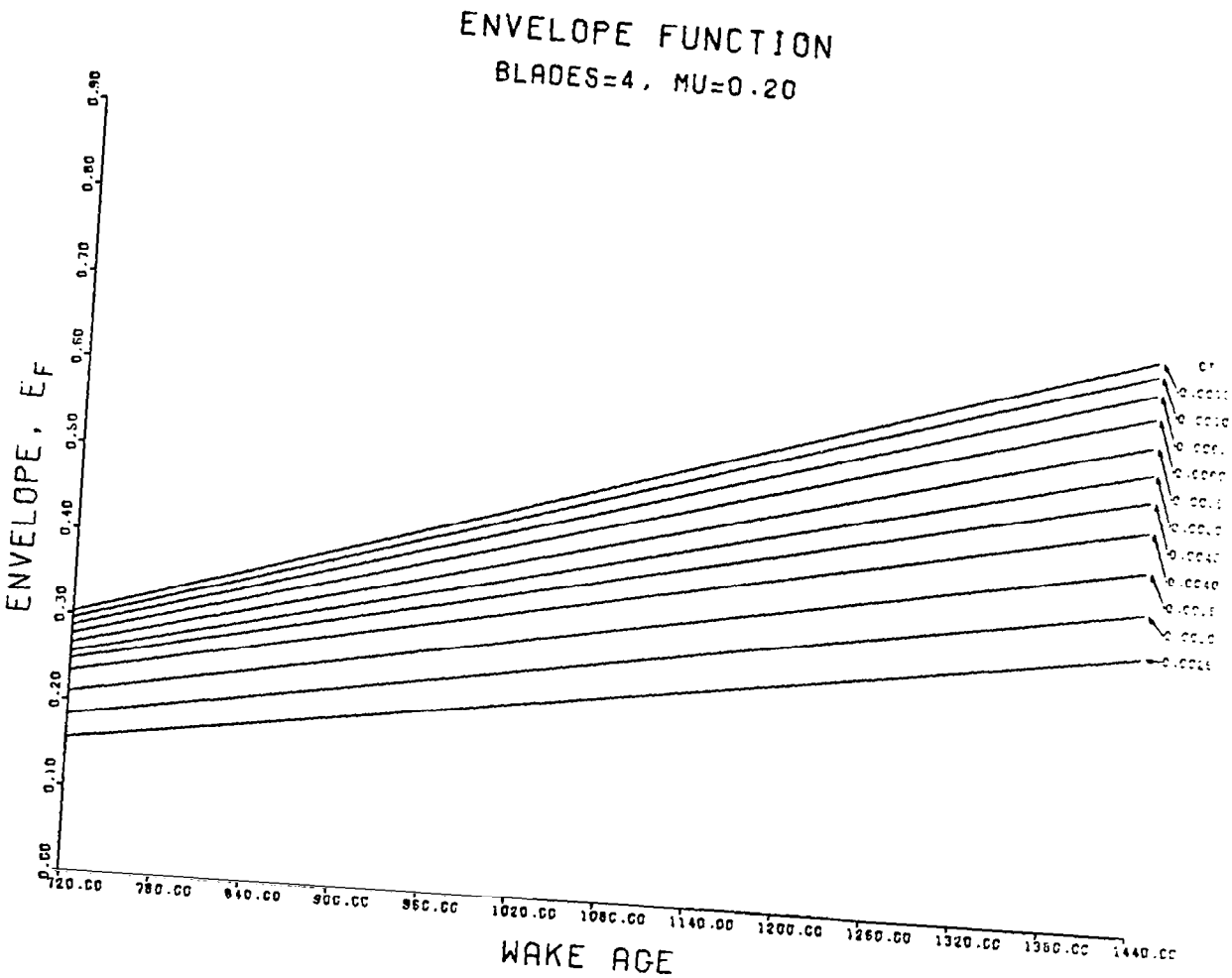

FIGURE 23D. CONTINUED

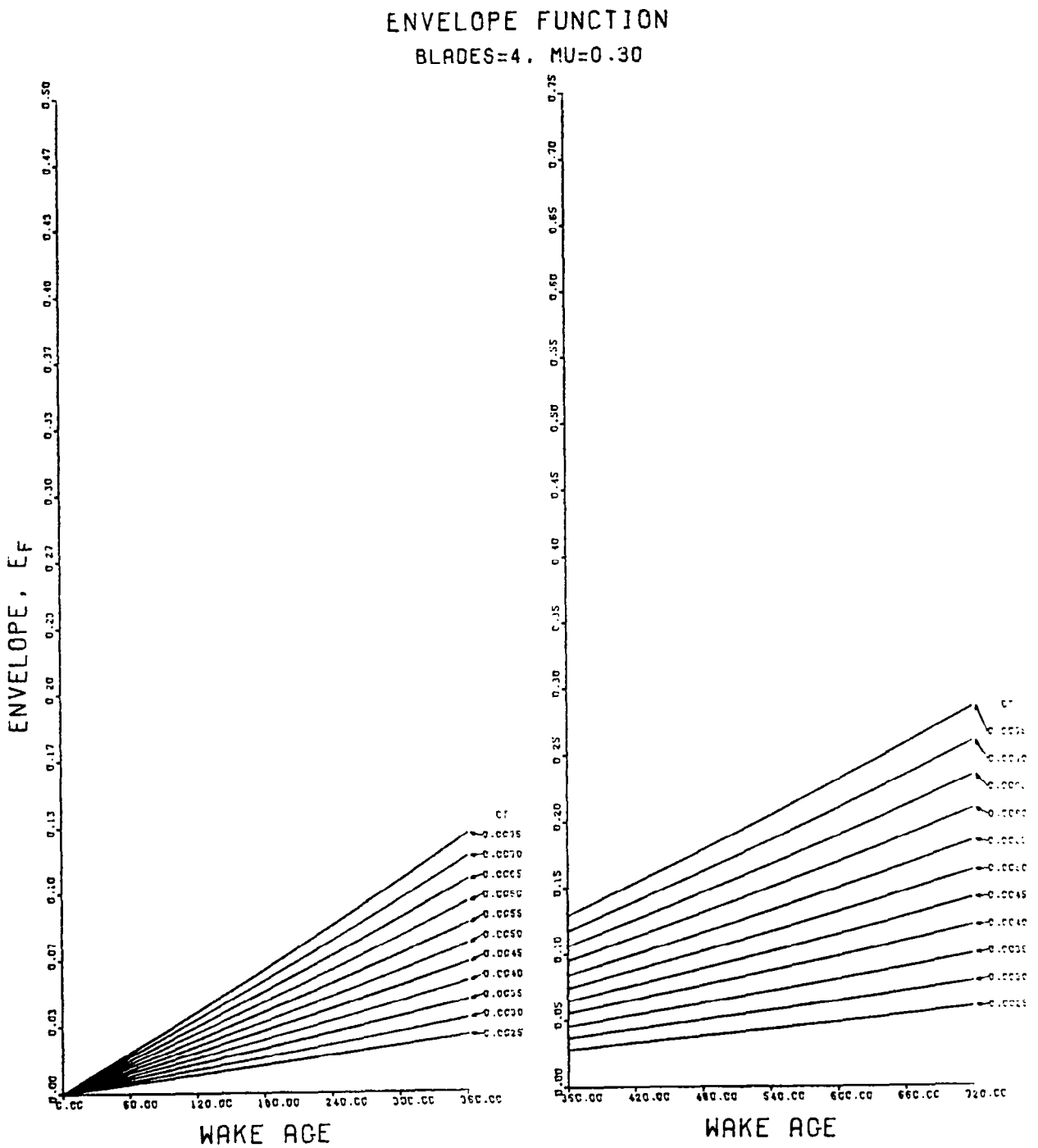

FIGURE 23E. GENERALIZED WAKE ENVELOPE FUNCTION CHARTS FOR FOUR BLADES (μ = .30)

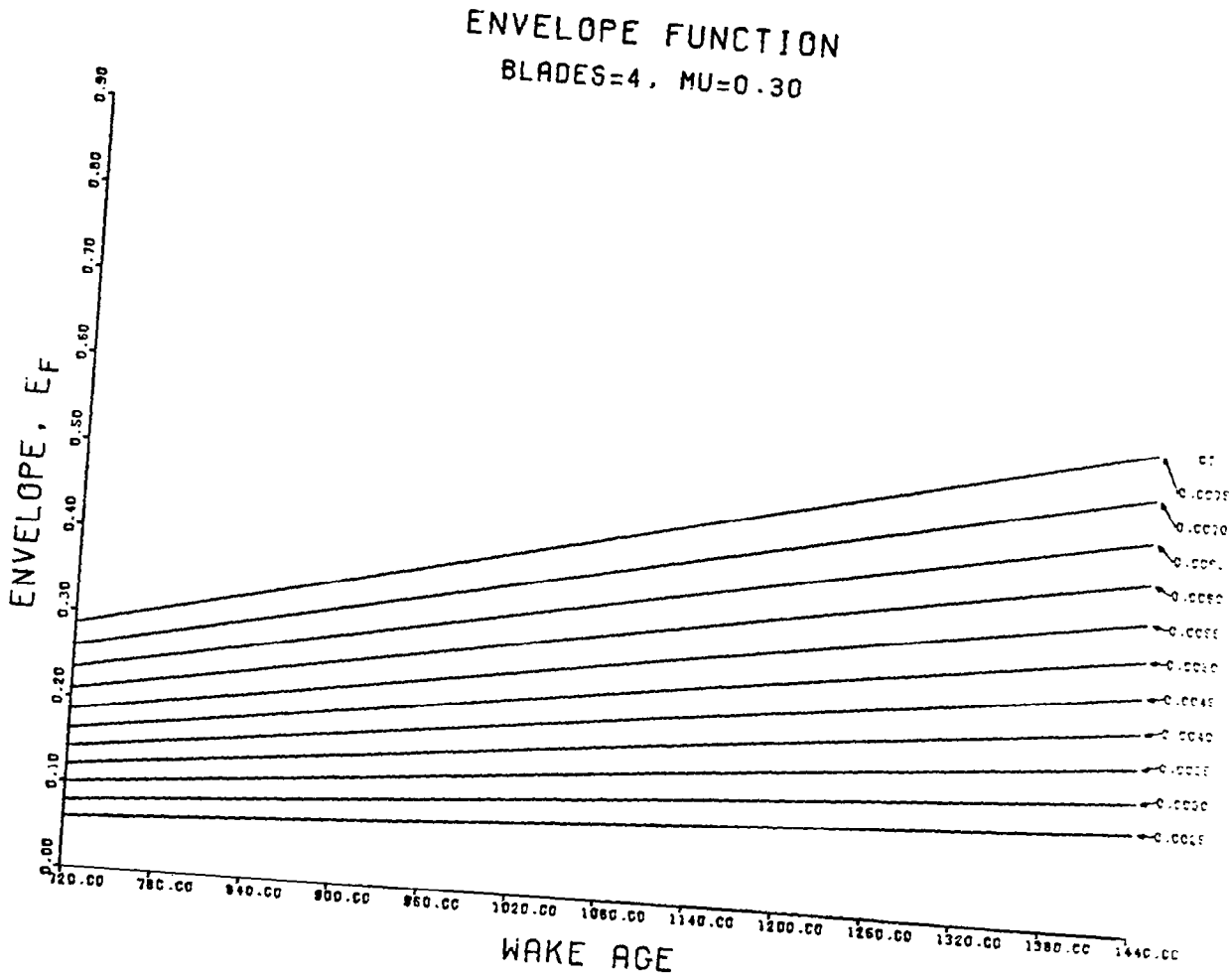

FIGURE 23E. CONTINUED

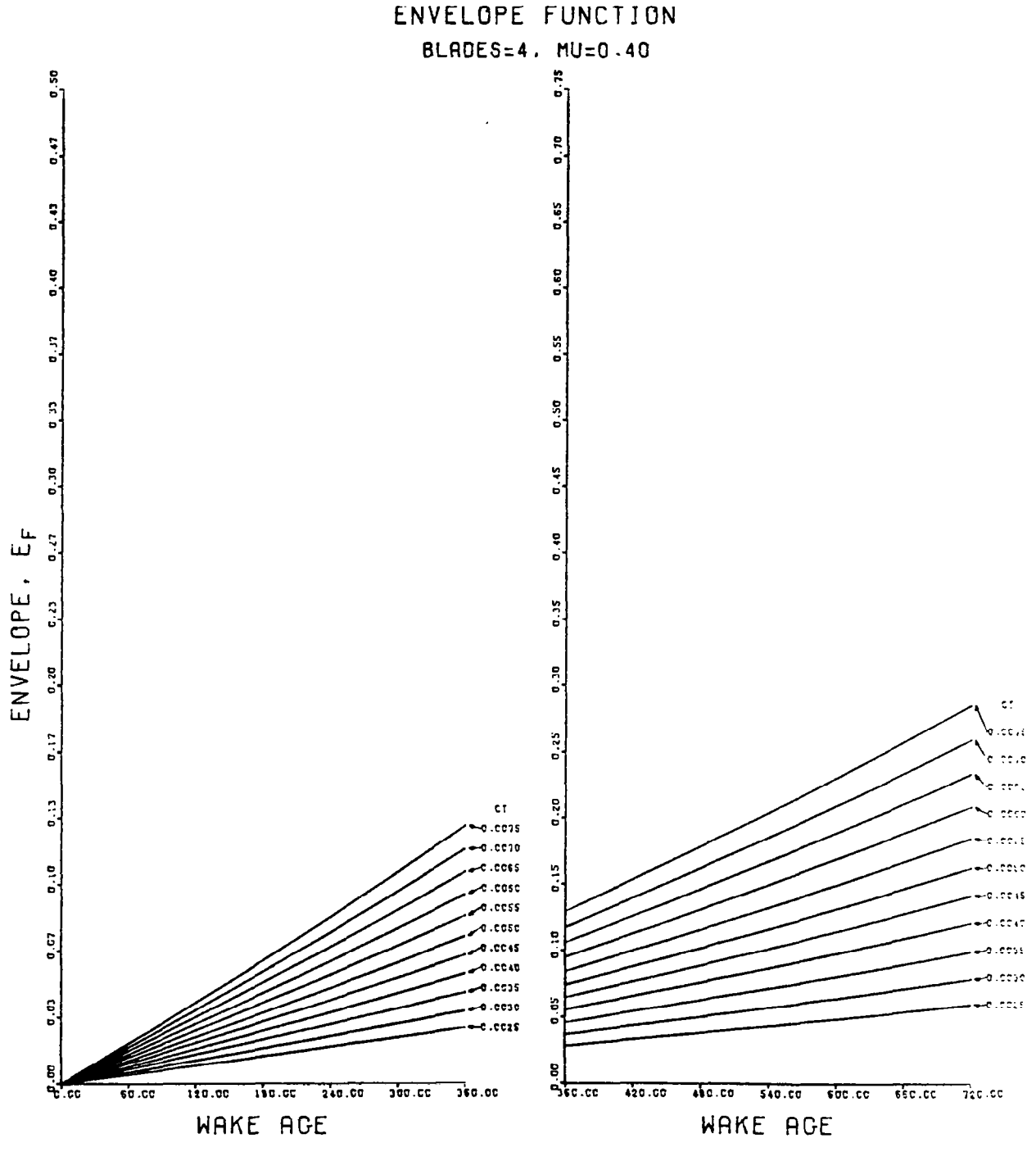

FIGURE 23F. GENERALIZED WAKE ENVELOPE FUNCTION CHARTS FOR FOUR BLADES (μ = .40)

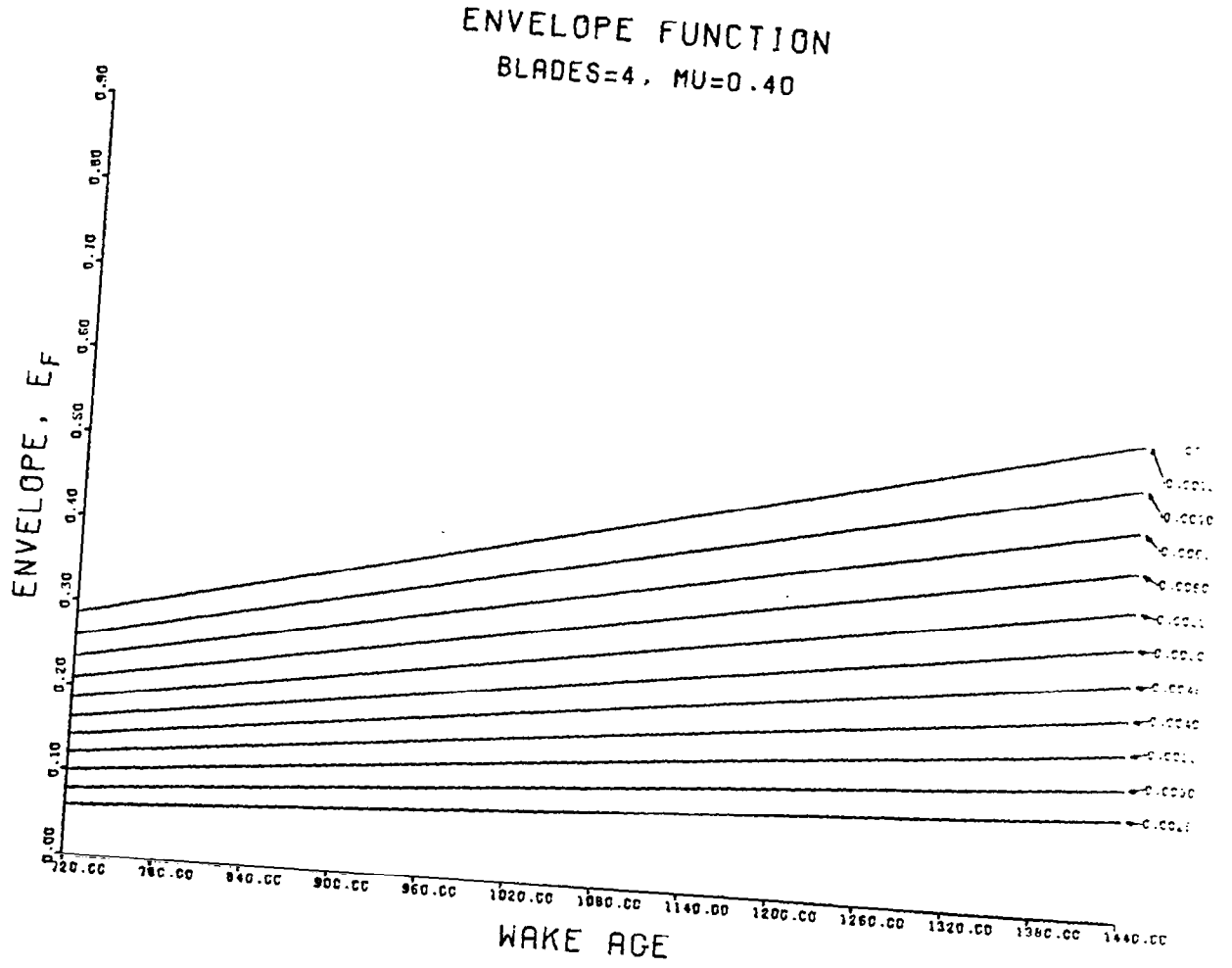

FIGURE 23F. CONTINUED

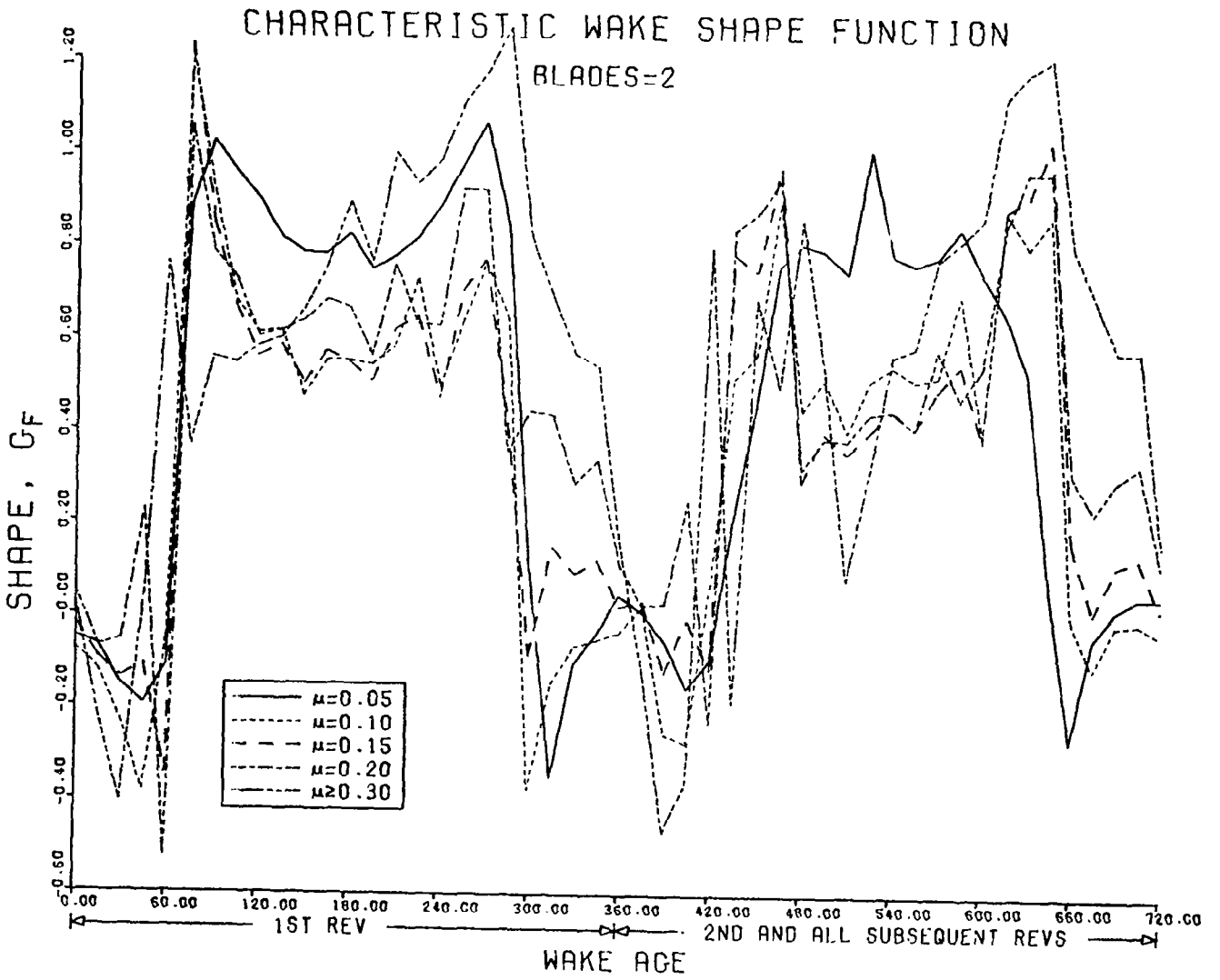

FIGURE 24. GENERALIZED WAKE SHAPE FUNCTION CHART FOR TWO BLADES

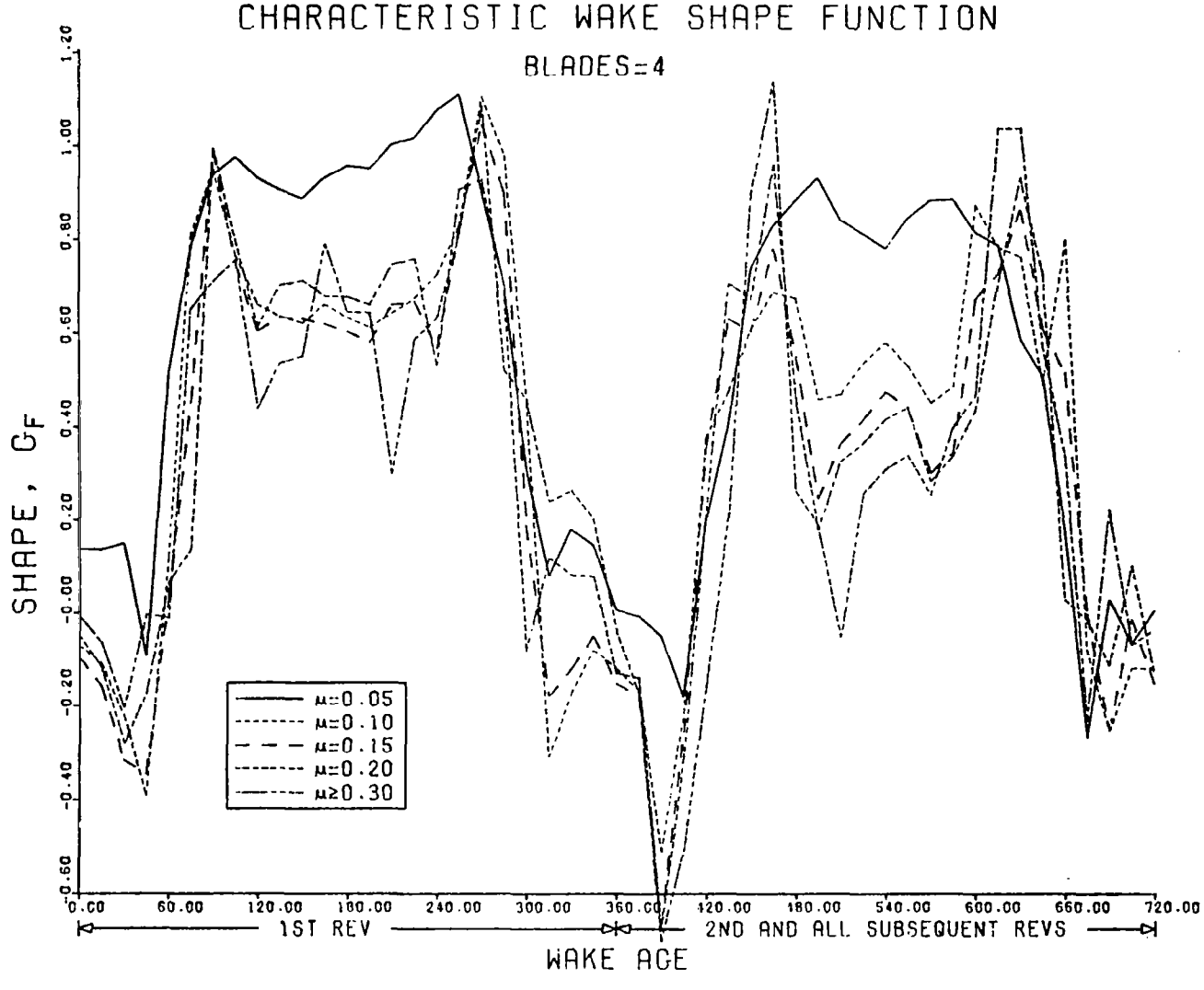

FIGURE 25. GENERALIZED WAKE SHAPE FUNCTION CHART FOR FOUR BLADES

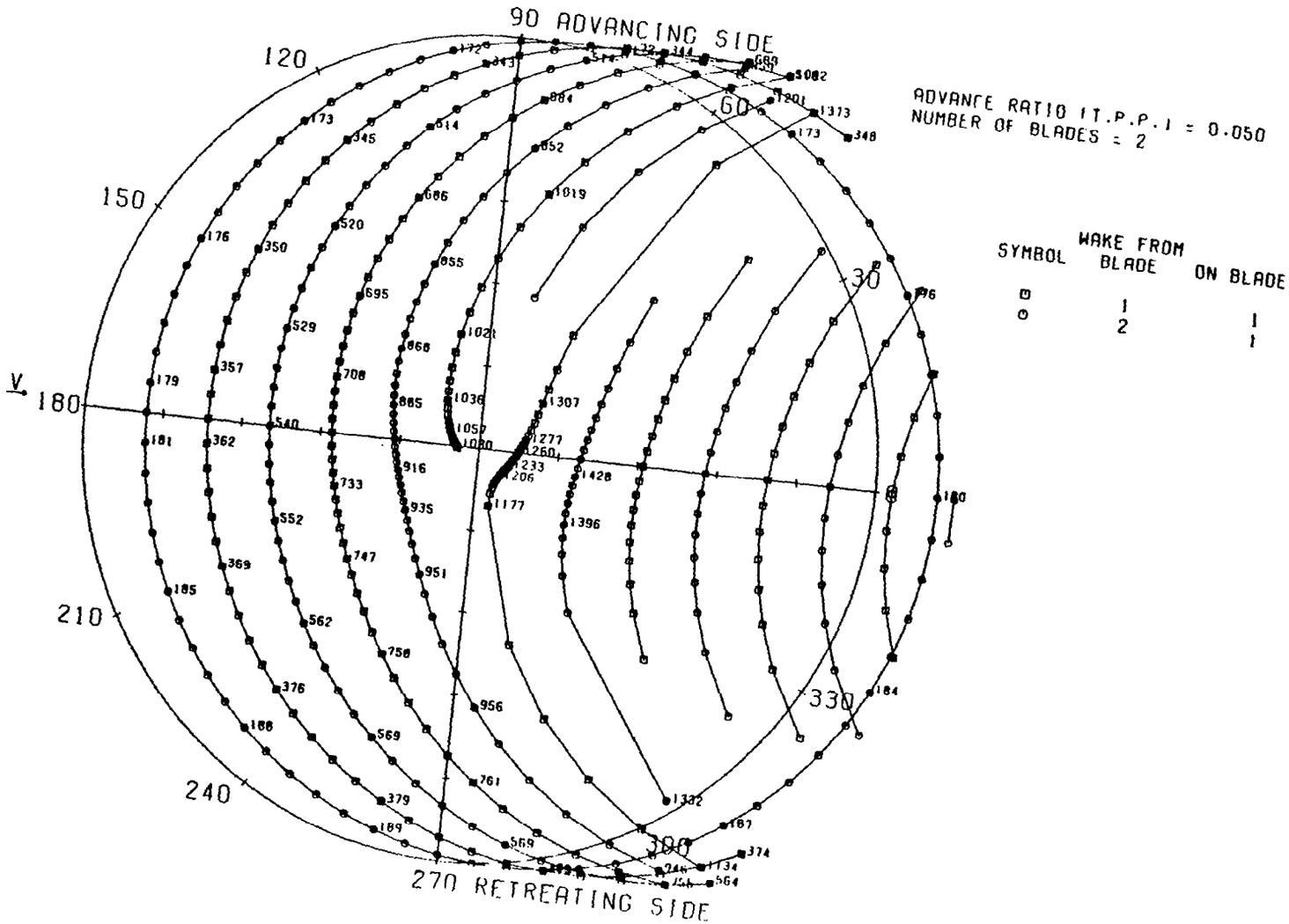

FIGURE 26A. POTENTIAL BLADE/TIP VORTEX INTERSECTION PLOT FOR TWO BLADES (POLAR FORMAT), μ = .05

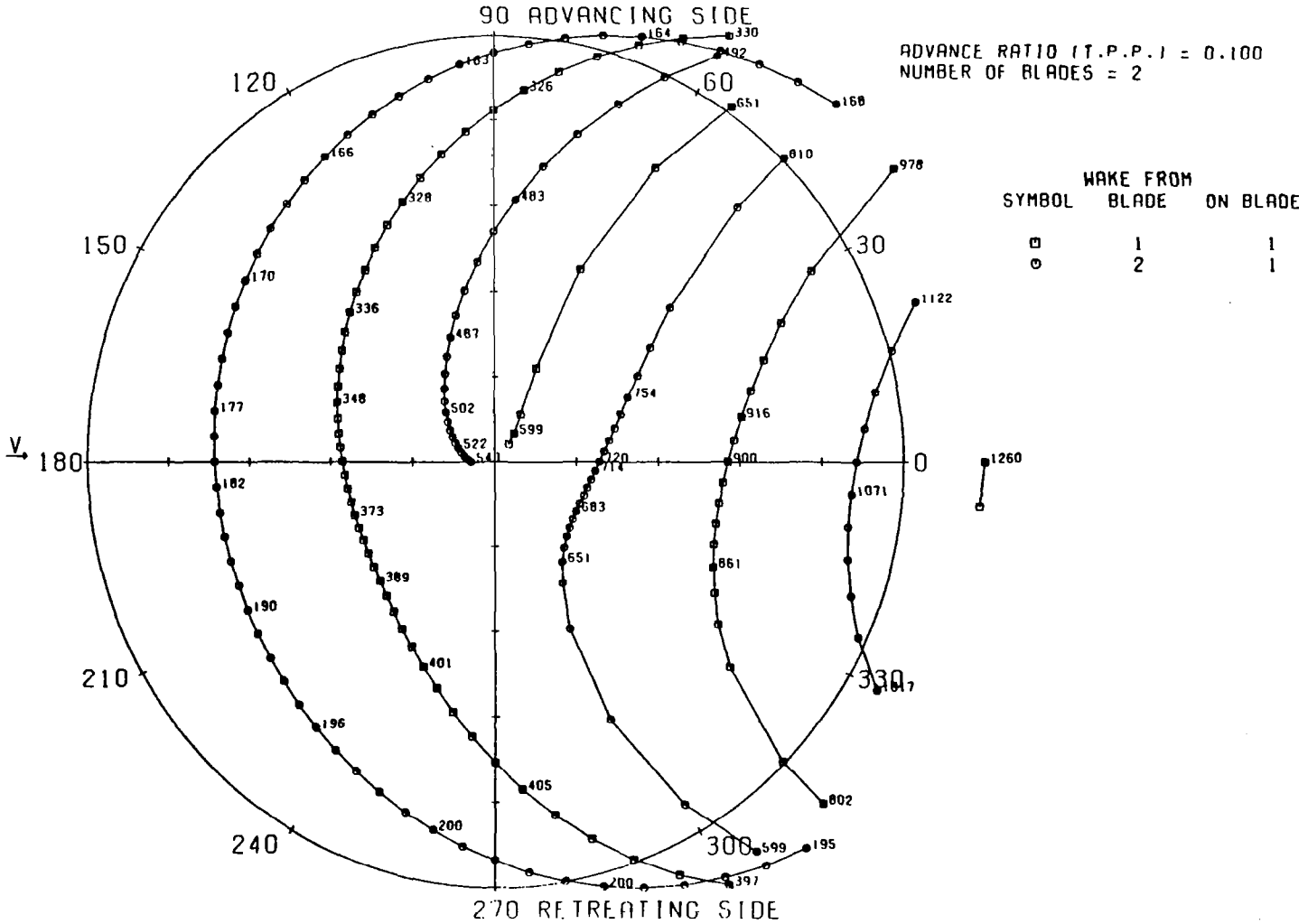

FIGURE 26B. POTENTIAL BLADE/TIP VORTEX INTERSECTION PLOT FOR TWO BLADES (POLAR FORMAT), μ = .10

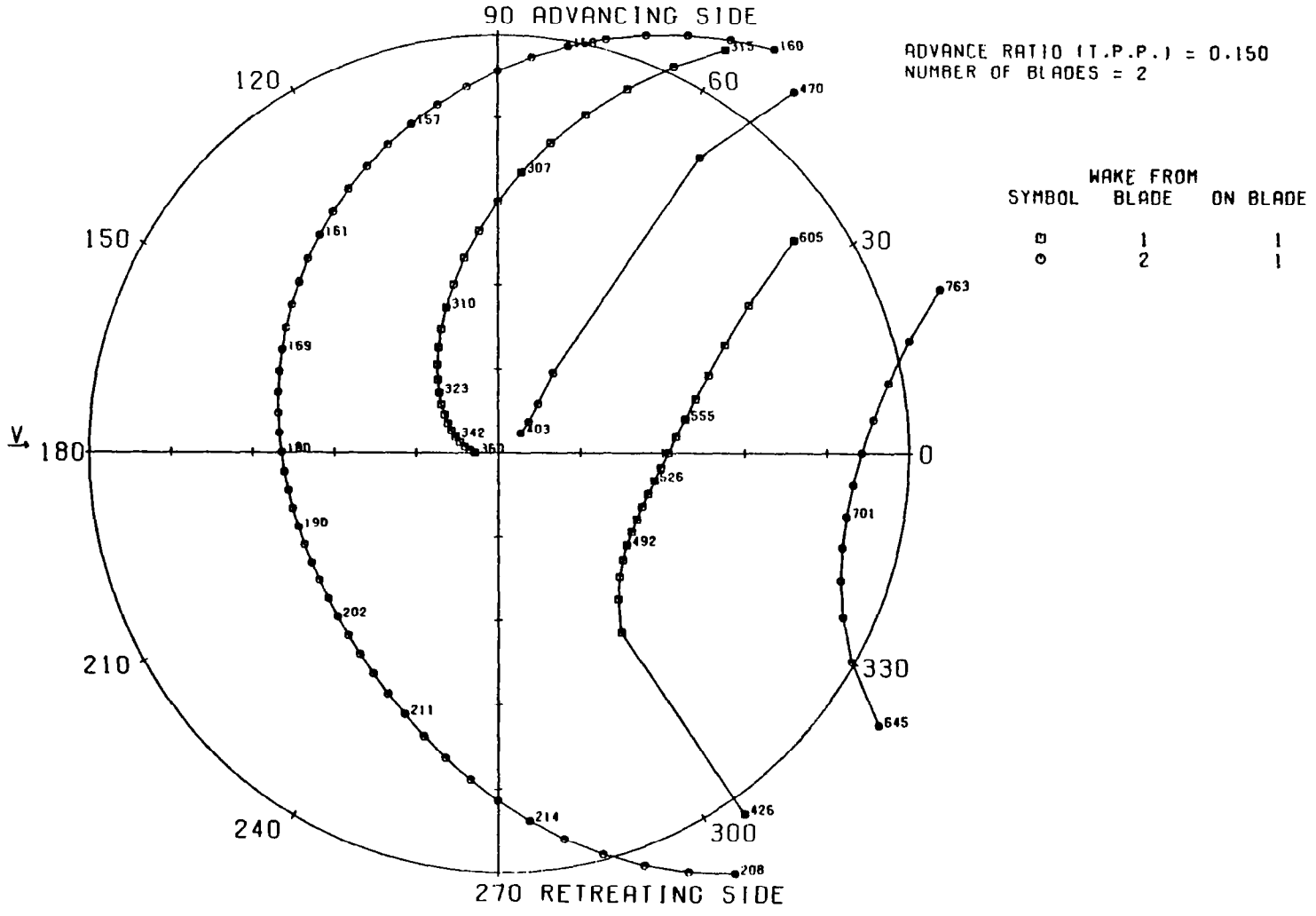

FIGURE 26C. POTENTIAL BLADE/TIP VORTEX INTERSECTION PLOT FOR TWO BLADES (POLAR FORMAT), μ = .15

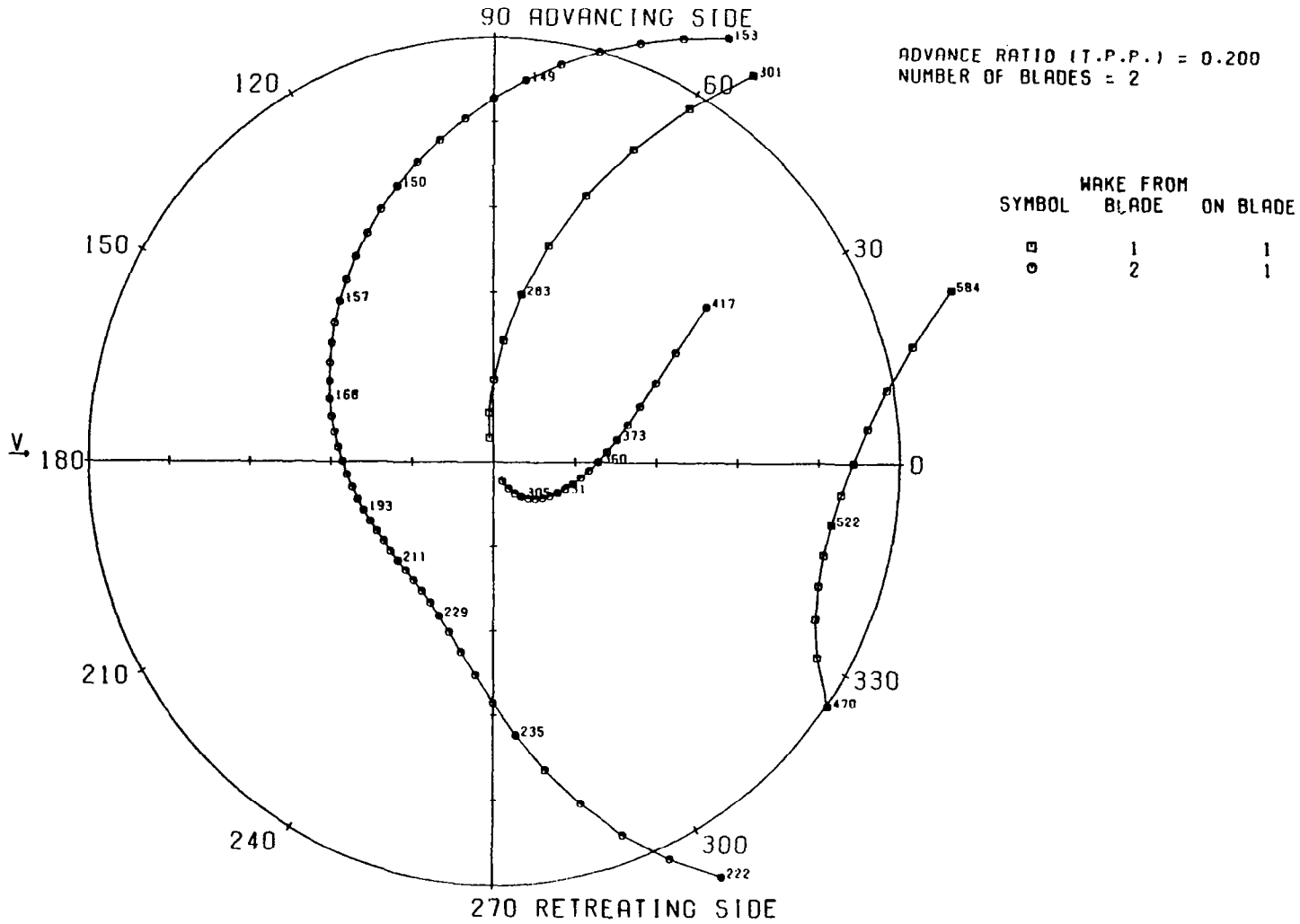

FIGURE 26D. POTENTIAL BLADE/TIP VORTEX INTERSECTION PLOT FOR TWO BLADES (POLAR FORMAT), μ = .20

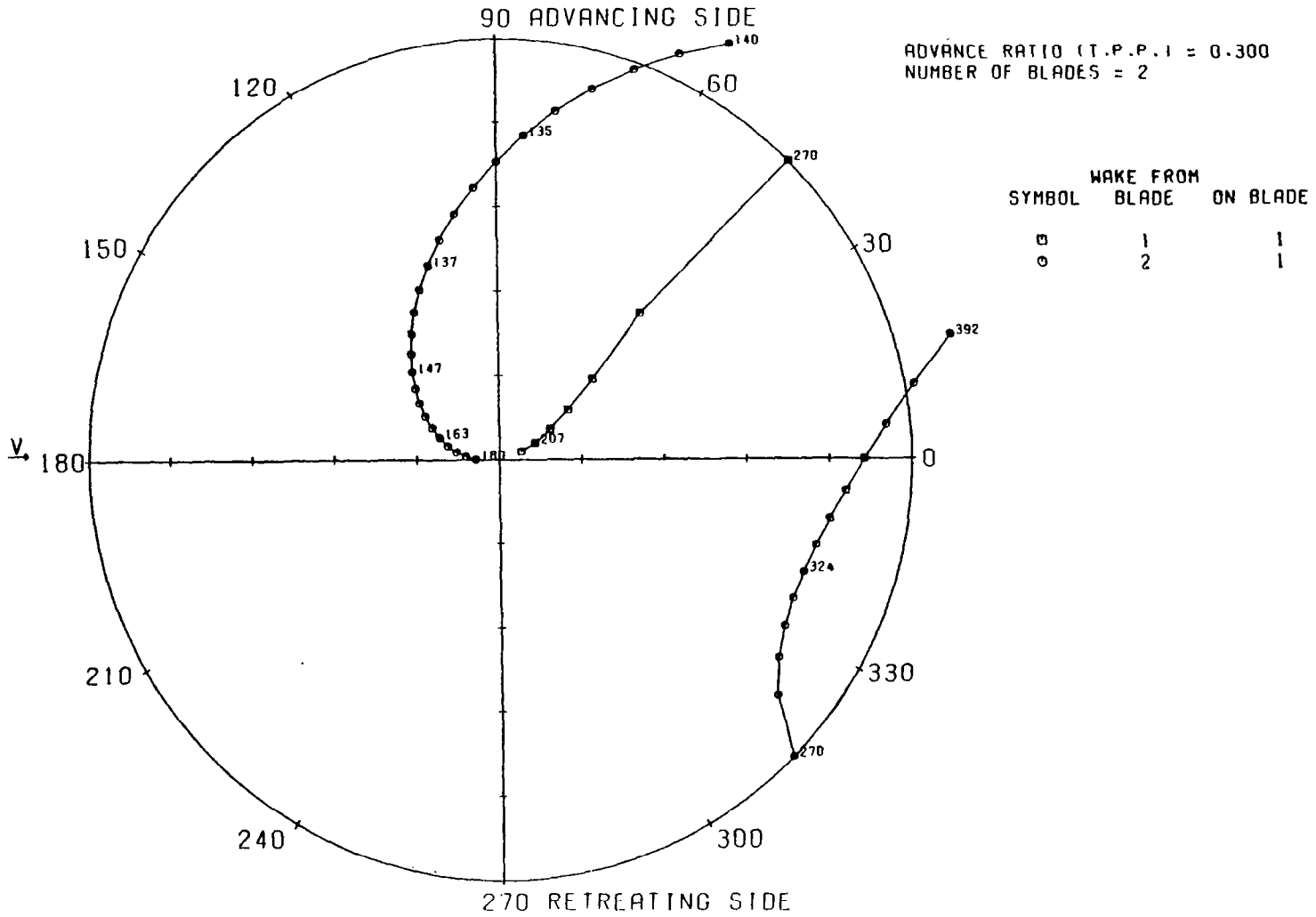

FIGURE 26E. POTENTIAL BLADE/TIP VORTEX INTERSECTION PLOT FOR TWO BLADES (POLAR FORMAT), μ = .30

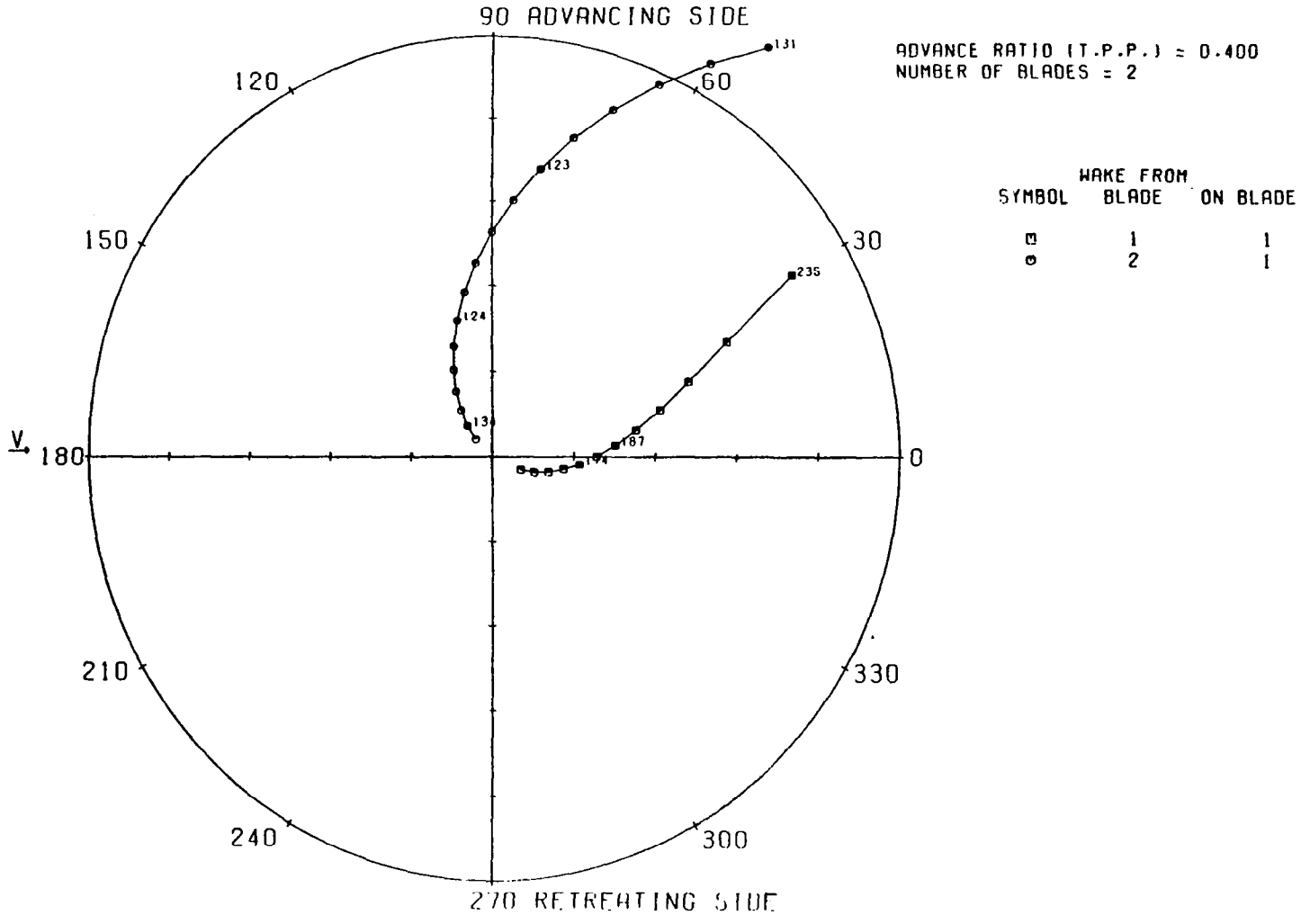

FIGURE 26F. POTENTIAL BLADE/TIP VORTEX INTERSECTION PLOT FOR TWO BLADES (POLAR FORMAT), μ = .40

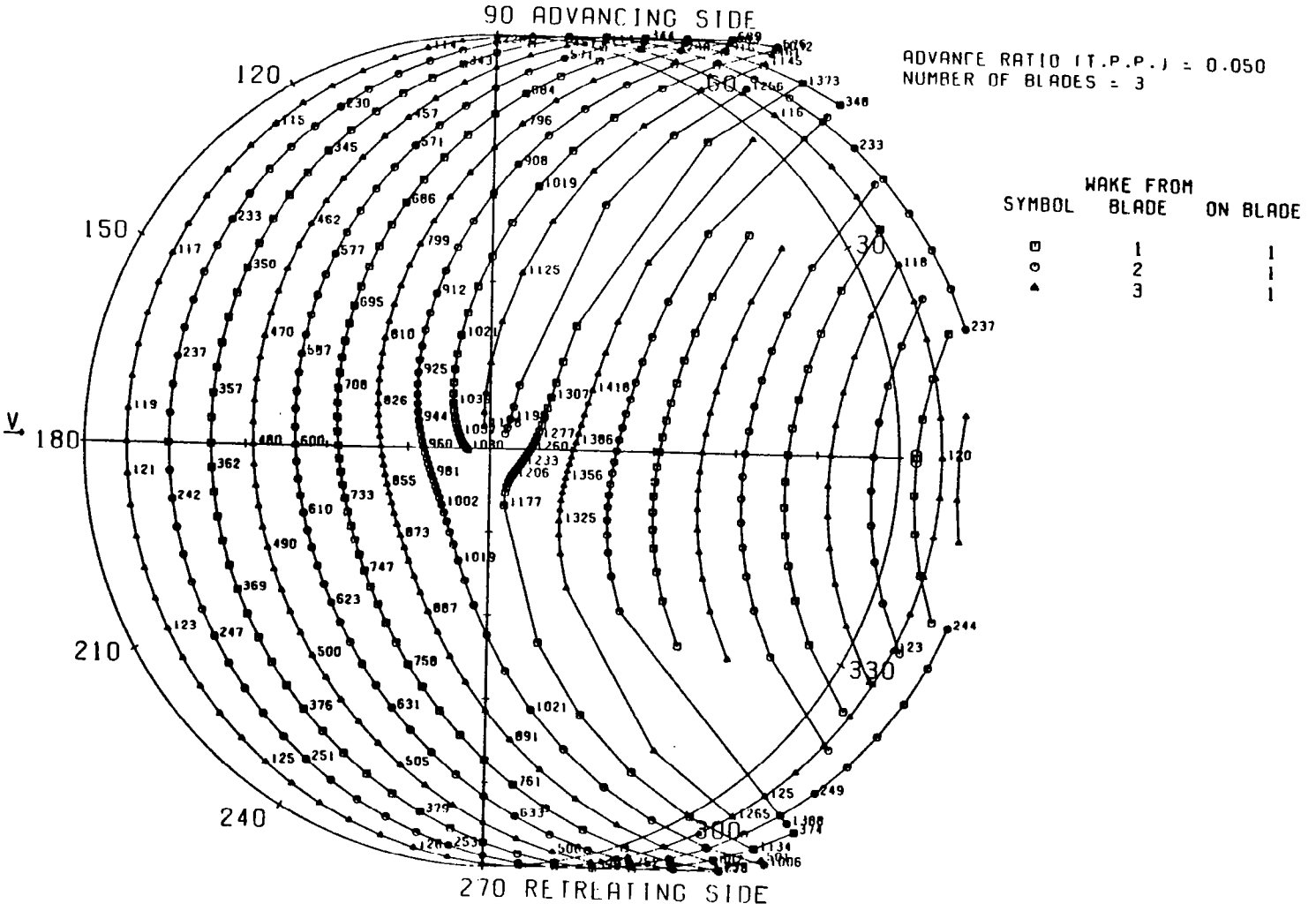

FIGURE 27A. POTENTIAL BLADE/TIP VORTEX INTERSECTION PLOT FOR THREE BLADES (POLAR FORMAT), μ = .05

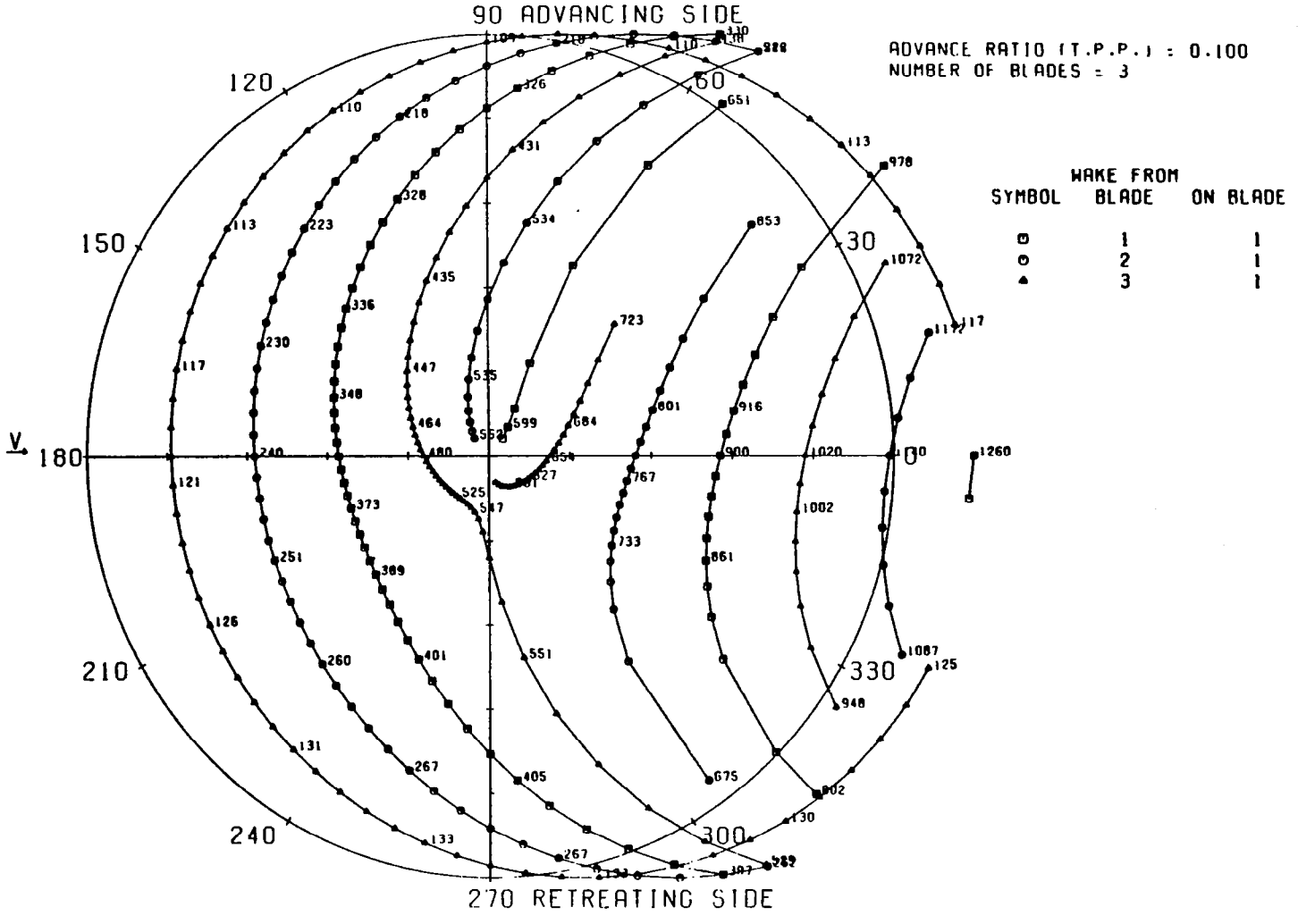

FIGURE 27B. POTENTIAL BLADE/TIP VORTEX INTERSECTION PLOT FOR THREE BLADES (POLAR FORMAT), μ = .10

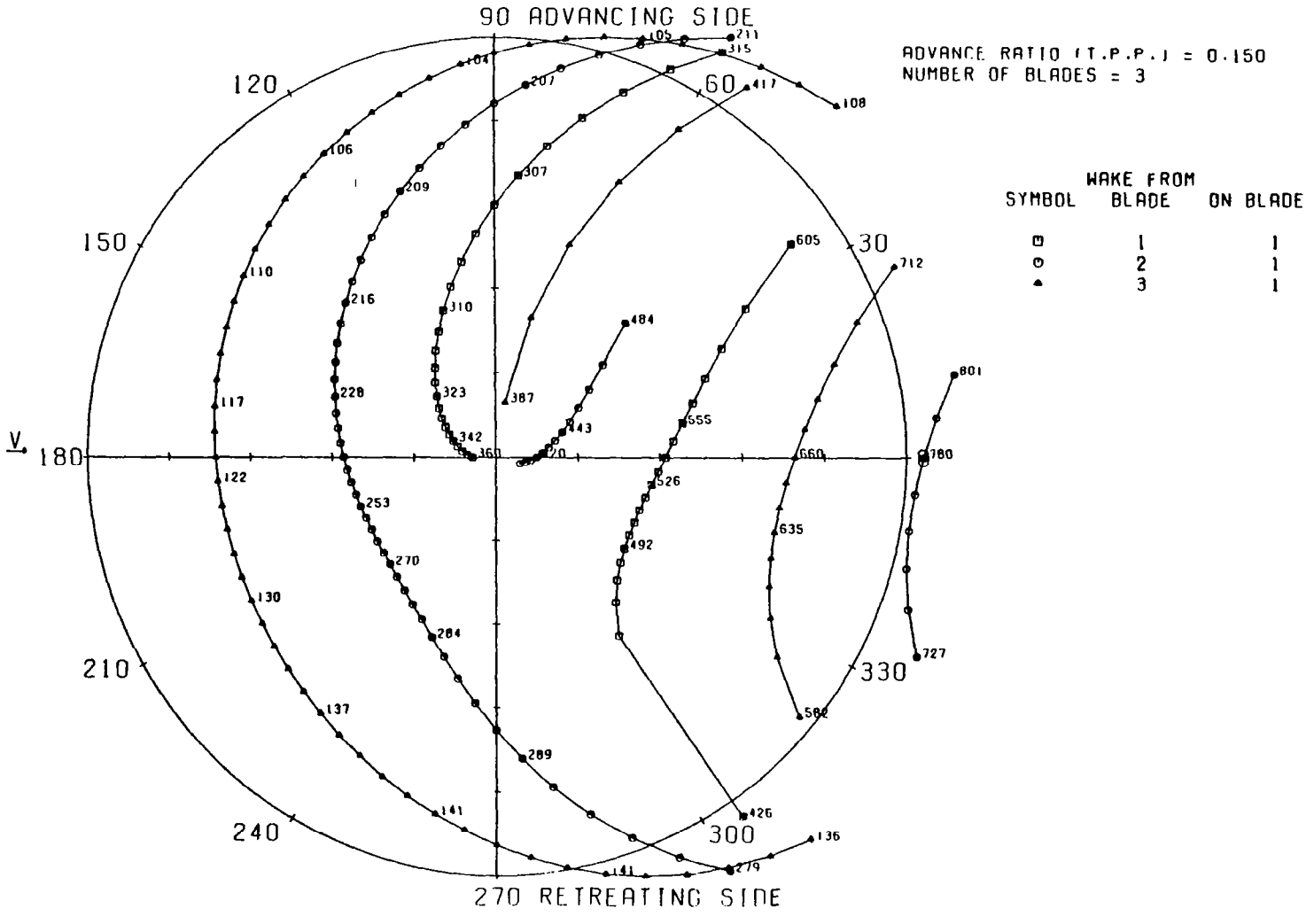

FIGURE 27C. POTENTIAL BLADE/TIP VORTEX INTERSECTION PLOT FOR THREE BLADES (POLAR FORMAT), μ = .15

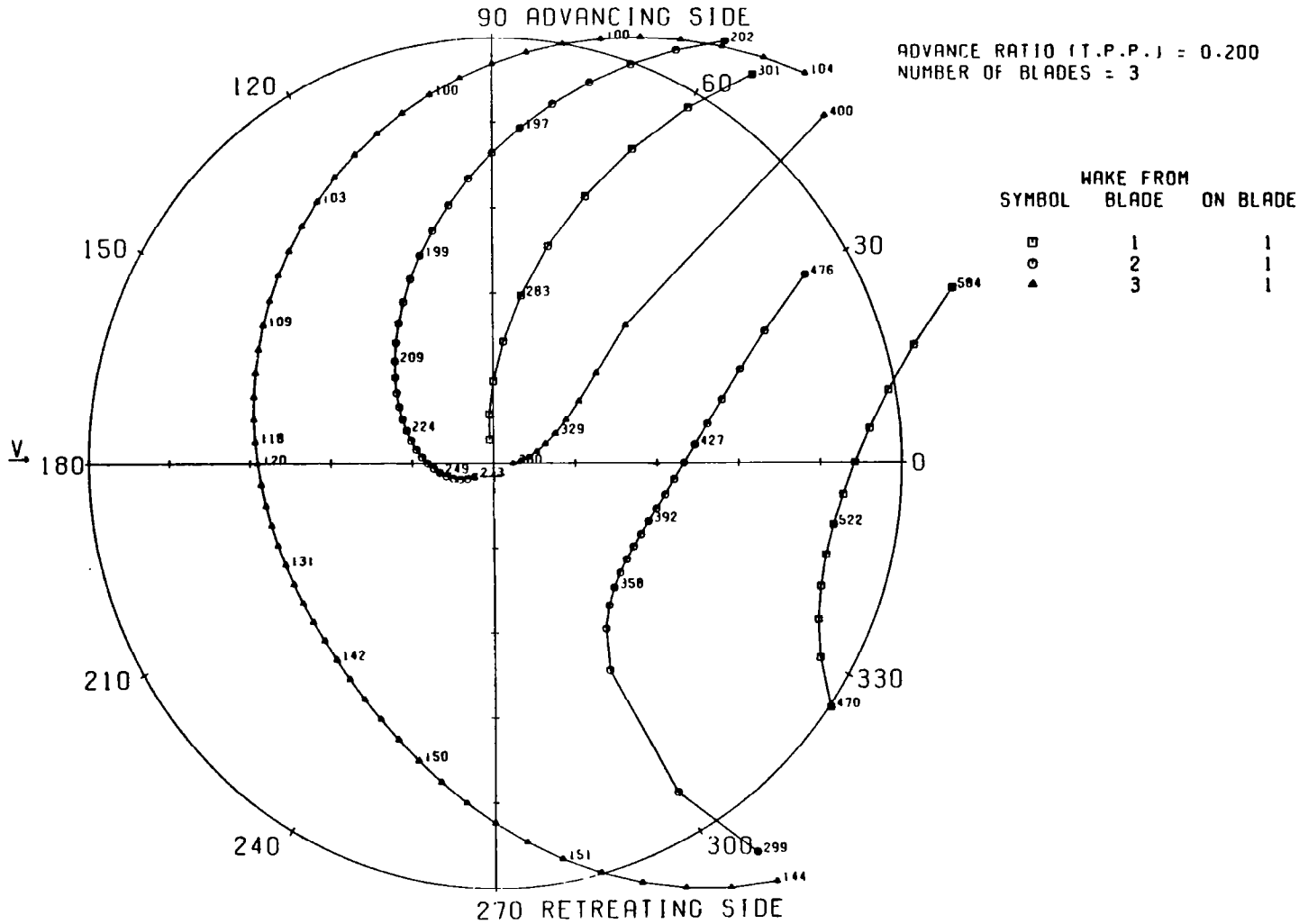

FIGURE 27D. POTENTIAL BLADE/TIP VORTEX INTERSECTION PLOT FOR THREE BLADES (POLAR FORMAT), μ = .20

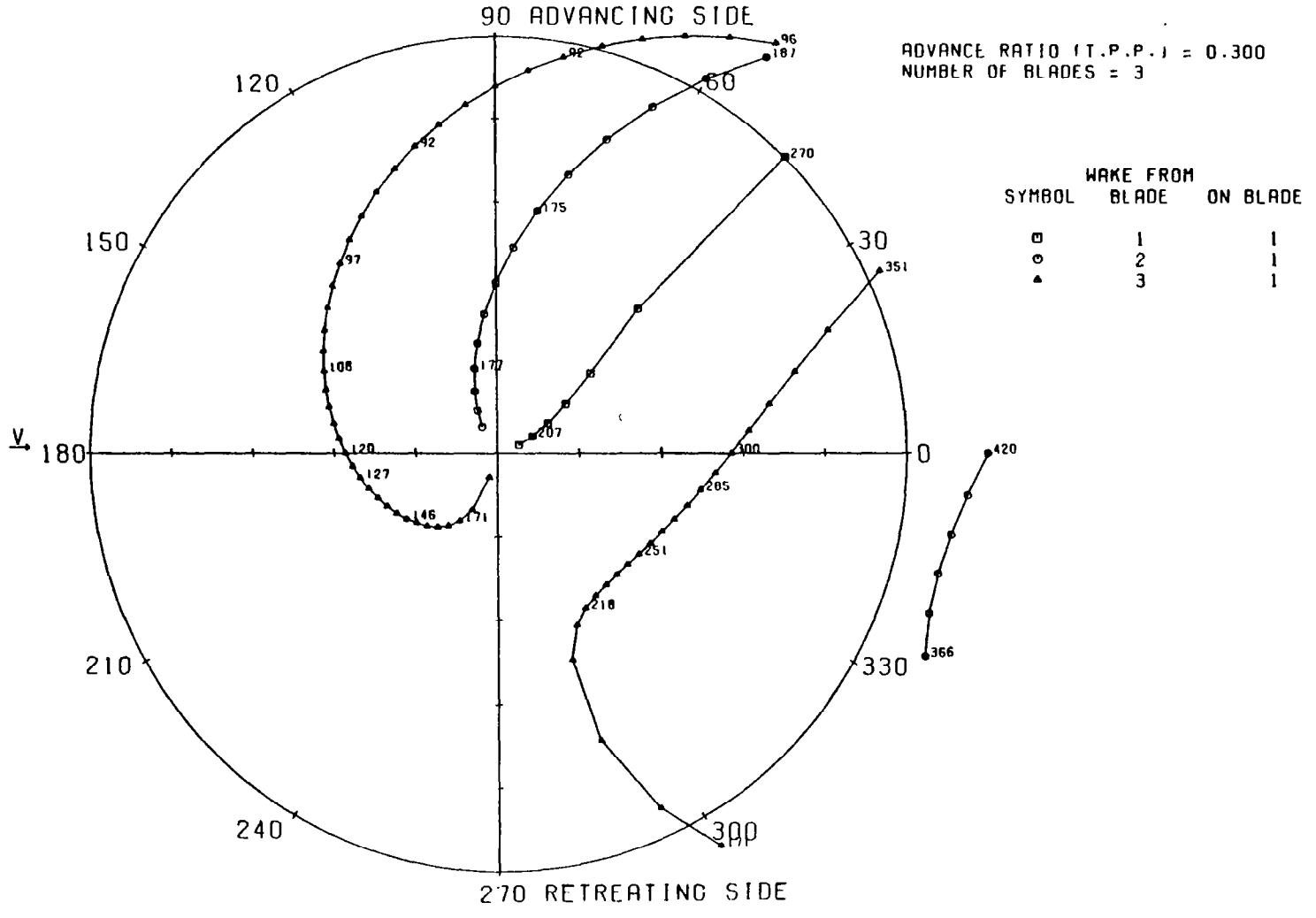

FIGURE 27E. POTENTIAL BLADE/TIP VORTEX INTERSECTION PLOT FOR THREE BLADES (POLAR FORMAT), μ = .30

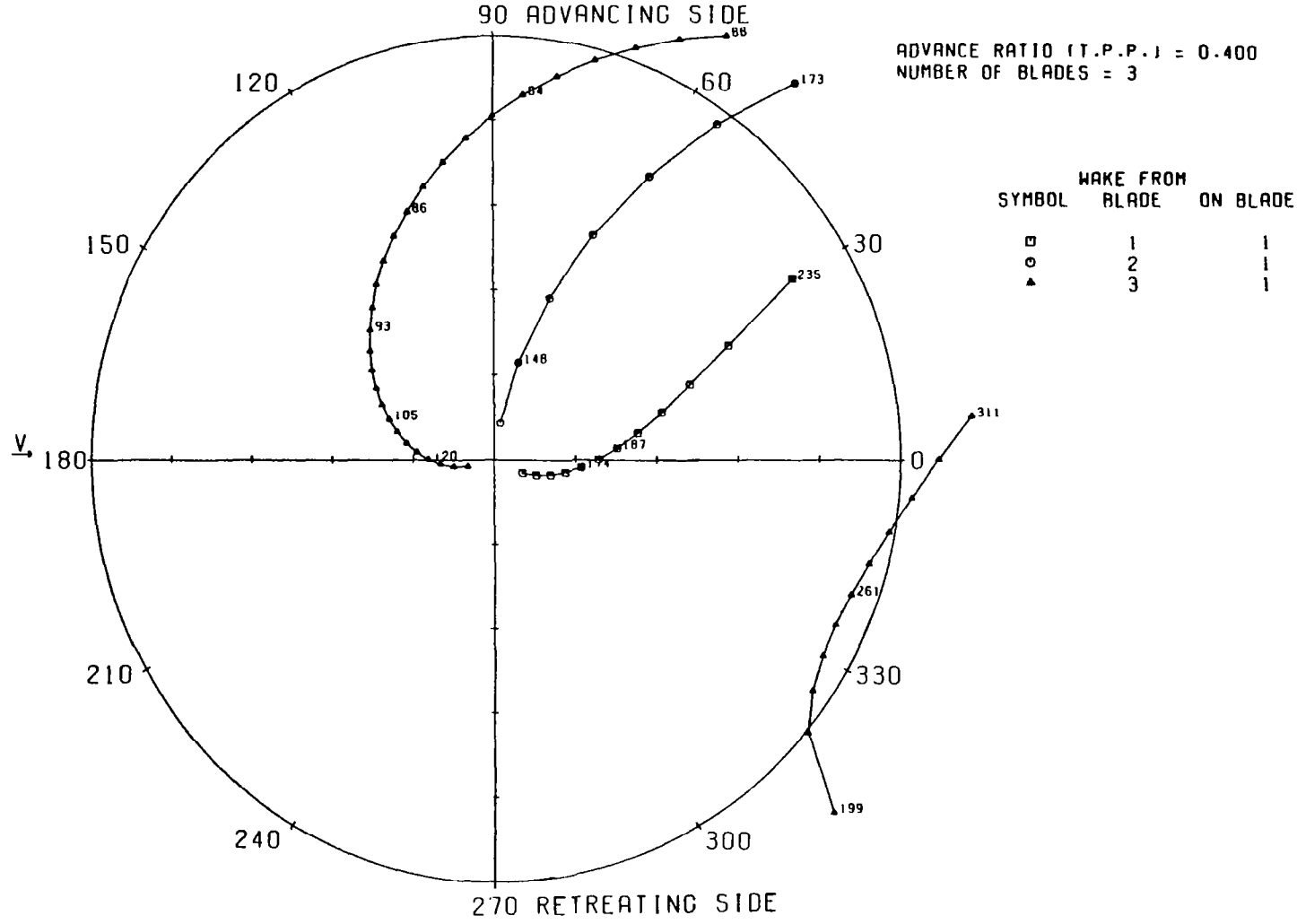

FIGURE 27F. POTENTIAL BLADE/TIP VORTEX INTERSECTION PLOT FOR THREE BLADES (POLAR FORMAT), μ = .40

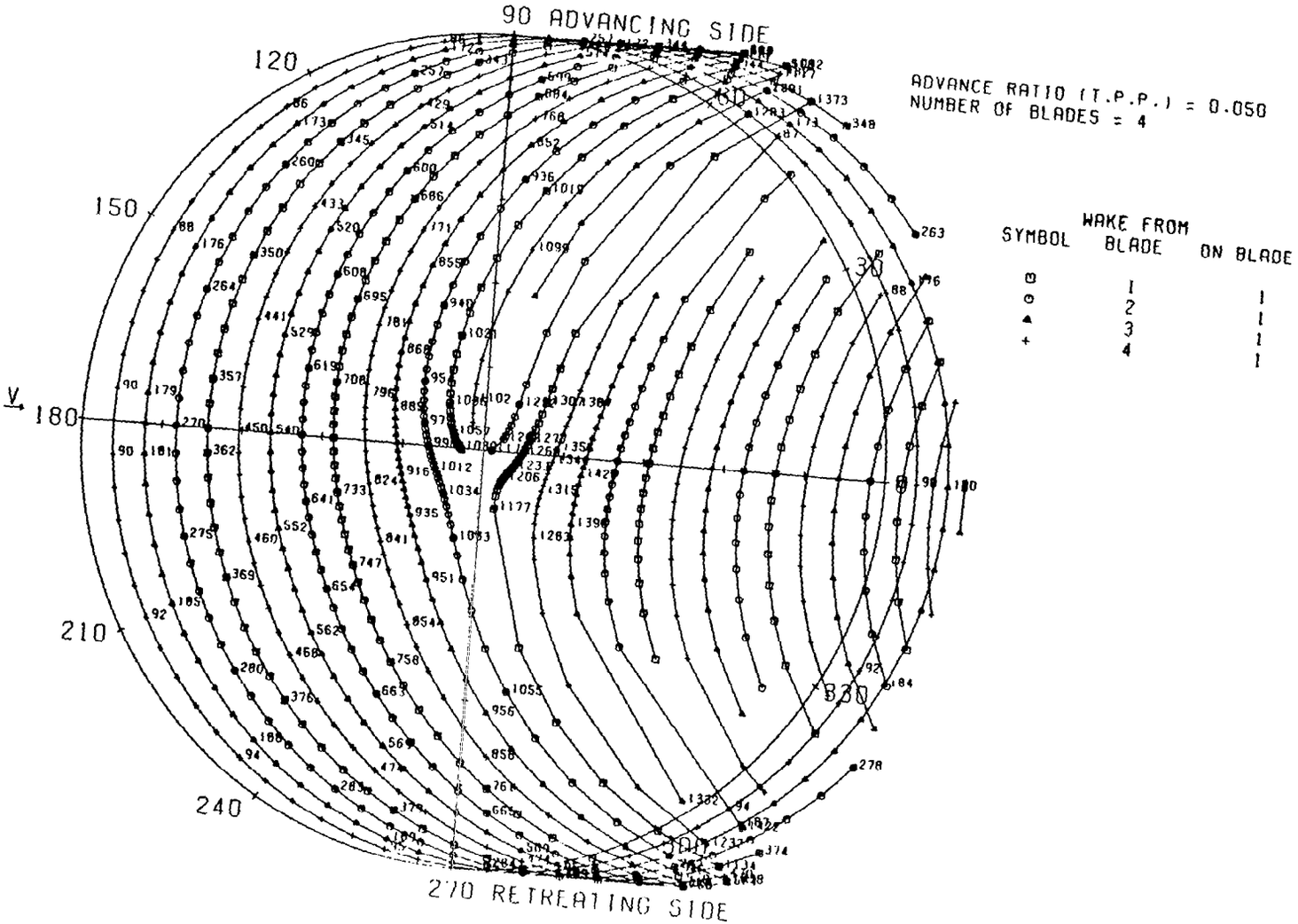

FIGURE 28A. POTENTIAL BLADE/TIP VORTEX INTERSECTION PLOT FOR FOUR BLADES (POLAR FORMAT), μ = .05

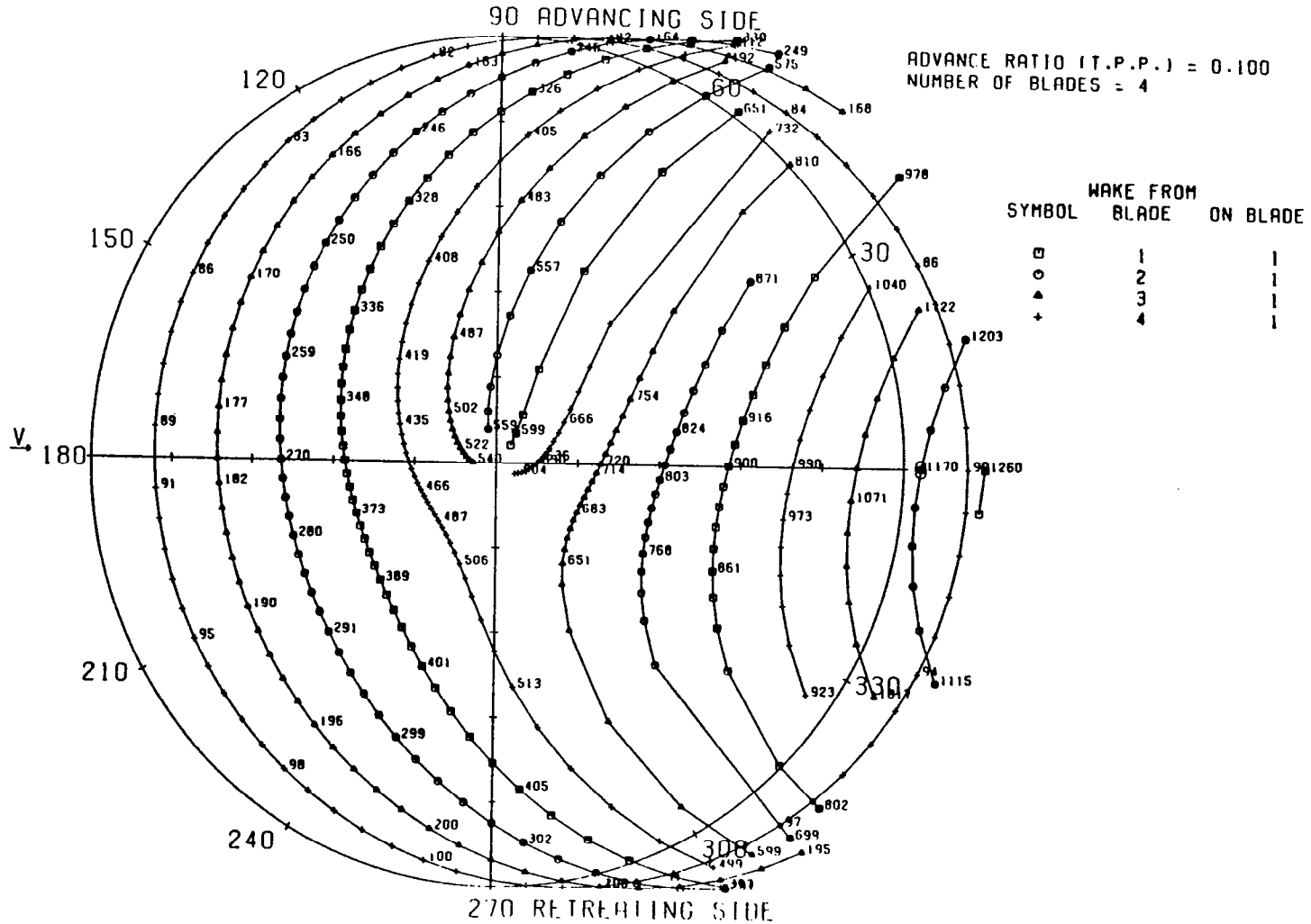

FIGURE 28B. POTENTIAL BLADE/TIP VORTEX INTERSECTION PLOT FOR FOUR BLADES (POLAR FORMAT), μ = .10

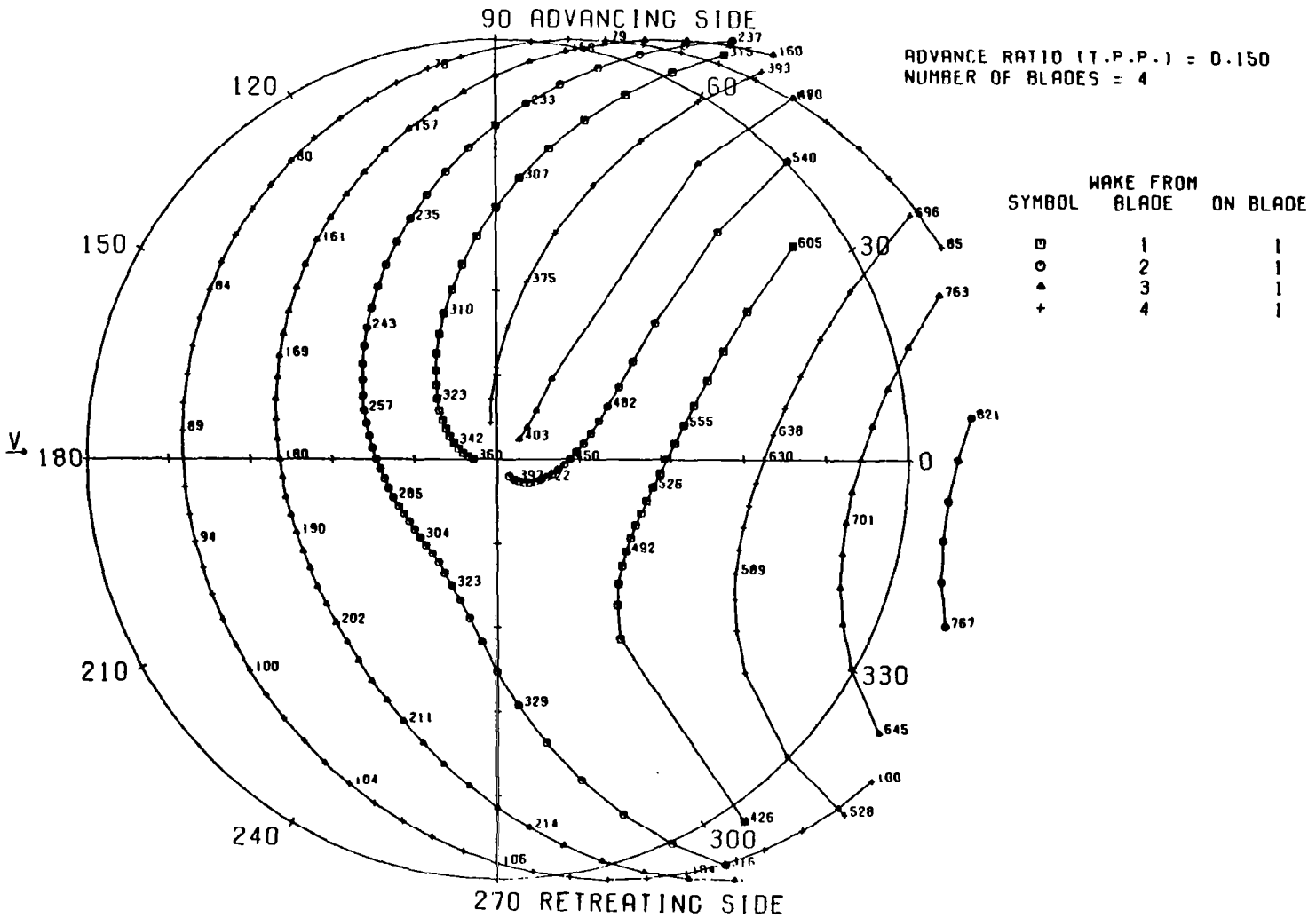

FIGURE 28C. POTENTIAL BLADE/TIP VORTEX INTERSECTION PLOT FOR FOUR BLADES (POLAR FORMAT), μ = .15

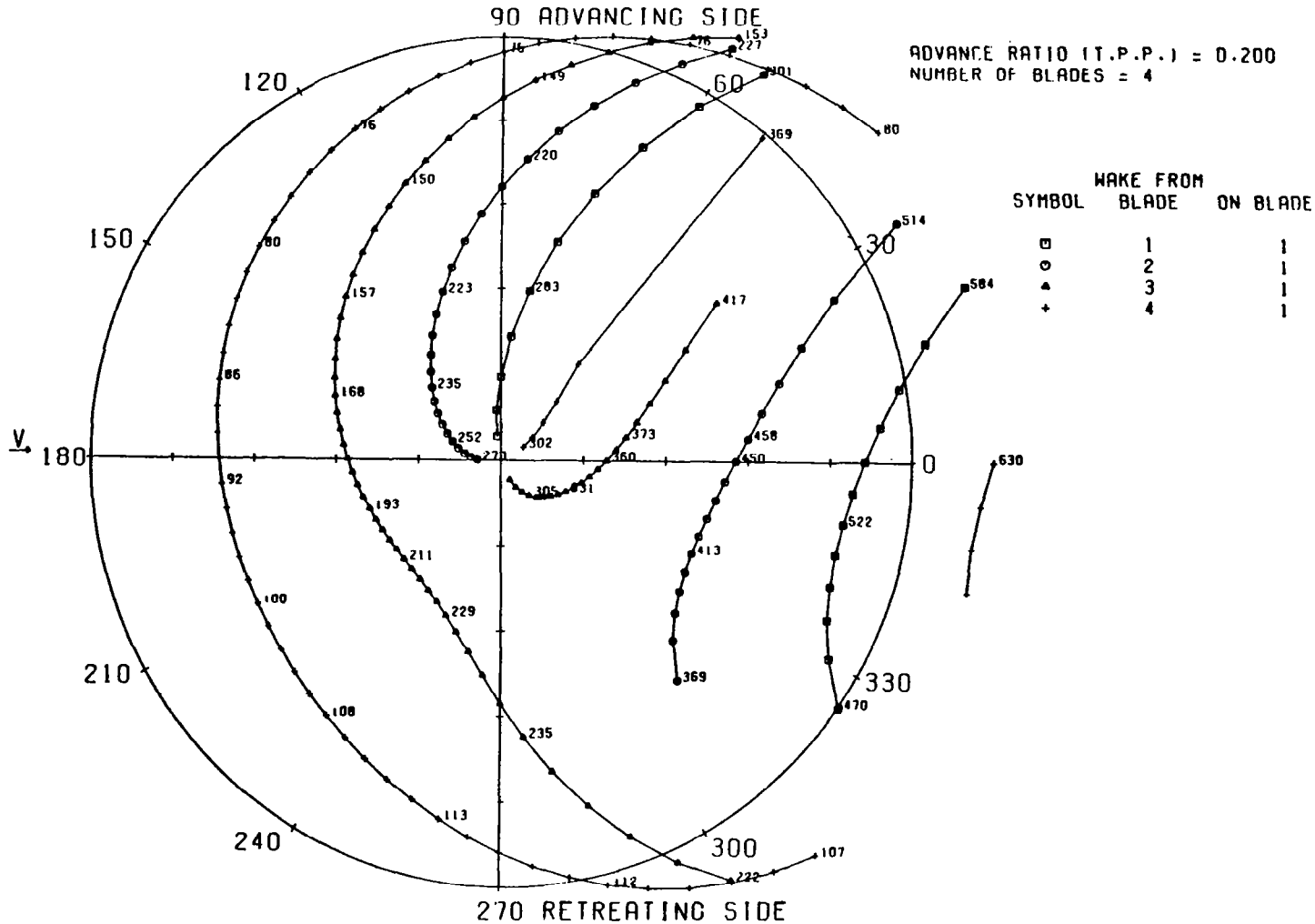

FIGURE 28D. POTENTIAL BLADE/TIP VORTEX INTERSECTION PLOT FOR FOUR BLADES (POLAR FORMAT), μ = .20

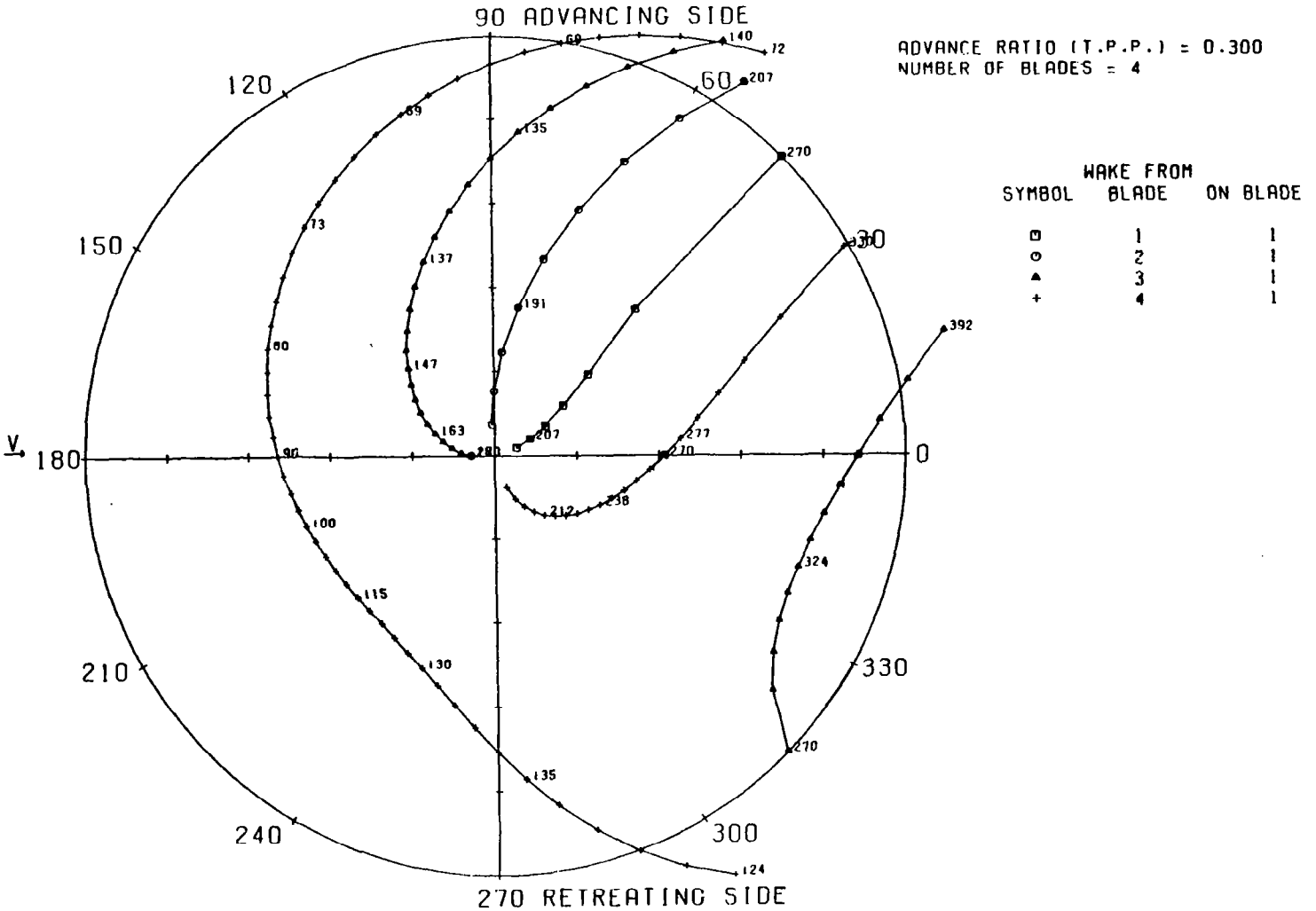

FIGURE 28E. POTENTIAL BLADE/TIP VORTEX INTERSECTION PLOT FOR FOUR BLADES (POLAR FORMAT), μ = .30

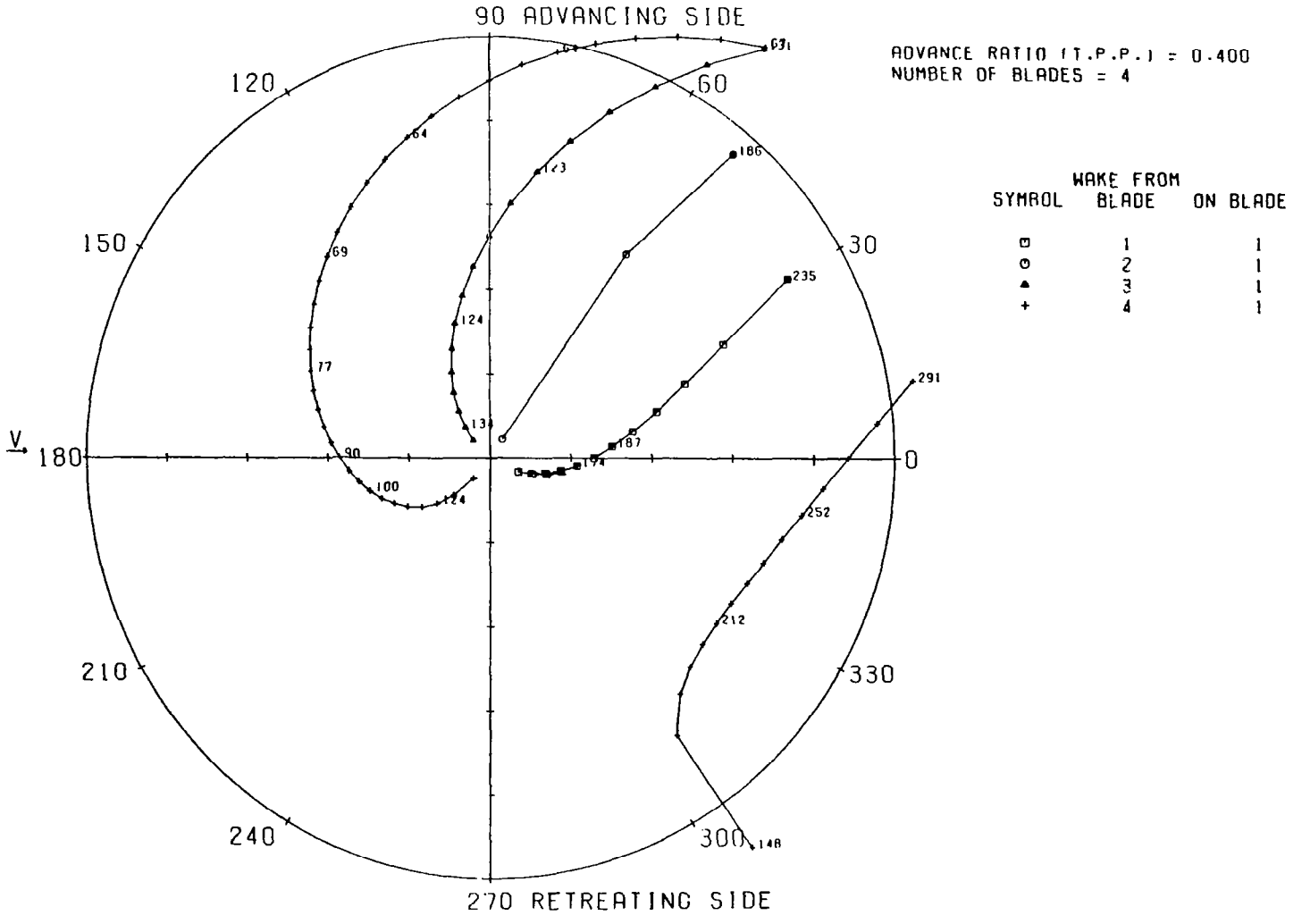

FIGURE 28F. POTENTIAL BLADE/TIP VORTEX INTERSECTION PLOT FOR FOUR BLADES (POLAR FORMAT), μ = .40

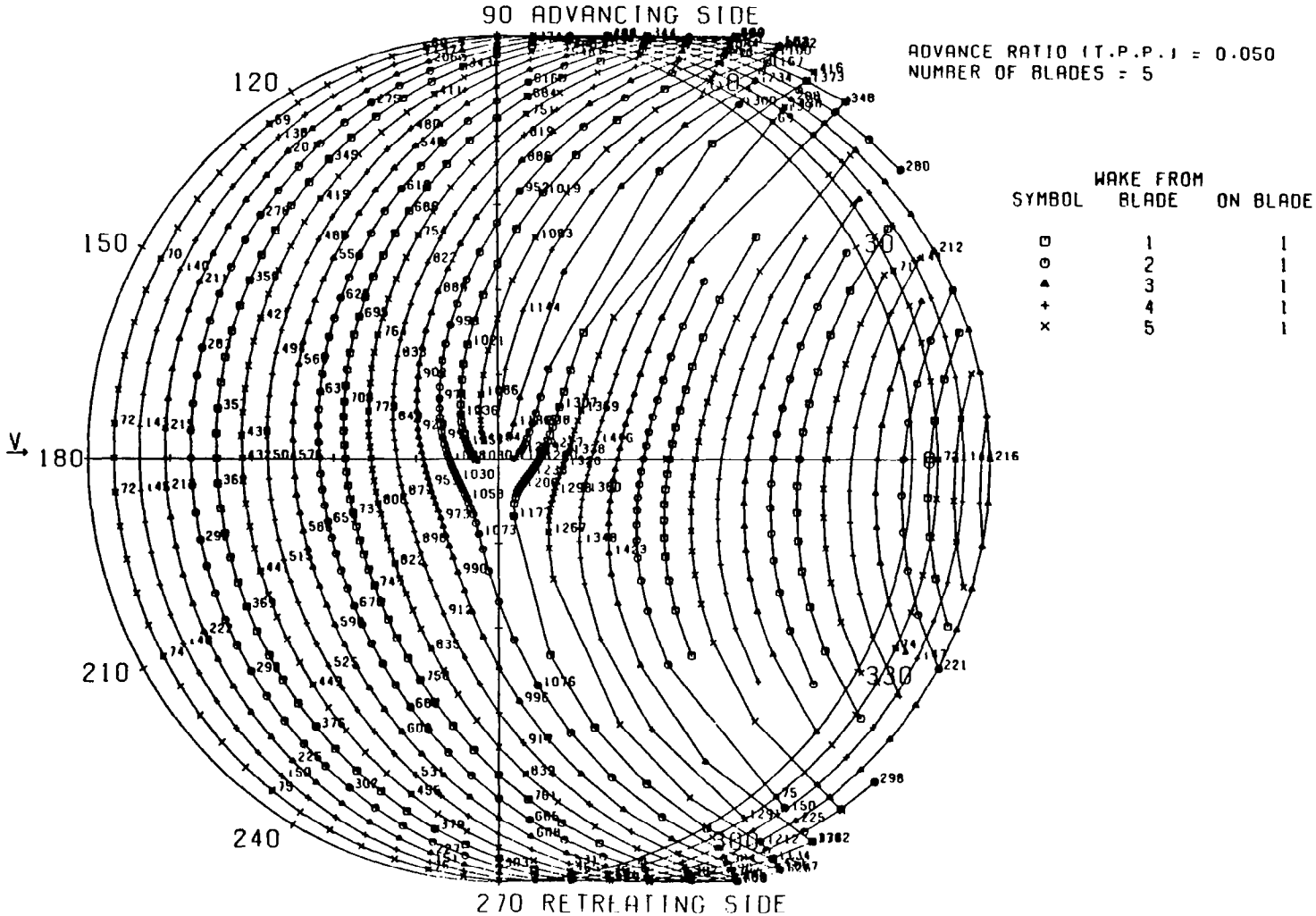

FIGURE 29A. POTENTIAL BLADE/TIP VORTEX INTERSECTION PLOT FOR FIVE BLADES (POLAR FORMAT), μ = .05

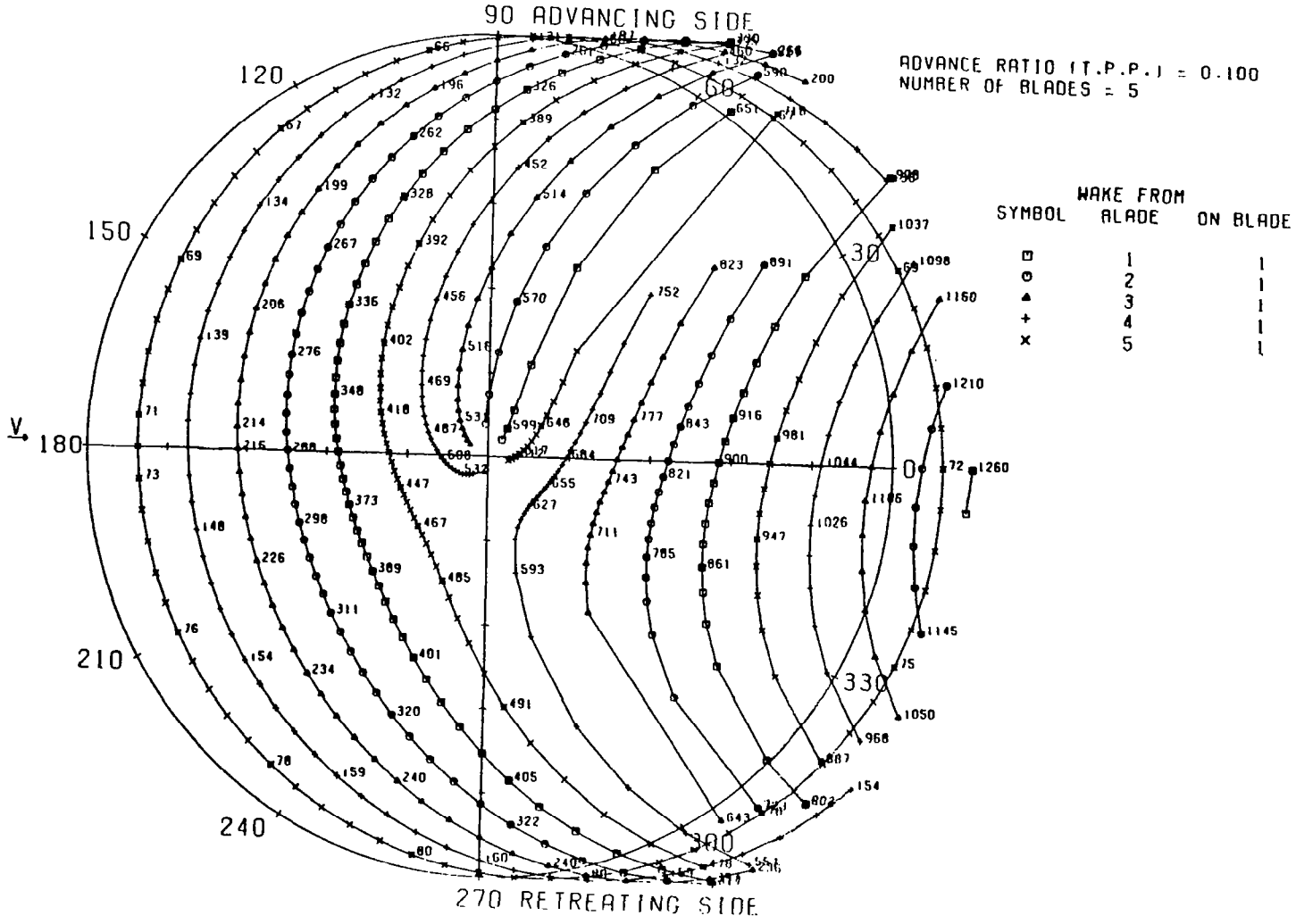

FIGURE 29B. POTENTIAL BLADE/TIP VORTEX INTERSECTION PLOT FOR FIVE BLADES (POLAR FORMAT), μ = .10

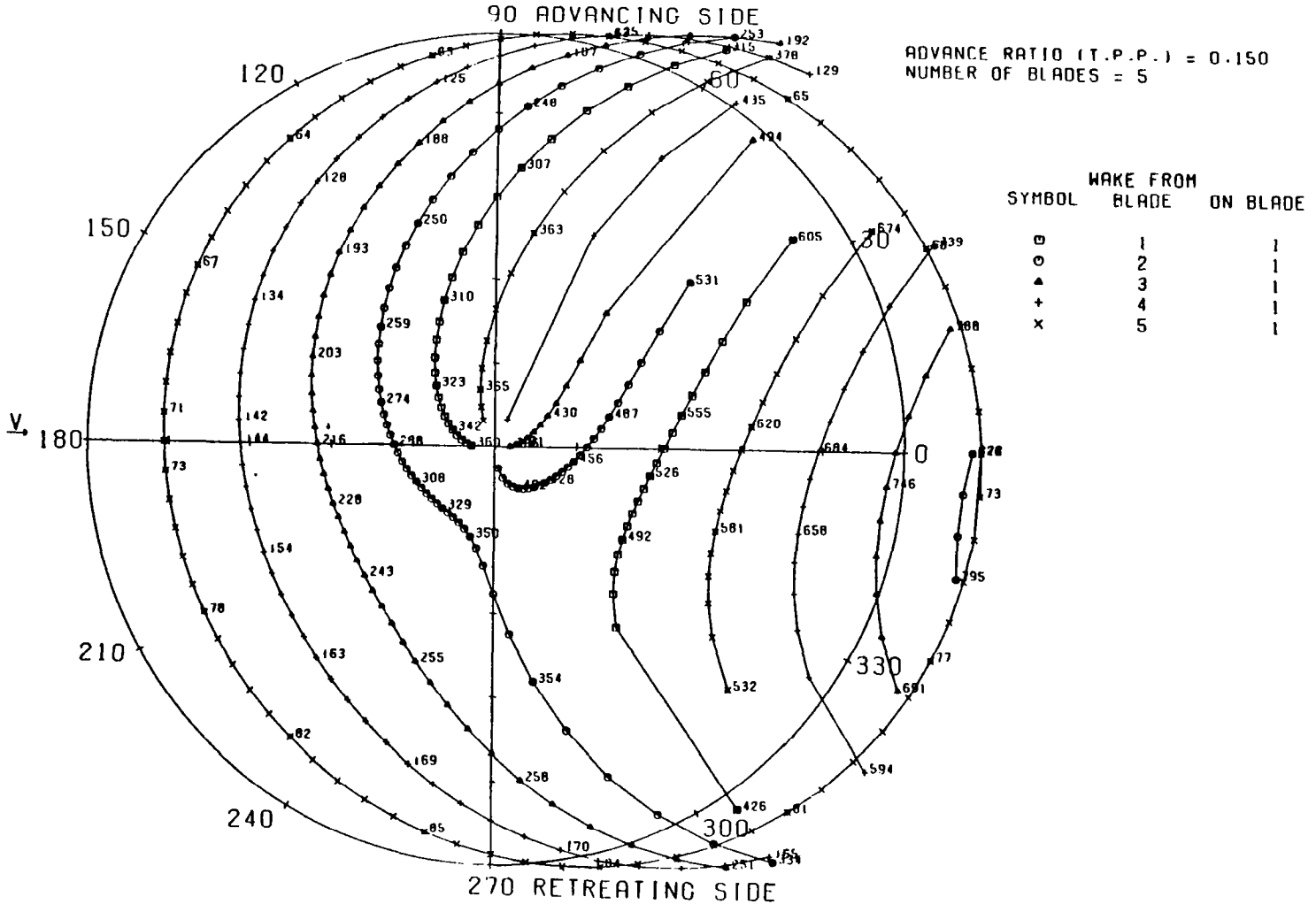

FIGURE 29C. POTENTIAL BLADE/TIP VORTEX INTERSECTION PLOT FOR FIVE BLADES (POLAR FORMAT), μ = .15

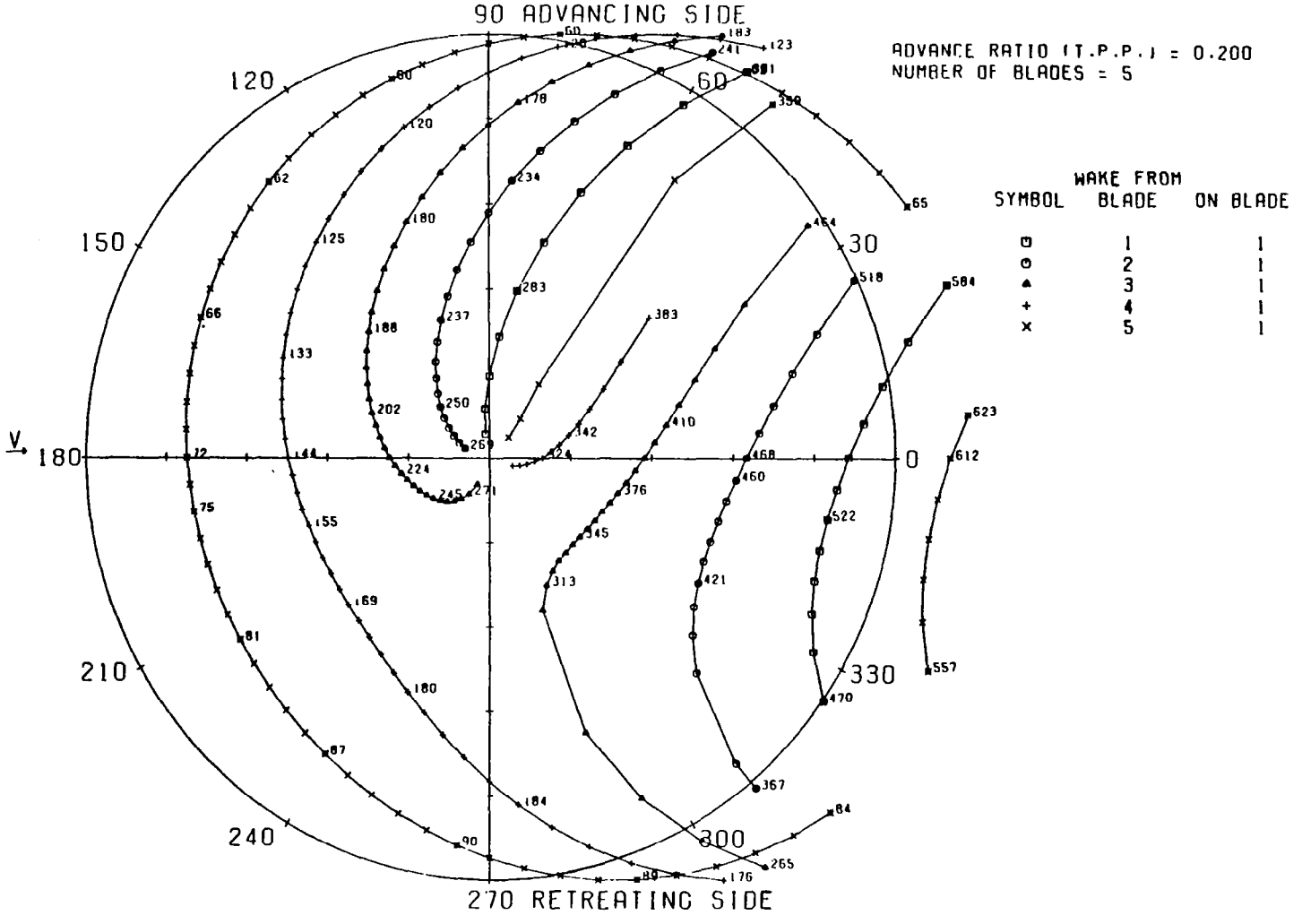

FIGURE 29D. POTENTIAL BLADE/TIP VORTEX INTERSECTION PLOT FOR FIVE BLADES (POLAR FORMAT), μ = .20

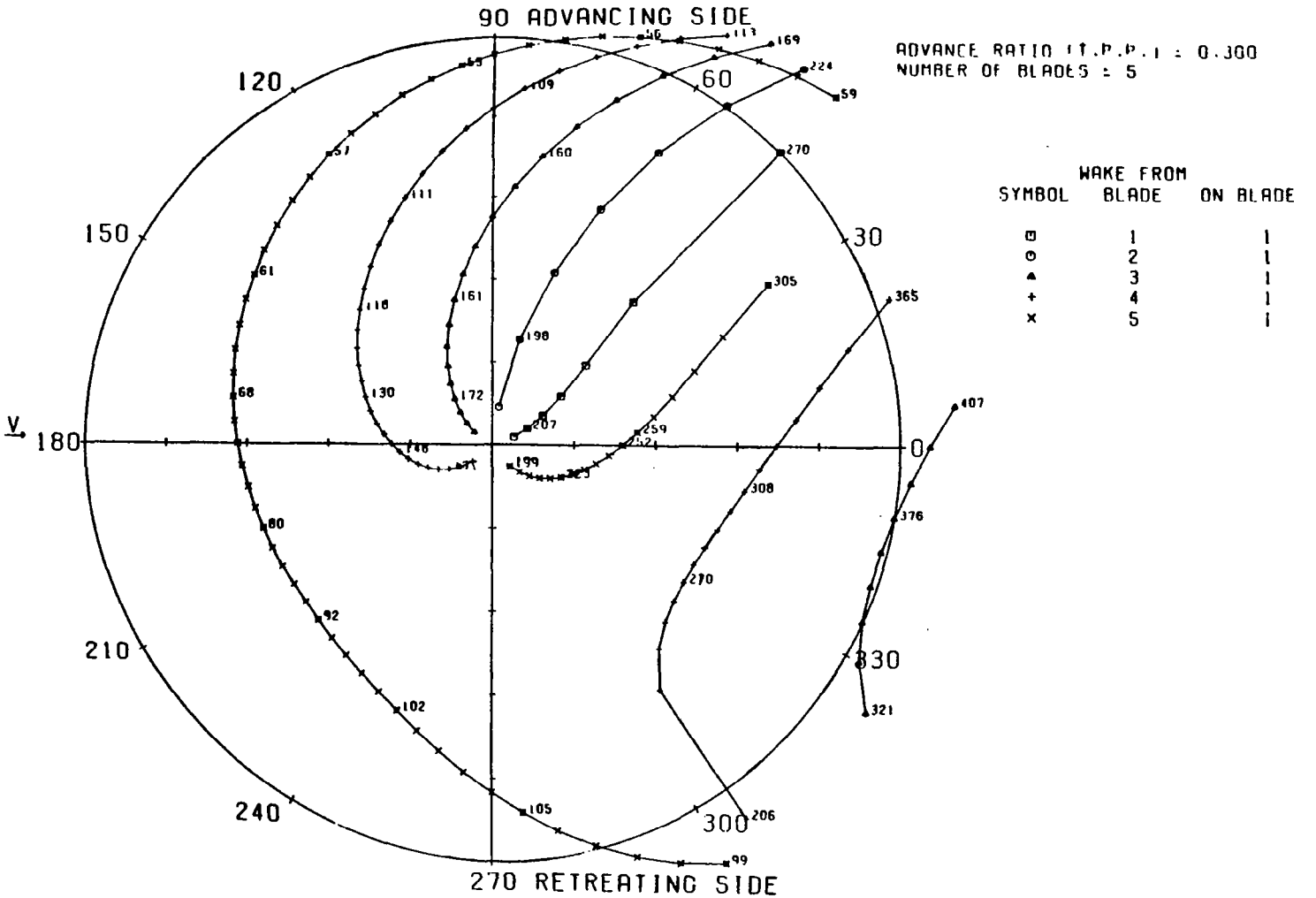

FIGURE 29E. POTENTIAL BLADE/TIP VORTEX INTERSECTION PLOT FOR FIVE BLADES (POLAR FORMAT), μ = .30

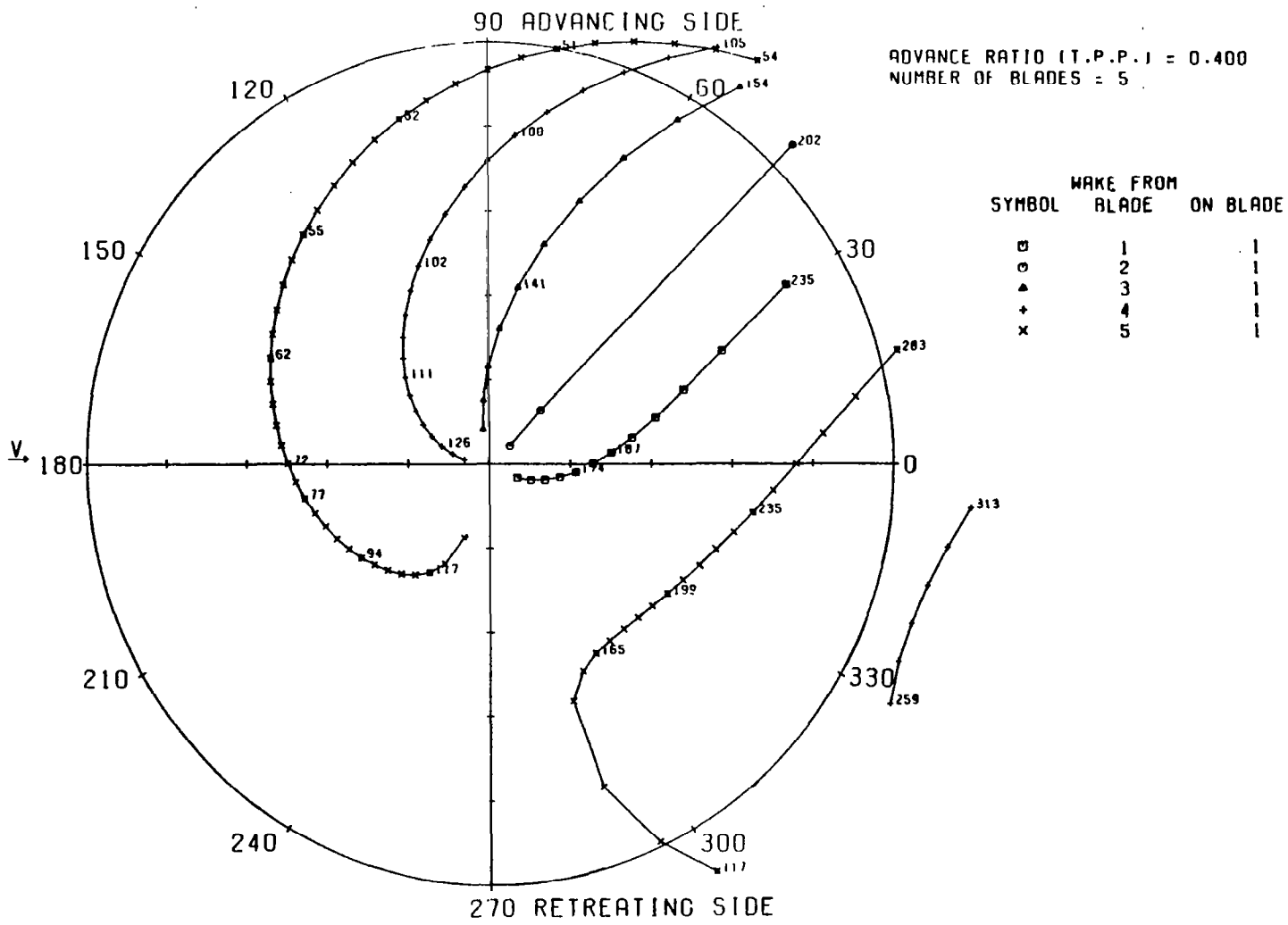

FIGURE 29F. POTENTIAL BLADE/TIP VORTEX INTERSECTION PLOT FOR FIVE BLADES (POLAR FORMAT), μ = .40

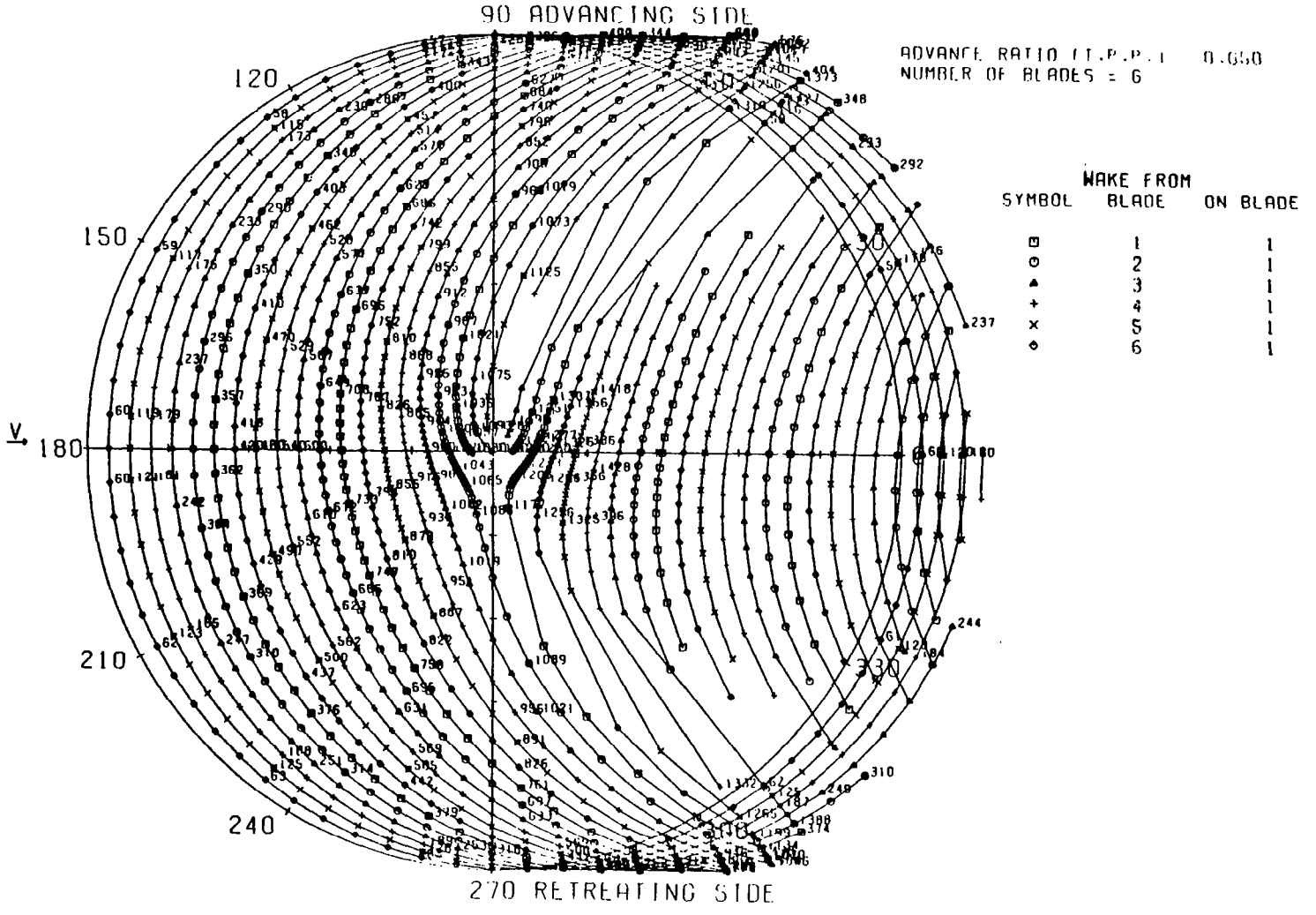

FIGURE 30A. POTENTIAL BLADE/TIP VORTEX INTERSECTION PLOT FOR SIX BLADES (POLAR FORMAT), μ = .05

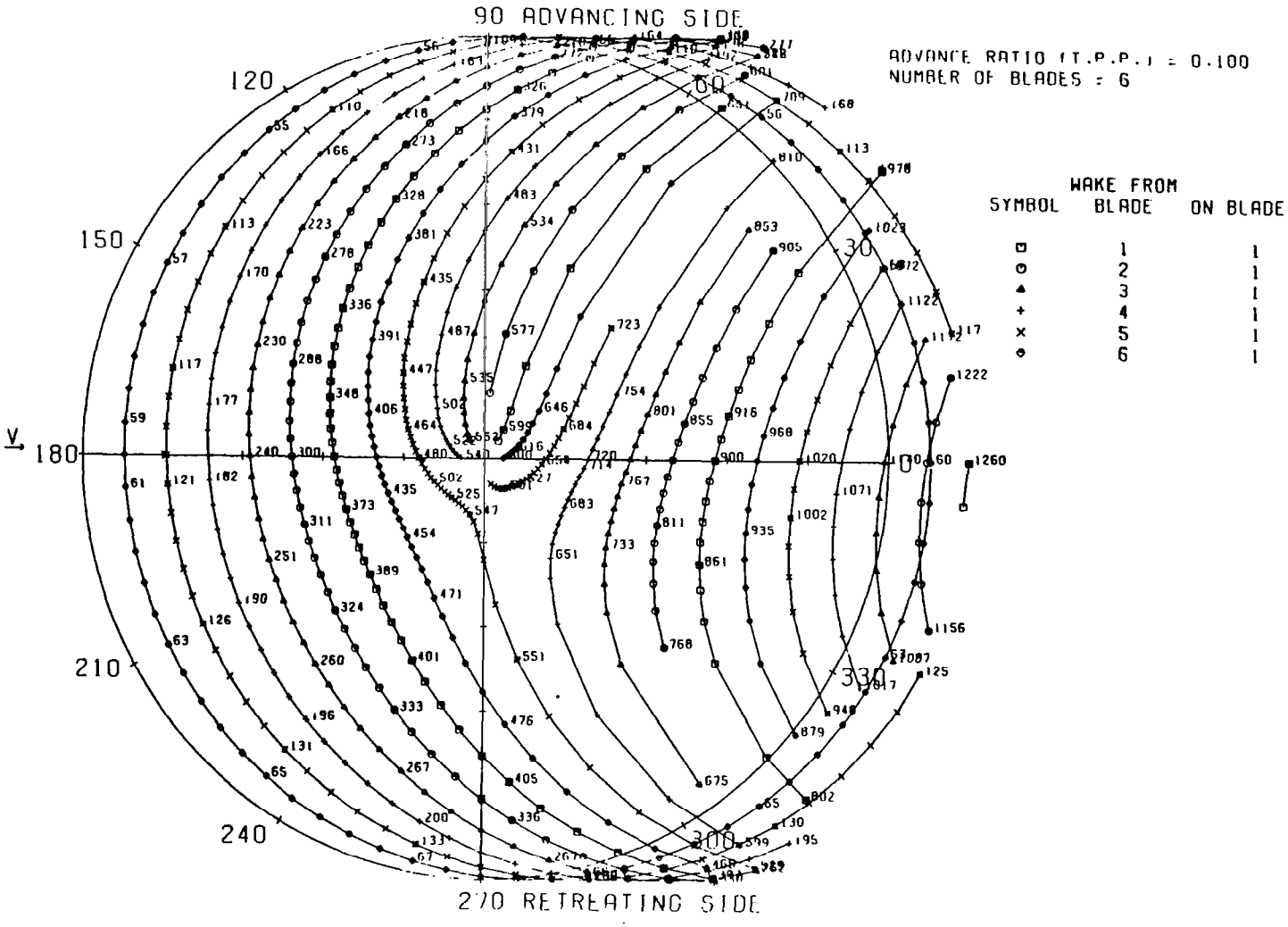

FIGURE 30B. POTENTIAL BLADE/TIP VORTEX INTERSECTION PLOT FOR SIX BLADES (POLAR FORMAT), μ = .10

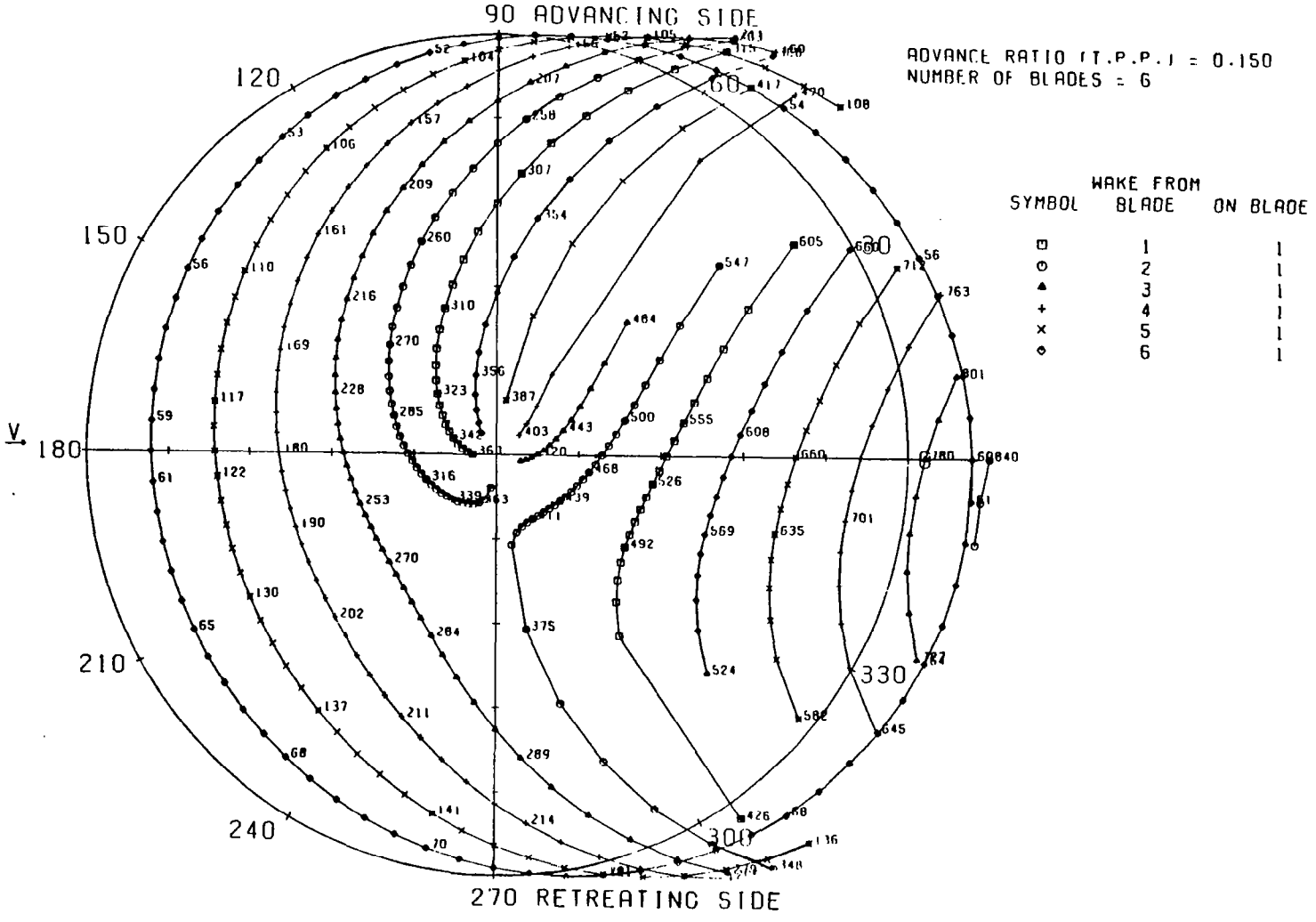

FIGURE 30C. POTENTIAL BLADE/TIP VORTEX INTERSECTION PLOT FOR SIX BLADES (POLAR FORMAT), μ = .15

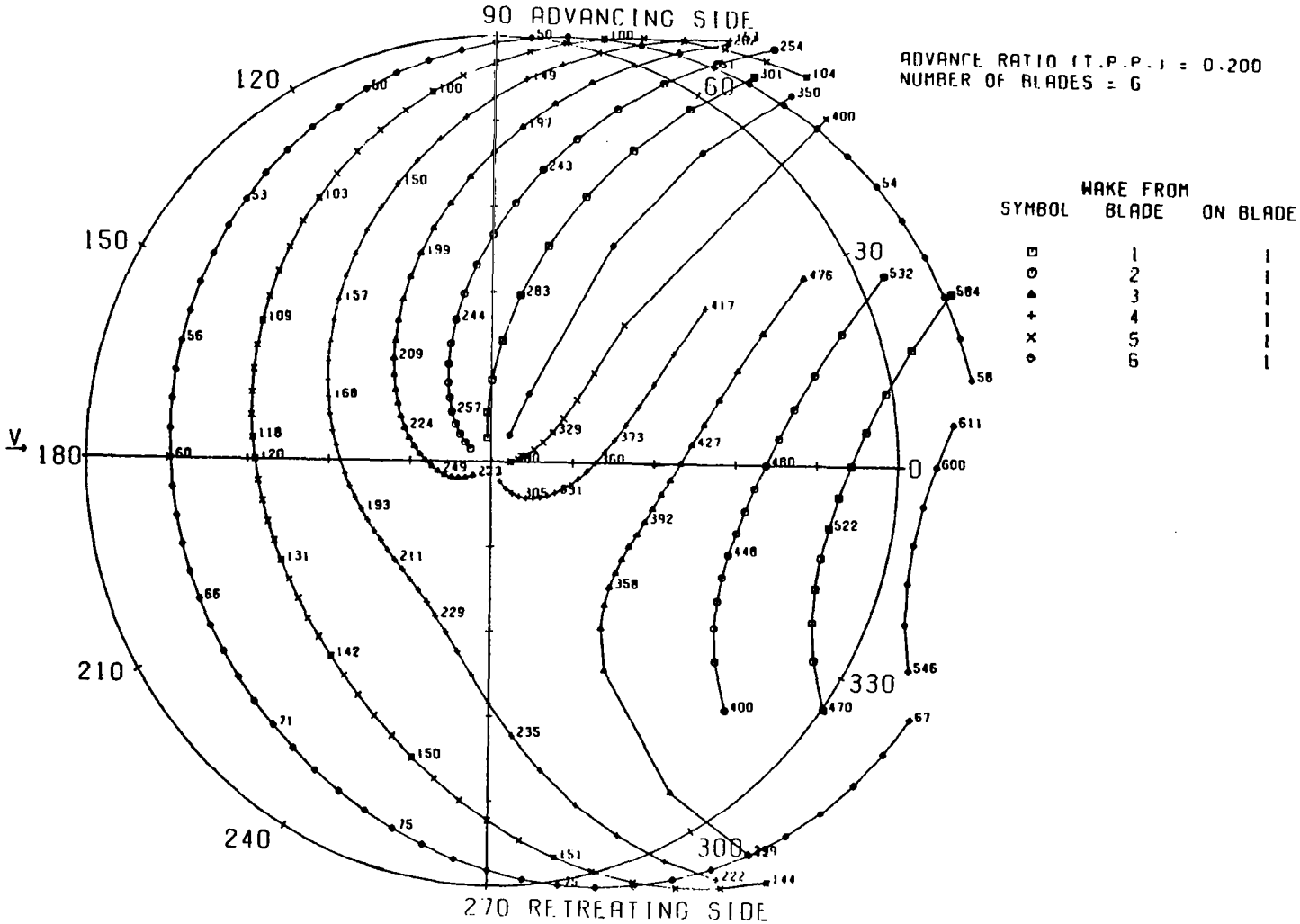

FIGURE 30D. POTENTIAL BLADE/TIP VORTEX INTERSECTION PLOT FOR SIX BLADES (POLAR FORMAT), μ = .20

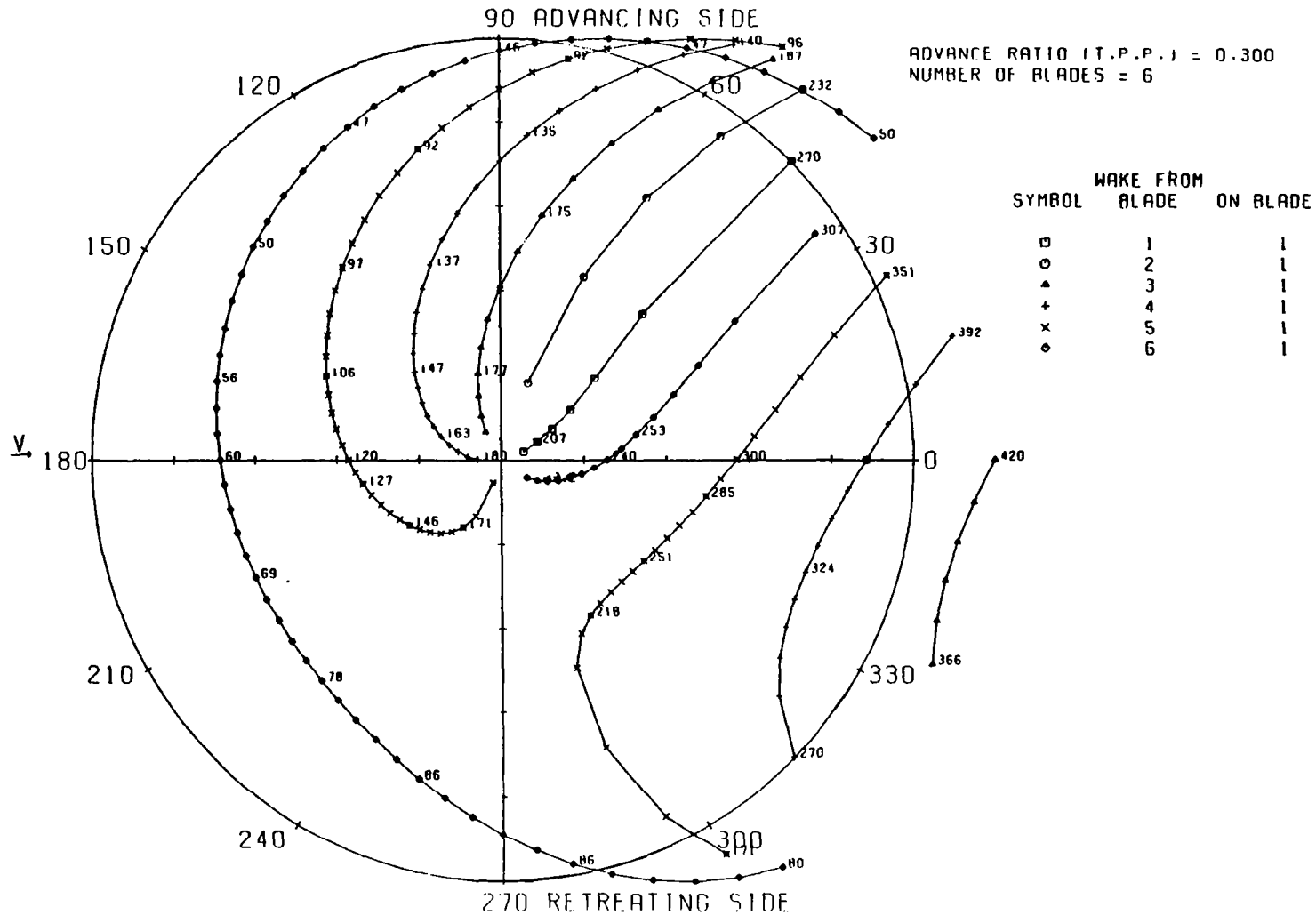

FIGURE 30E. POTENTIAL BLADE/TIP VORTEX INTERSECTION PLOT FOR SIX BLADES (POLAR FORMAT), μ = .30

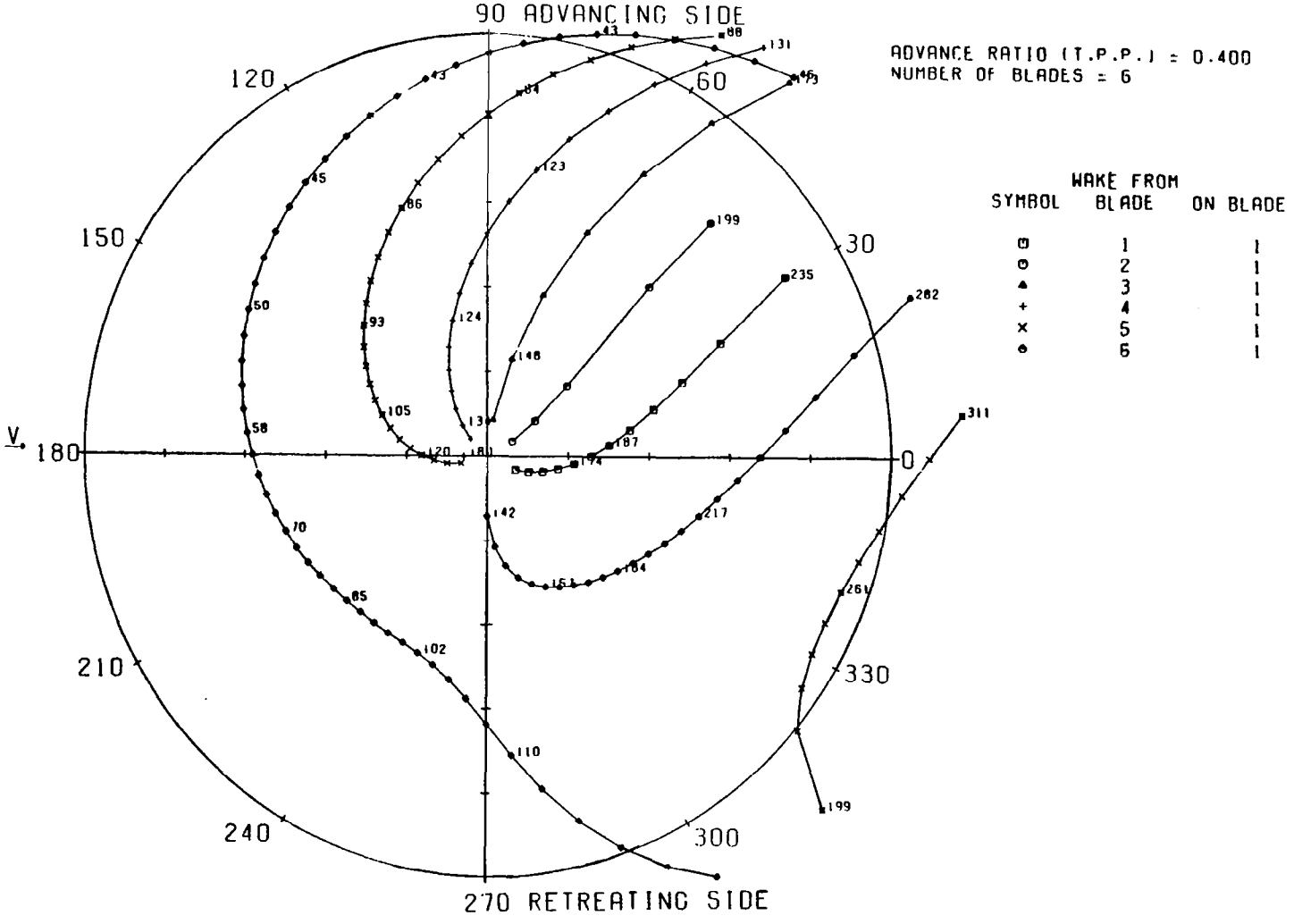

FIGURE 30F. POTENTIAL BLADE/TIP VORTEX INTERSECTION PLOT FOR SIX BLADES (POLAR FORMAT), μ = .40

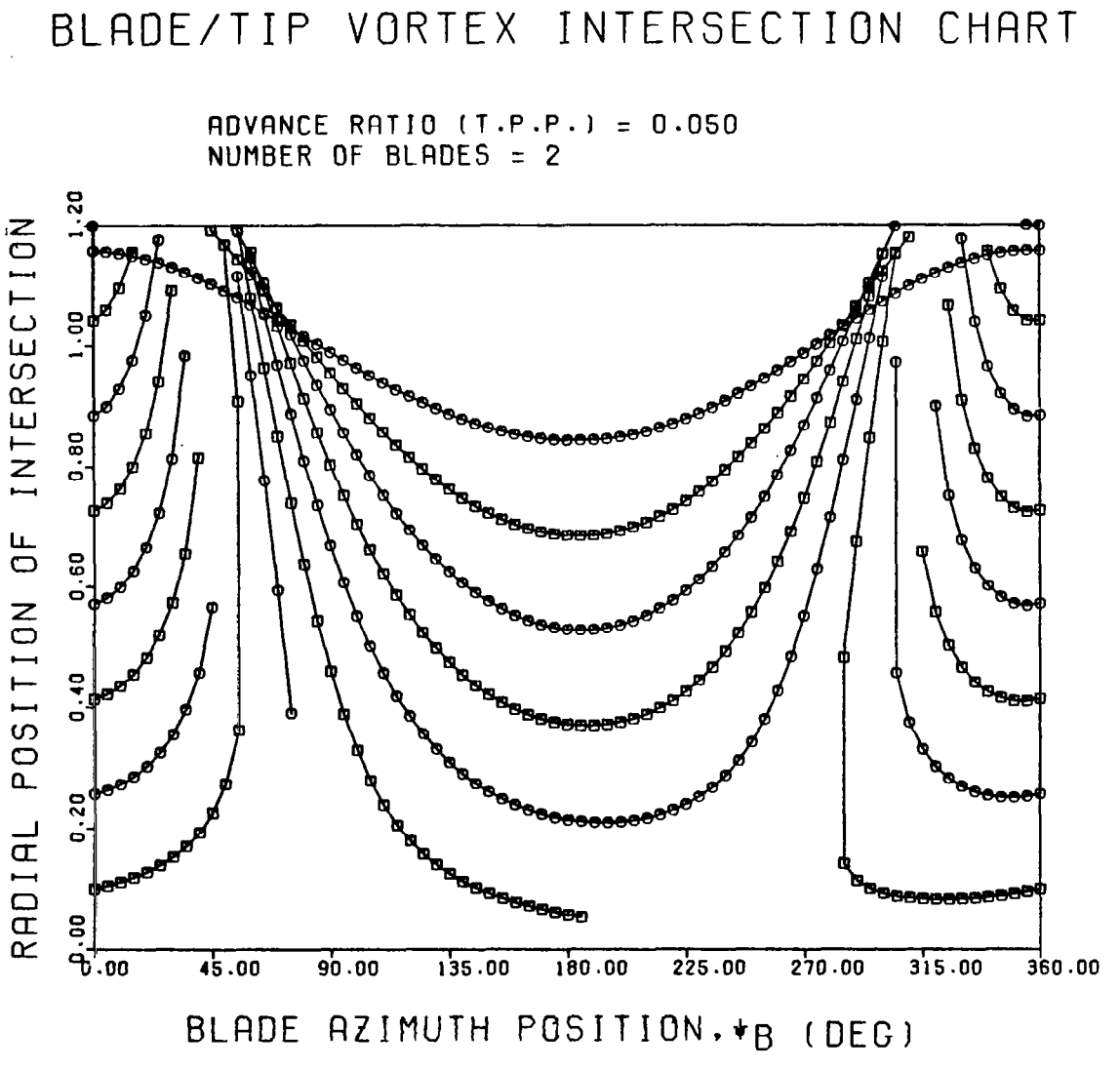

FIGURE 31A. POTENTIAL BLADE/TIP VORTEX INTERSECTION PLOT FOR TWO BLADES (RECTILINEAR FORMAT), μ = .05

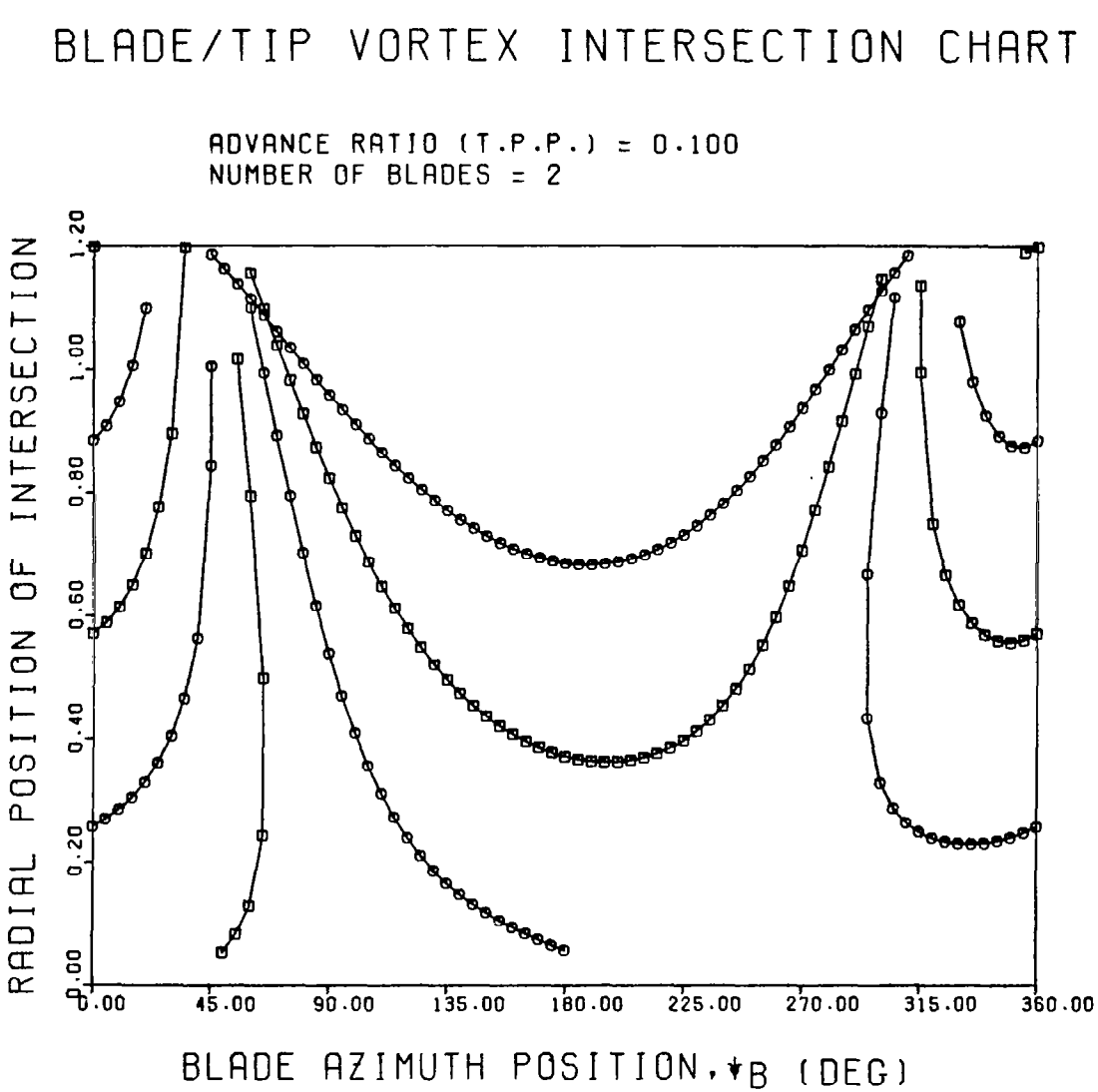

FIGURE 31B. POTENTIAL BLADE/TIP VORTEX INTERSECTION PLOT FOR TWO BLADES (RECTILINEAR FORMAT), μ = .10

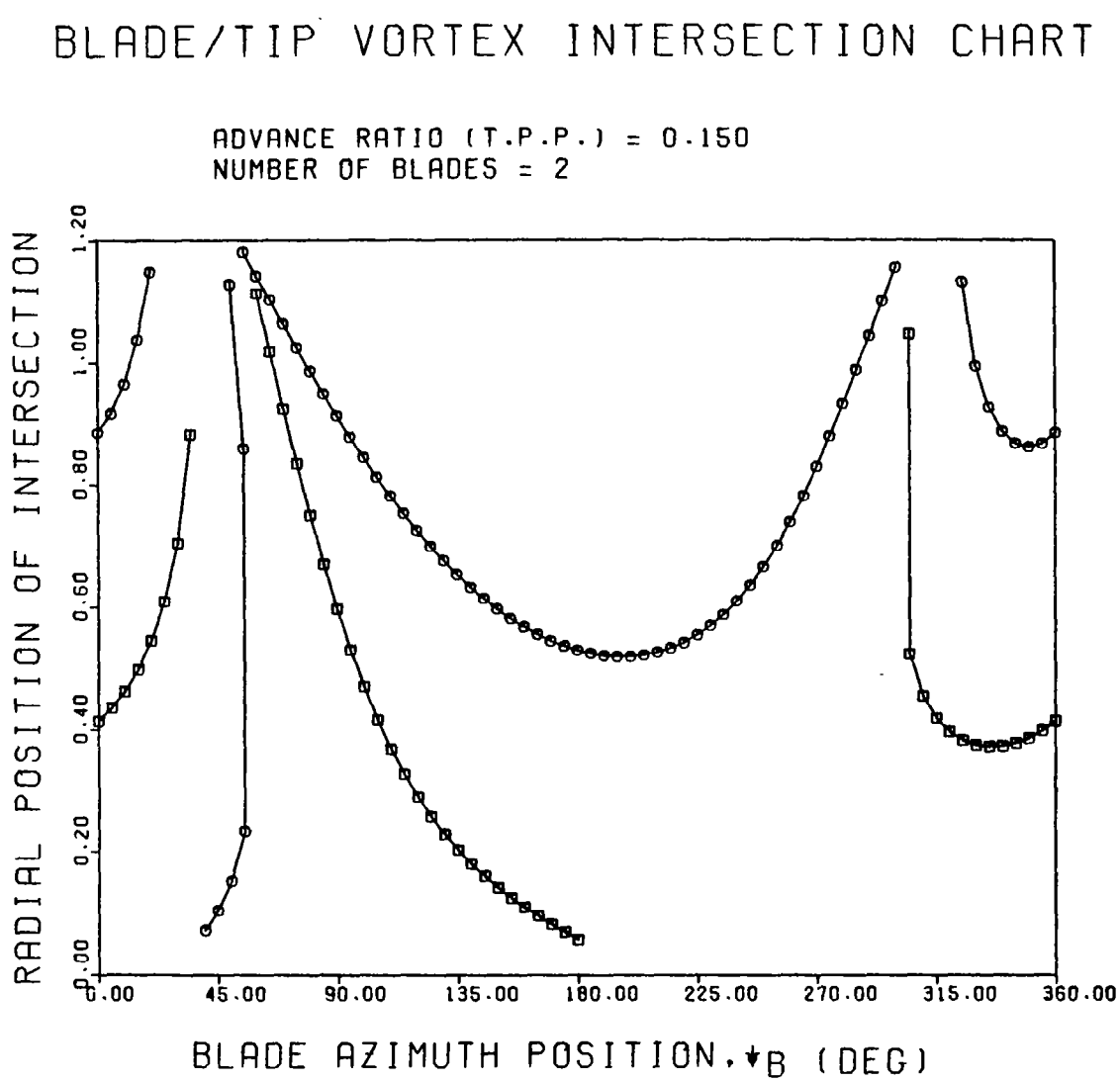

FIGURE 31C. POTENTIAL BLADE/TIP VORTEX INTERSECTION PLOT FOR TWO BLADES (RECTILINEAR FORMAT), μ = .15

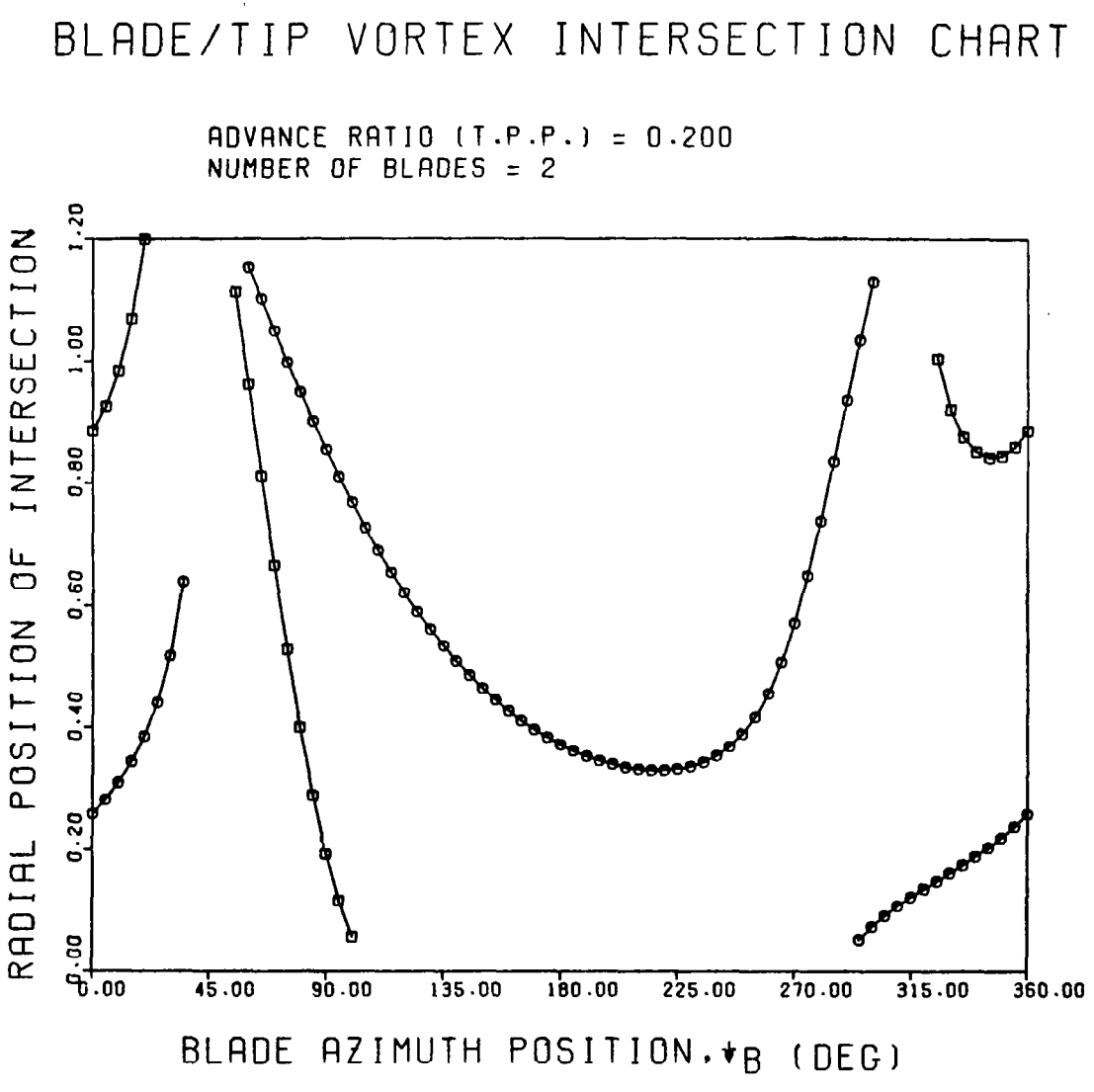

FIGURE 31D. POTENTIAL BLADE/TIP VORTEX INTERSECTION PLOT FOR TWO BLADES (RECTILINEAR FORMAT), μ = .20

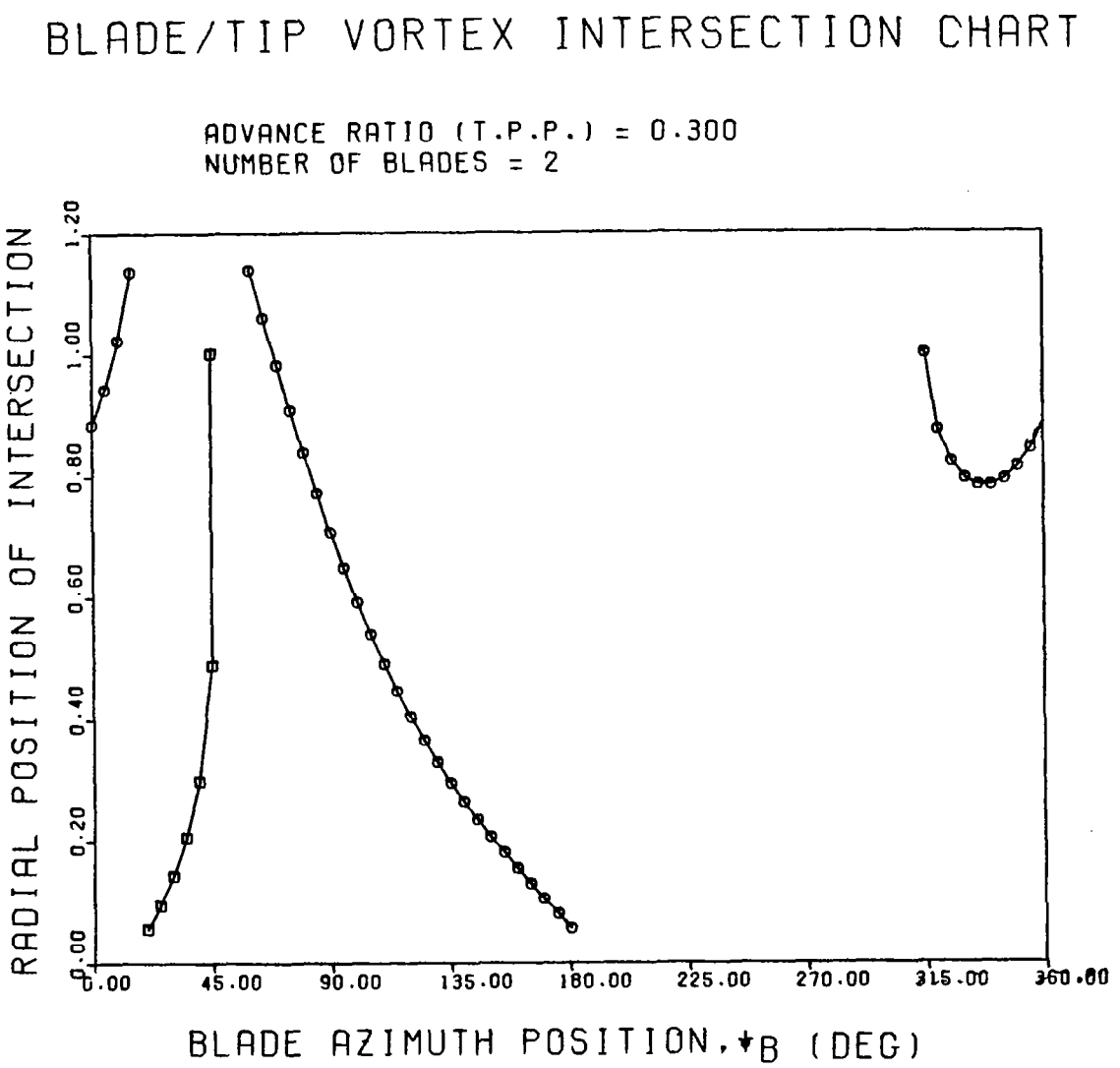

FIGURE 31E. POTENTIAL BLADE/TIP VORTEX INTERSECTION PLOT FOR TWO BLADES (RECTILINEAR FORMAT), μ = .30

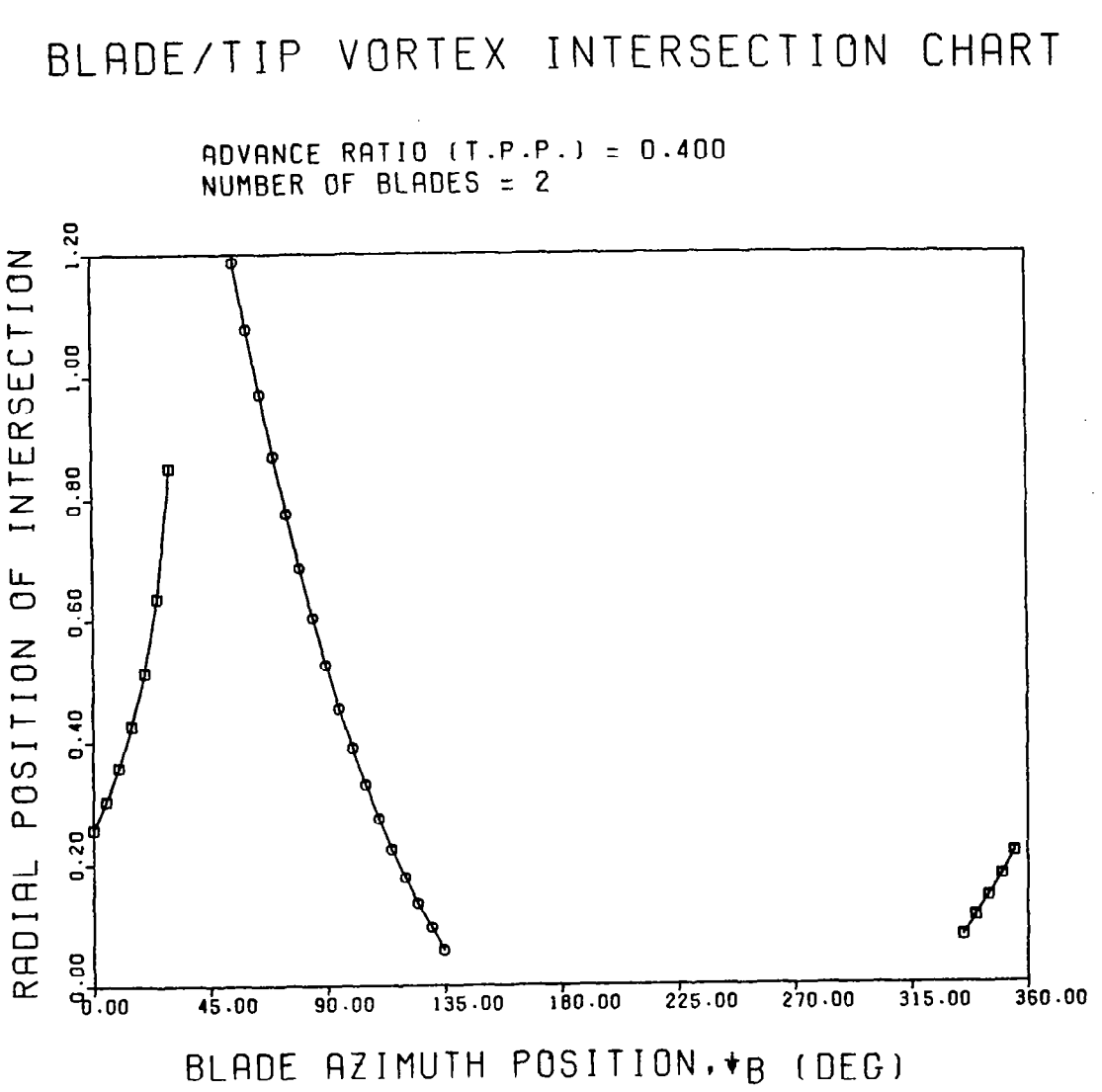

FIGURE 31F. POTENTIAL BLADE/TIP VORTEX INTERSECTION PLOT FOR TWO BLADES (RECTILINEAR FORMAT), μ = .40

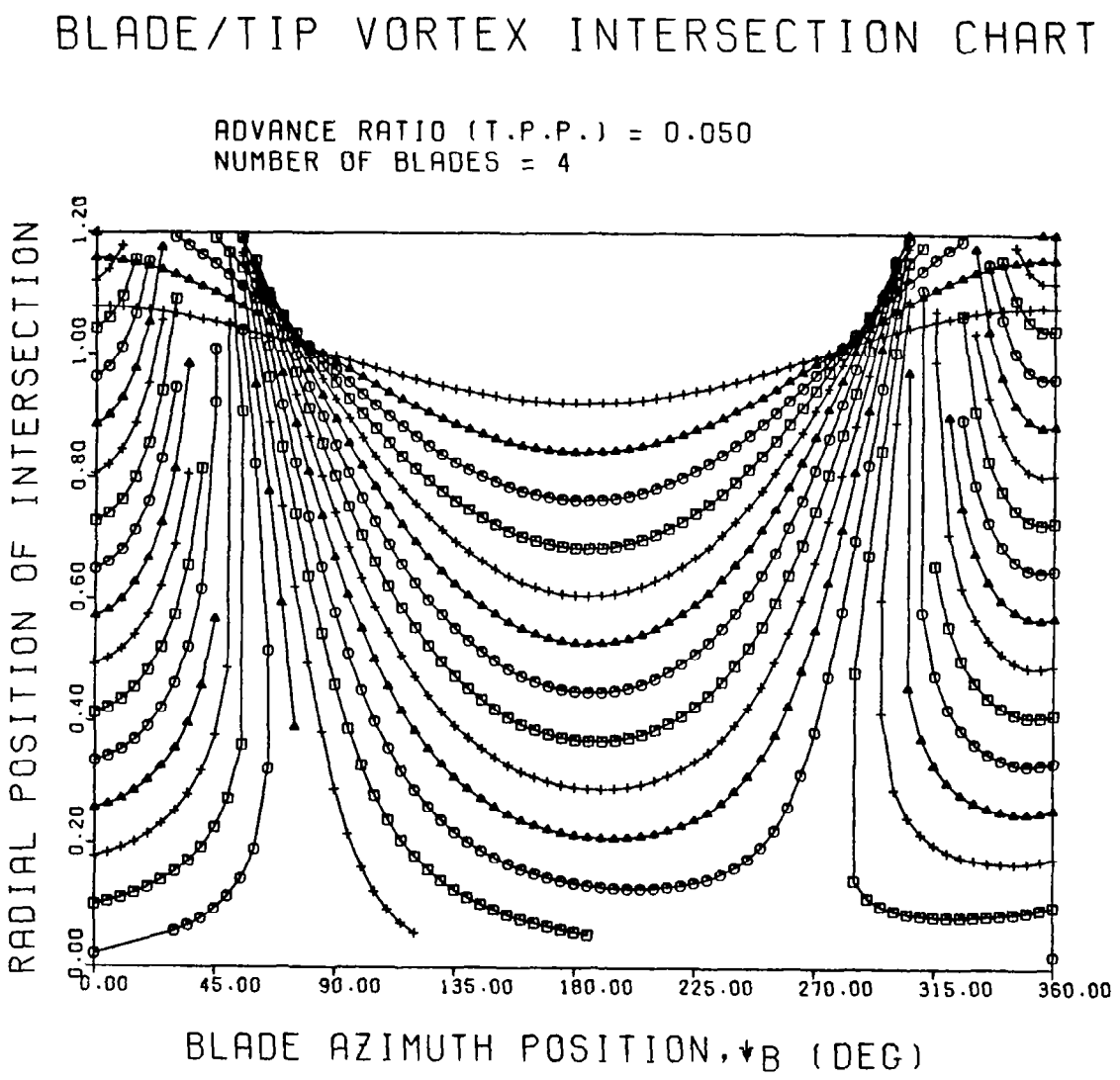

FIGURE 32A. POTENTIAL BLADE/TIP VORTEX INTERSECTION PLOT FOR FOUR BLADES (RECTILINEAR FORMAT), μ = .05

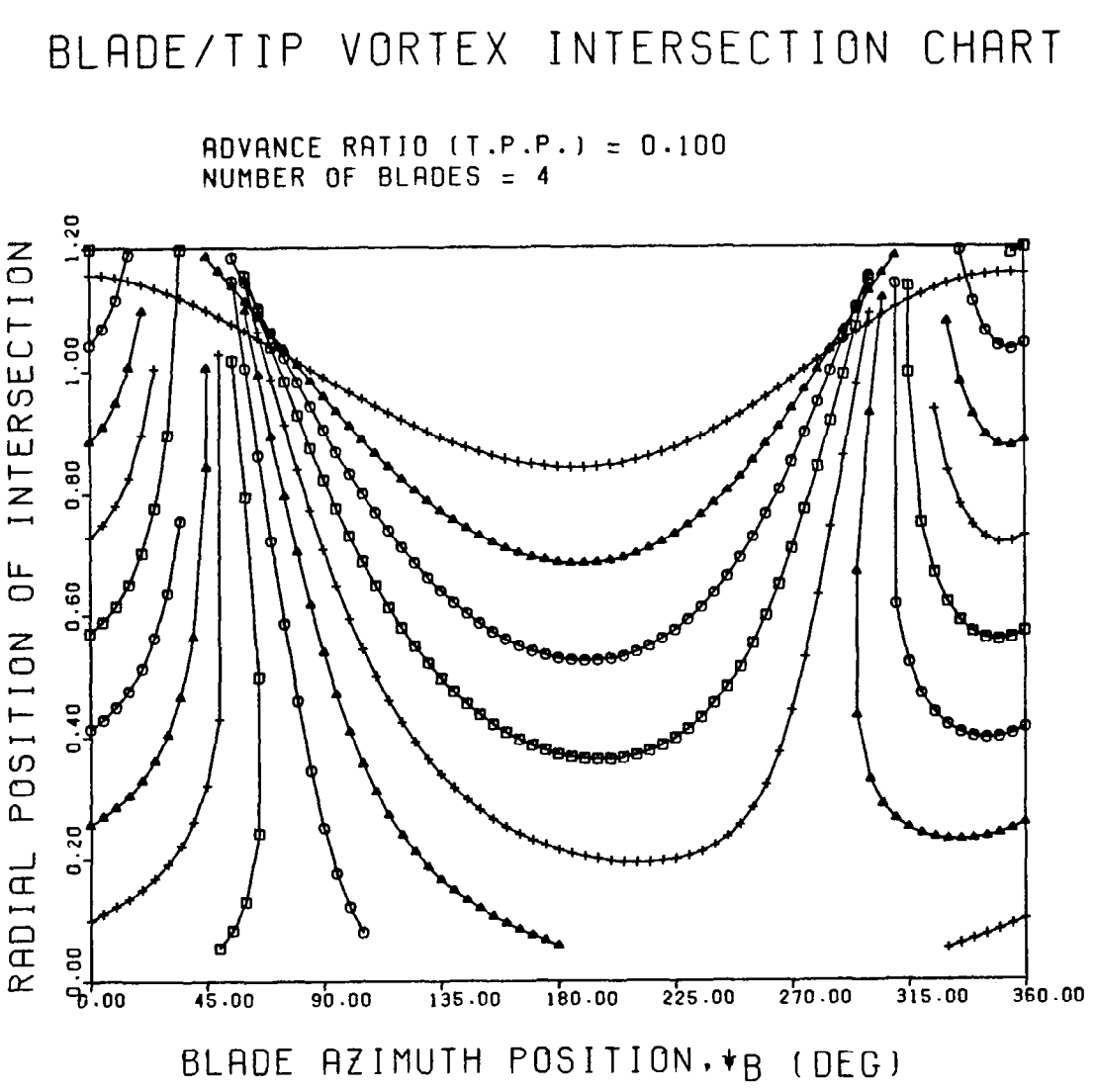

FIGURE 32B. POTENTIAL BLADE/TIP VORTEX INTERSECTION PLOT FOR FOUR BLADES (RECTILINEAR FORMAT), μ = .10

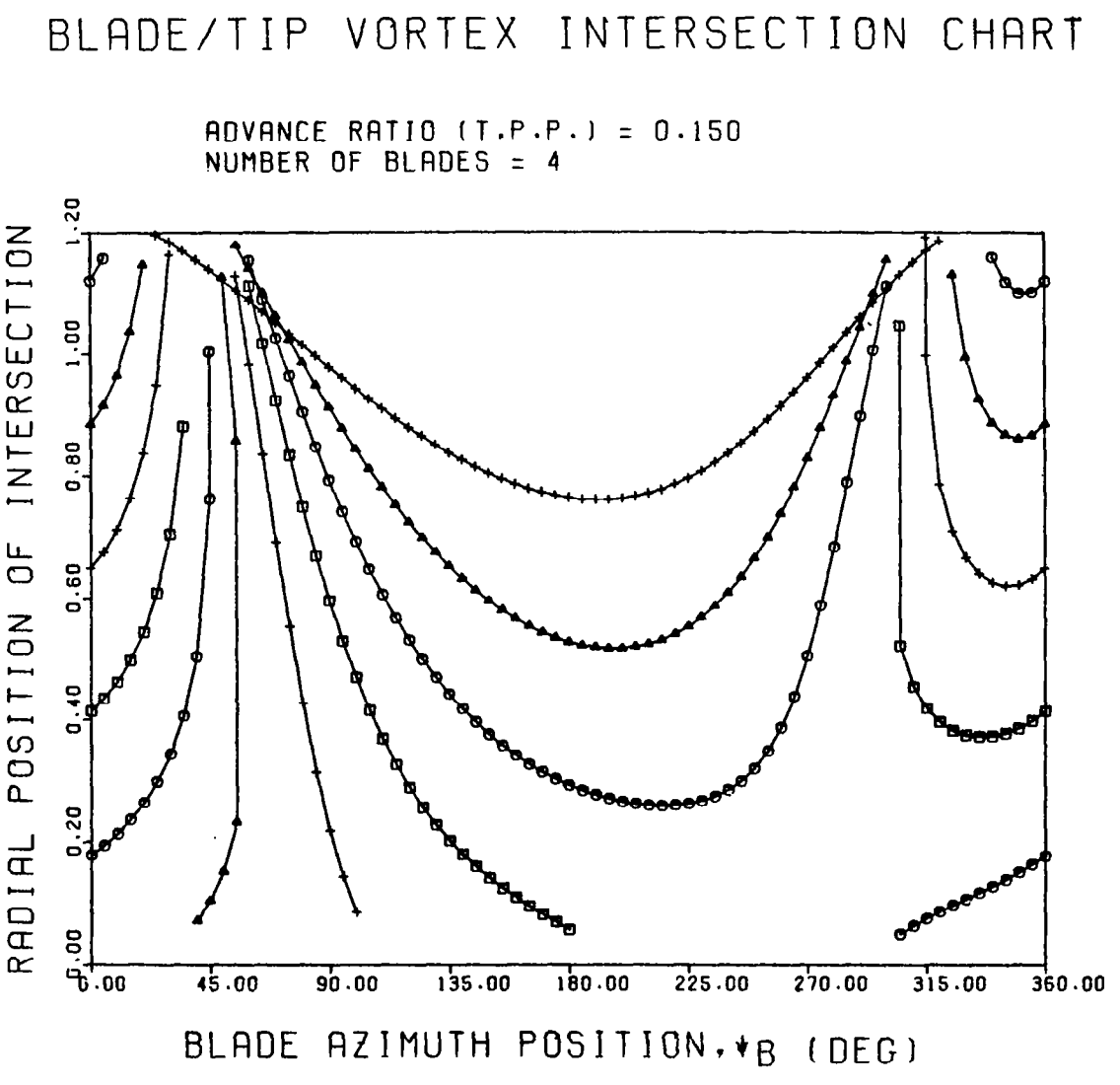

FIGURE 32C. POTENTIAL BLADE/TIP VORTEX INTERSECTION PLOT FOR FOUR BLADES (RECTILINEAR FORMAT), μ = .15

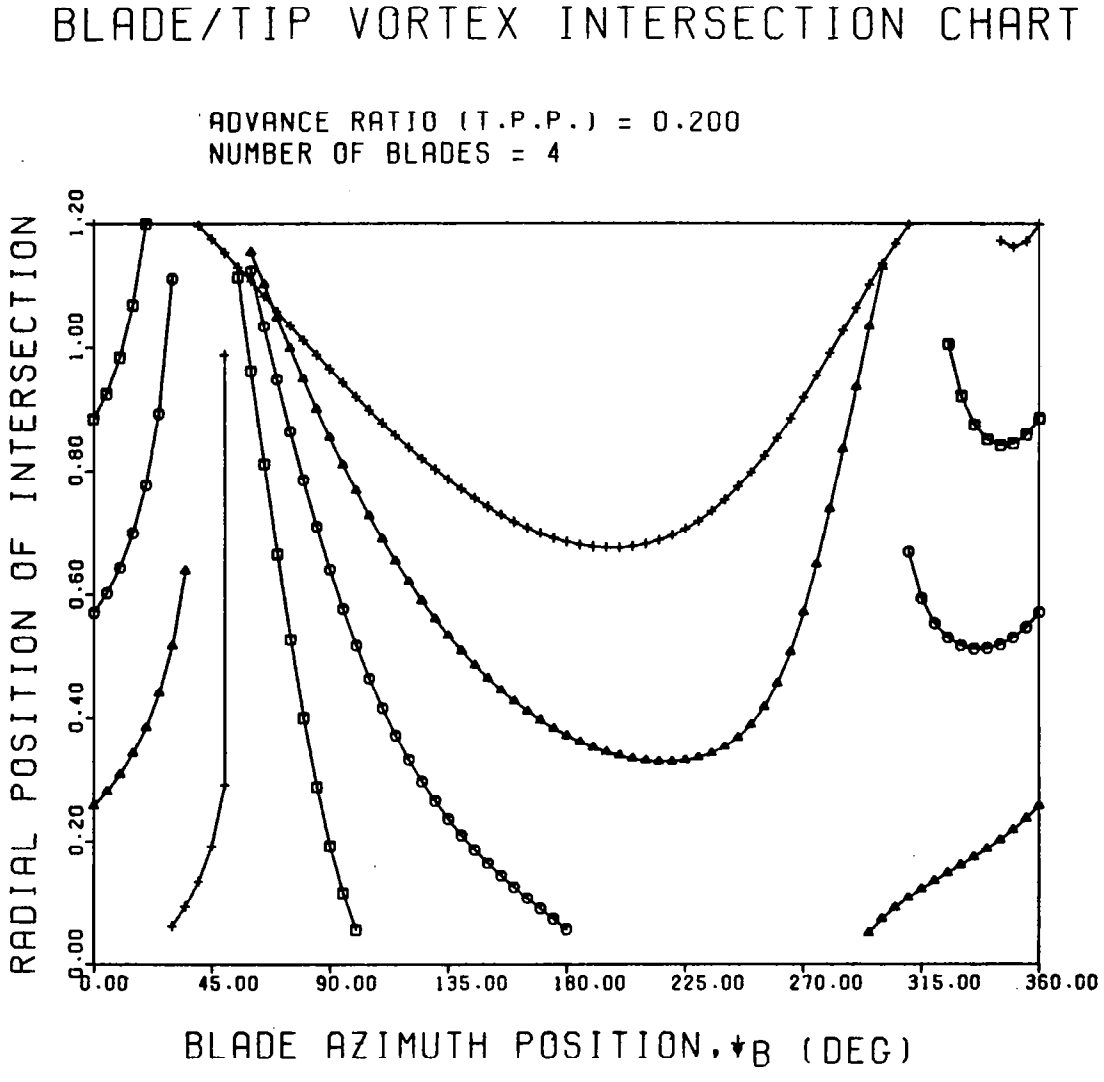

FIGURE 32D. POTENTIAL BLADE/TIP VORTEX INTERSECTION PLOT FOR FOUR BLADES (RECTILINEAR FORMAT), μ = .20

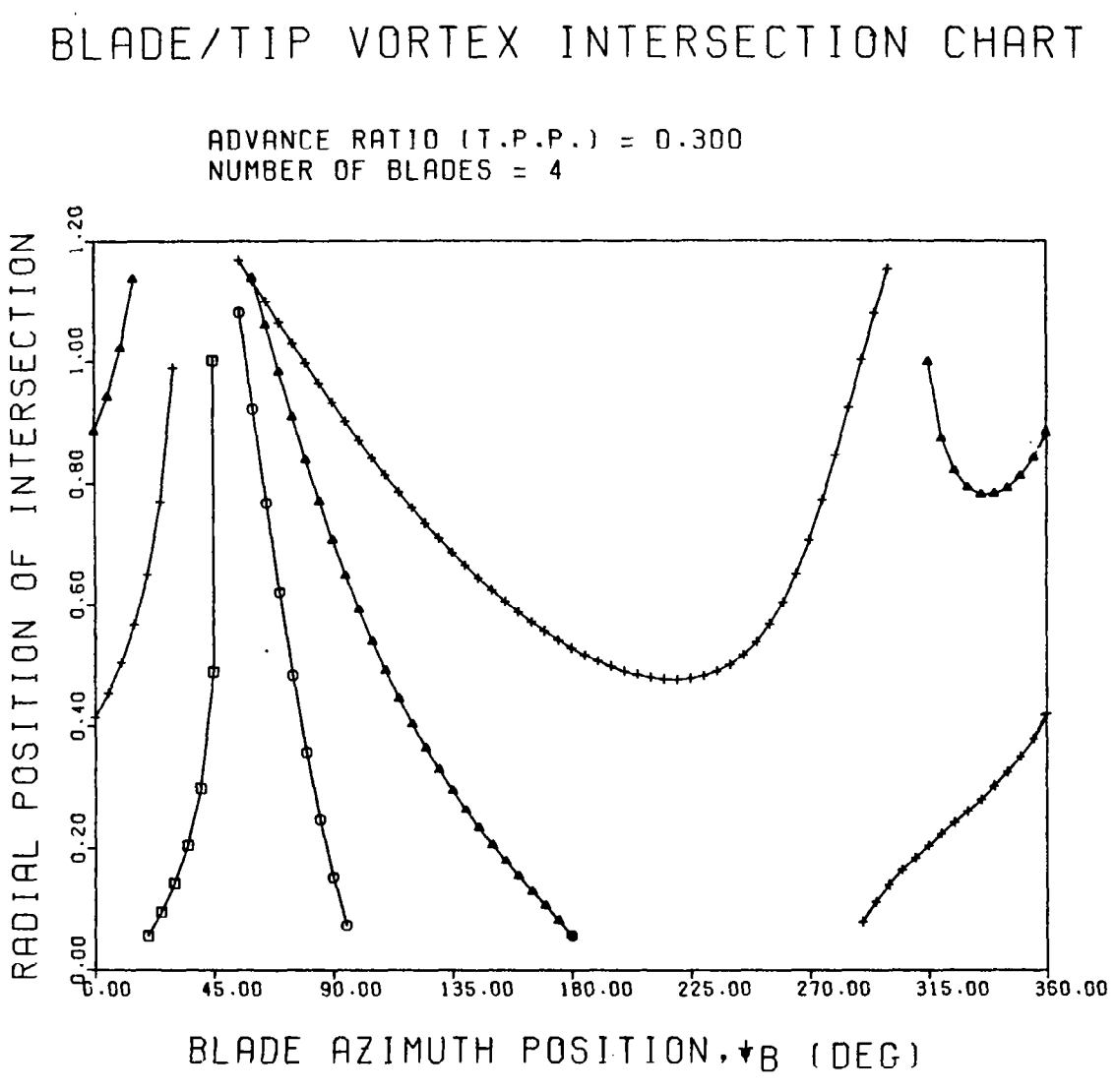

FIGURE 32E. POTENTIAL BLADE/TIP VORTEX INTERSECTION PLOT FOR FOUR BLADES (RECTILINEAR FORMAT), μ = .30

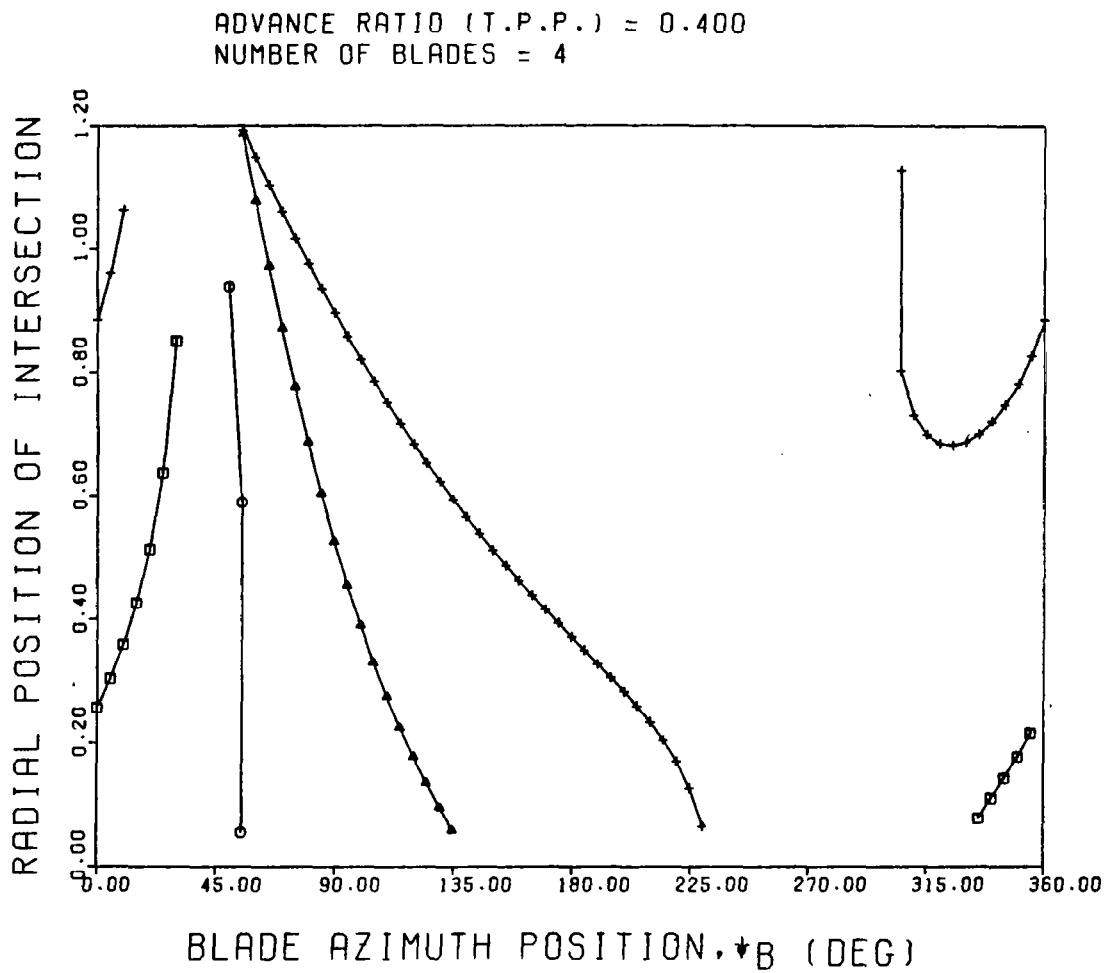

FIGURE 32F. POTENTIAL BLADE/TIP VORTEX INTERSECTION PLOT FOR FOUR BLADES (RECTILINEAR FORMAT), μ = .40

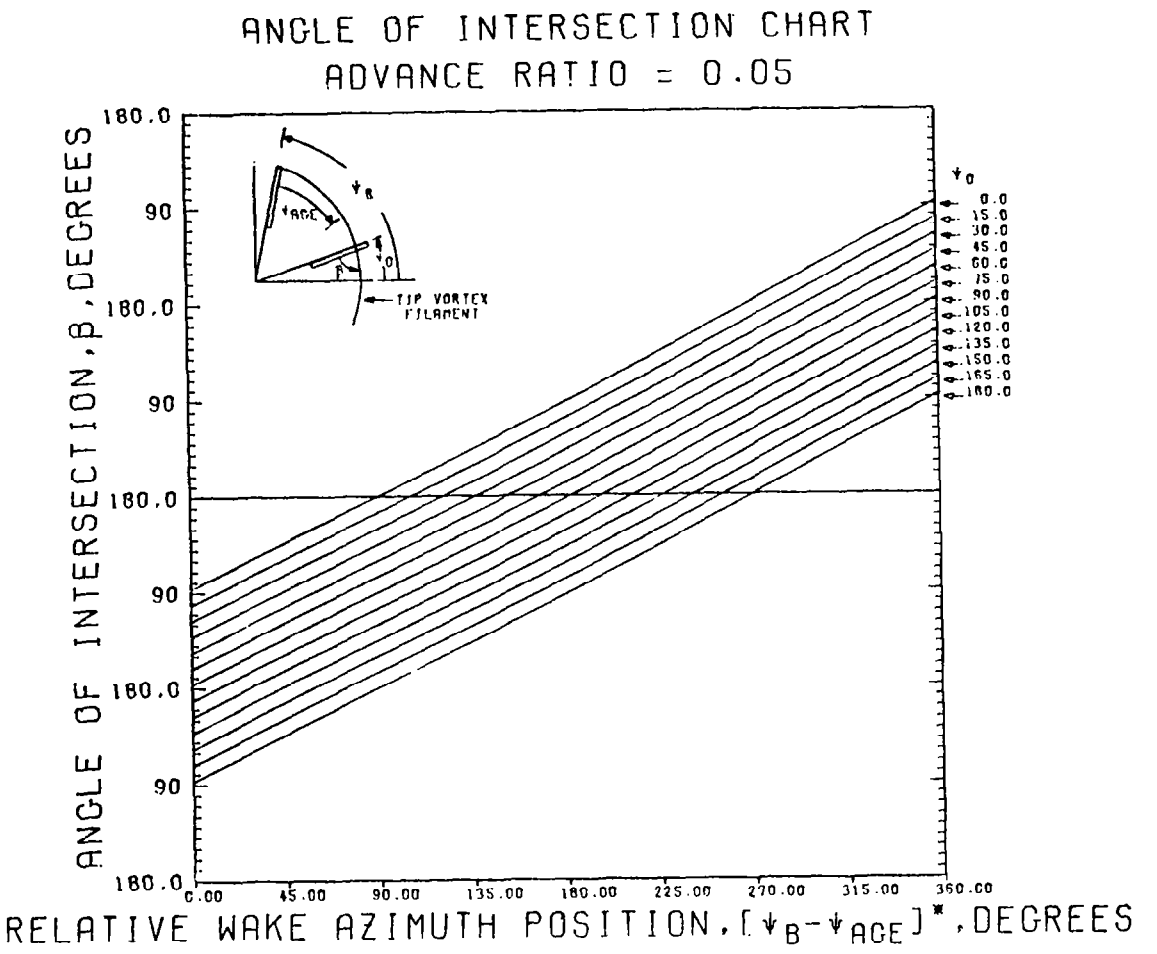

* POSITIVE RESIDUAL OF MULTIPLES OF 360 DEGREES

FIGURE 33A. BLADE/TIP VORTEX INTERSECTION ANGLE, μ = .05

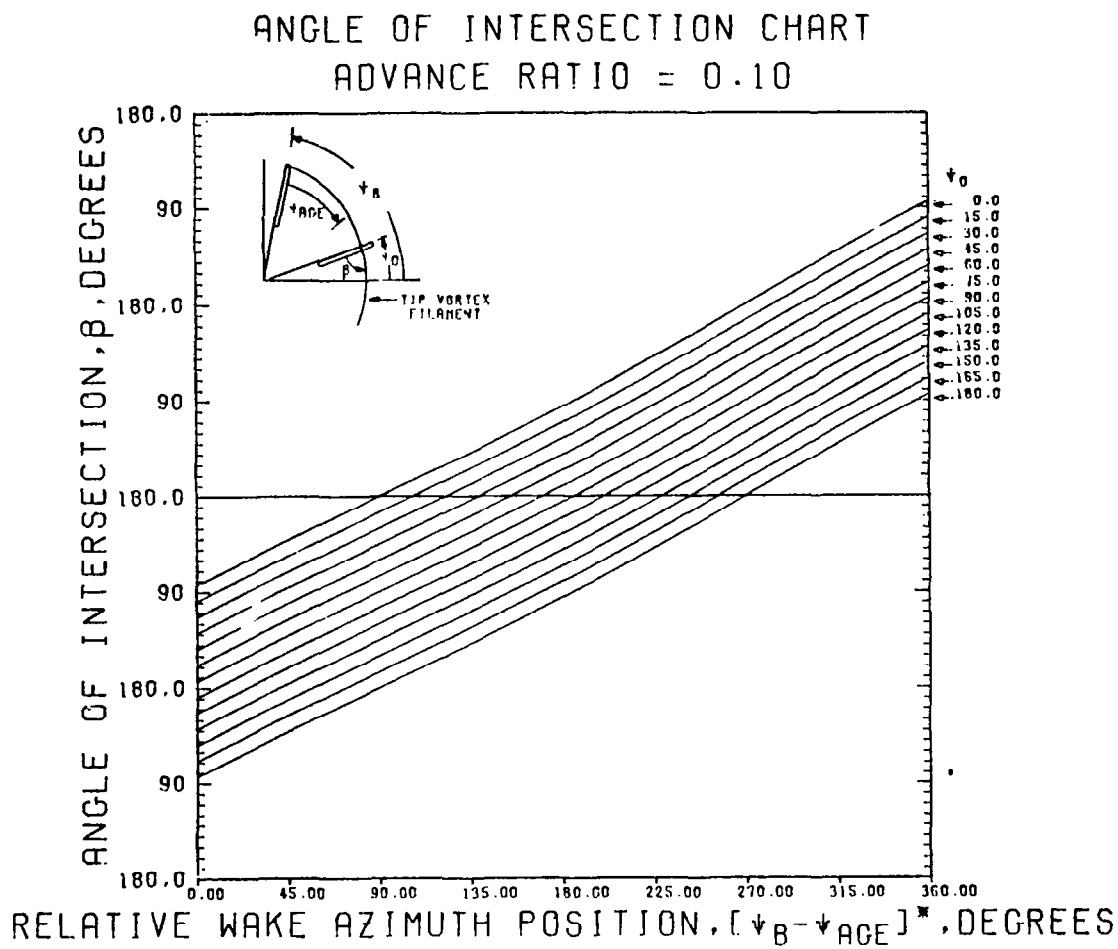

FIGURE 33B. BLADE/TIP VORTEX INTERSECTION ANGLE, μ = .10

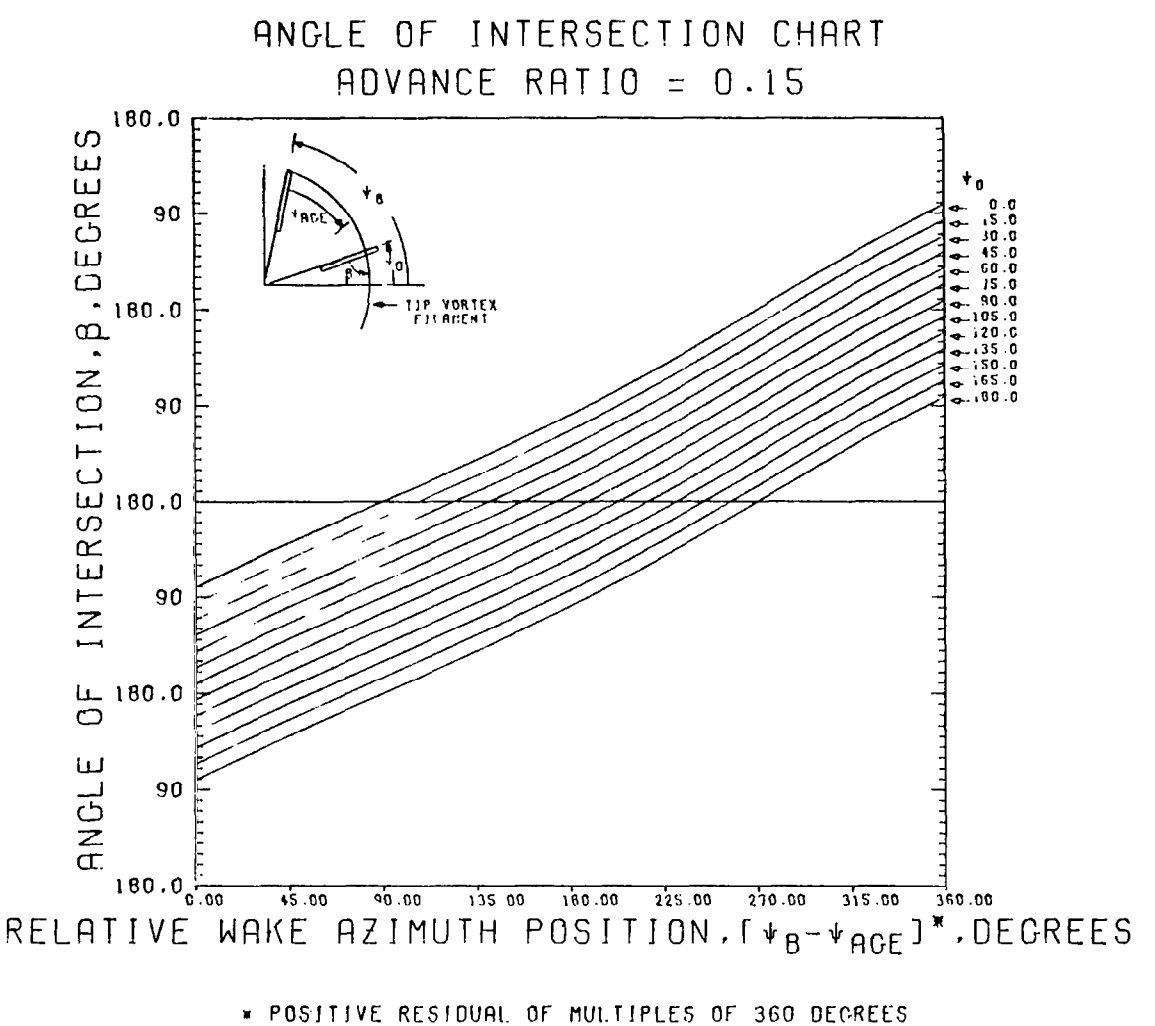

FIGURE 33C. BLADE/TIP VORTEX INTERSECTION ANGLE, μ = .15

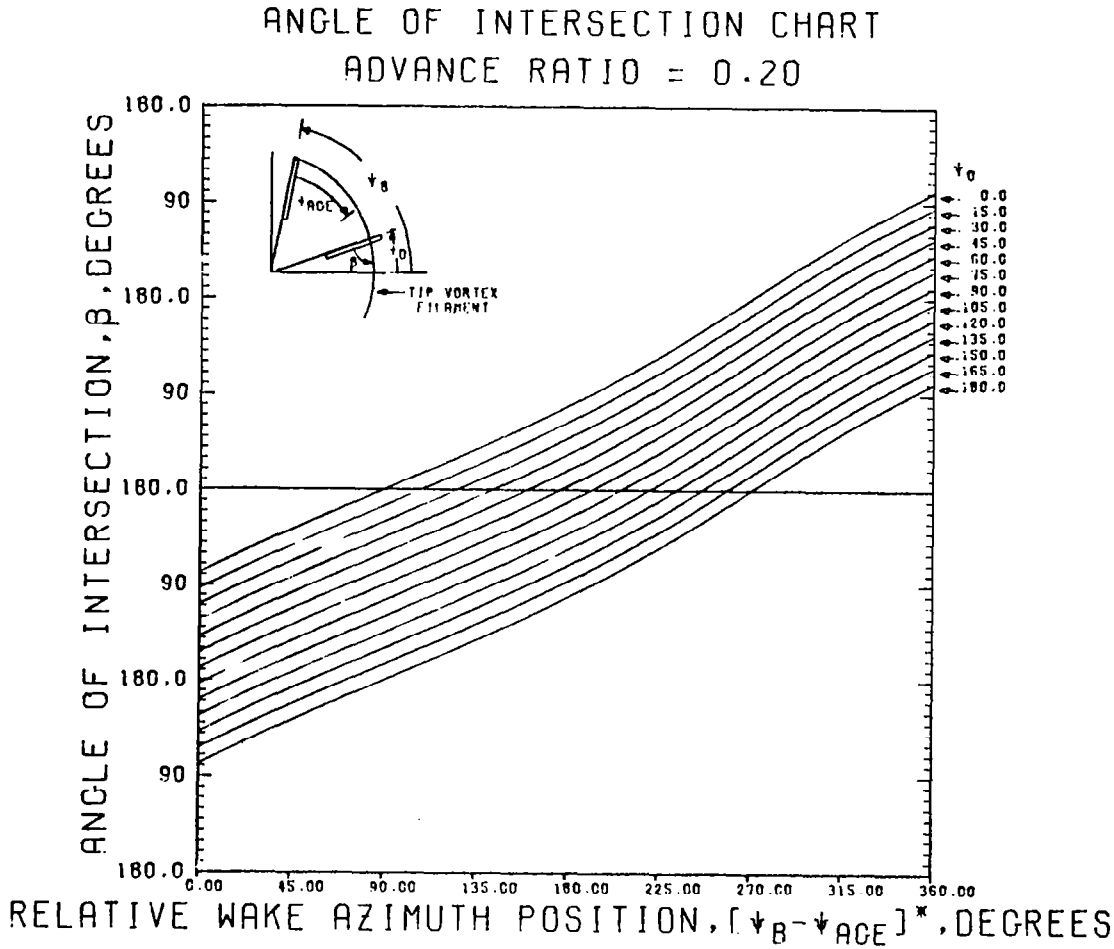

FIGURE 33D. BLADE/TIP VORTEX INTERSECTION ANGLE, μ = .20

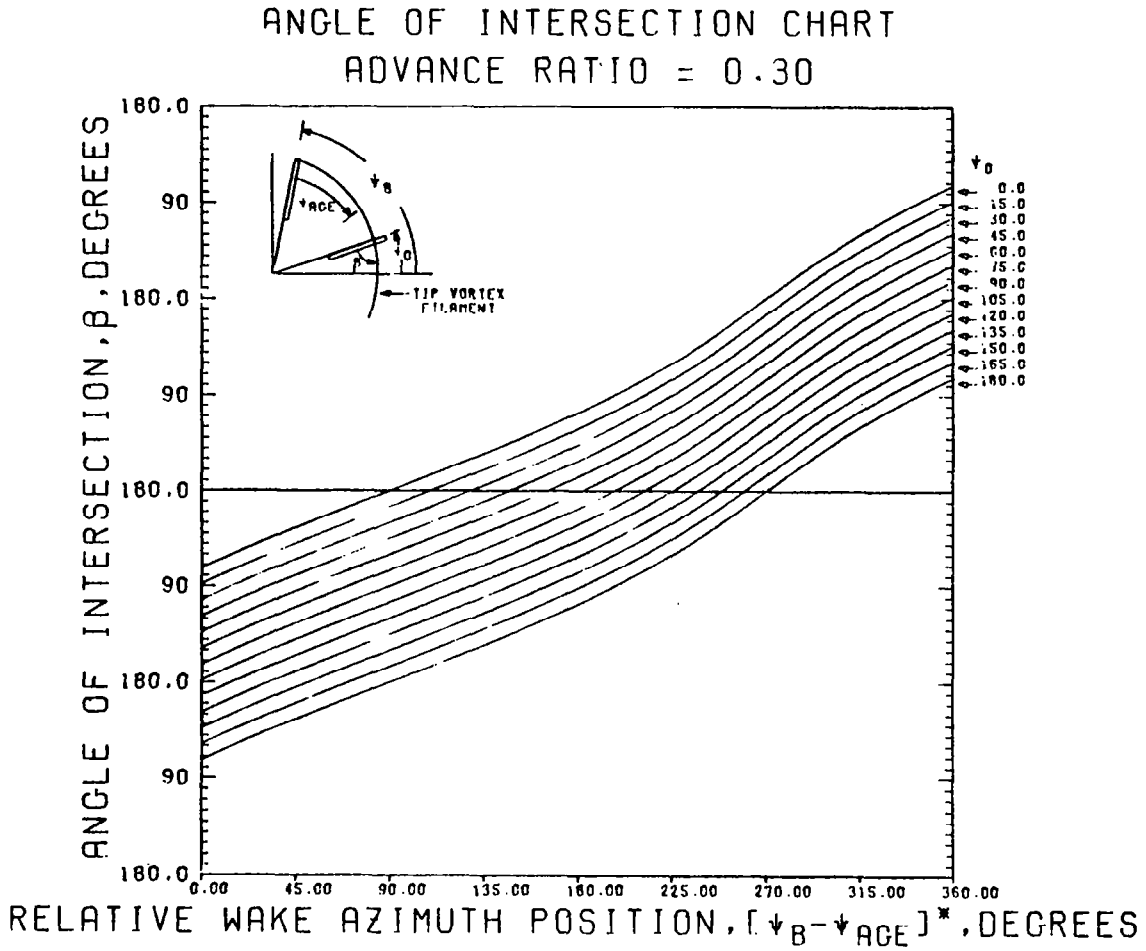

* POSITIVE RESIDUAL OF MULTIPLES OF 360 DEGREES

FIGURE 33E. BLADE/TIP VORTEX INTERSECTION ANGLE, μ = .30

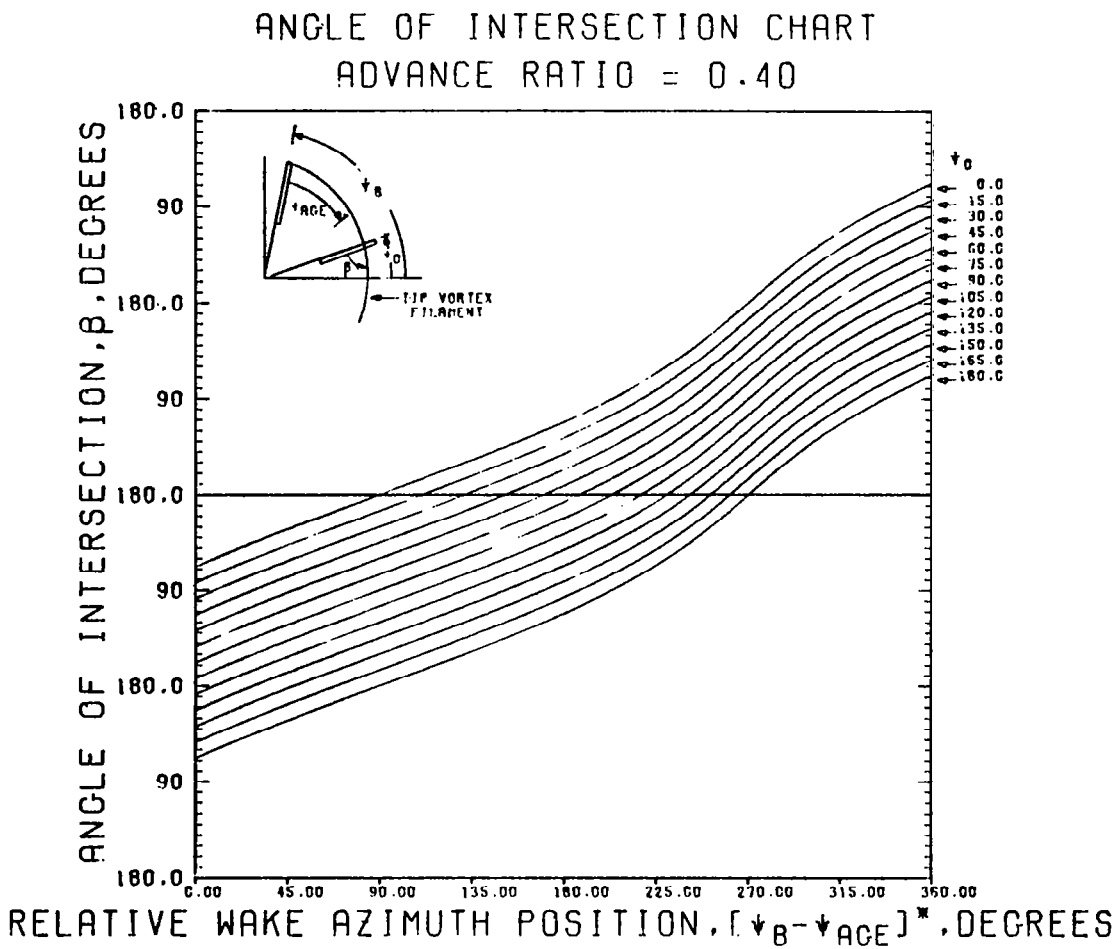

FIGURE 33F. BLADE/TIP VORTEX INTERSECTION ANGLE, μ = .40

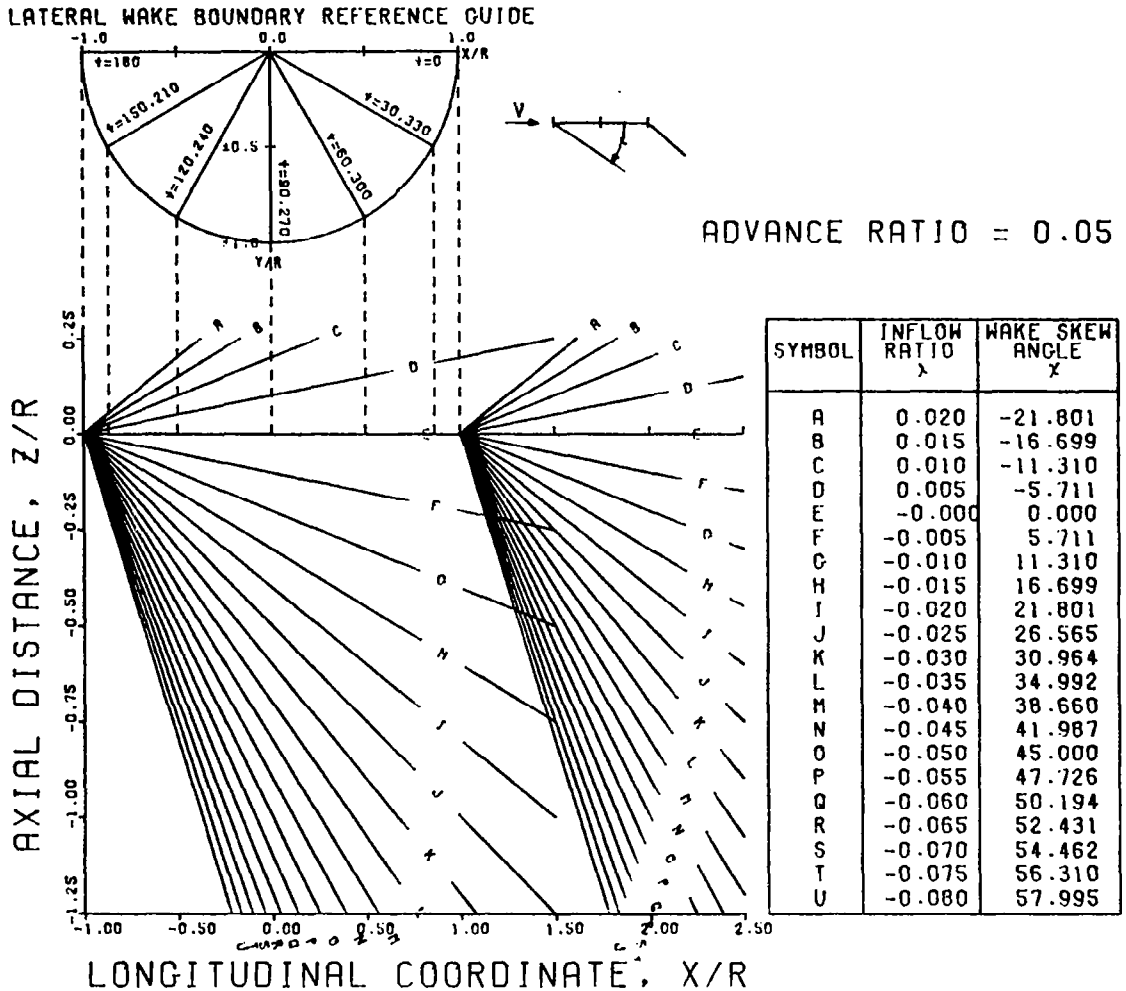

SYMBOL	INFLOW RATIO λ	WAKE SKEW ANGLE χ
A	0.020	-21.801
B	0.015	-16.699
C	0.010	-11.310
D	0.005	-5.711
E	-0.000	0.000
F	-0.005	5.711
G	-0.010	11.310
H	-0.015	16.699
I	-0.020	21.801
J	-0.025	26.565
K	-0.030	30.964
L	-0.035	34.992
M	-0.040	38.660
N	-0.045	41.987
O	-0.050	45.000
P	-0.055	47.726
Q	-0.060	50.194
R	-0.065	52.431
S	-0.070	54.462
T	-0.075	56.310
U	-0.080	57.995

FIGURE 34A. FORE AND AFT WAKE BOUNDARIES FOR THE UNDISTORTED WAKE MODEL, μ = .05

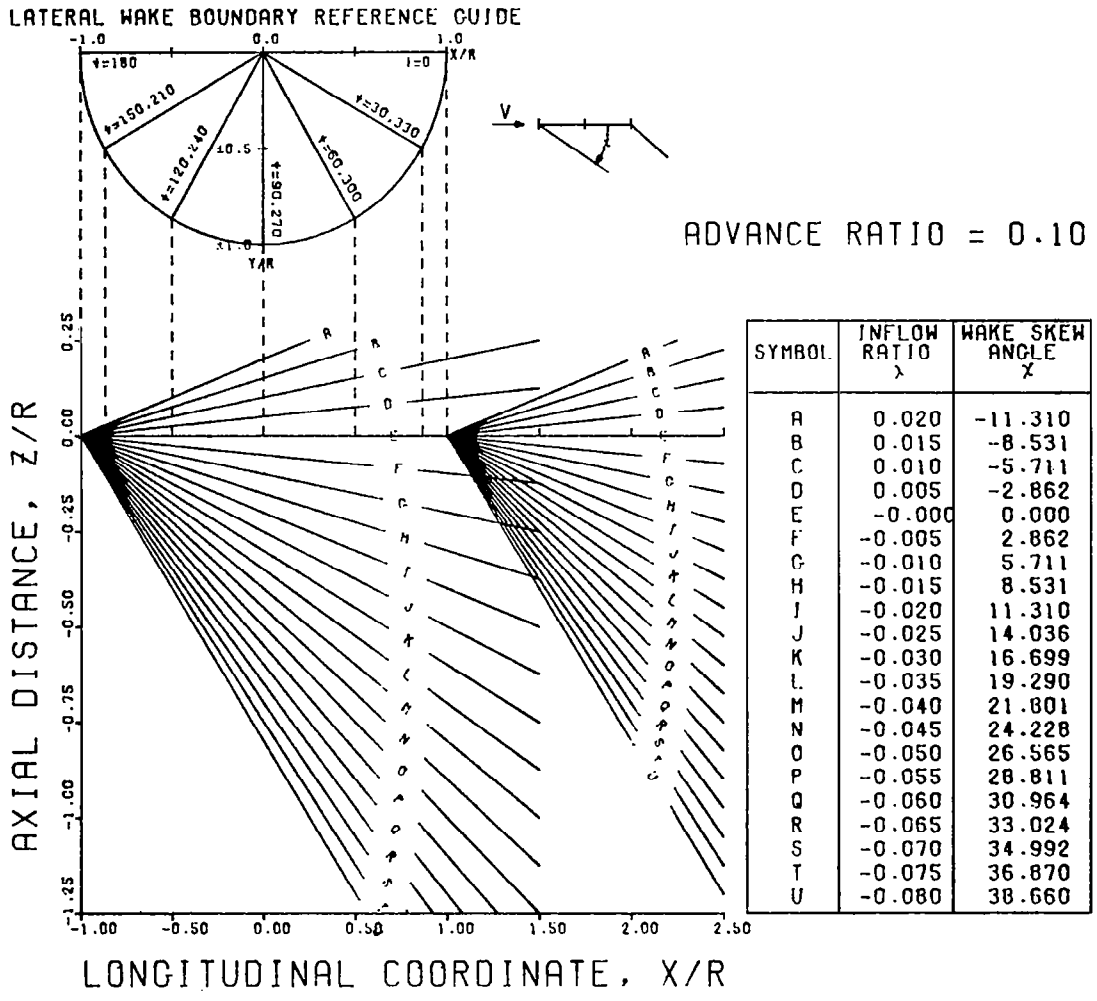

FIGURE 34B. FORE AND AFT WAKE BOUNDARIES FOR THE UNDISTORTED WAKE MODEL, μ = .10

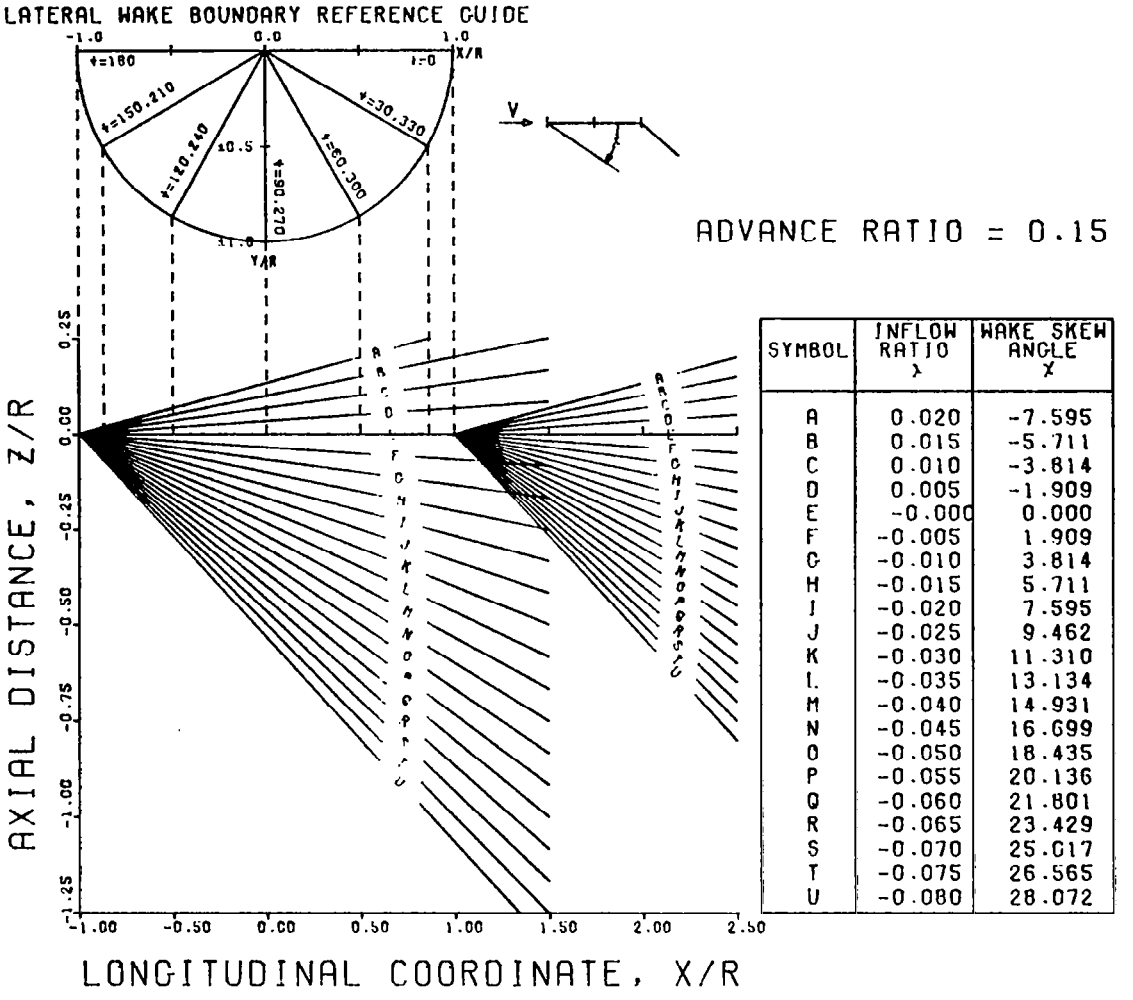

FIGURE 34C. FORE AND AFT WAKE BOUNDARIES FOR THE UNDISTORTED WAKE MODEL, μ = .15

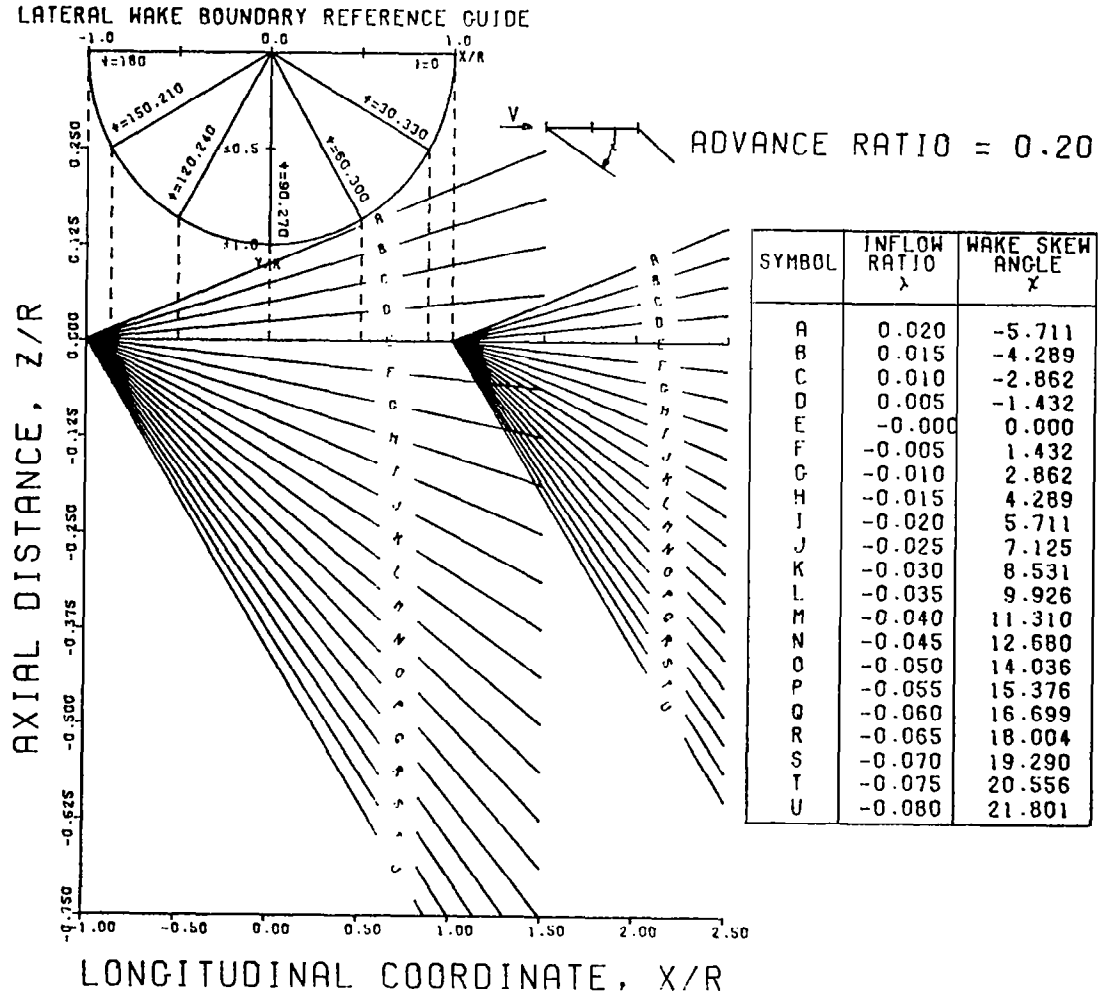

SYMBOL	INFLOW RATIO λ	WAKE SKEW ANGLE χ
A	0.020	-5.711
B	0.015	-4.289
C	0.010	-2.862
D	0.005	-1.432
E	-0.000	0.000
F	-0.005	1.432
G	-0.010	2.862
H	-0.015	4.289
I	-0.020	5.711
J	-0.025	7.125
K	-0.030	8.531
L	-0.035	9.926
M	-0.040	11.310
N	-0.045	12.680
O	-0.050	14.036
P	-0.055	15.376
Q	-0.060	16.699
R	-0.065	18.004
S	-0.070	19.290
T	-0.075	20.556
U	-0.080	21.801

FIGURE 34D. FORE AND AFT WAKE BOUNDARIES FOR THE UNDISTORTED WAKE MODEL, μ = .20

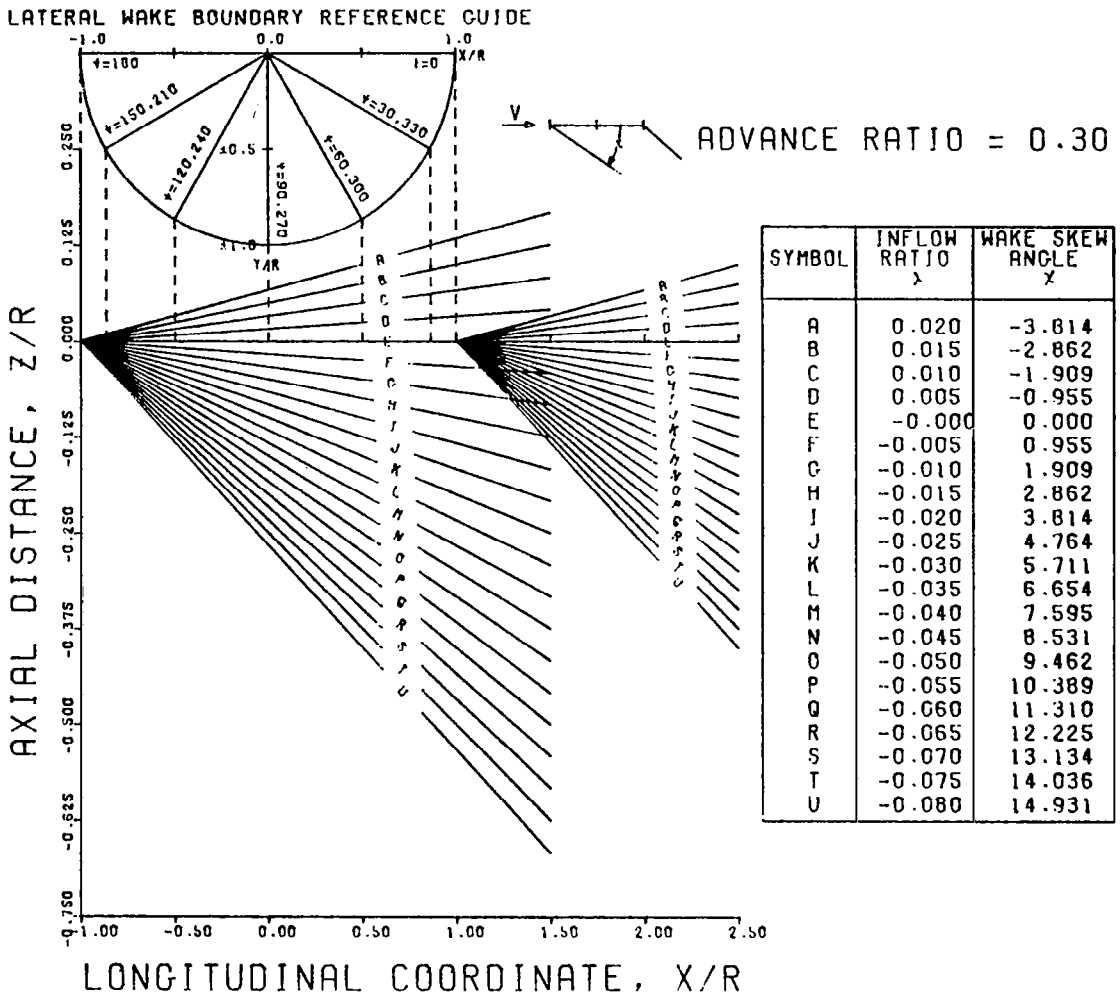

FIGURE 34E. FORE AND AFT WAKE BOUNDARIES FOR THE UNDISTORTED WAKE MODEL, μ = .30

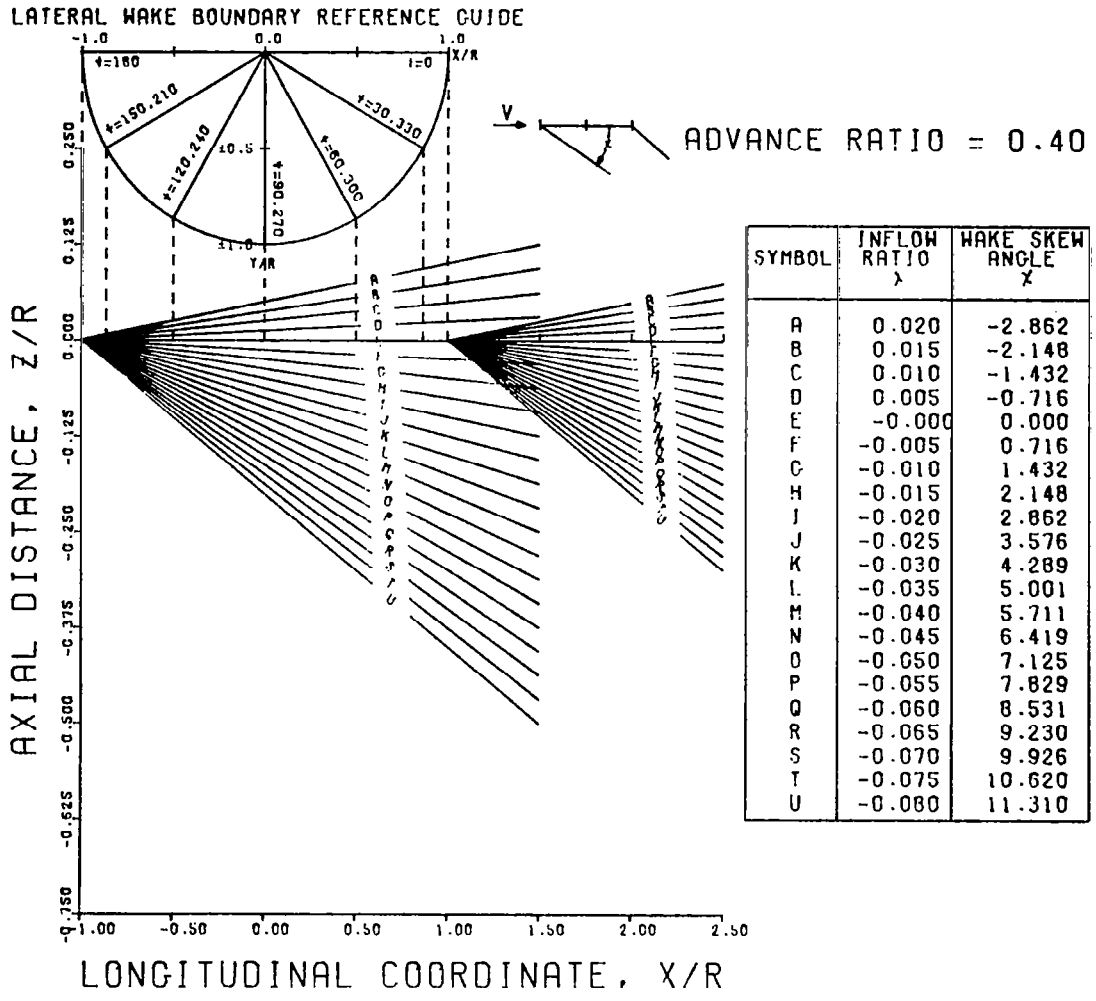

SYMBOL	INFLOW RATIO λ	WAKE SKEW ANGLE χ
A	0.020	-2.862
B	0.015	-2.148
C	0.010	-1.432
D	0.005	-0.716
E	-0.000	0.000
F	-0.005	0.716
G	-0.010	1.432
H	-0.015	2.148
I	-0.020	2.862
J	-0.025	3.576
K	-0.030	4.289
L	-0.035	5.001
M	-0.040	5.711
N	-0.045	6.419
O	-0.050	7.125
P	-0.055	7.829
Q	-0.060	8.531
R	-0.065	9.230
S	-0.070	9.926
T	-0.075	10.620
U	-0.080	11.310

FIGURE 34F. FORE AND AFT WAKE BOUNDARIES FOR THE UNDISTORTED WAKE MODEL, μ = .40

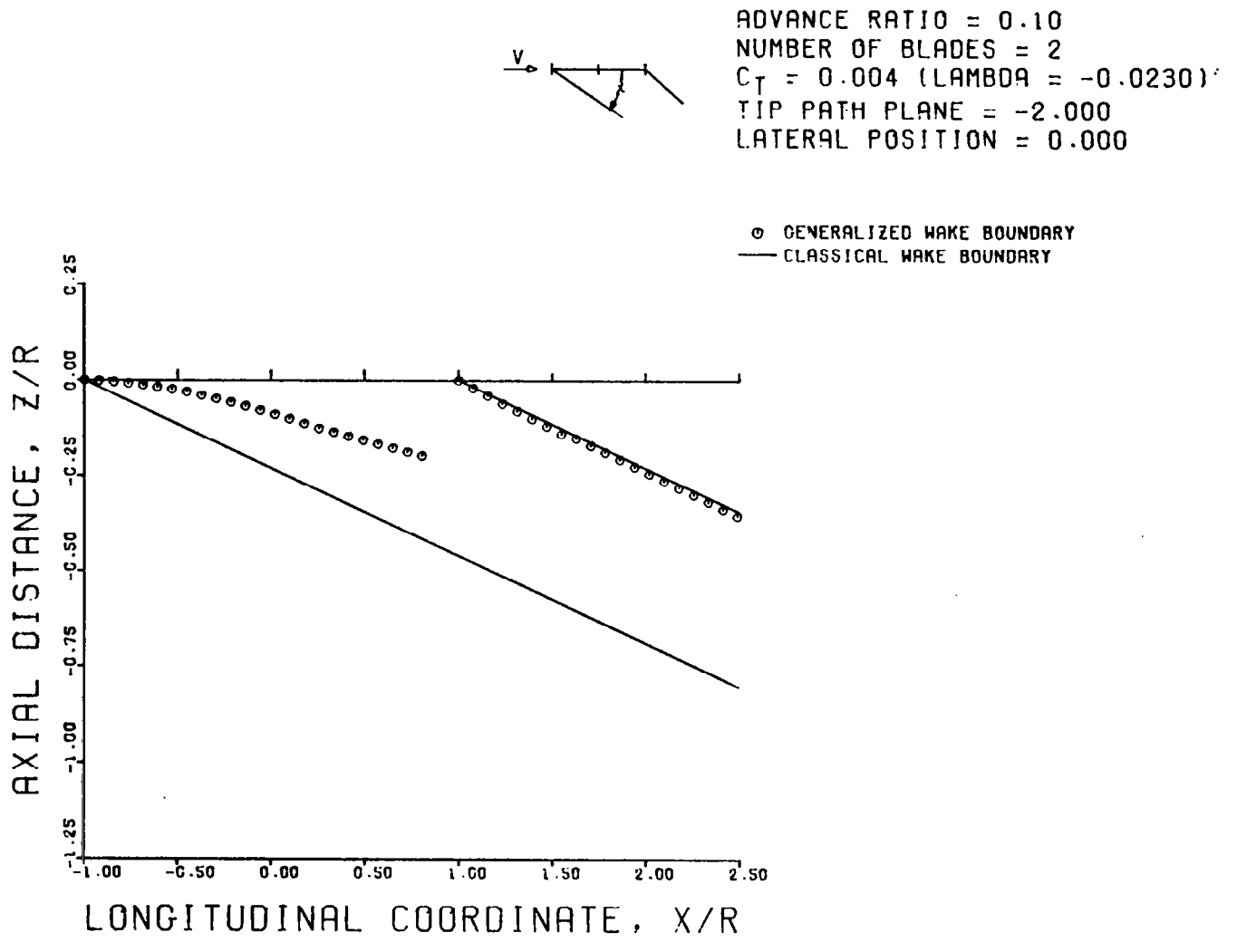

FIGURE 35A. FORE AND AFT WAKE BOUNDARY CHARTS FOR THE GENERALIZED DISTORTED TIP VORTEX (μ = .1, B = 2, C_T = .004, α = -2), Y/R = 0.0

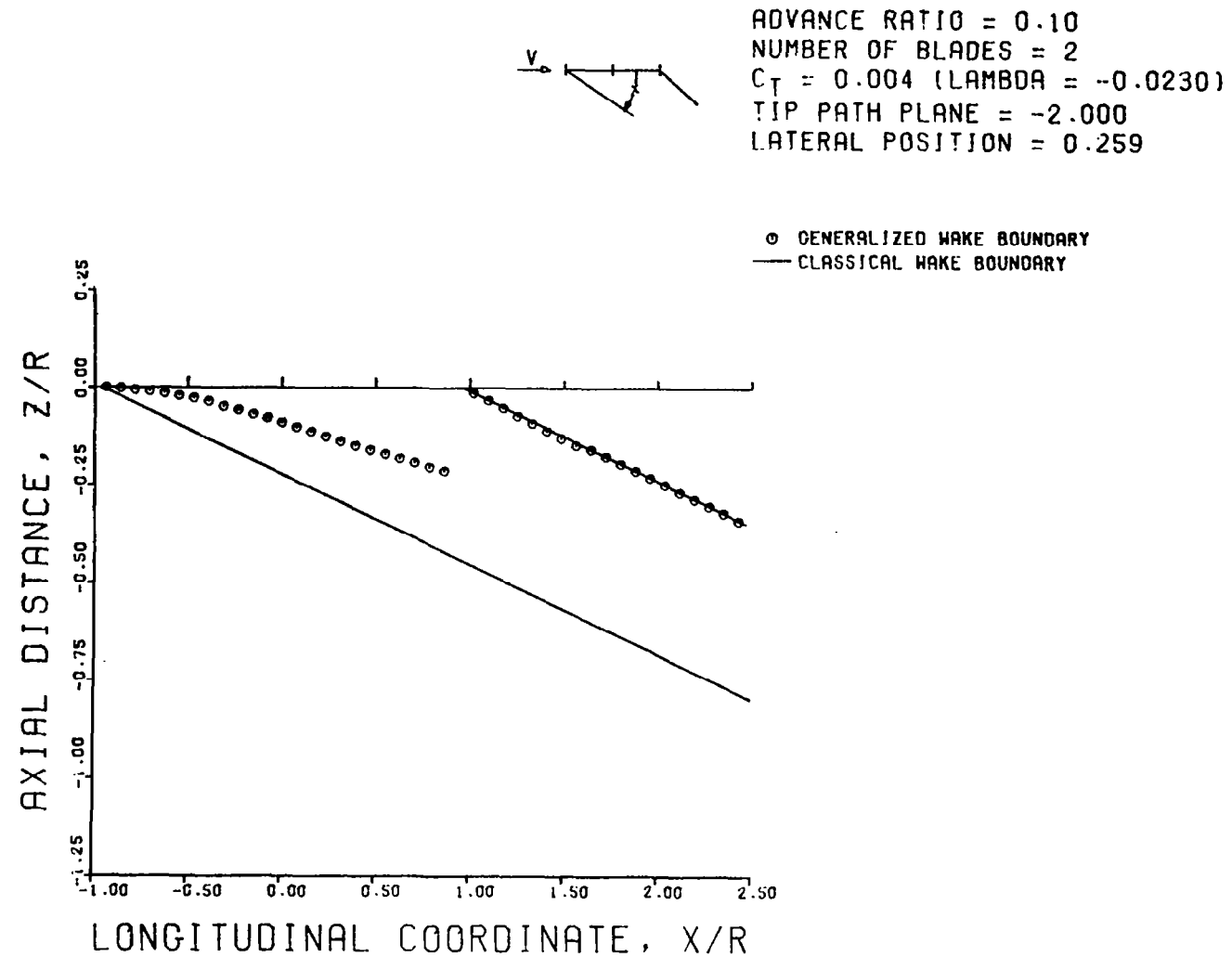

FIGURE 35B. FORE AND AFT WAKE BOUNDARY CHARTS FOR THE GENERALIZED DISTORTED TIP VORTEX (μ = .1, B = 2, C_T = .004, α = -2), Y/R = .259

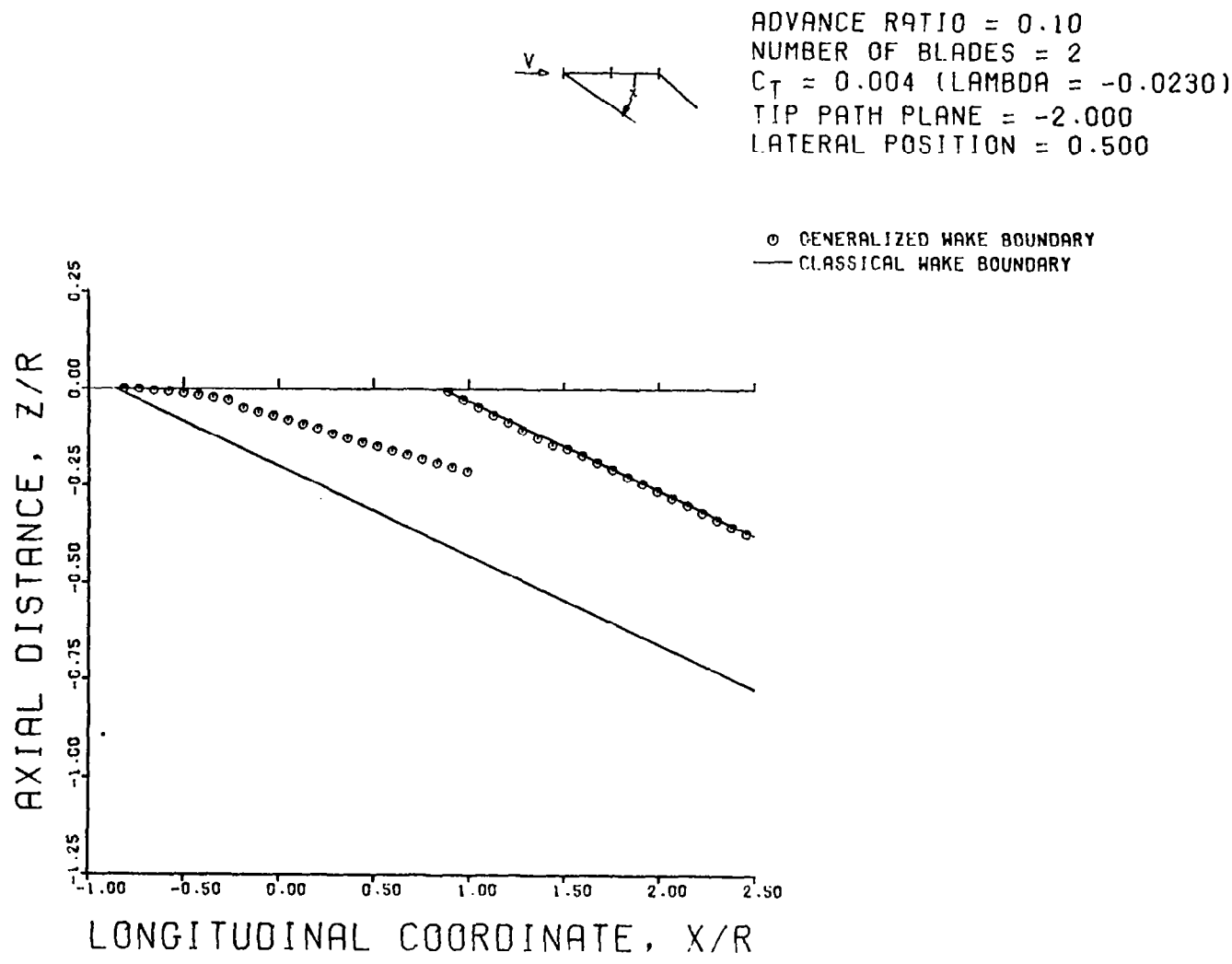

FIGURE 35C. FORE AND AFT WAKE BOUNDARY CHARTS FOR THE GENERALIZED DISTORTED TIP VORTEX (μ = .1, B = 2, C_T = .004, α = -2), Y/R = .500

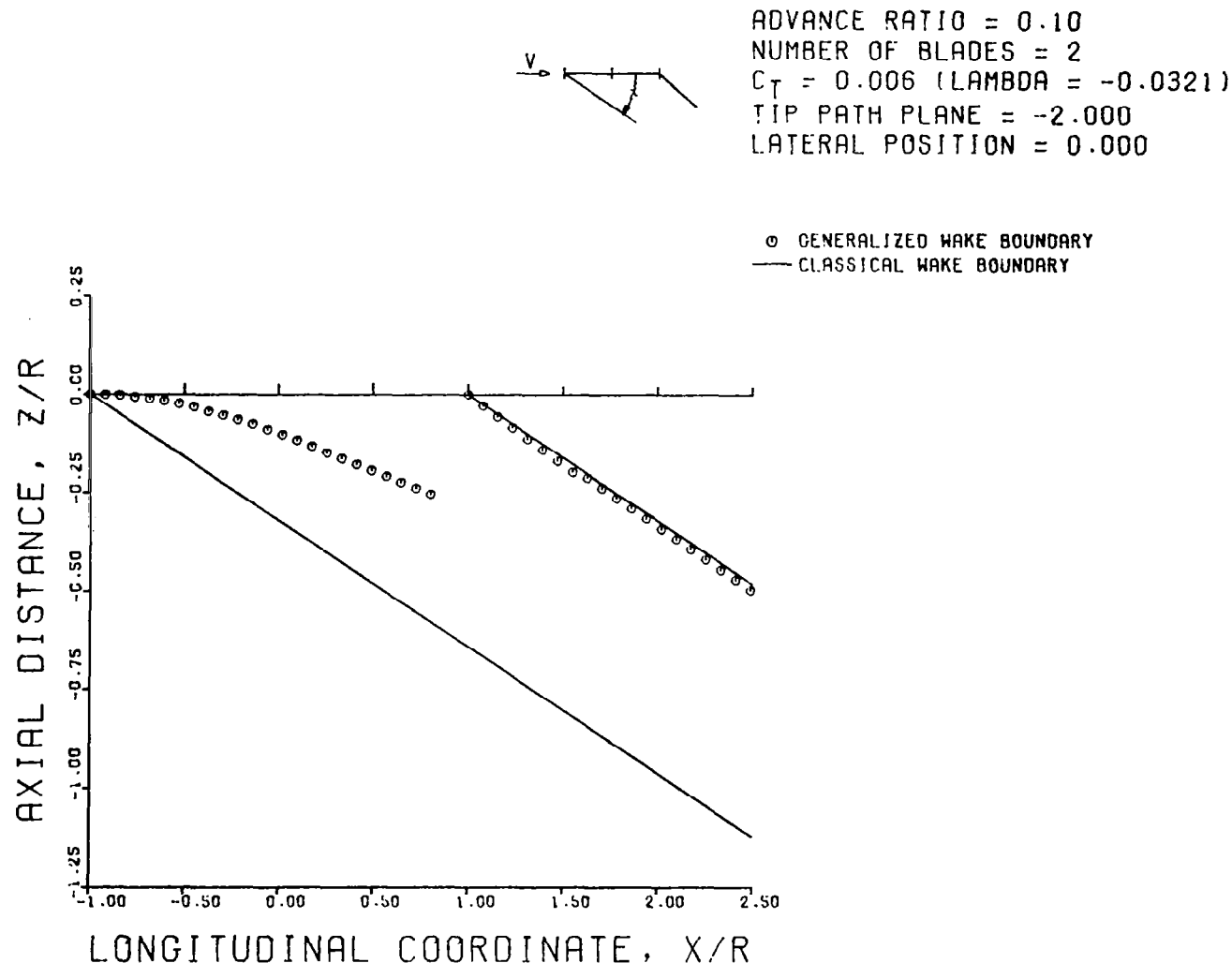

FIGURE 36A. FORE AND AFT WAKE BOUNDARY CHARTS FOR THE GENERALIZED DISTORTED TIP VORTEX (μ = .1, B = 2, C_T = .006, α = -2), Y/R = 0.0

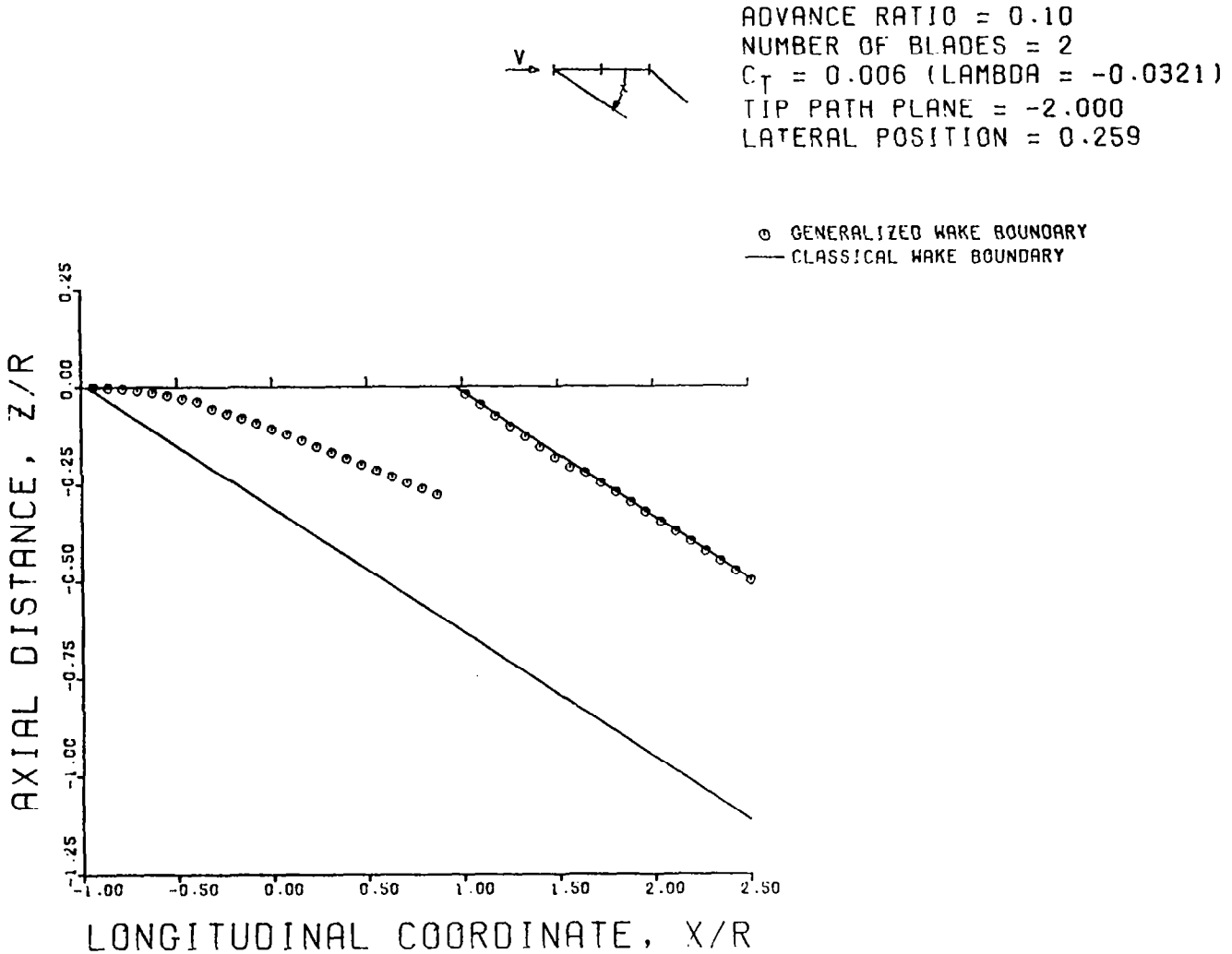

FIGURE 36B. FORE AND AFT WAKE BOUNDARY CHARTS FOR THE GENERALIZED DISTORTED TIP VORTEX (μ = .1, B = 2, C_T = .006, α = -2), Y/R = .259

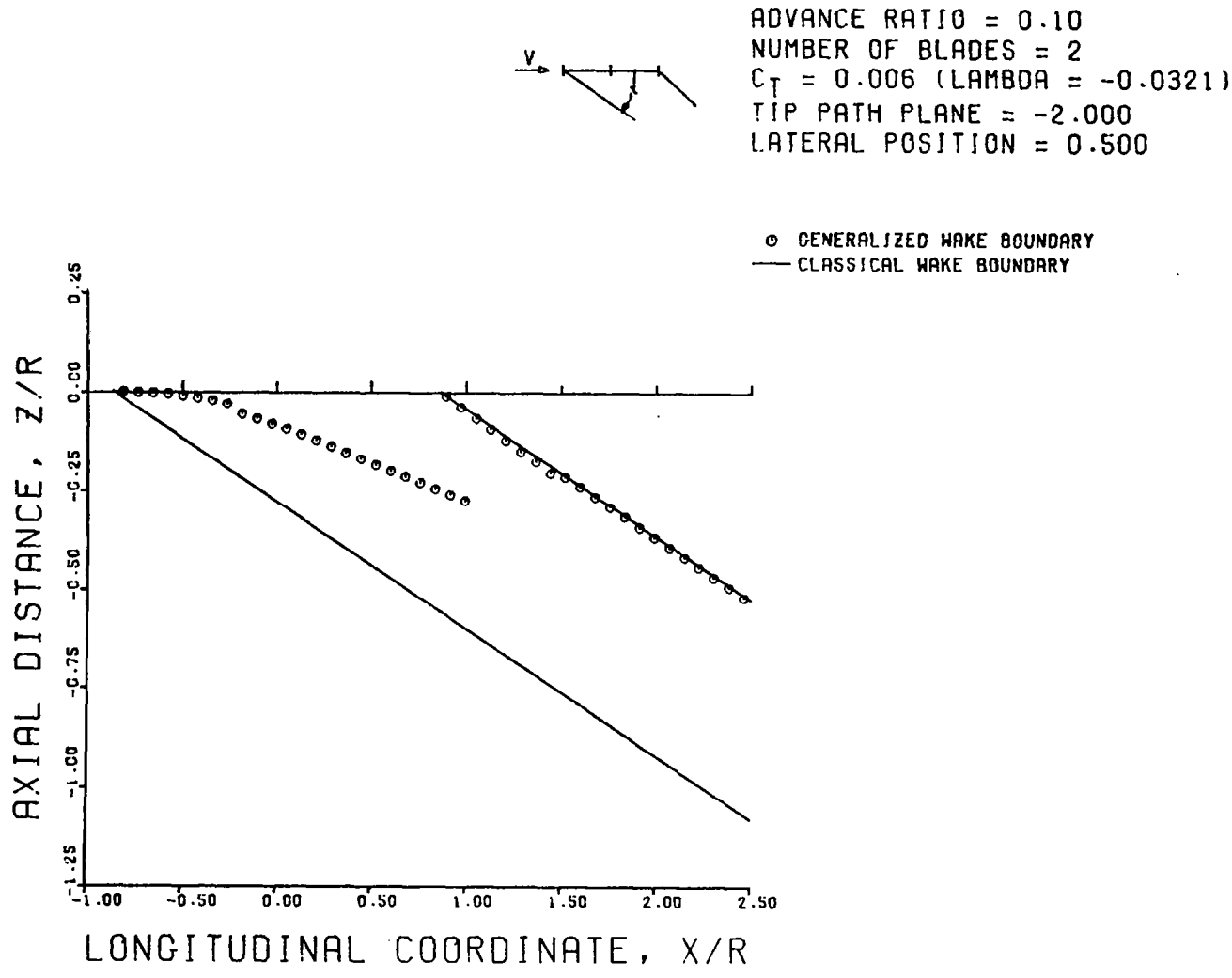

FIGURE 36C. FORE AND AFT WAKE BOUNDARY CHARTS FOR THE GENERALIZED DISTORTED TIP VORTEX (μ = .1, B = 2, C_T = .006, α = -2), Y/R = .500

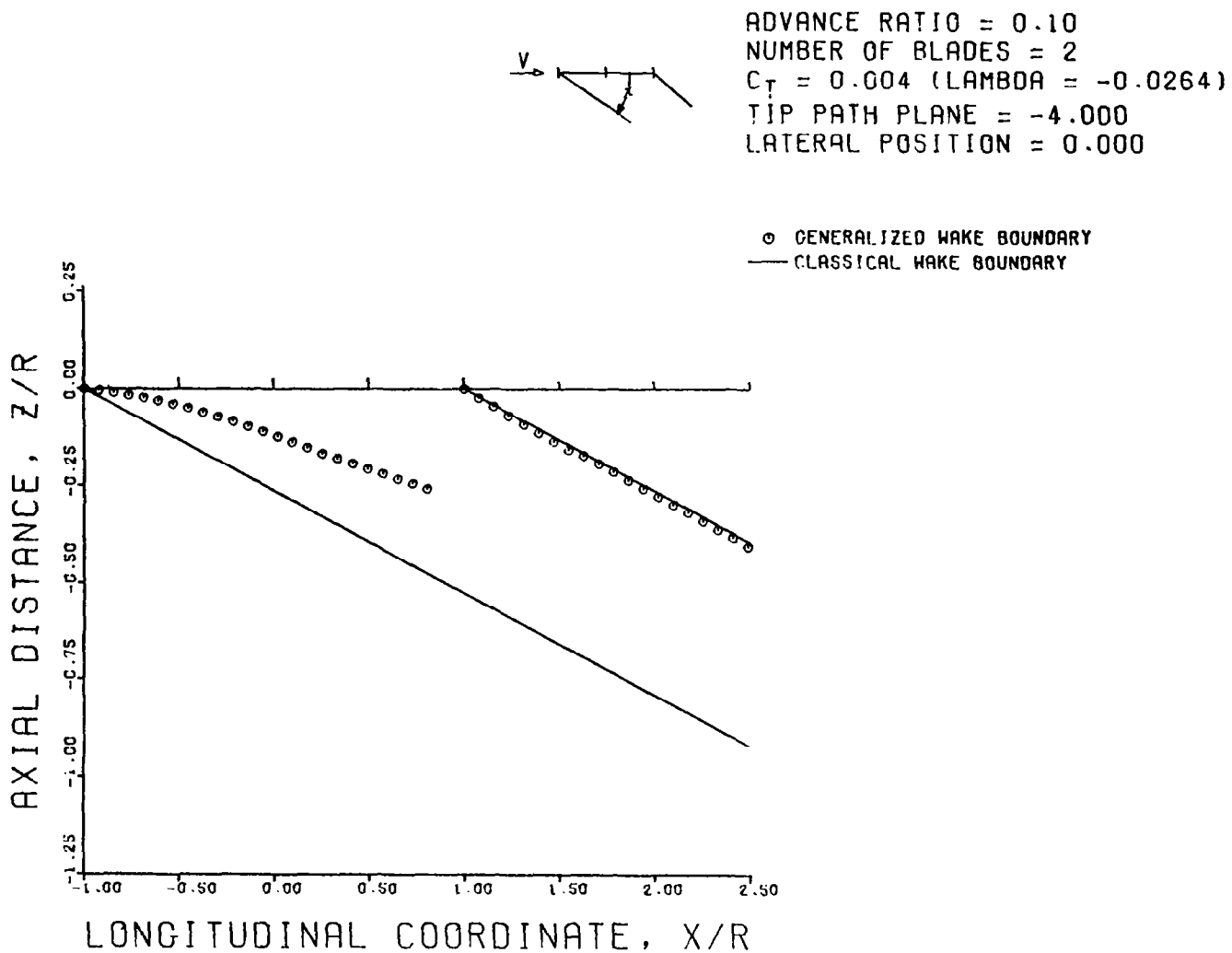

FIGURE 37A. FORE AND AFT WAKE BOUNDARY CHARTS FOR THE GENERALIZED DISTORTED TIP VORTEX (μ = .1, B = 2, C_T = .004, α = -4), Y/R = 0.0

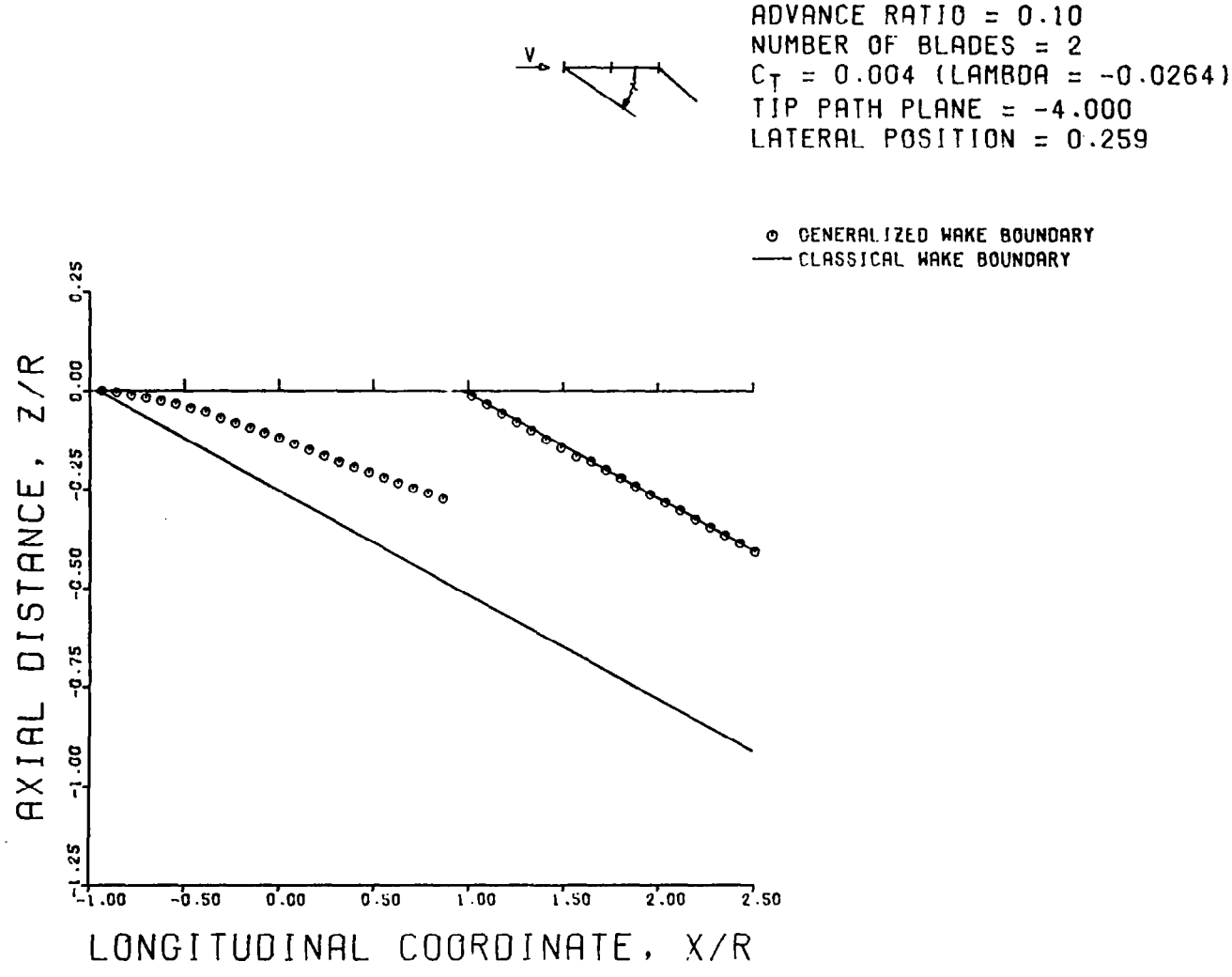

FIGURE 37B. FORE AND AFT WAKE BOUNDARY CHARTS FOR THE GENERALIZED DISTORTED TIP VORTEX (μ = .1, B = 2, C_T = .004, α = -4), Y/R = .259

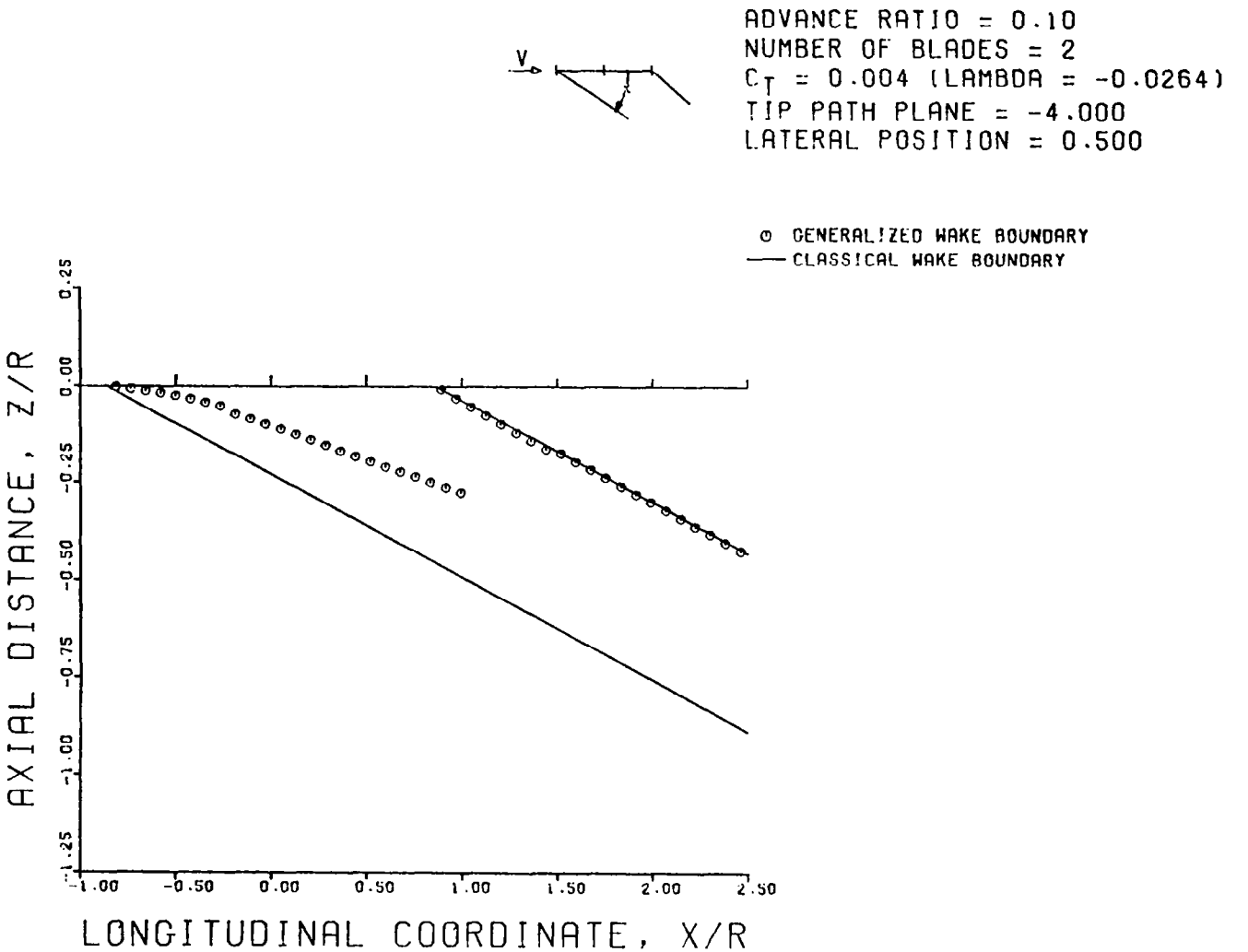

FIGURE 37C. FORE AND AFT WAKE BOUNDARY CHARTS FOR THE GENERALIZED DISTORTED TIP VORTEX (μ = .1, B = 2, C_T = .004, α = -4), Y/R = .500

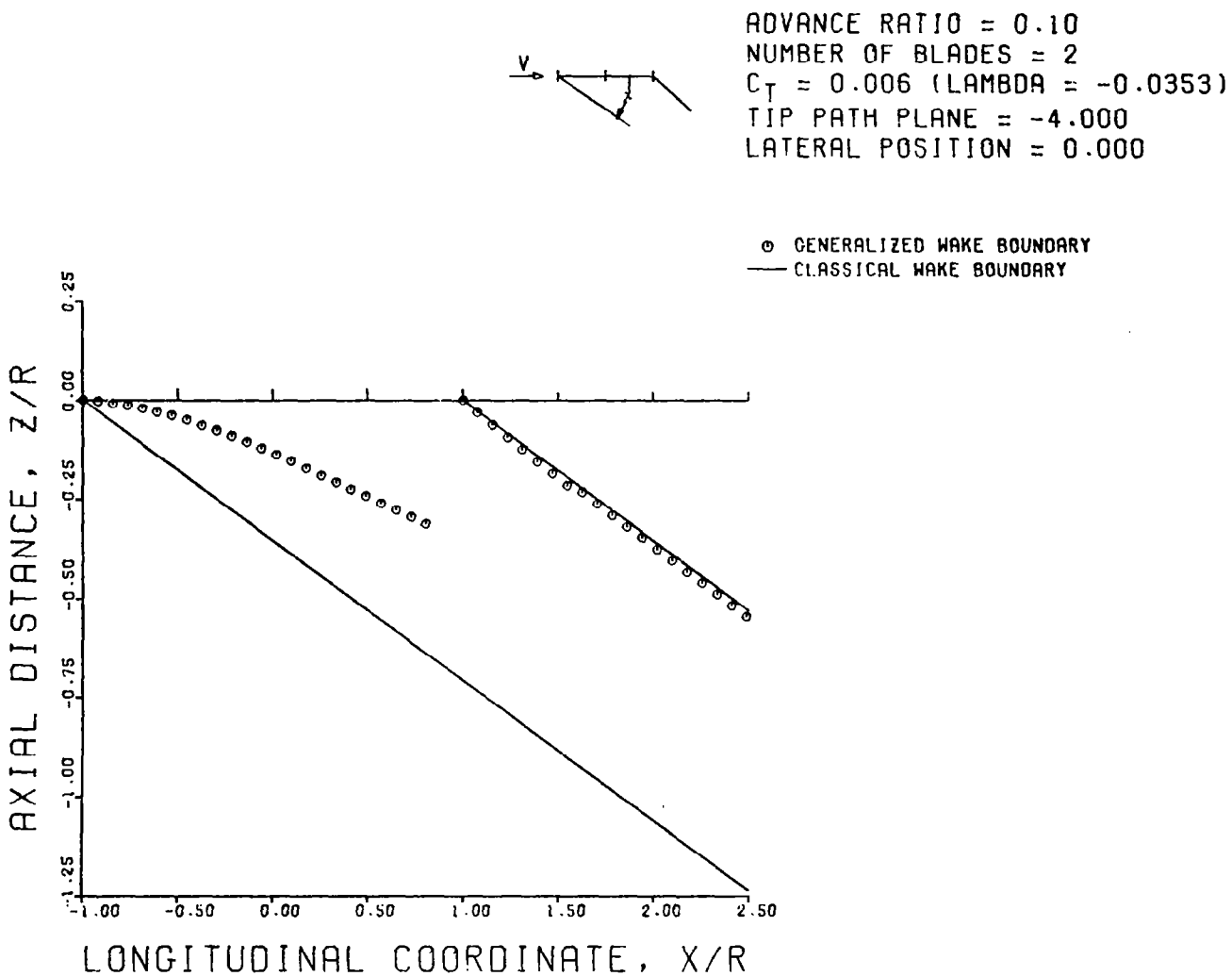

FIGURE 38A. FORE AND AFT WAKE BOUNDARY CHARTS FOR THE GENERALIZED DISTORTED TIP VORTEX (μ = .1, B = 2, C_T = .006, α = -4), Y/R = 0.0

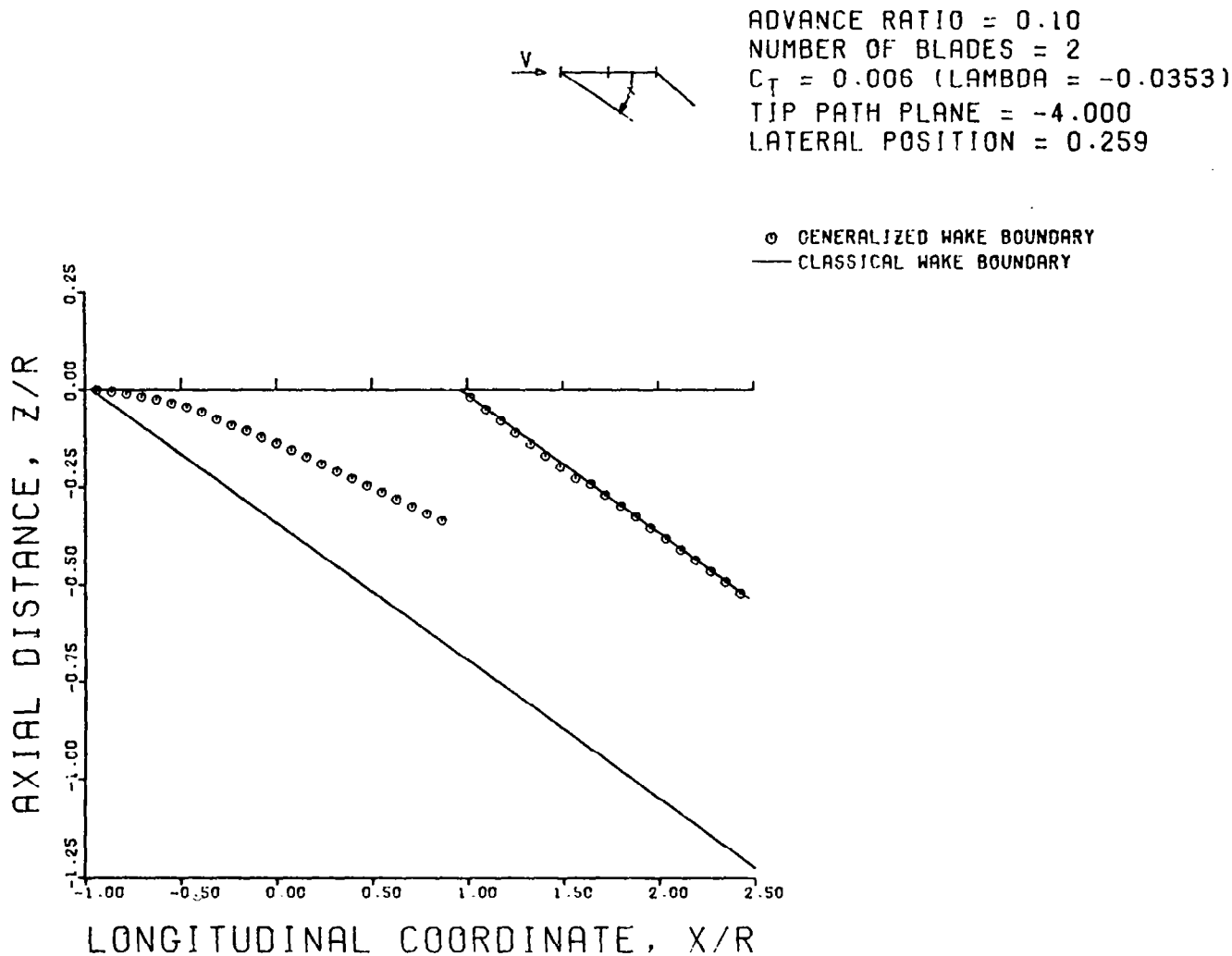

FIGURE 38B. FORE AND AFT WAKE BOUNDARY CHARTS FOR THE GENERALIZED DISTORTED TIP VORTEX (μ = .1, B = 2, C_T = .006, α = -4), Y/R = .259

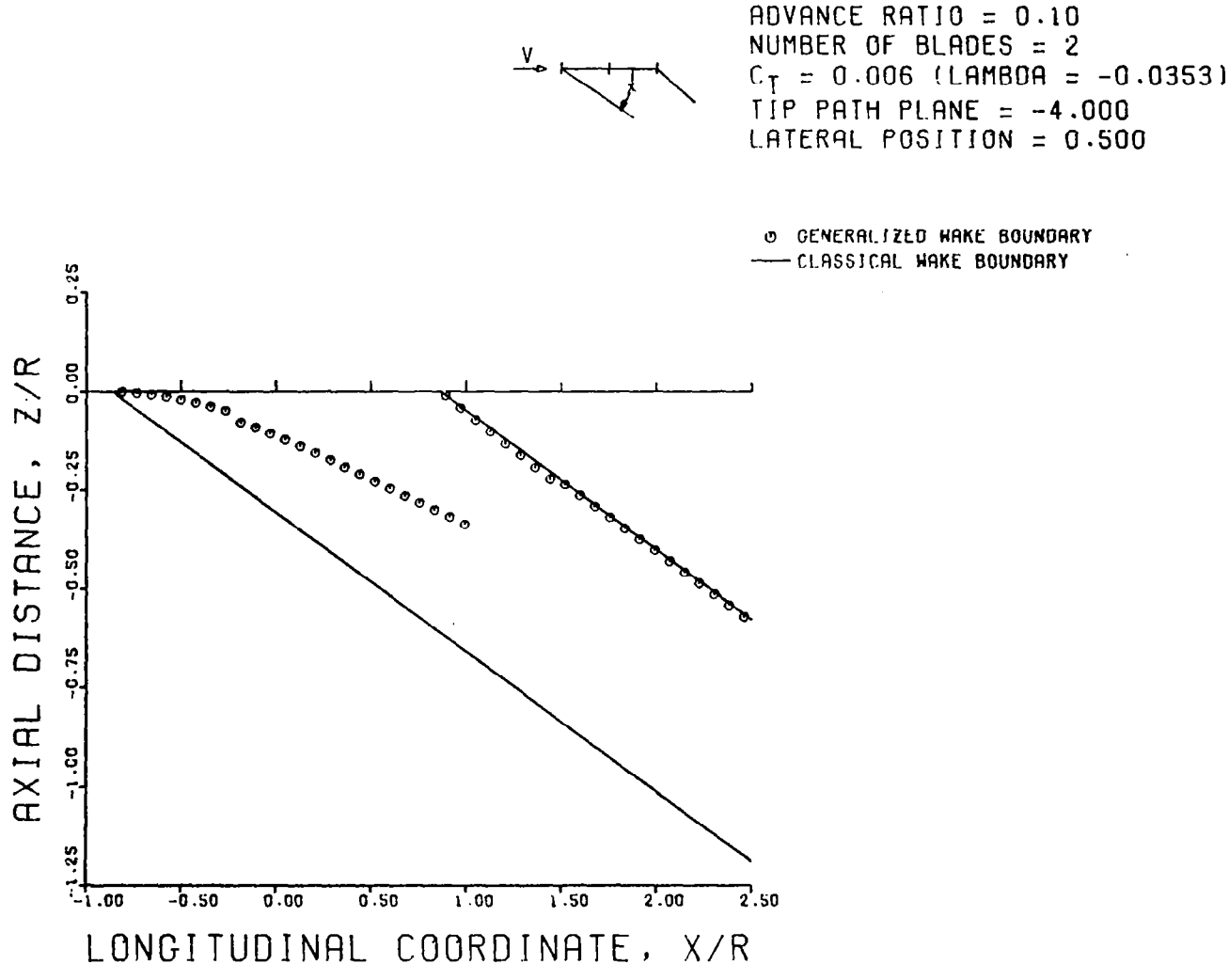

FIGURE 38C. FORE AND AFT WAKE BOUNDARY CHARTS FOR THE GENERALIZED DISTORTED TIP VORTEX (μ = .1, B = 2, C_T = .006, α = -4), Y/R = .500

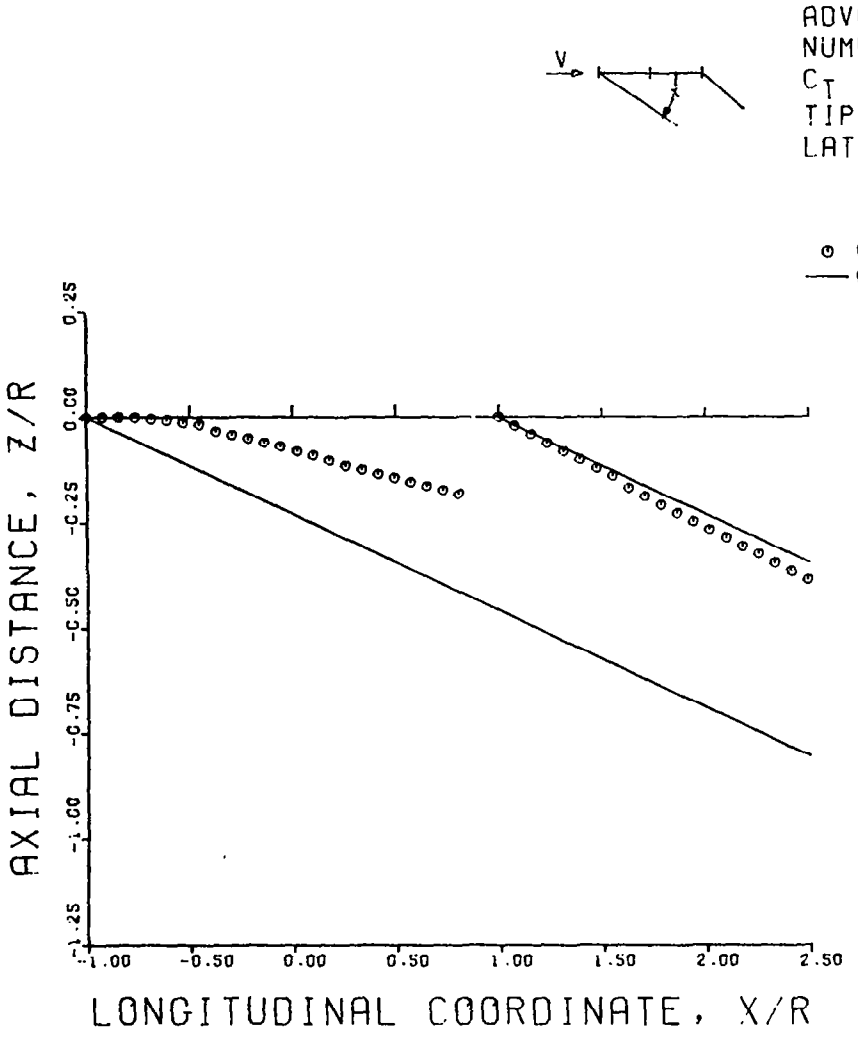

FIGURE 39A. FORE AND AFT WAKE BOUNDARY CHARTS FOR THE GENERALIZED DISTORTED TIP VORTEX (μ = .1, B = 4, C_T = .004, α = -2), Y/R = 0.0

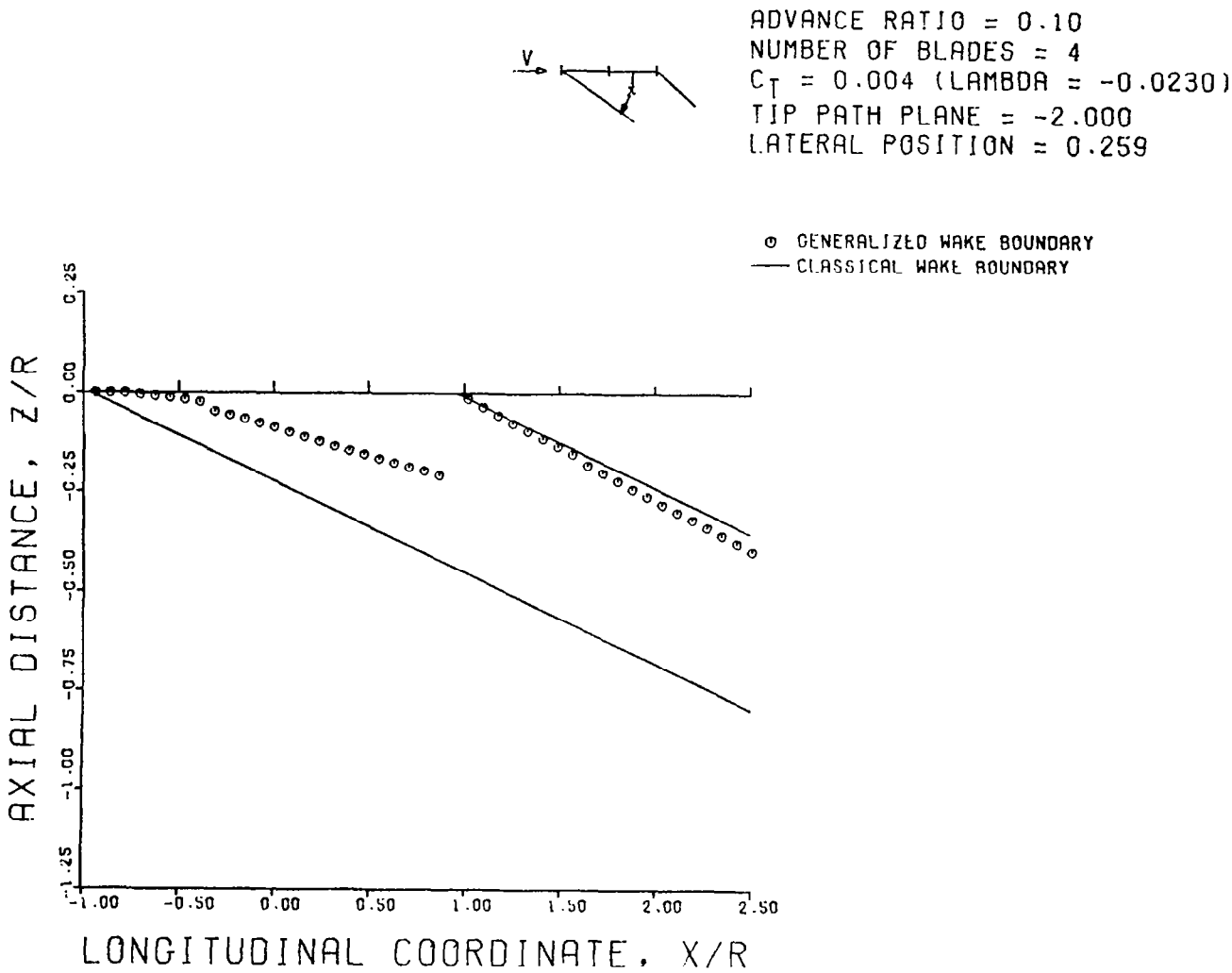

FIGURE 39B. FORE AND AFT WAKE BOUNDARY CHARTS FOR THE GENERALIZED DISTORTED TIP VORTEX (μ = .1, B = 4, C_T = .004, α = -2), Y/R = .259

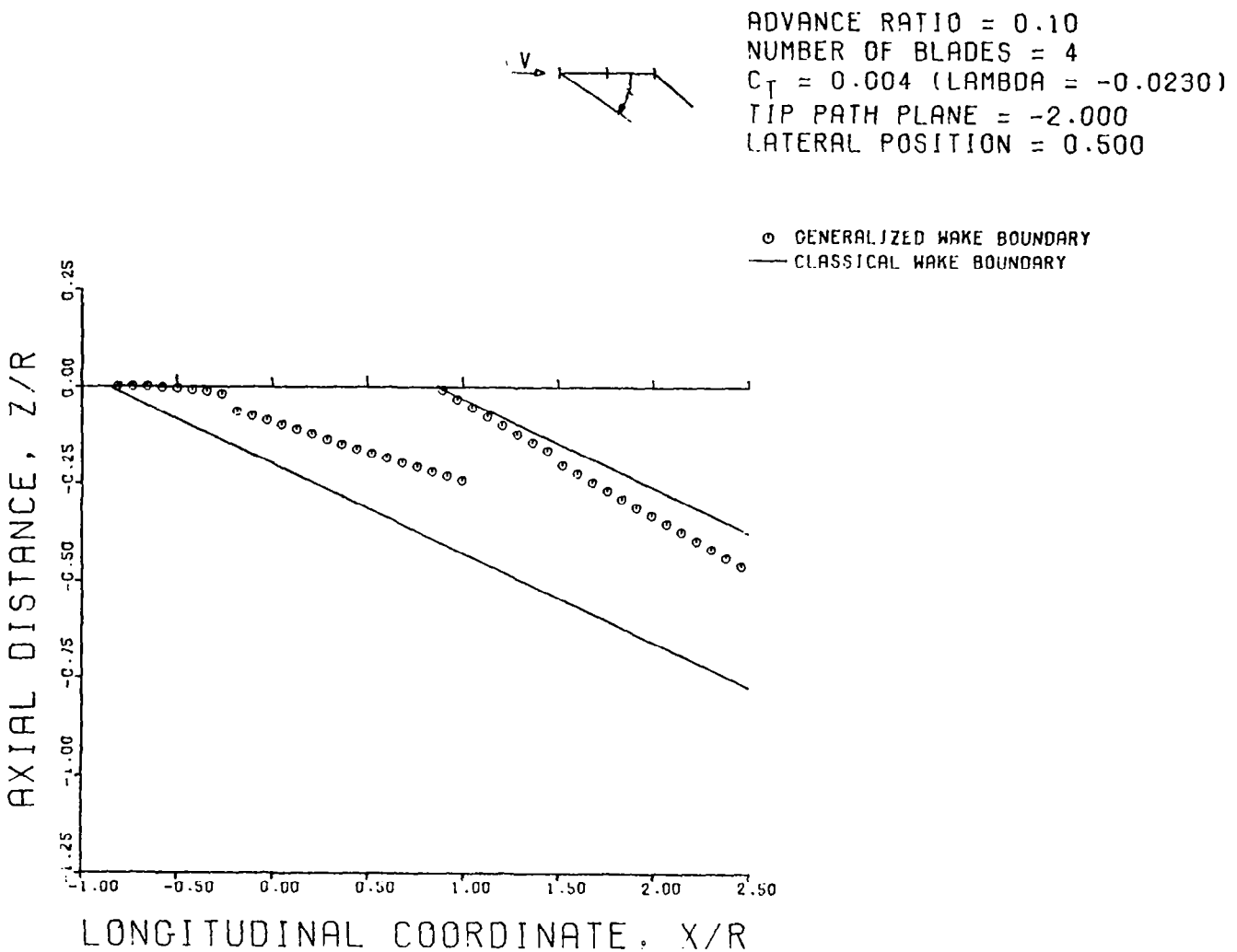

FIGURE 39C. FORE AND AFT WAKE BOUNDARY CHARTS FOR THE GENERALIZED DISTORTED TIP VORTEX (μ = .1, B = 4, C_T = .004, α = -2), Y/R = .500

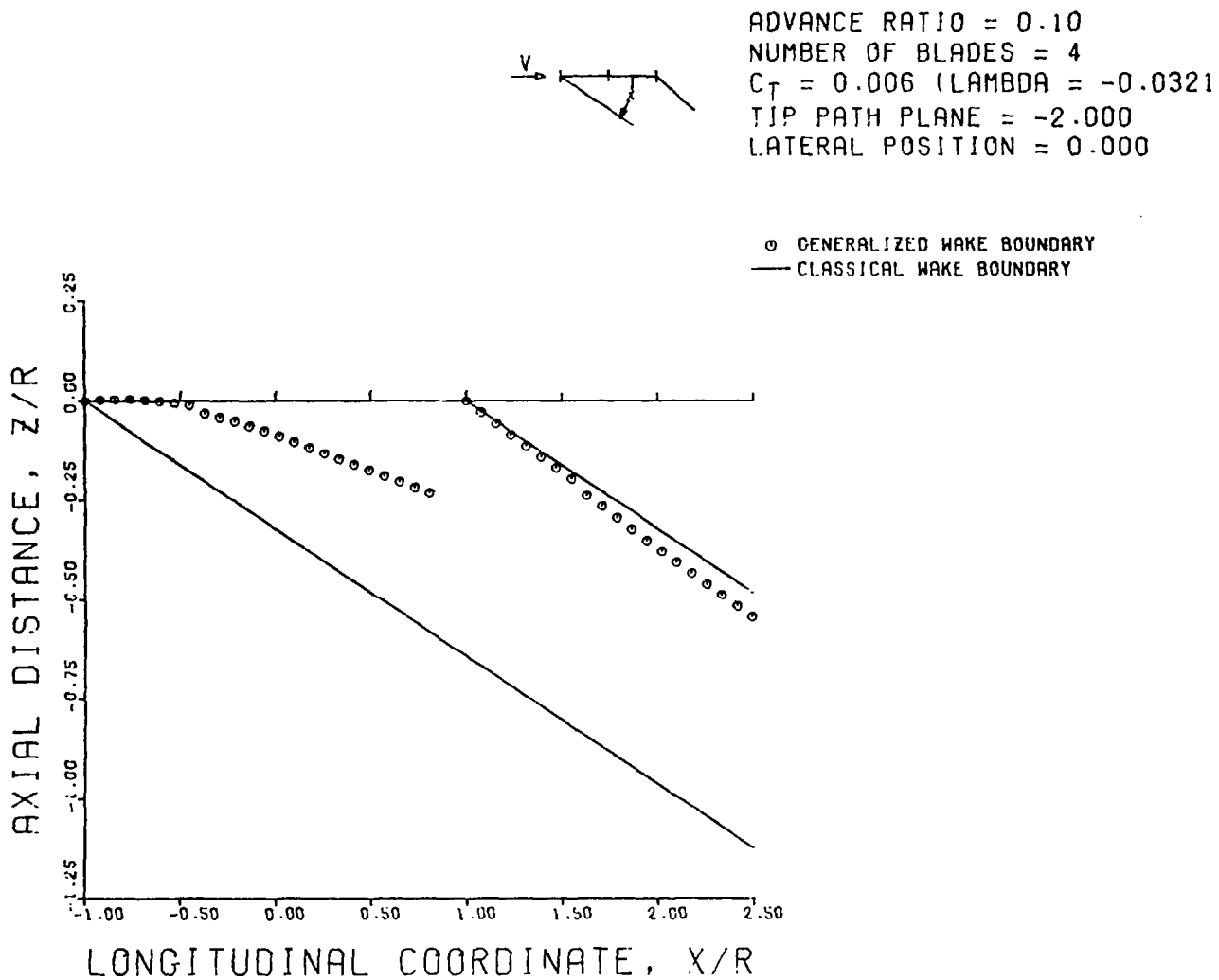

FIGURE 40A. FORE AND AFT WAKE BOUNDARY CHARTS FOR THE GENERALIZED DISTORTED TIP VORTEX (μ = .1, B = 4, C_T = .006, α = -2), Y/R = 0.0

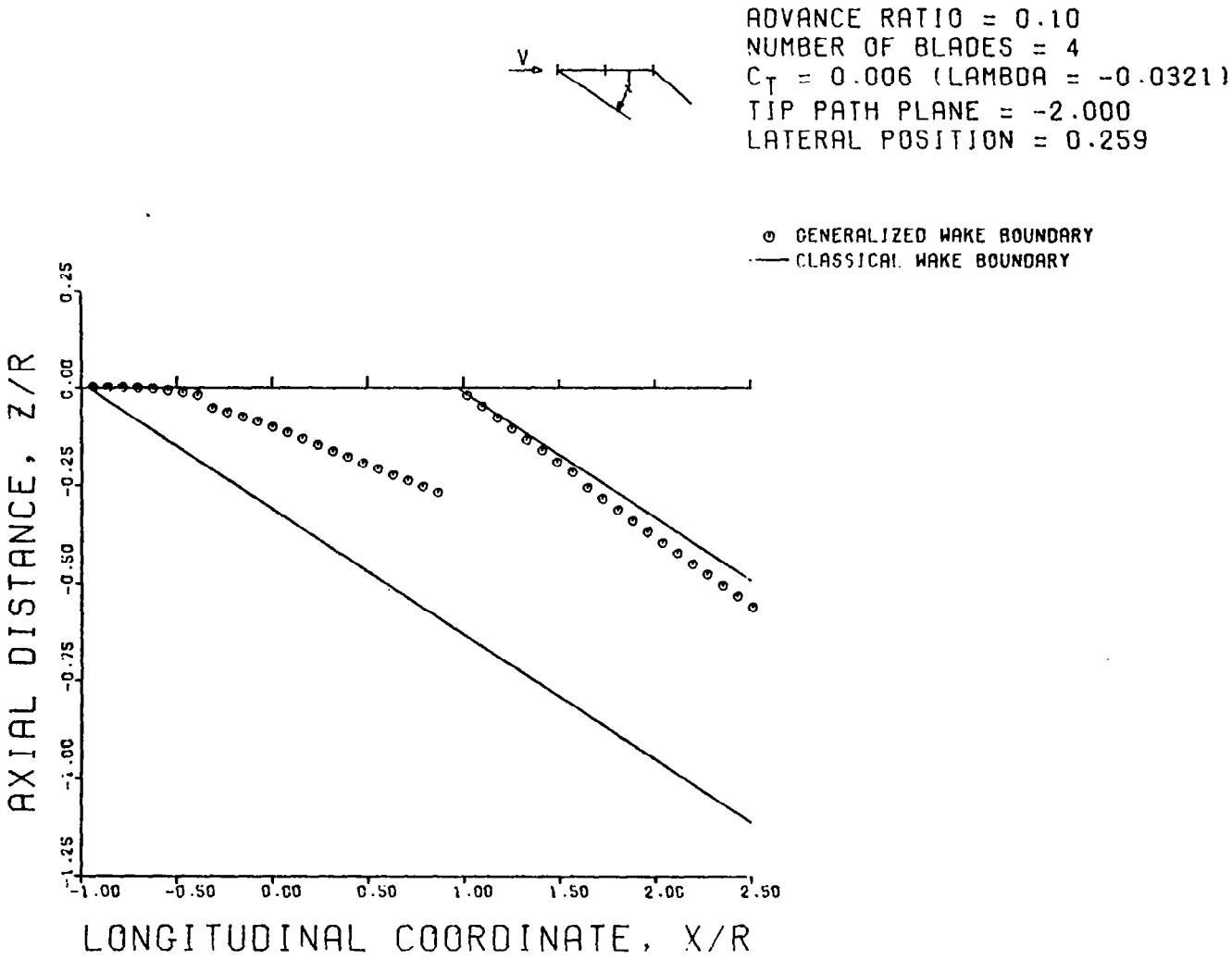

FIGURE 40B. FORE AND AFT WAKE BOUNDARY CHARTS FOR THE GENERALIZED DISTORTED TIP VORTEX (μ = .1, B = 4, C_T = .006, α = -2), Y/R = .259

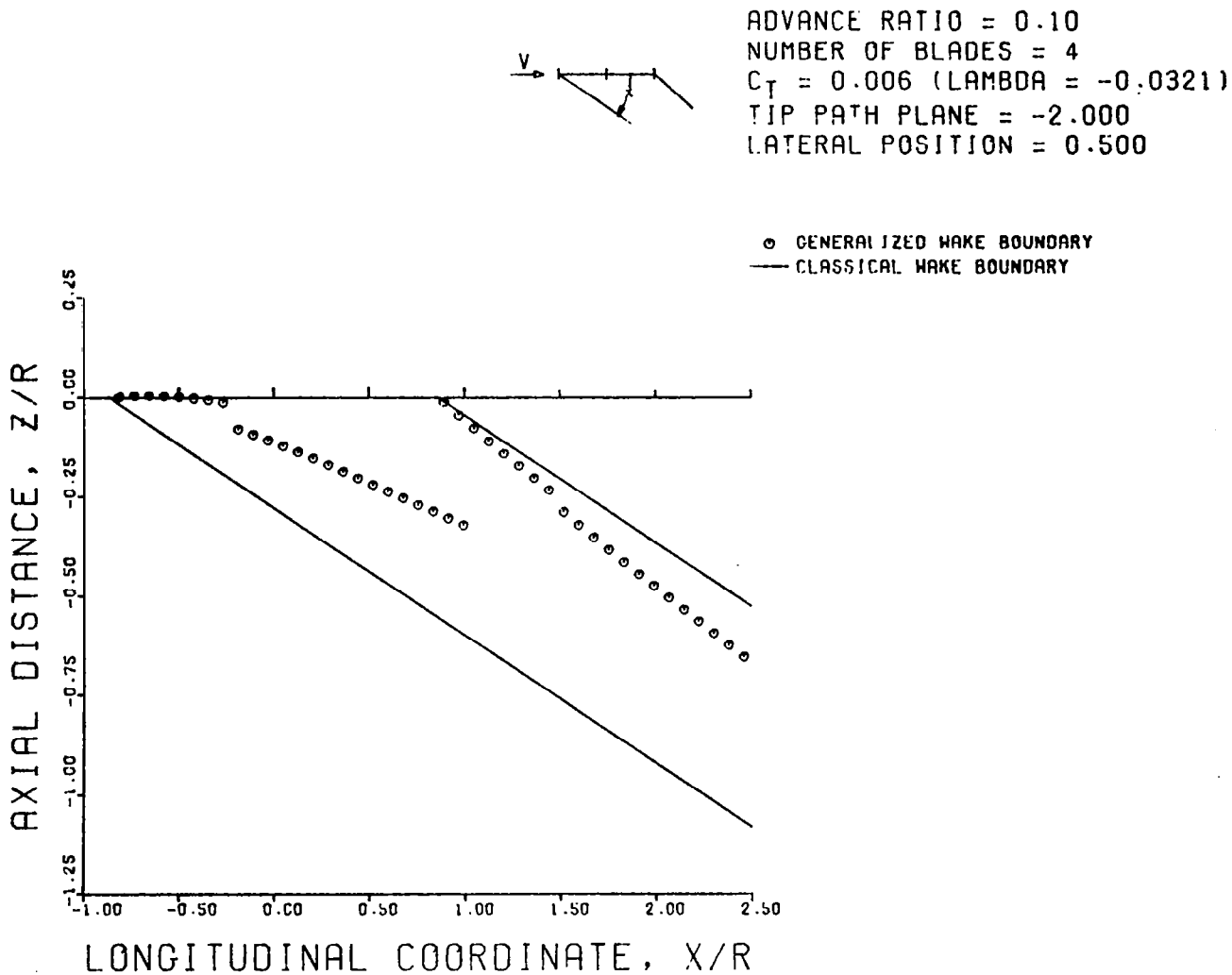

FIGURE 40C. FORE AND AFT WAKE BOUNDARY CHARTS FOR THE GENERALIZED DISTORTED TIP VORTEX (μ = .1, B = 4, C_T = .006, α = -2), Y/R = .500

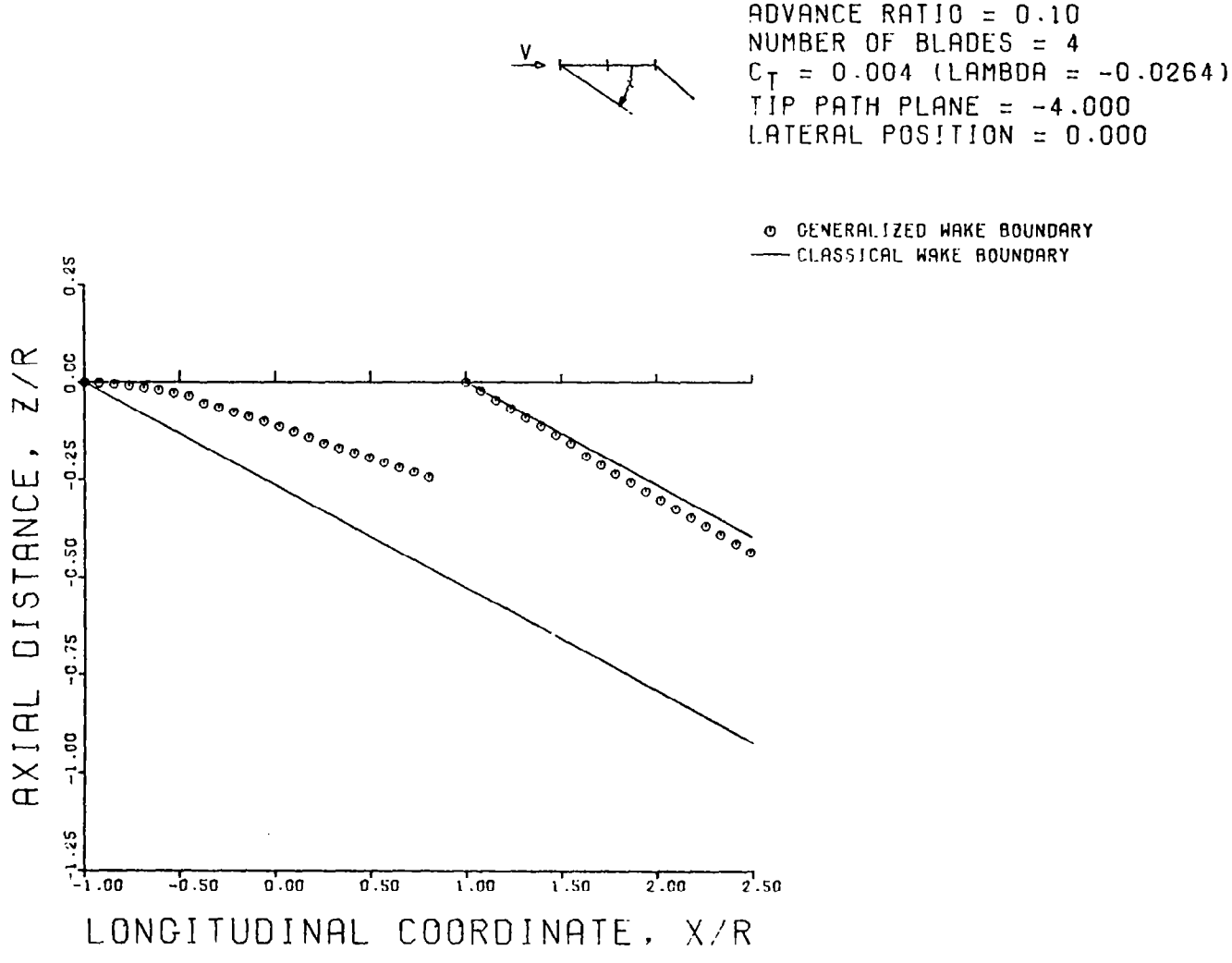

FIGURE 41A. FORE AND AFT WAKE BOUNDARY CHARTS FOR THE GENERALIZED DISTORTED TIP VORTEX (μ = .1, B = 4, C_T = .004, α = -4), Y/R = 0.0

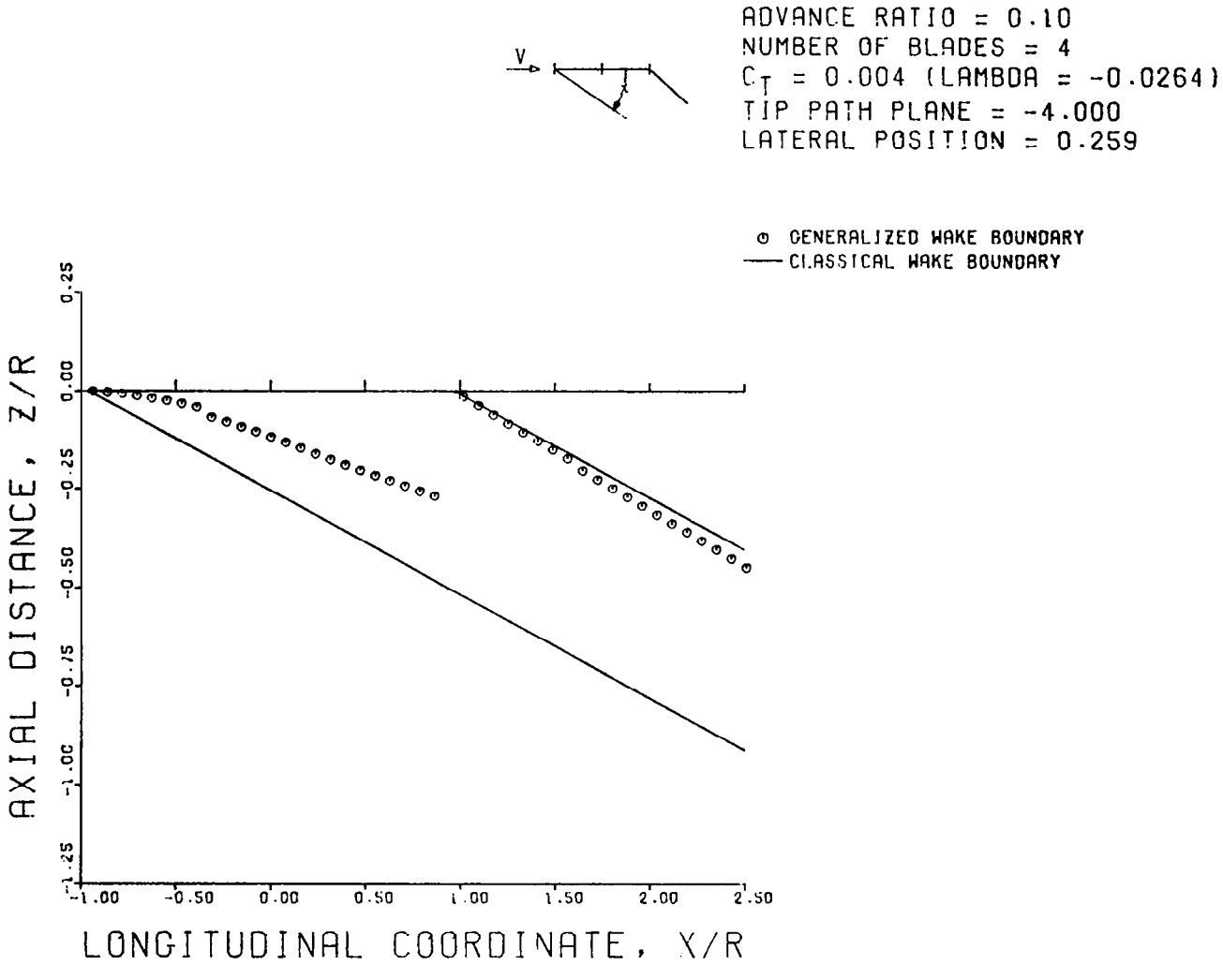

FIGURE 41B. FORE AND AFT WAKE BOUNDARY CHARTS FOR THE GENERALIZED DISTORTED TIP VORTEX (μ = .1, B = 4, C_T = .004, α = -4), Y/R = .259

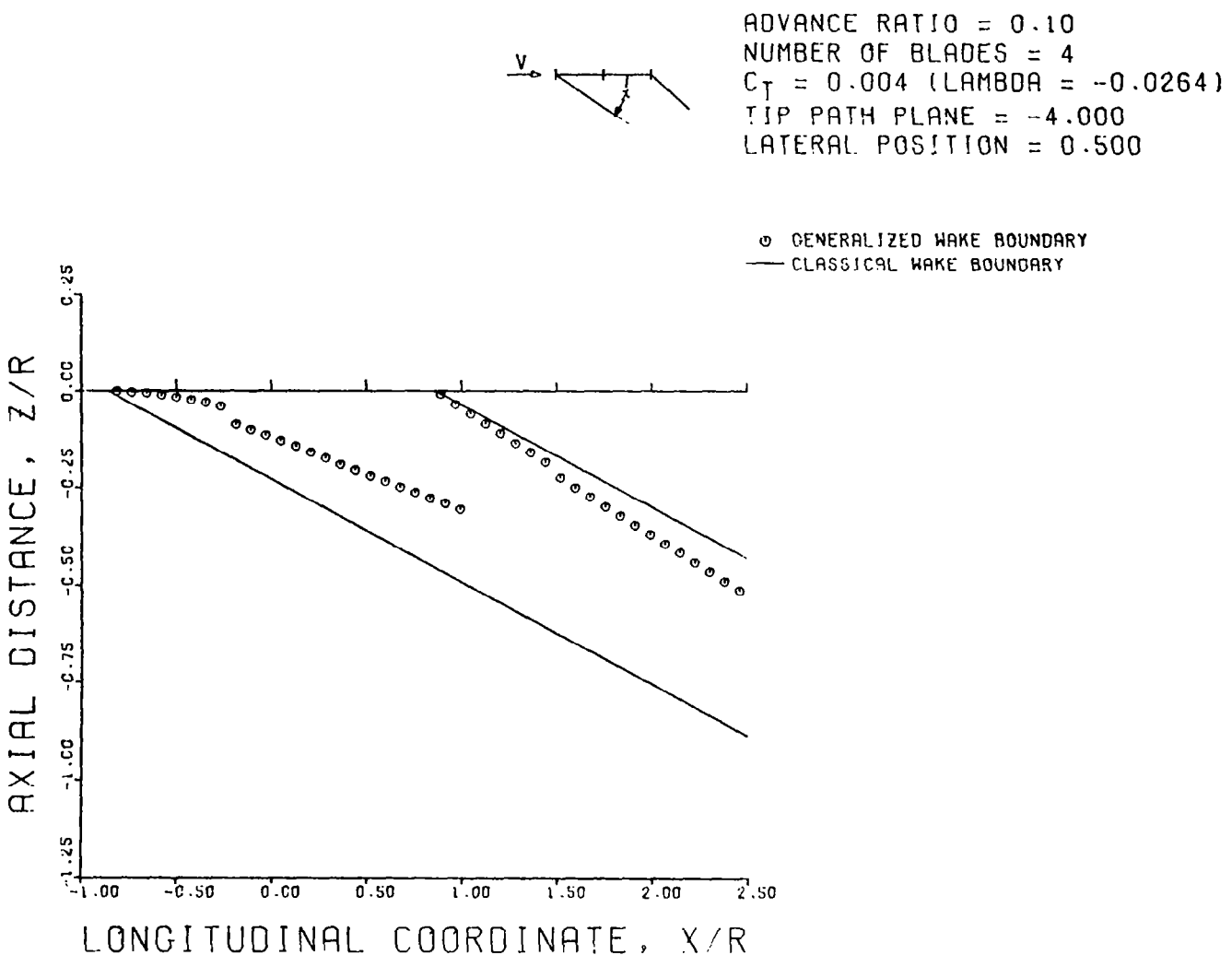

FIGURE 41C. FORE AND AFT WAKE BOUNDARY CHARTS FOR THE GENERALIZED DISTORTED TIP VORTEX (μ = .1, B = 4, C_T = .004, α = -4), Y/R = .500

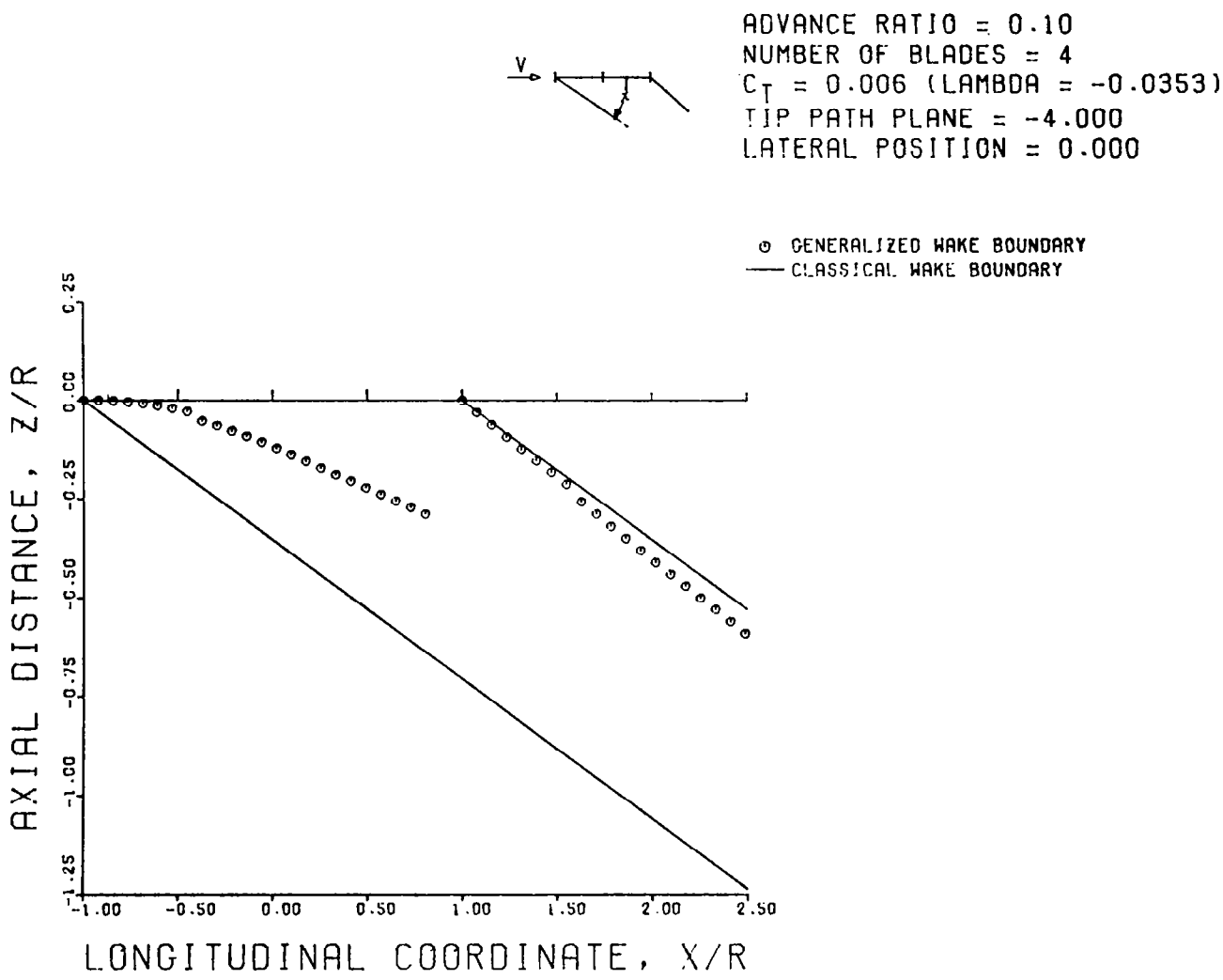

FIGURE 42A. FORE AND AFT WAKE BOUNDARY CHARTS FOR THE GENERALIZED DISTORTED TIP VORTEX (μ = .1, B = 4, C_T = .006, α = -4), Y/R = 0.0

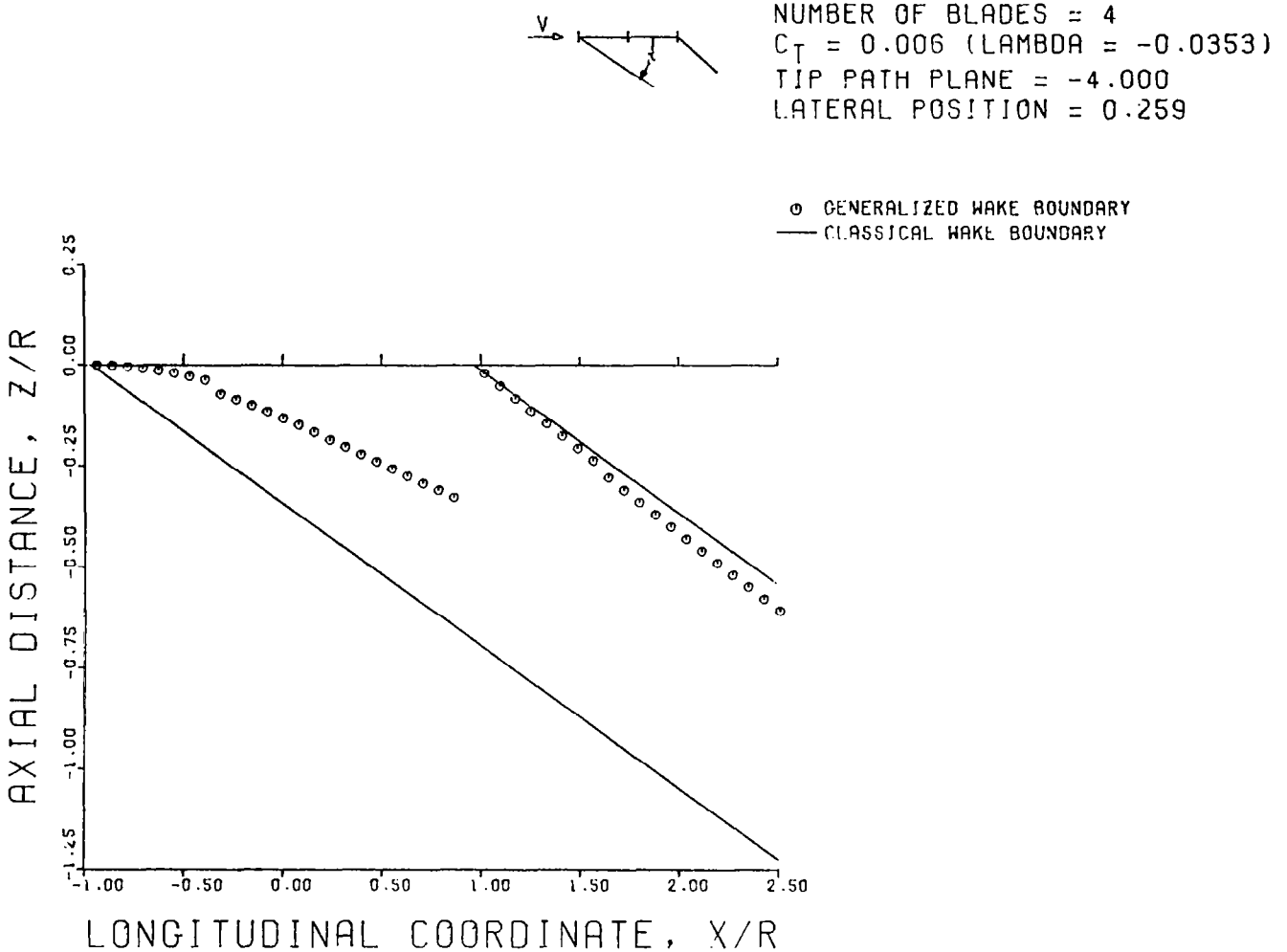

FIGURE 42B. FORE AND AFT WAKE BOUNDARY CHARTS FOR THE GENERALIZED DISTORTED TIP VORTEX (μ = .1, B = 4, C_T = .006, α = -4), Y/R = .259

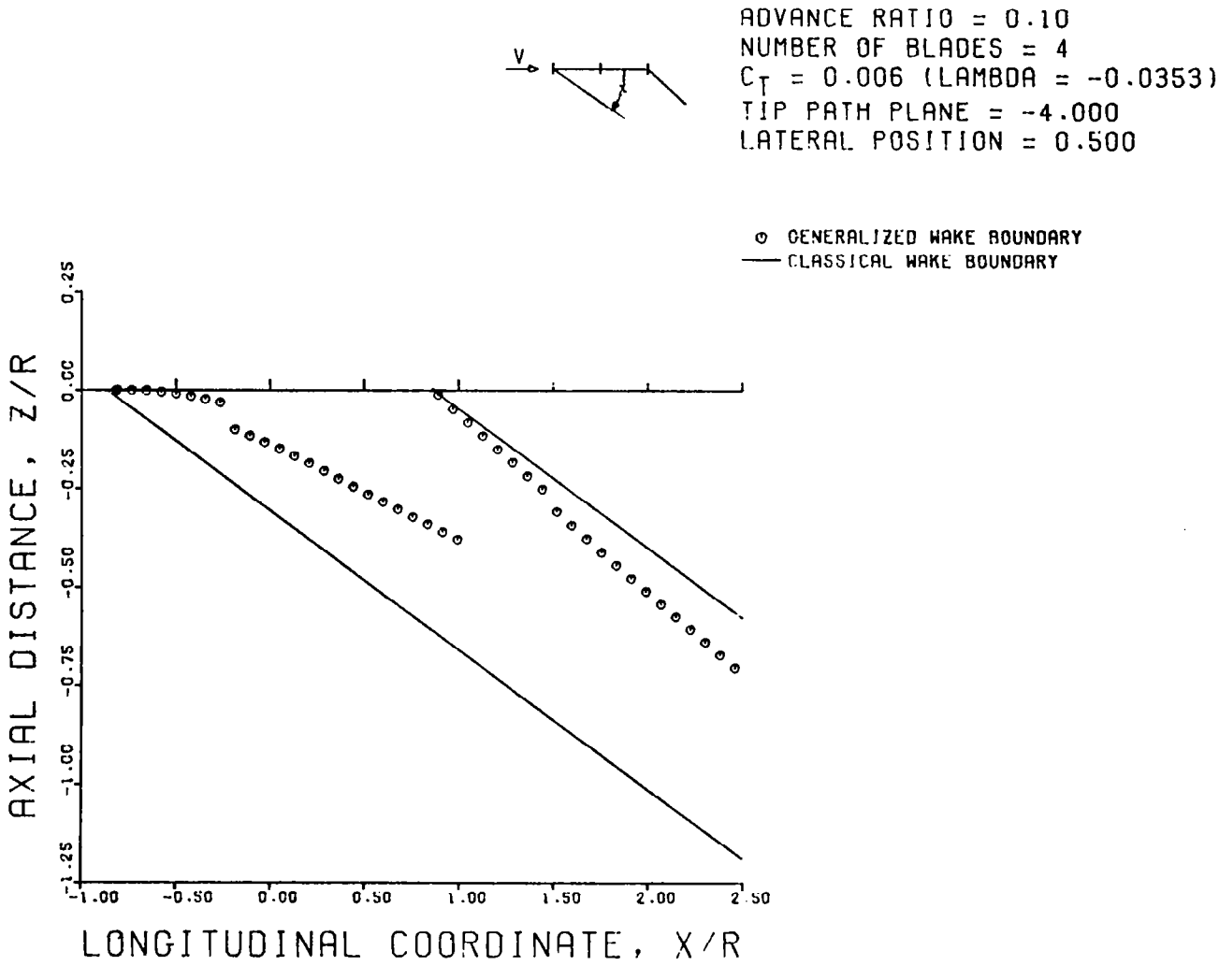

FIGURE 42C. FORE AND AFT WAKE BOUNDARY CHARTS FOR THE GENERALIZED DISTORTED TIP VORTEX (μ = .1, B = 4, C_T = .006, α = -4), Y/R = .500

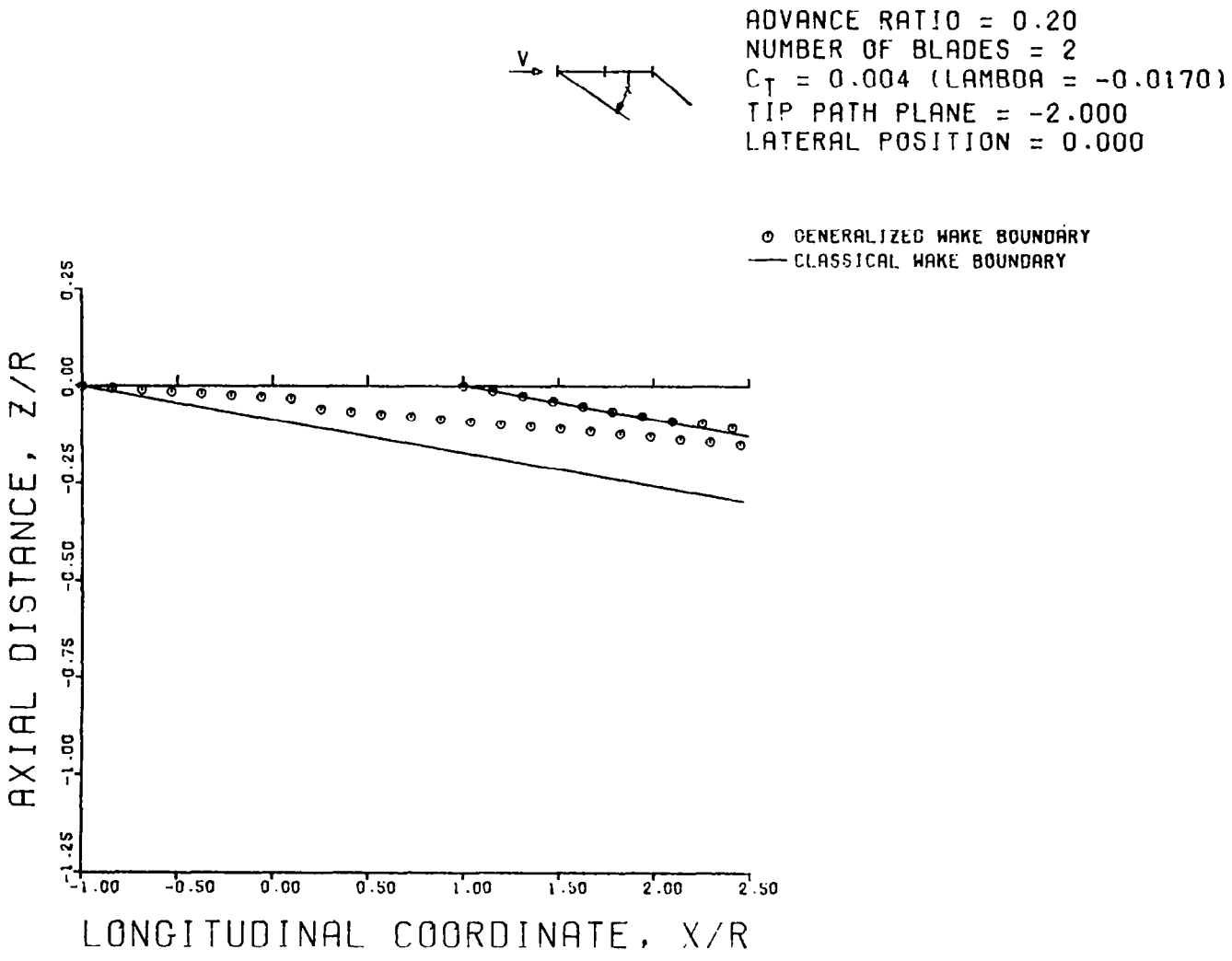

FIGURE 43A. FORE AND AFT WAKE BOUNDARY CHARTS FOR THE GENERALIZED DISTORTED TIP VORTEX (μ = .2, B = 2, C_T = .004, α = -2), Y/R = 0.0

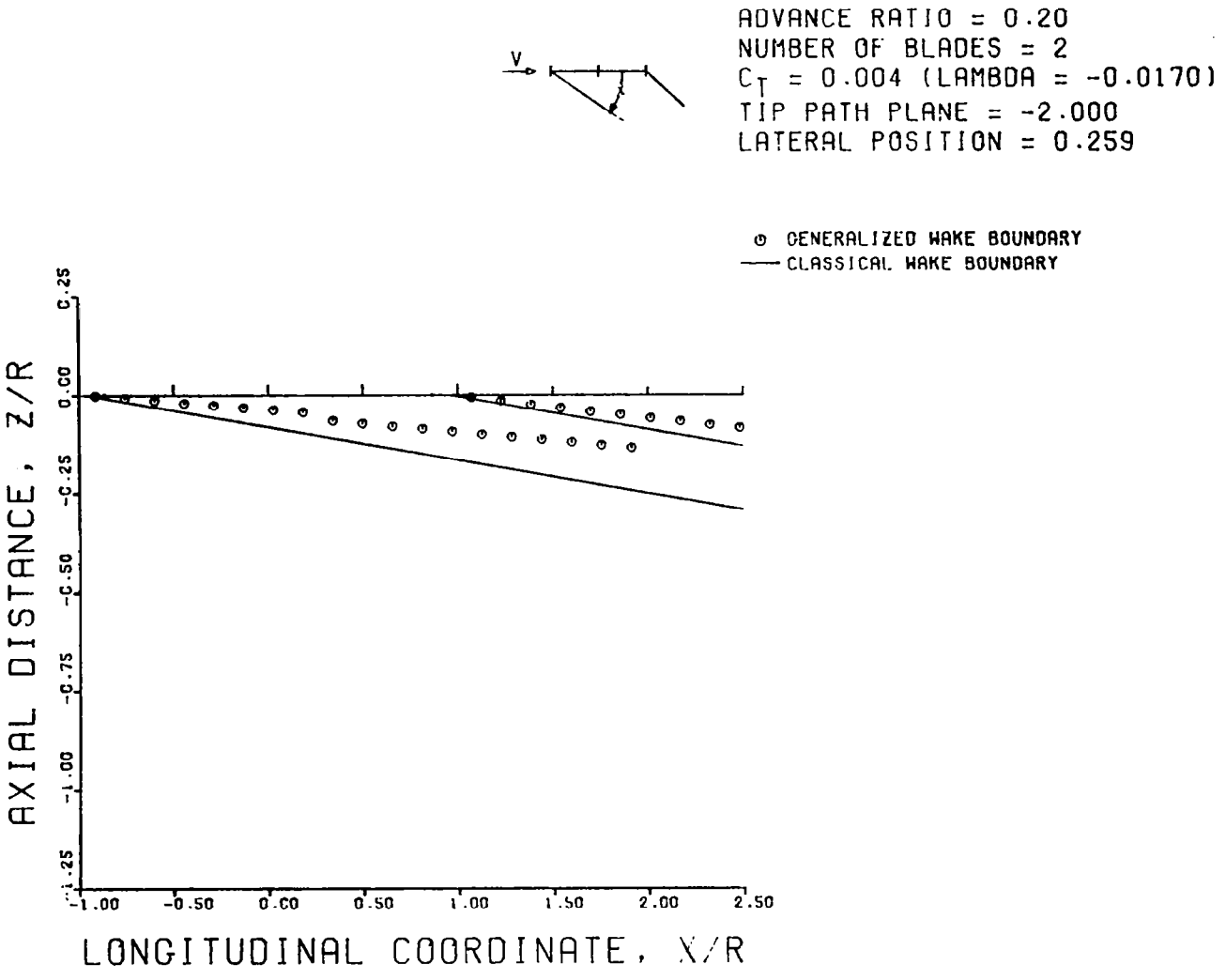

FIGURE 43B. FORE AND AFT WAKE BOUNDARY CHARTS FOR THE GENERALIZED DISTORTED TIP VORTEX (μ = .2, B = 2, C_T = .004, α = -2), Y/R = .259

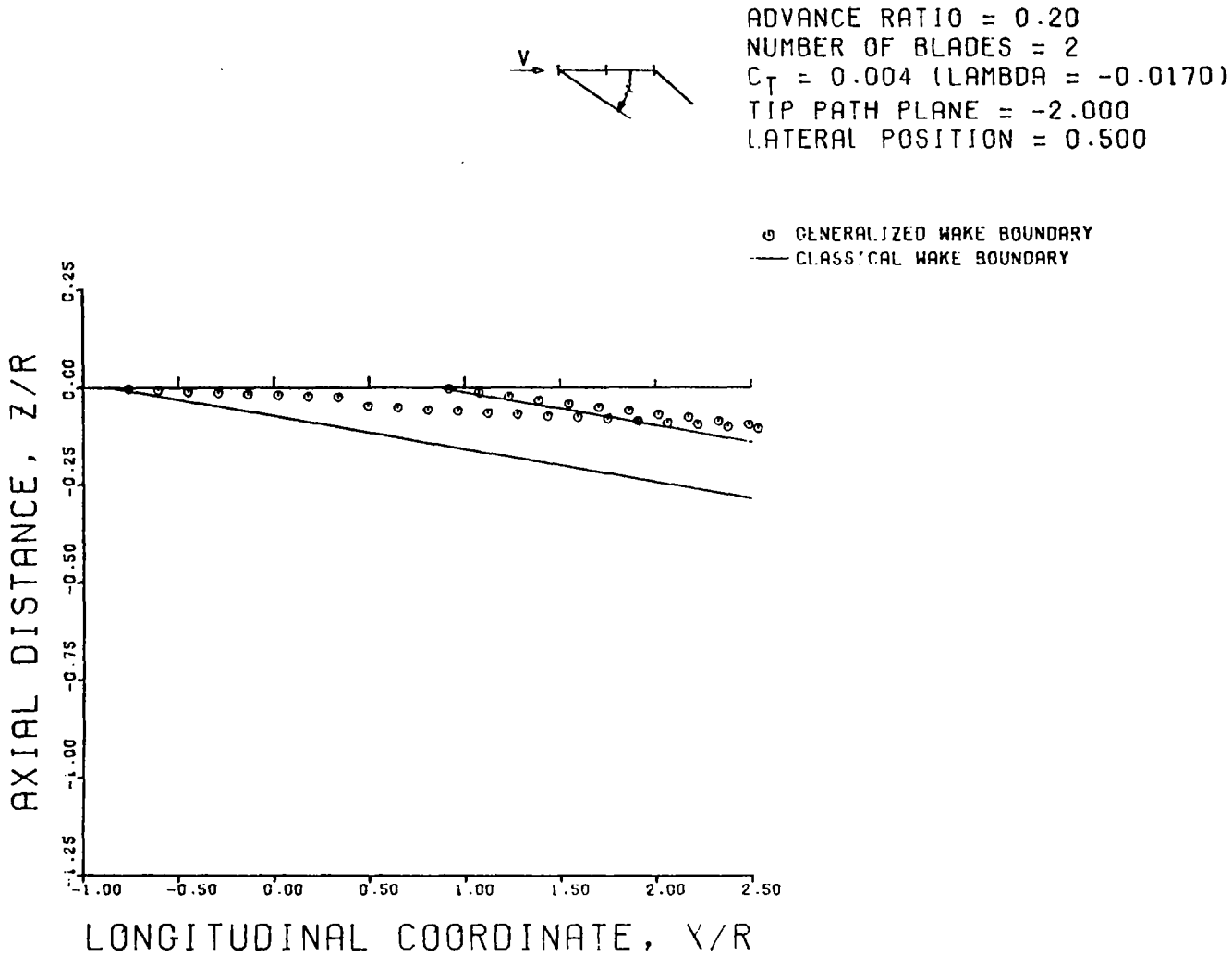

FIGURE 43C. FORE AND AFT WAKE BOUNDARY CHARTS FOR THE GENERALIZED DISTORTED TIP VORTEX (μ = .2, B = 2, C_T = .004, α = -2), Y/R = .500

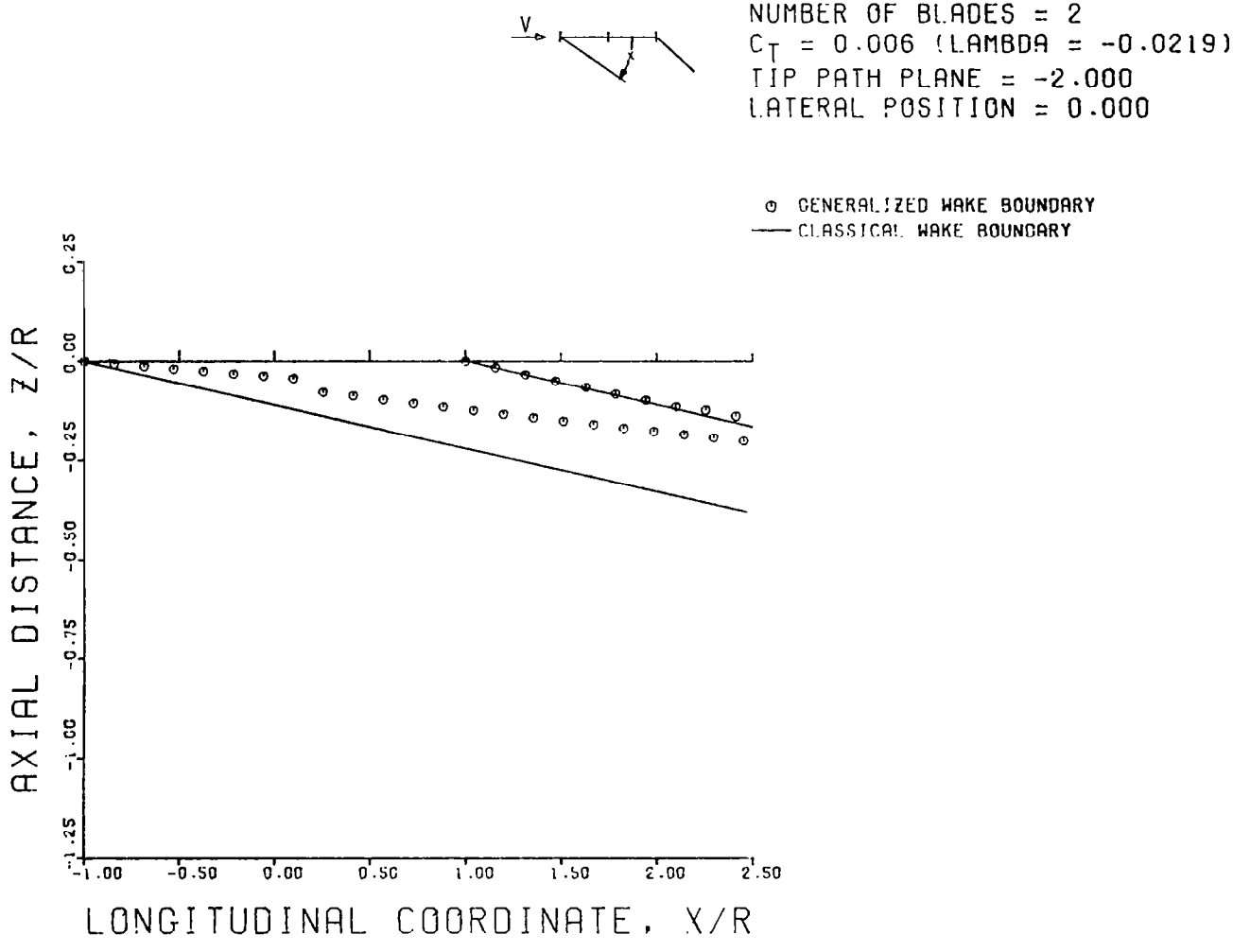

FIGURE 44A. FORE AND AFT WAKE BOUNDARY CHARTS FOR THE GENERALIZED DISTORTED TIP VORTEX (μ = .2, B = 2, C_T = .006, α = -2), Y/R = 0.0

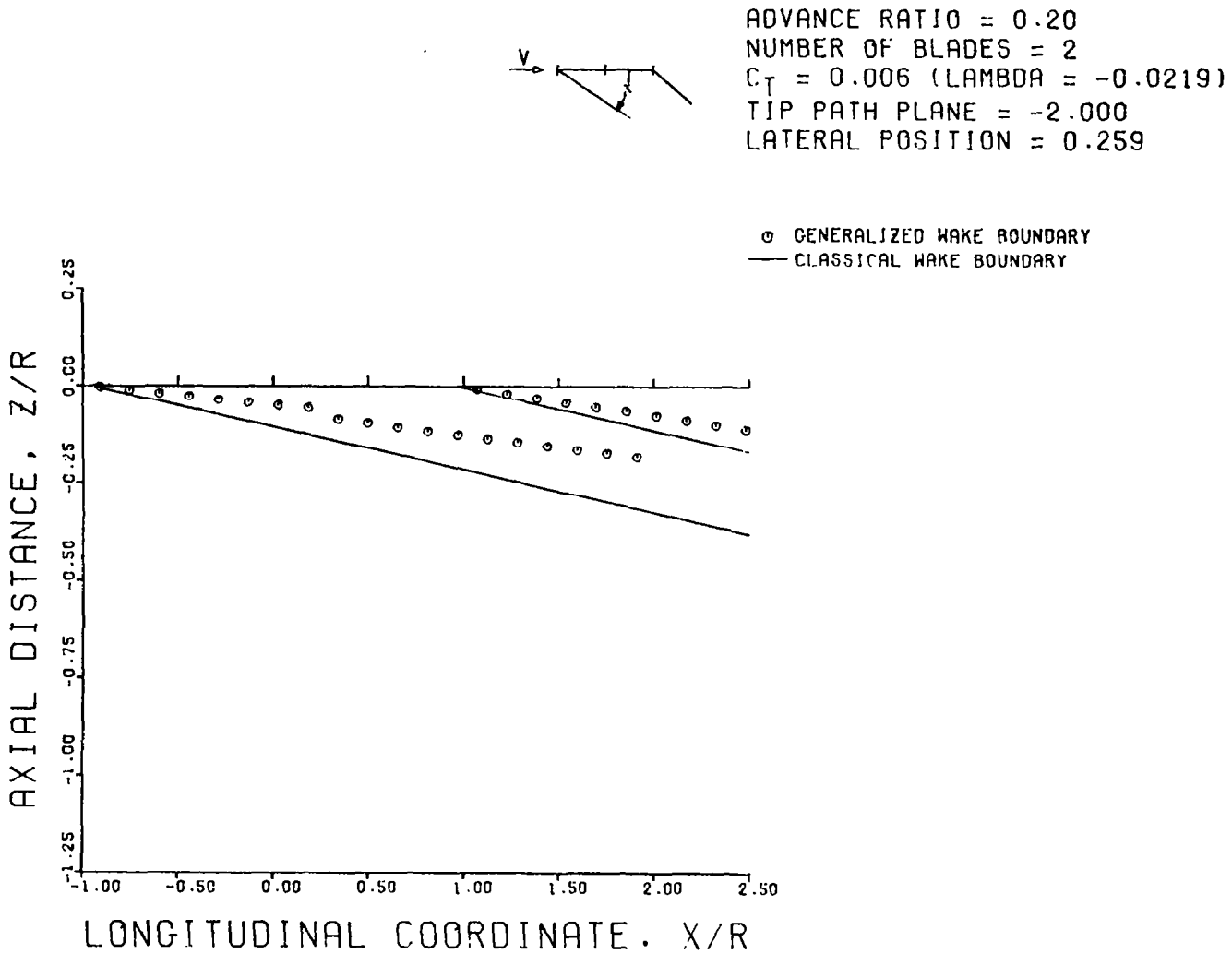

FIGURE 44B. FORE AND AFT WAKE BOUNDARY CHARTS FOR THE GENERALIZED DISTORTED TIP VORTEX (μ = .2, B = 2, C_T = .006, α = -2), Y/R = .259

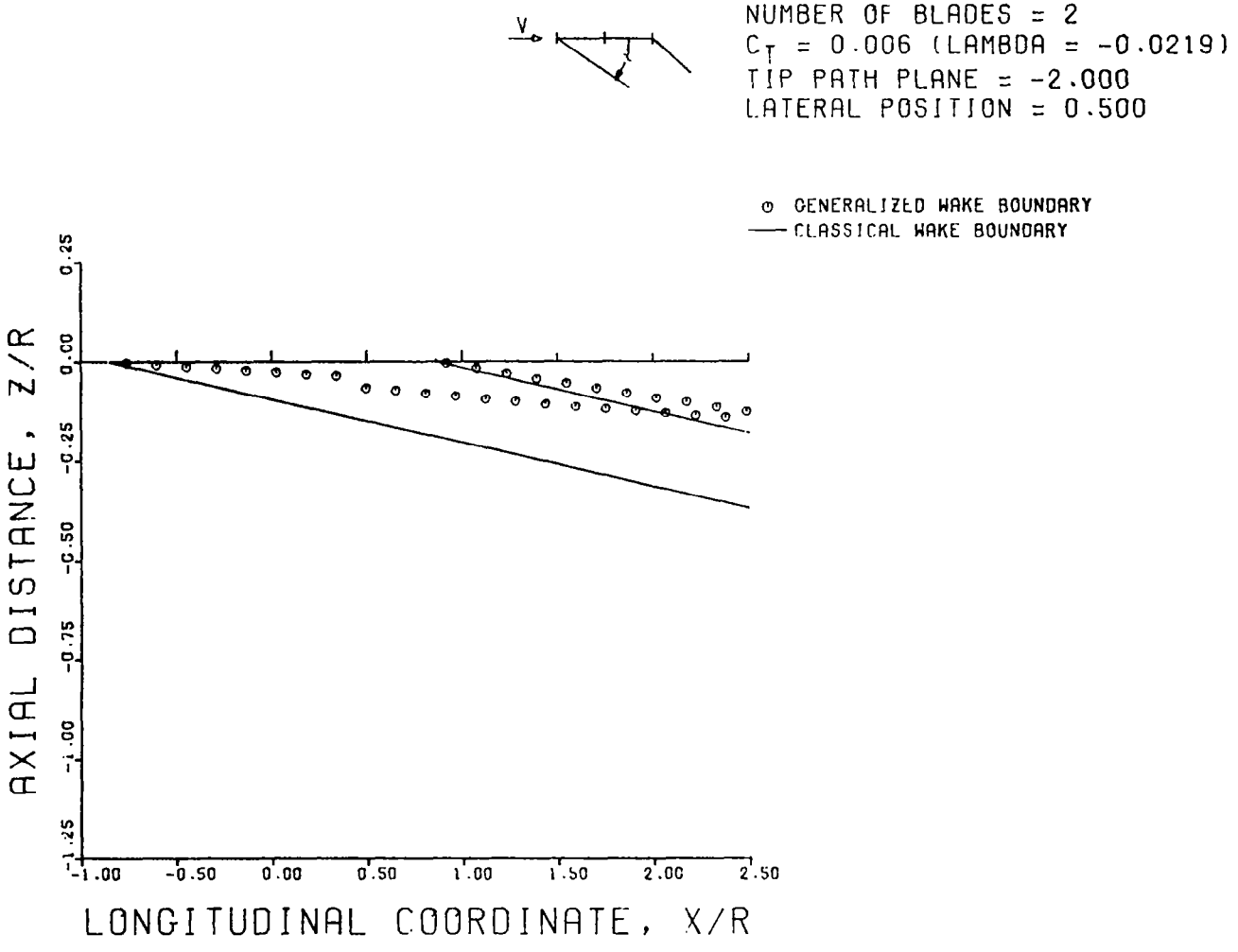

FIGURE 44C. FORE AND AFT WAKE BOUNDARY CHARTS FOR THE GENERALIZED DISTORTED TIP VORTEX (μ = .2, B = 2, C_T = .006, α = -2), Y/R = .500

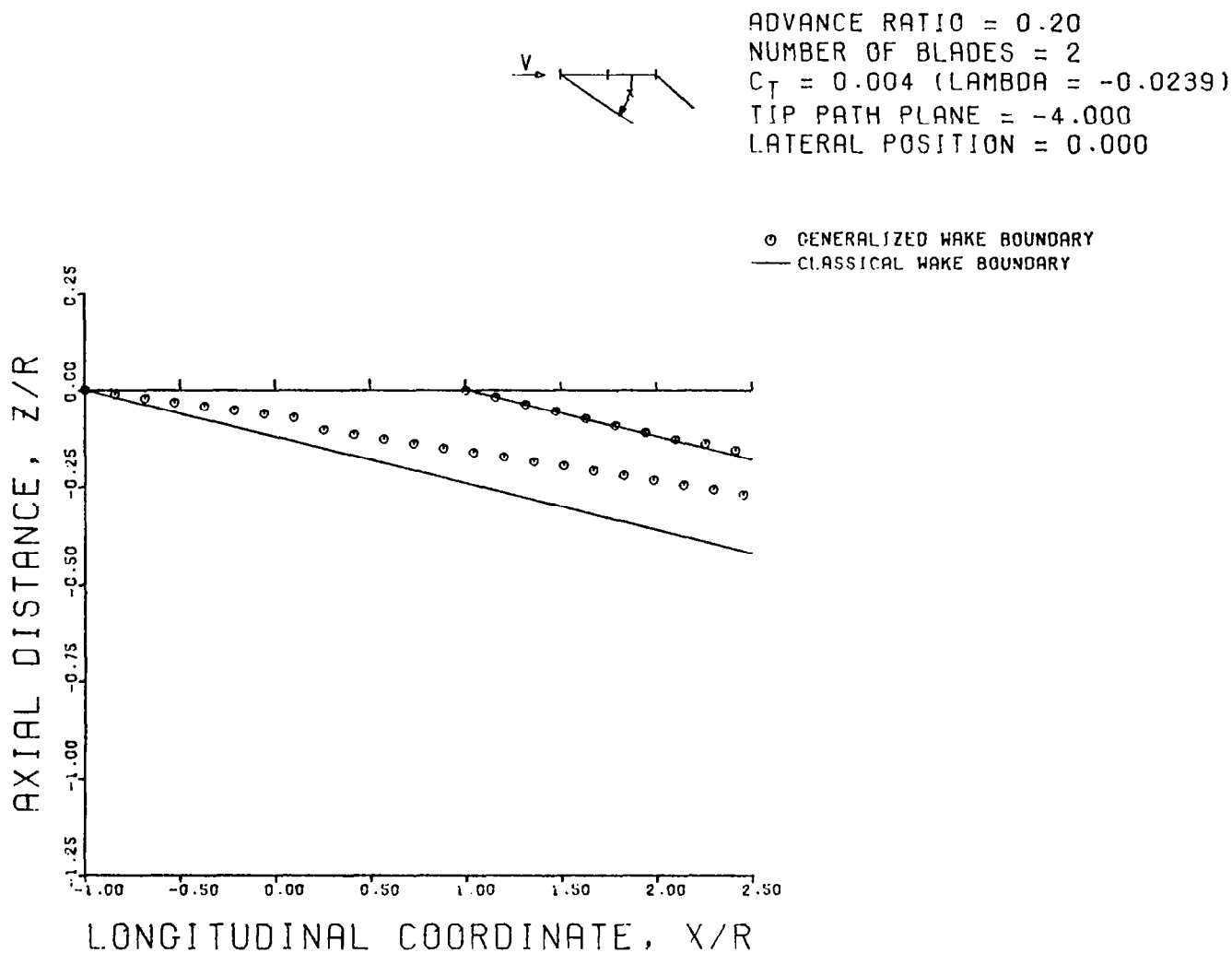

FIGURE 45A. FORE AND AFT WAKE BOUNDARY CHARTS FOR THE GENERALIZED DISTORTED TIP VORTEX (μ = .2, B = 2, C_T = .004, α = -4), Y/R = 0.0

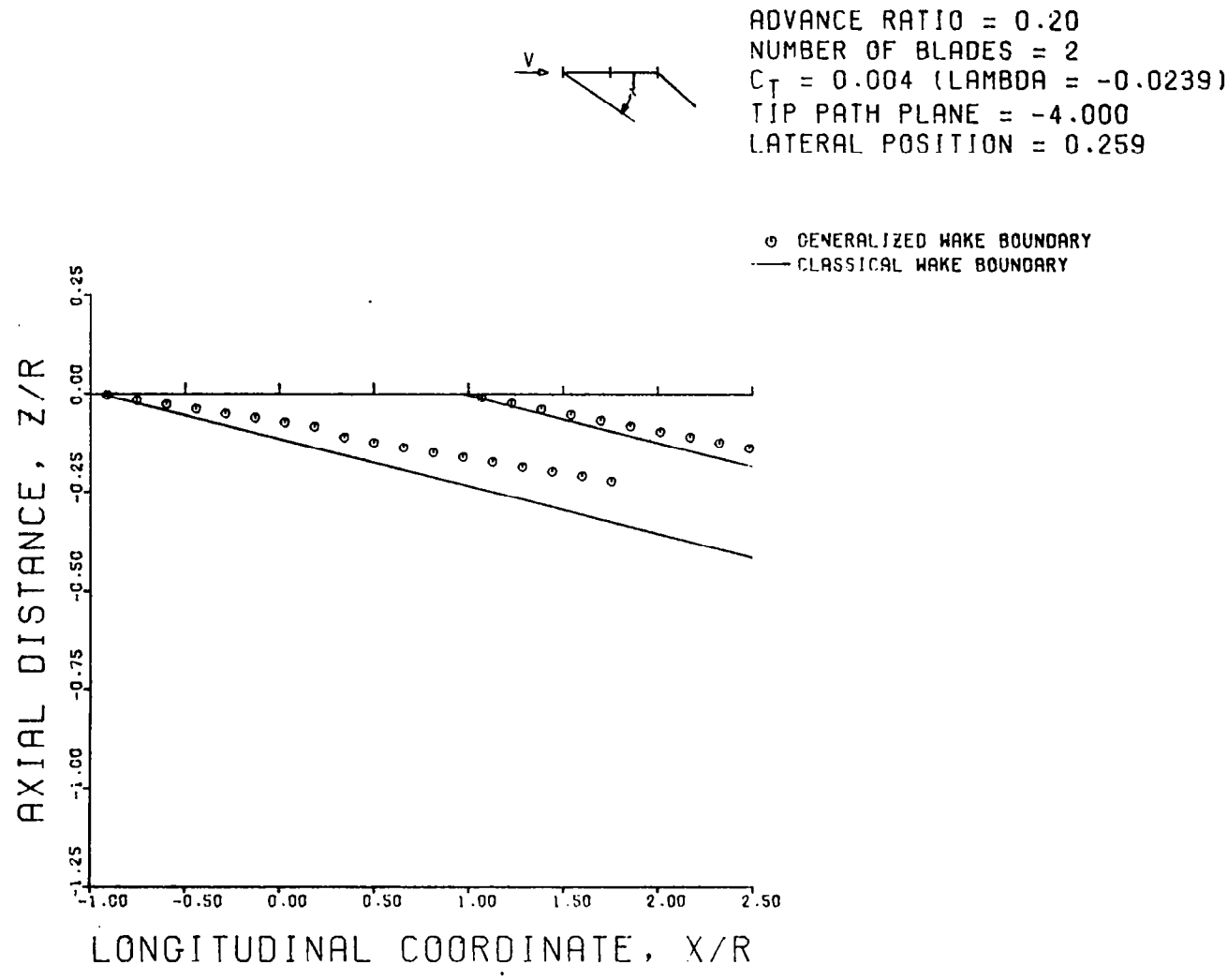

FIGURE 45B. FORE AND AFT WAKE BOUNDARY CHARTS FOR THE GENERALIZED DISTORTED TIP VORTEX (μ = .2, B = 2, C_T = .004, α = -4), Y/R = .259

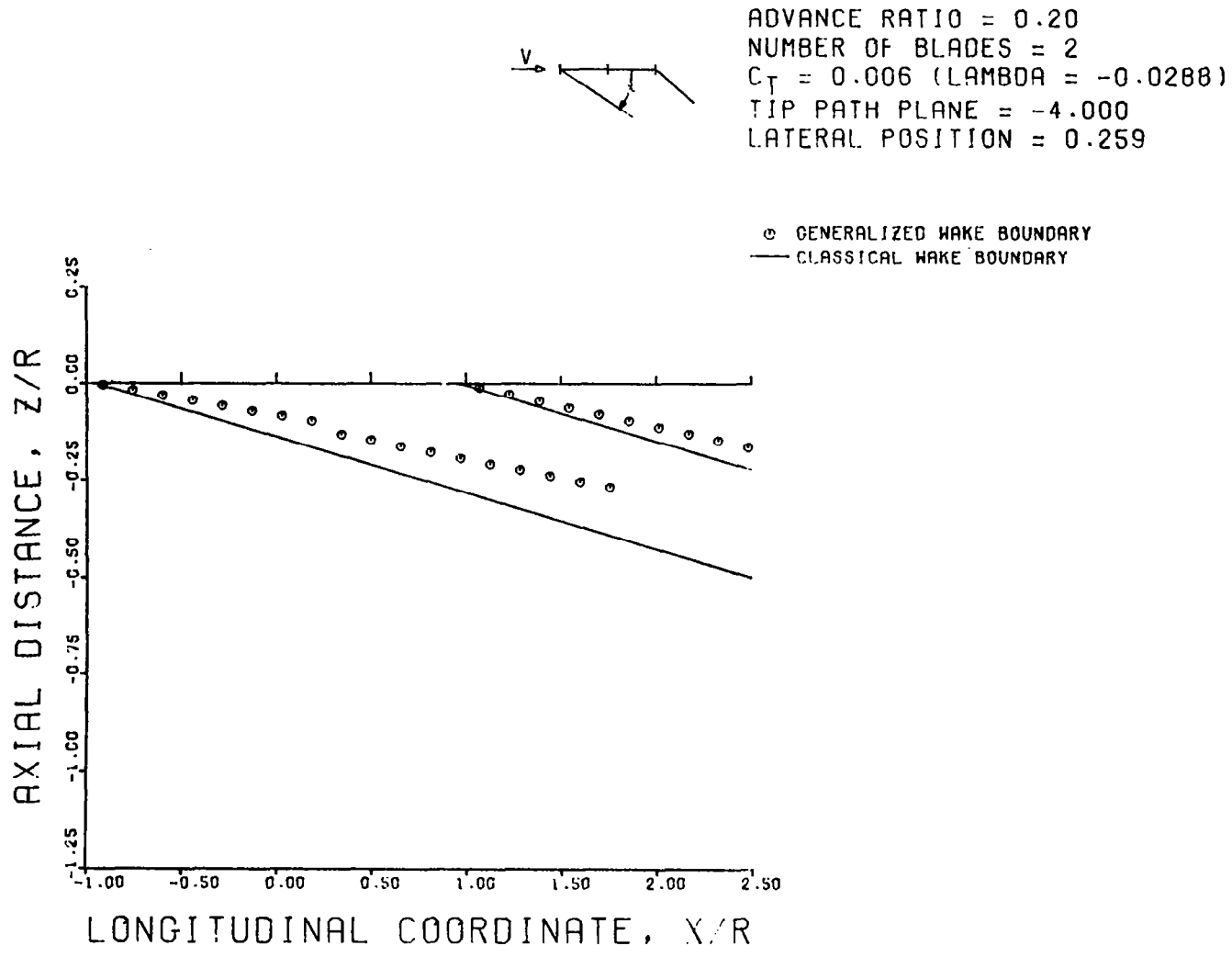

FIGURE 46B. FORE AND AFT WAKE BOUNDARY CHARTS FOR THE GENERALIZED DISTORTED TIP VORTEX (μ = .2, B = 2, C_T = .006, α = -4), Y/R = .259

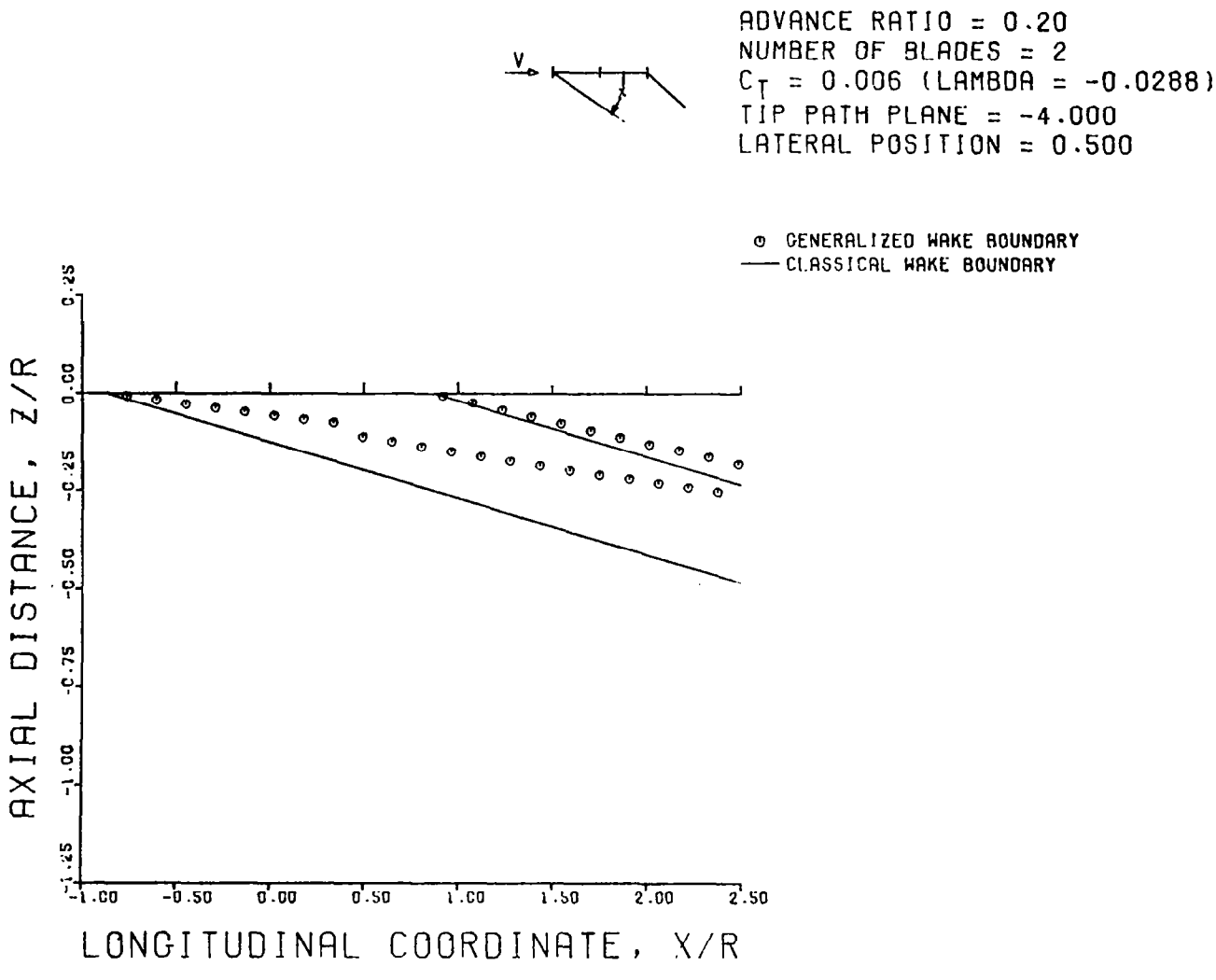

FIGURE 46C. FORE AND AFT WAKE BOUNDARY CHARTS FOR THE GENERALIZED DISTORTED TIP VORTEX (μ = .2, B = 2, C_T = .006, α = -4), Y/R = .500

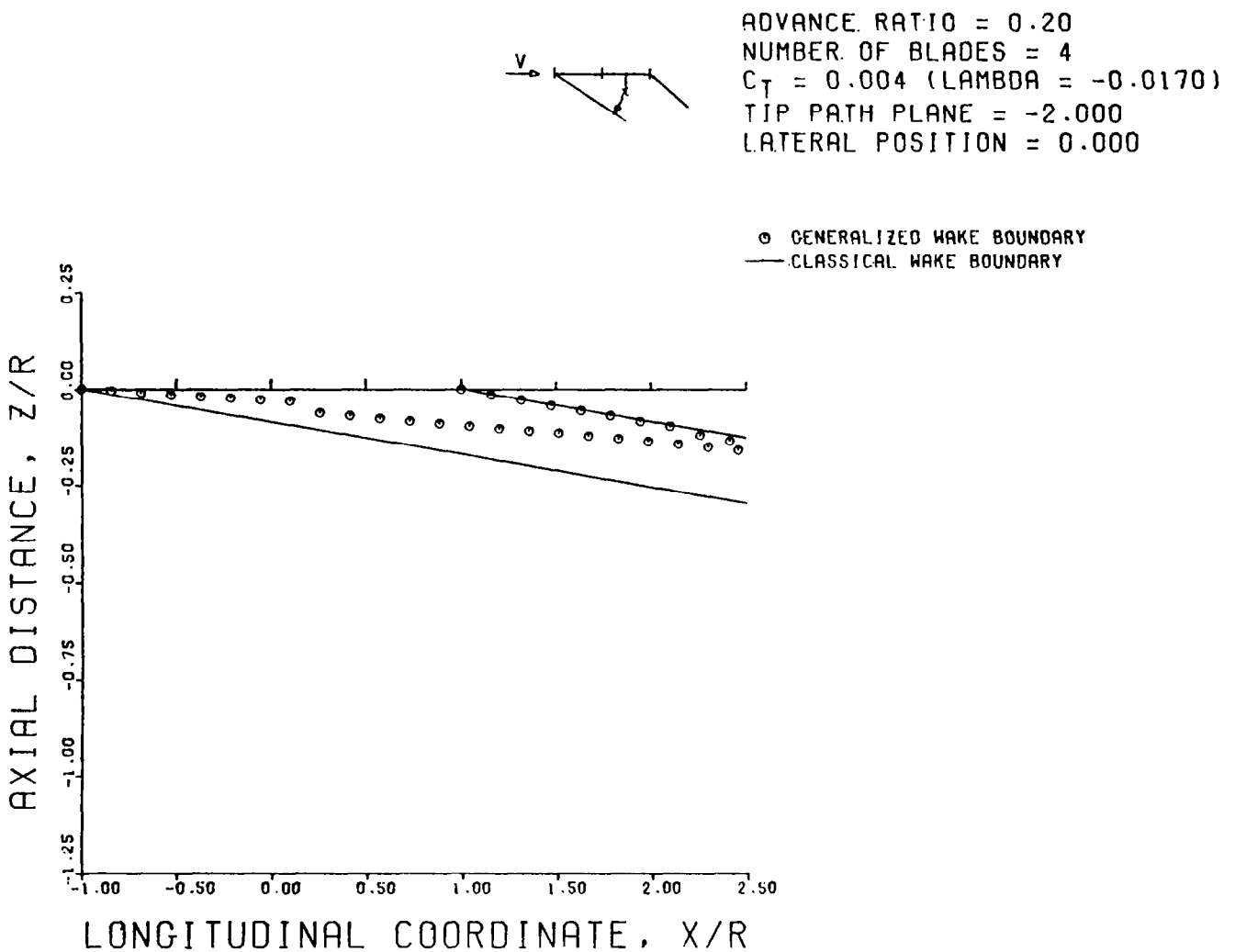

FIGURE 47A. FORE AND AFT WAKE BOUNDARY CHARTS FOR THE GENERALIZED DISTORTED TIP VORTEX (μ = .2, B = 4, C_T = .004, α = -2), Y/R = 0.0

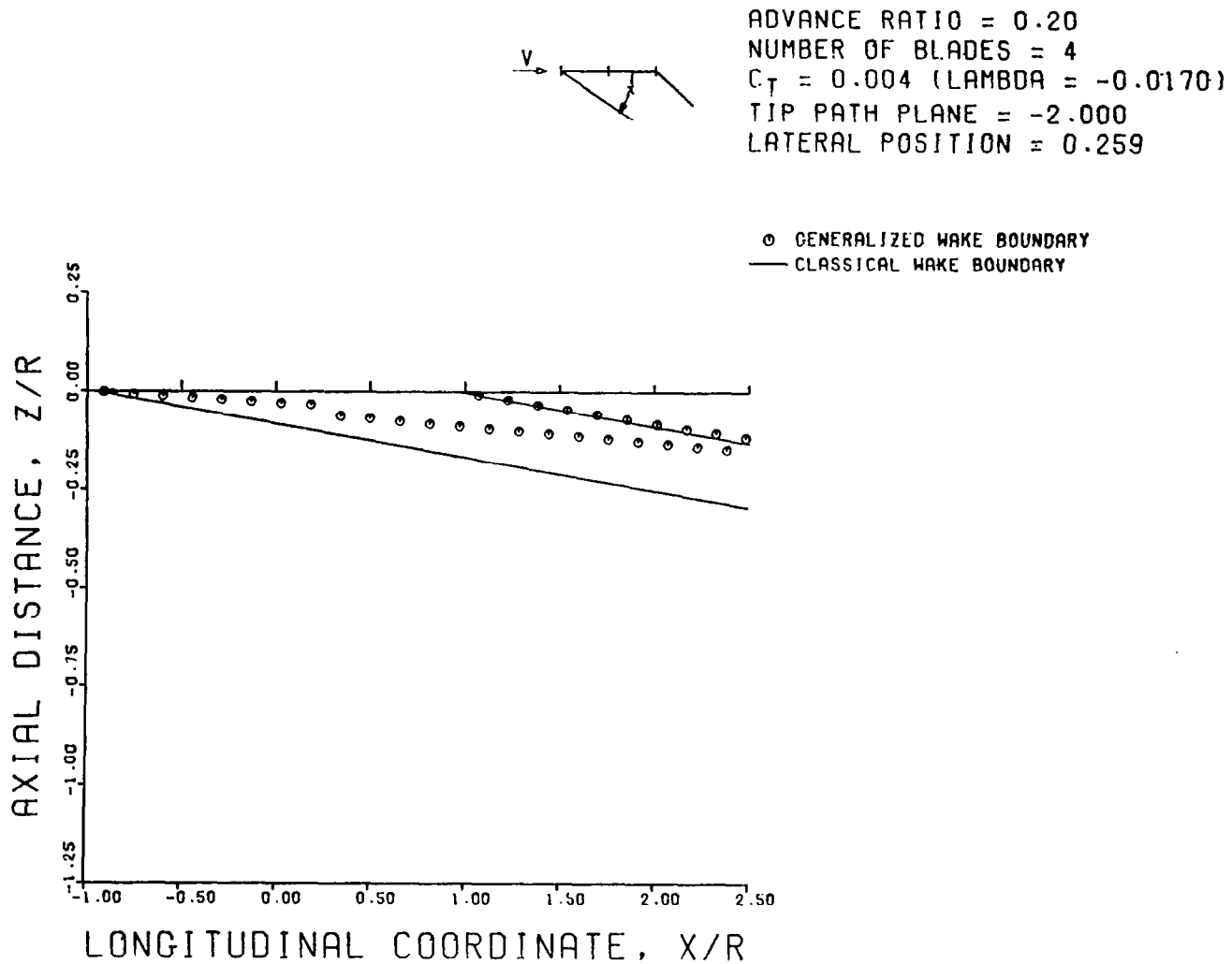

FIGURE 47B. FORE AND AFT WAKE BOUNDARY CHARTS FOR THE GENERALIZED DISTORTED TIP VORTEX (μ = .2, B = 4, C_T = .004, α = -2), Y/R = .259

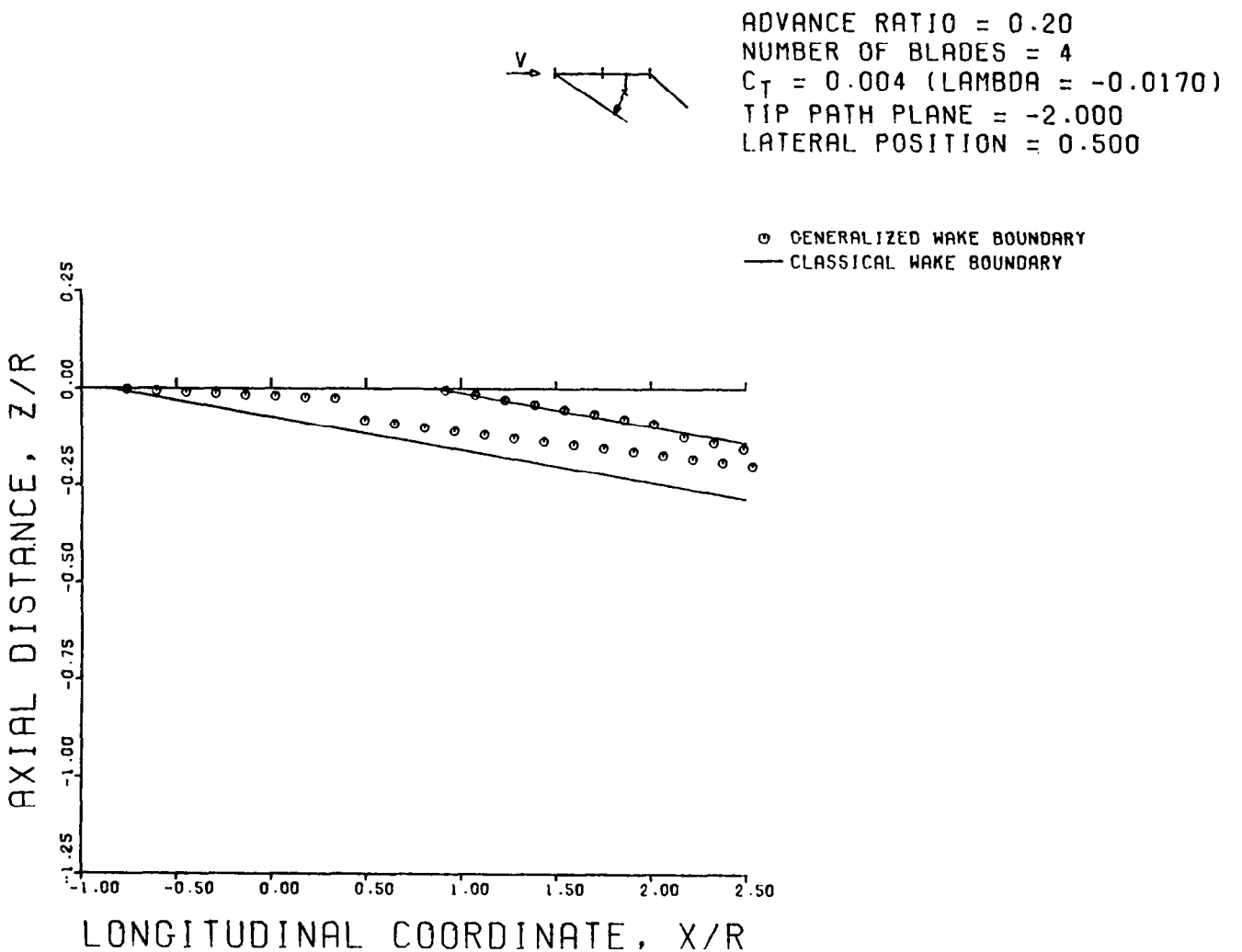

FIGURE 47C. FORE AND AFT WAKE BOUNDARY CHARTS FOR THE GENERALIZED DISTORTED TIP VORTEX (μ = .2, B = 4, C_T = .004, α = -2), Y/R = .500

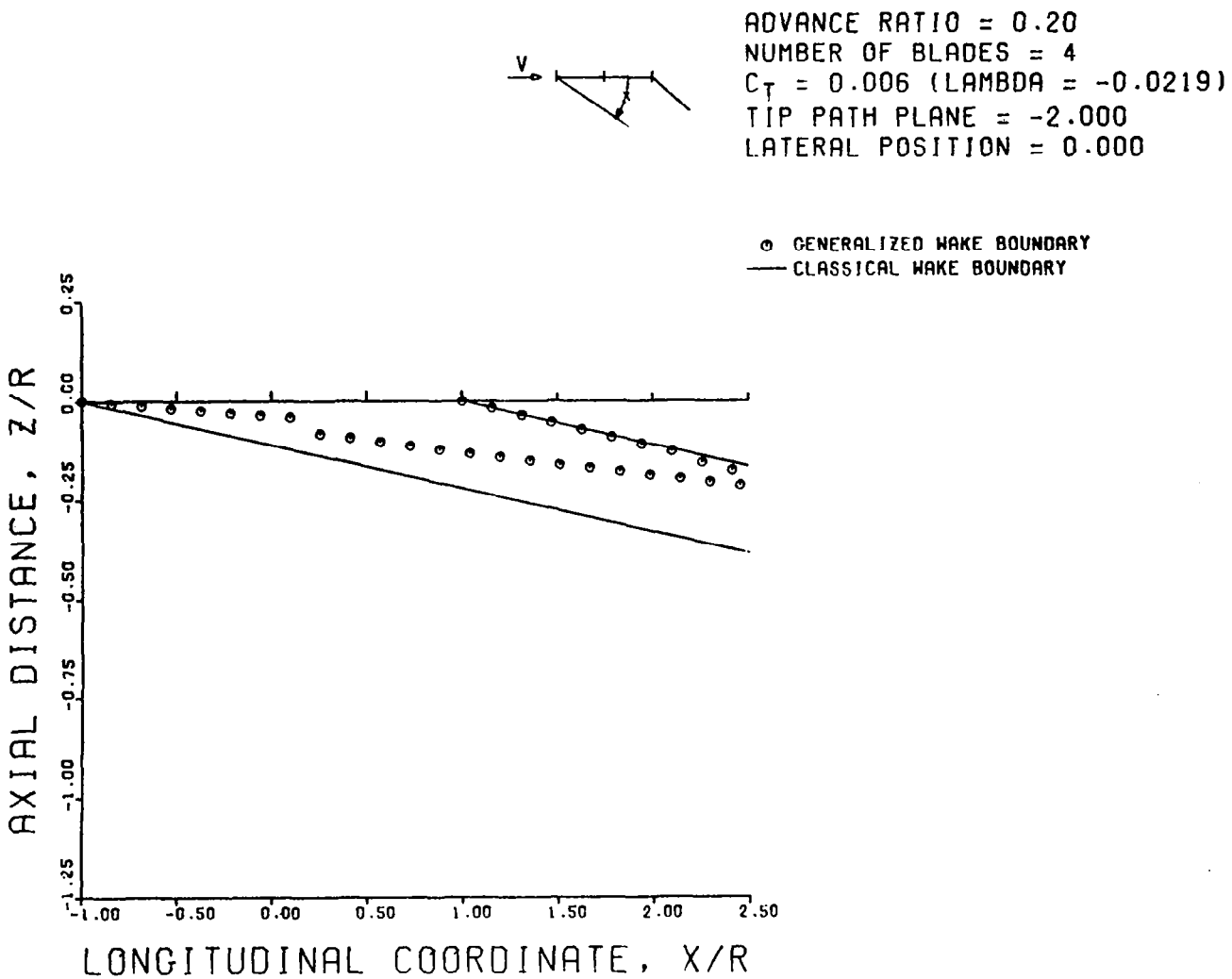

FIGURE 48A. FORE AND AFT WAKE BOUNDARY CHARTS FOR THE GENERALIZED DISTORTED TIP VORTEX (μ = .2, B = 4, C_T = .006, α = -2), Y/R = 0.0

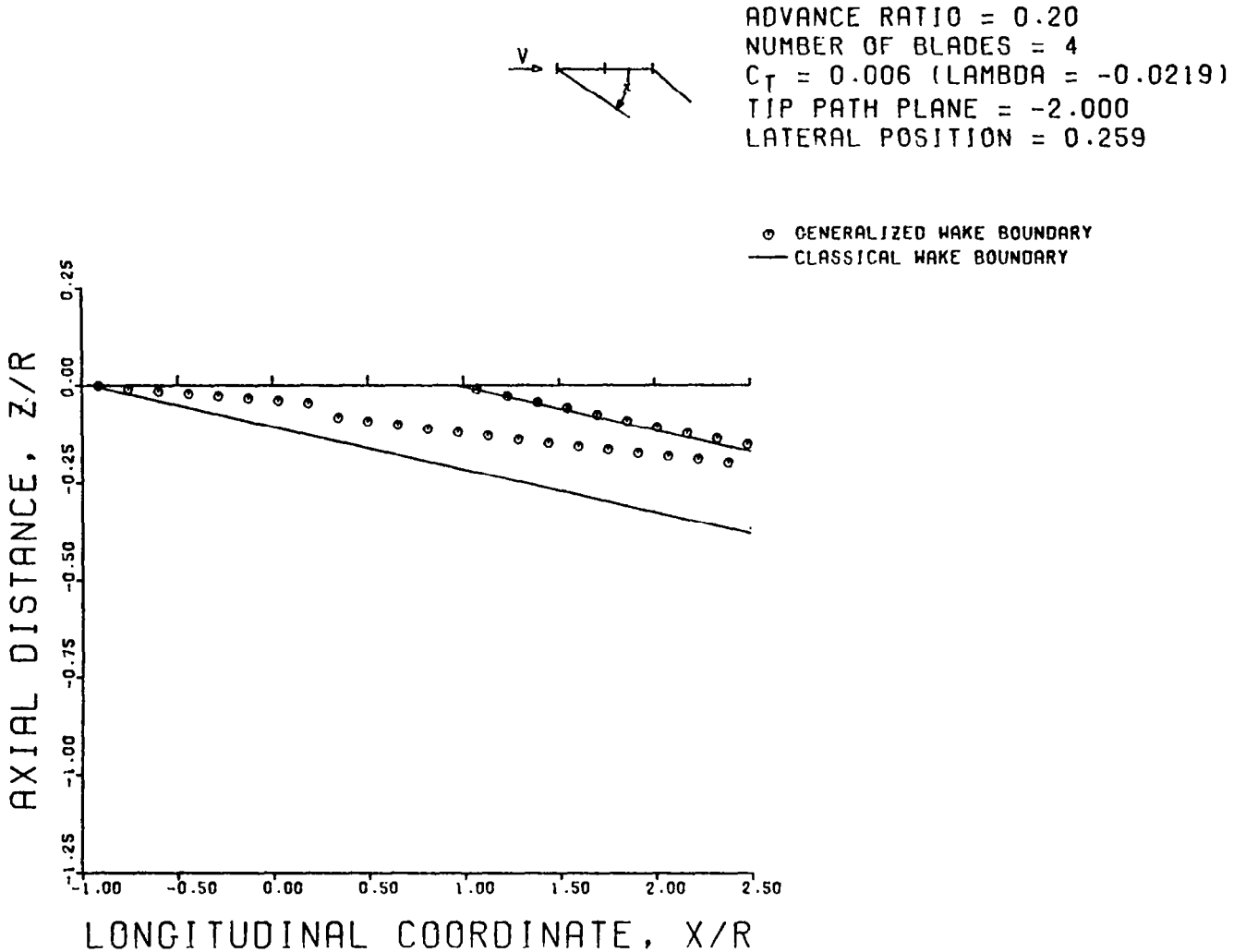

FIGURE 48B. FORE AND AFT WAKE BOUNDARY CHARTS FOR THE GENERALIZED DISTORTED TIP VORTEX (μ = .2, B = 4, C_T = .006, α = -2), Y/R = .259

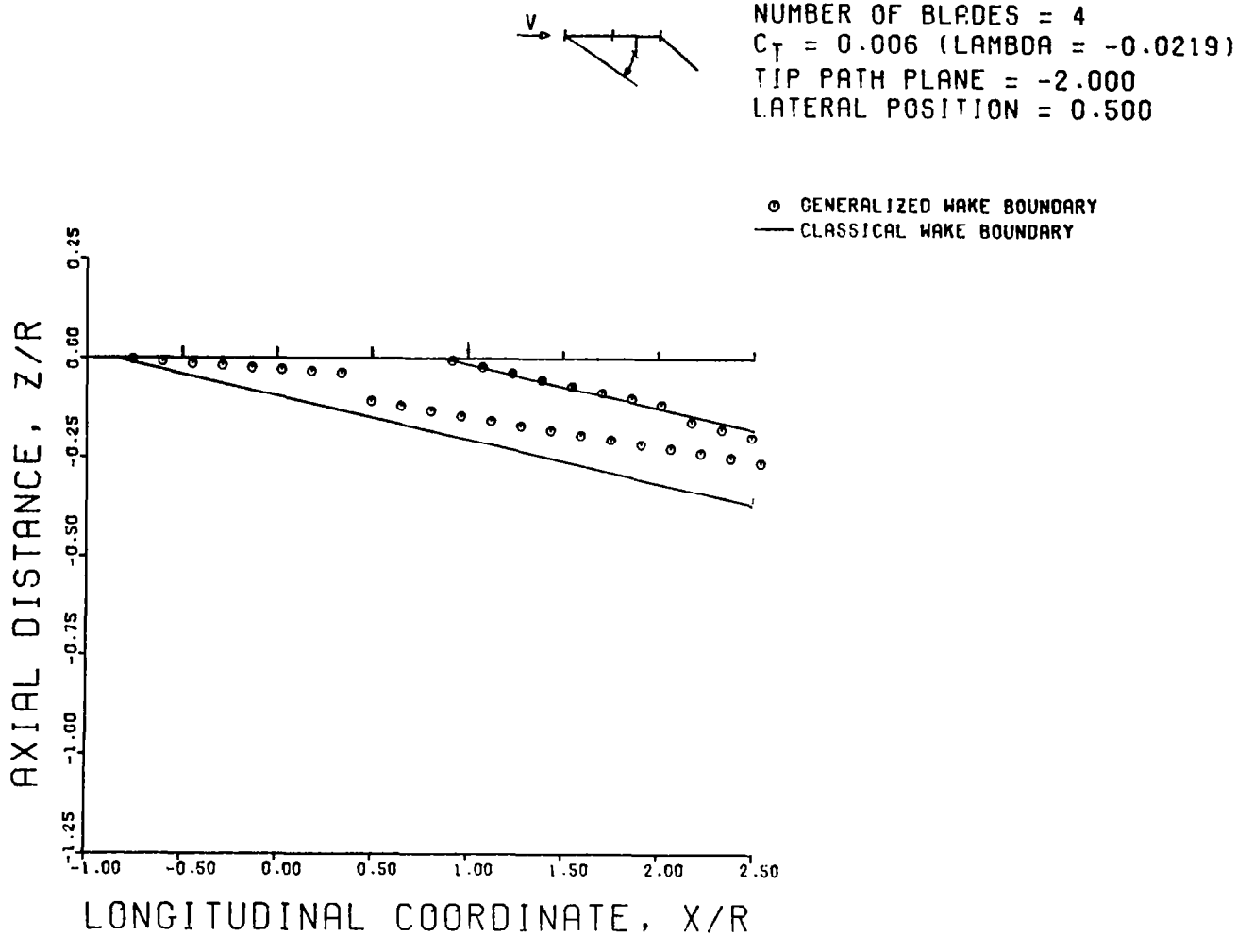

FIGURE 48C. FORE AND AFT WAKE BOUNDARY CHARTS FOR THE GENERALIZED DISTORTED TIP VORTEX (μ = .2, B = 4, C_T = .006, α = -2), Y/R = .500

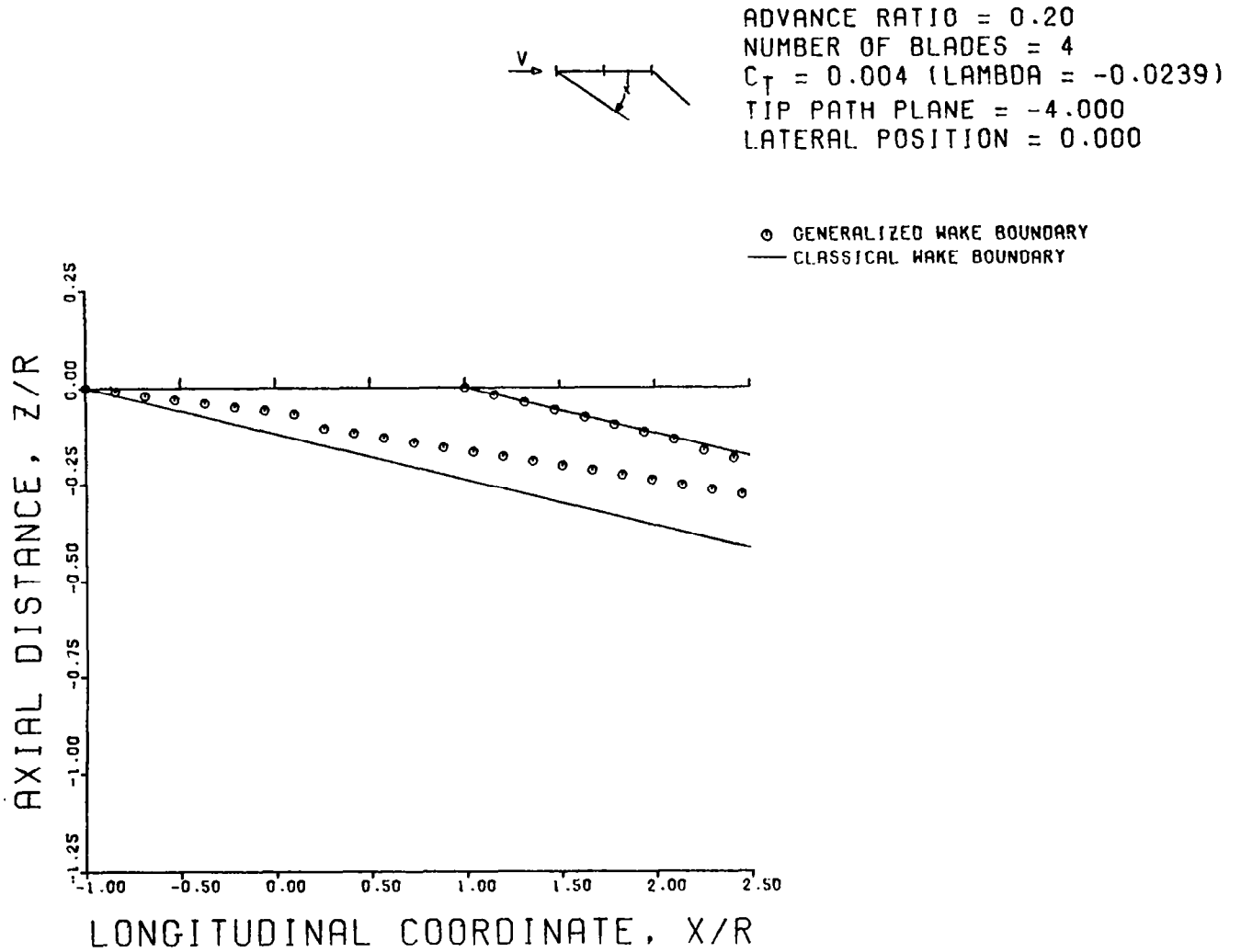

FIGURE 49A. FORE AND AFT WAKE BOUNDARY CHARTS FOR THE GENERALIZED DISTORTED TIP VORTEX (μ = .2, B = 4, C_T = .004, α = -4), Y/R = 0.0

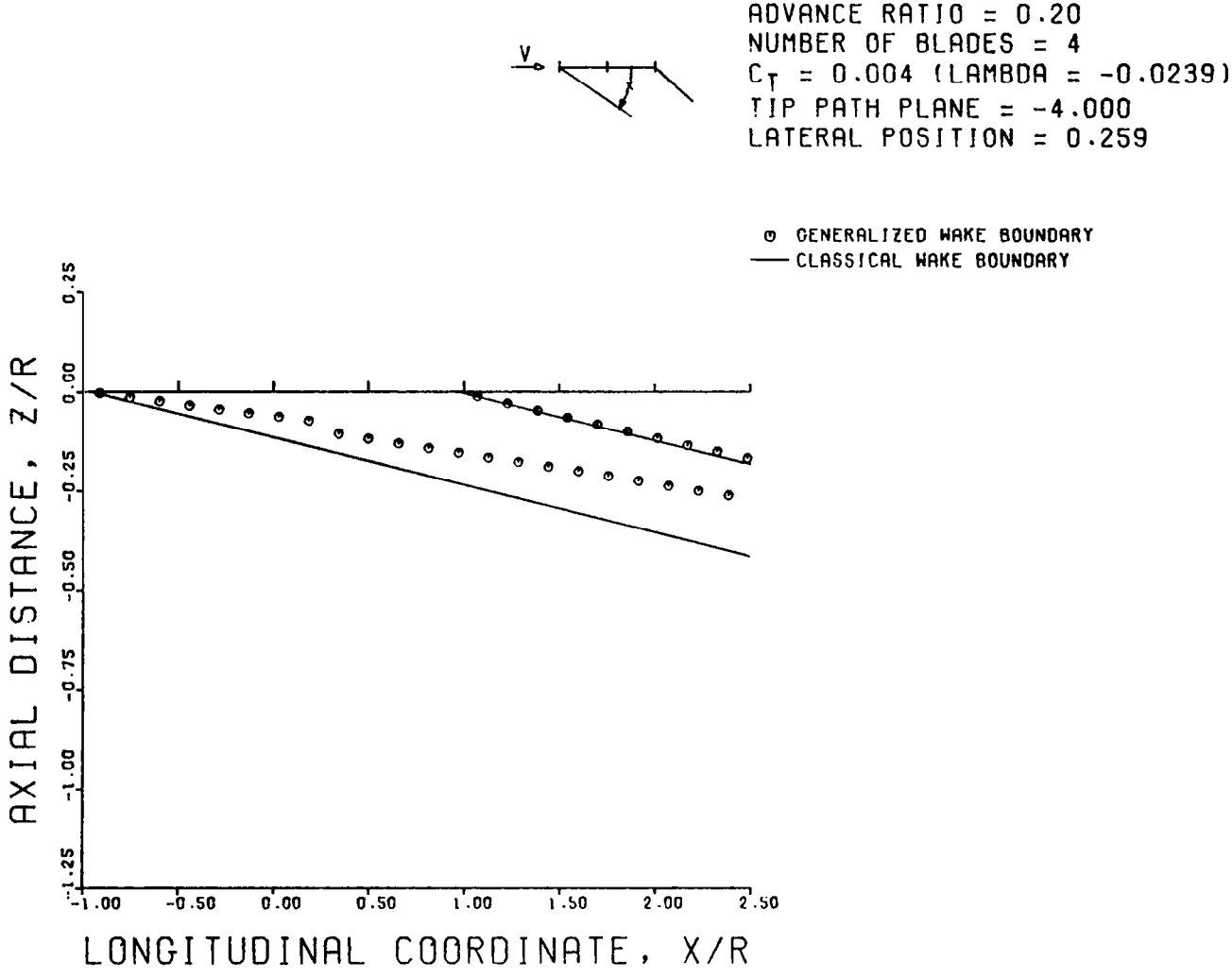

FIGURE 49B. FORE AND AFT WAKE BOUNDARY CHARTS FOR THE GENERALIZED DISTORTED TIP VORTEX (μ = .2, B = 4, C_T = .004, α = -4), Y/R = .259

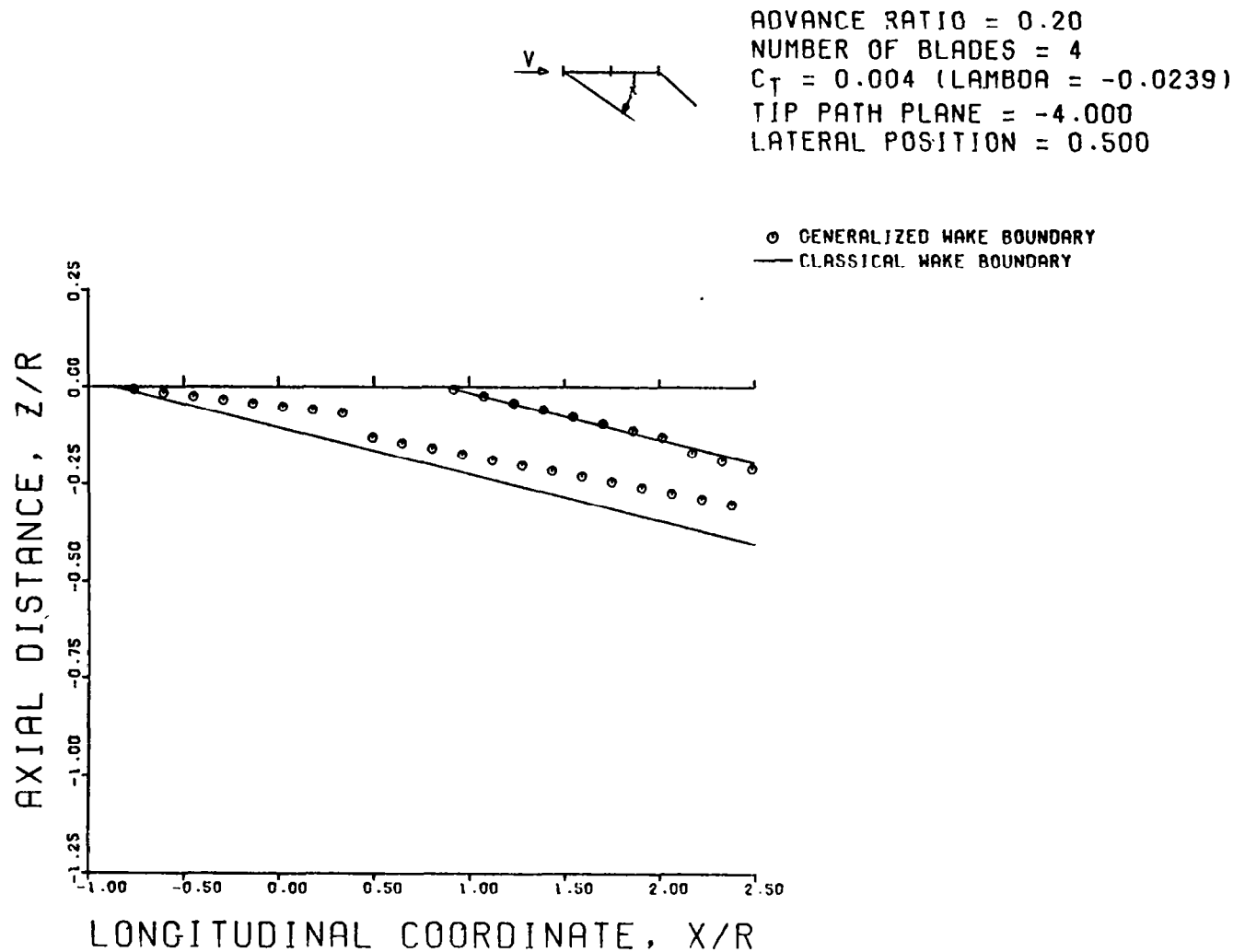

FIGURE 49C. FORE AND AFT WAKE BOUNDARY CHARTS FOR THE GENERALIZED DISTORTED TIP VORTEX (μ = .2, B = 4, C_T = .004, α = -4), Y/R = .500

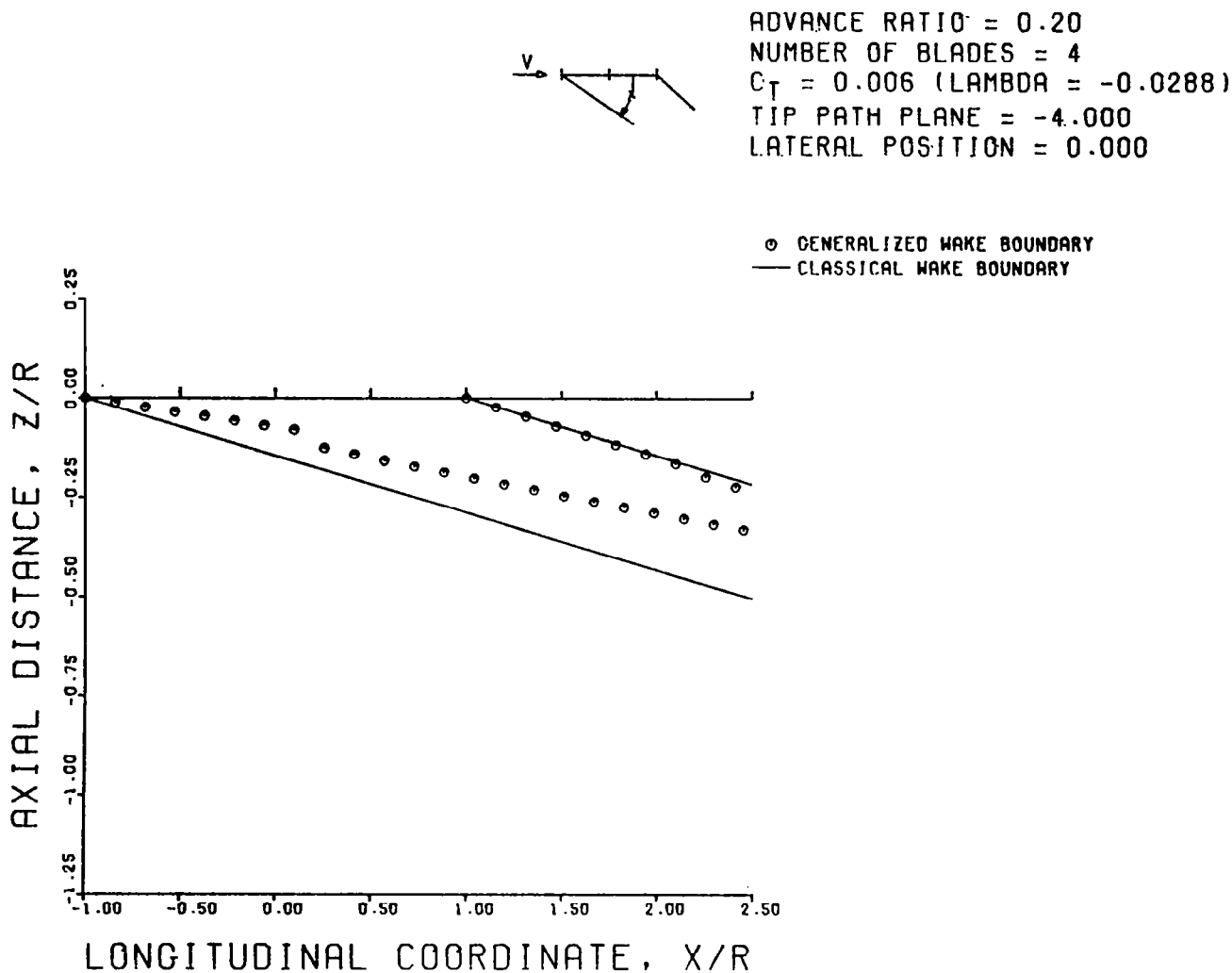

FIGURE 50A. FORE AND AFT WAKE BOUNDARY CHARTS FOR THE GENERALIZED DISTORTED TIP VORTEX (μ = .2, B = 4, C_T = .006, α = -4), Y/R = 0.0

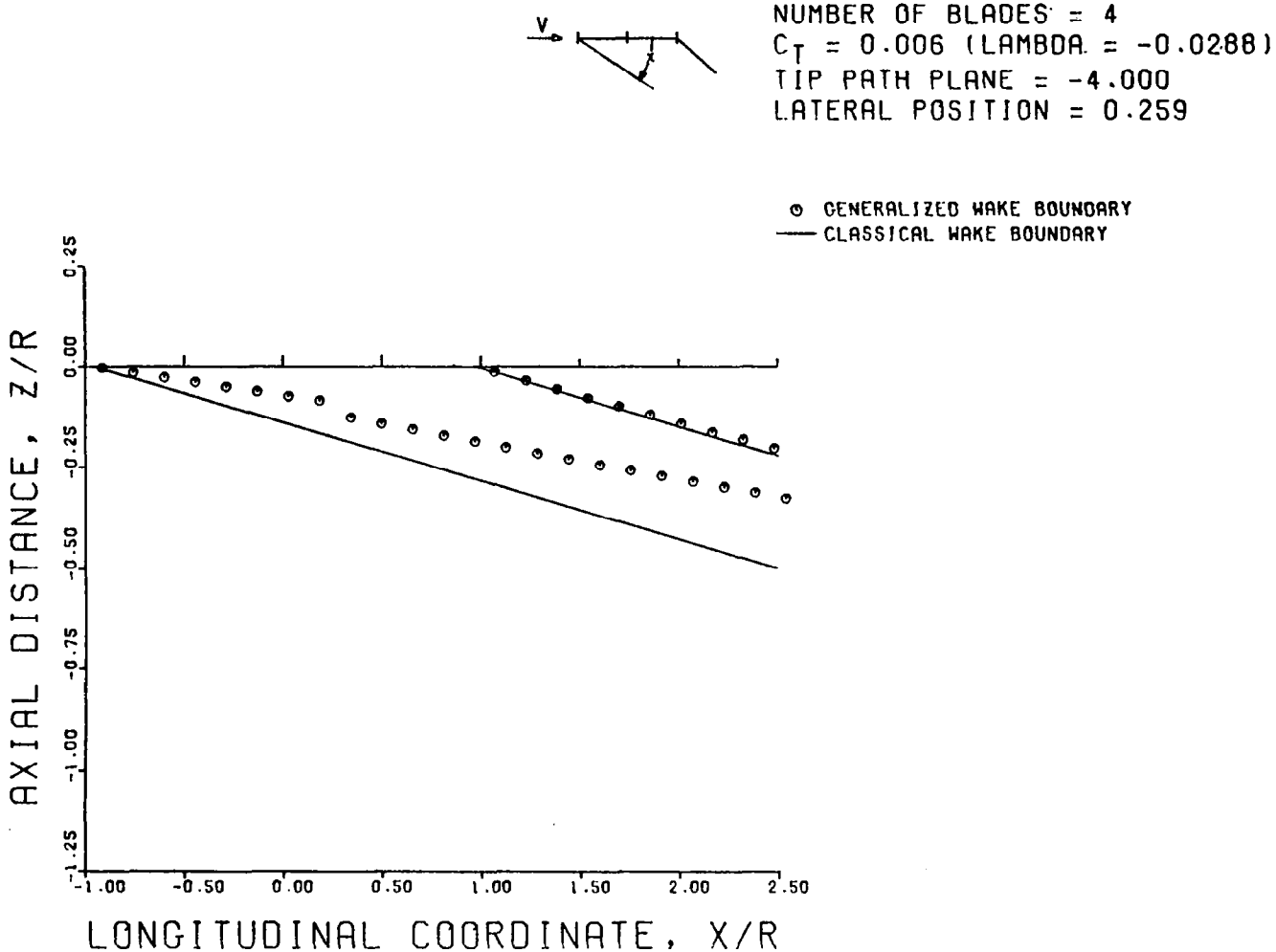

FIGURE 50B. FORE AND AFT WAKE BOUNDARY CHARTS FOR THE GENERALIZED DISTORTED TIP VORTEX (μ = .2, B = 4, C_T = .006, α = -4), Y/R = .259

*U.S. GOVERNMENT PRINTING OFFICE:1983-639-008/37

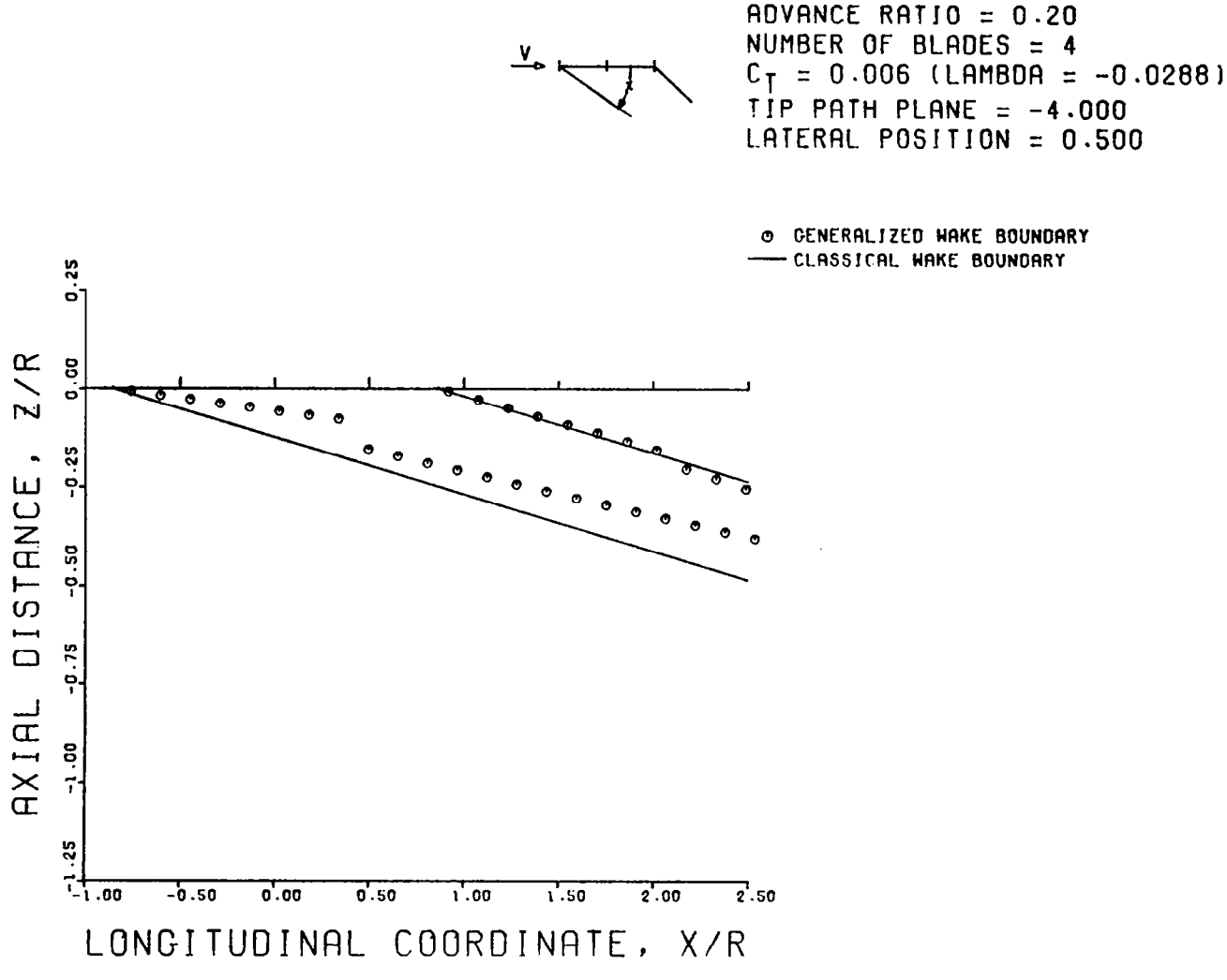

FIGURE 50C. FORE AND AFT WAKE BOUNDARY CHARTS FOR THE GENERALIZED DISTORTED TIP VORTEX (μ = .2, B = 4, C_T = .006, α = -4), Y/R = .500

1. Report No.	2. Government Accession No.	3. Recipient's Catalog No.
NASA CR-3727		

4. Title and Subtitle	5. Report Date
HELICOPTER ROTOR WAKE GEOMETRY AND ITS INFLUENCE IN FORWARD FLIGHT Volume II - Wake Geometry Charts	October 1983 6. Performing Organization Code
7. Author(s) T. Alan Egolf and Anton J. Landgrebe	8. Performing Organization Report No. R83-912666-58 10. Work Unit No.
9. Performing Organization Name and Address United Technologies Research Center East Hartford, CT 06108	11. Contract or Grant No. NAS1-14568
12. Sponsoring Agency Name and Address National Aeronautics and Space Administration Washington, DC 20546	13. Type of Report and Period Covered Contractor Report 14. Sponsoring Agency Code

15. Supplementary Notes The contract research effort which has led to the results in this report was financially supported by the structures Laboratory, USARTL, (AVRADCOM). Langley Technical Monitor: Wayne R. Mantay, Final Report - Volume II of two Volumes

16. Abstract An analytical investigation to generalize the wake geometry of a helicopter rotor in steady level forward flight and to demonstrate the influence of wake deformation in the prediction of rotor airloads and performance is described.

In Volume I, a first level generalized wake model is presented which is based on theoretically predicted tip vortex geometries for a selected representative blade design. The tip vortex distortions are generalized in equation form as displacements from the classical undistorted tip vortex geometry in terms of vortex age, blade azimuth, rotor advance ratio, thrust coefficient, and number of blades. These equations were programmed in a computer module to provide distorted wake coordinates at very low cost for use in rotor airflow and airloads prediction analyses. The sensitivity of predicted rotor airloads, performance, and blade bending moments to the modeling of the tip vortex distortion are demonstrated for low to moderately high advance ratios for a representative rotor and the H-34 rotor. Comparisons with H-34 rotor test data demonstrate the effects of the classical, predicted distorted, and the newly developed generalized wake models on airloads and blade bending moments. The use of distorted wake models results in the occurrence of numerous blade-vortex interactions on the forward and lateral sides of the rotor disk. The significance of these interactions is related to the number and degree of proximity to the blades of the tip vortices. The correlation obtained with the distorted wake models (generalized and predicted) is encouraging. However, the resulting high sensitivity of the predicted airloads to small deviations in tip vortex position demonstrate the requirement for improved blade-vortex interaction modeling.

A set of wake geometry charts are presented in Volume II to provide a convenient, readily accessible source for approximating rotor forward flight wake geometry and identifying wake boundaries and locations of blade-vortex passage.

17. Key Words (Suggested by Author(s))	18. Distribution Statement
Rotor Wake Geometry Distorted Wake Generalized Wake Rotor Airloads Rotor Performance Helicopter Wake Geometry Charts Tip Vortex	Unclassified - Unlimited Subject Category 02

19. Security Classif. (of this report)	20. Security Classif. (of this page)	21. No. of Pages	22. Price
Unclassified	Unclassified	208	A10

For sale by the National Technical Information Service, Springfield, Virginia 22161